



**CYTOTOXIC ACTIVITIES AND MOLECULAR  
TARGETS OF ATRACTYLODIN AND BETA-  
EUDESMOL IN CHOLANGIOCARCINOMA**

**BY**

**MR. VIVEK BHAKTA MATHEMA**

**A DISSERTATION SUBMITTED IN PARTIAL FULFILLMENT  
OF THE REQUIREMENTS FOR THE DEGREE OF  
DOCTOR OF PHILOSOPHY (BIOCLINICAL SCIENCES)  
CHULABHORN INTERNATIONAL COLLEGE OF MEDICINE  
THAMMASAT UNIVERSITY  
ACADEMIC YEAR 2017  
COPYRIGHT OF THAMMASAT UNIVERSITY**

**CYTOTOXIC ACTIVITIES AND MOLECULAR  
TARGETS OF ATRACTYLODIN AND BETA-  
EUDESMOL IN CHOLANGIOCARCINOMA**

**BY**

**MR. VIVEK BHAKTA MATHEMA**

**A DISSERTATION SUBMITTED IN PARTIAL FULFILLMENT  
OF THE REQUIREMENTS FOR THE DEGREE OF  
DOCTOR OF PHILOSOPHY (BIOCLINICAL SCIENCES)  
CHULABHORN INTERNATIONAL COLLEGE OF MEDICINE  
THAMMASAT UNIVERSITY  
ACADEMIC YEAR 2017  
COPYRIGHT OF THAMMASAT UNIVERSITY**

THAMMASAT UNIVERSITY  
CHULABHORN INTERNATIONAL COLLEGE OF MEDICINE

DISSERTATION

BY

MR.VIVEK BHAKTA MATHEMA


ENTITLED

CYTOTOXIC ACTIVITIES AND MOLECULAR TARGETS OF  
ATRACTYLODIN AND BETA-EUDESOL IN  
CHOLANGIOCARCINOMA

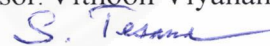
was approved as partial fulfillment of the requirements for  
the degree of Doctor of Philosophy in Bioclinical Sciences

on November 29, 2017

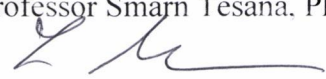
Chairman

  
(Professor Vithoon Viyanant, Ph.D.)


Member

  
(Associate Professor Smarn Tesana, Ph.D.)

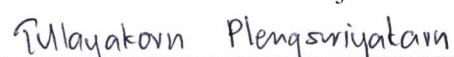
Member and Advisor

  
(Professor Kesara Na-Bangchang, Ph.D.)

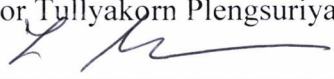
Member and Co-Advisor

  
(Assistant Professor Wanna Chaijaroenkul, Ph.D.)


Member and Co-Advisor

  
(Assistant Professor Tullyakorn Plengsuriyakarn, Ph.D.)

Director, Graduate Studies

  
(Professor Kesara Na-Bangchang, Ph.D.)

Dean

  
(Associate Professor Kammal Kumar Pawa, M.D.)

THAMMASAT UNIVERSITY  
CHULABHORN INTERNATIONAL COLLEGE OF MEDICINE

DISSERTATION

BY

MR.VIVEK BHAKTA MATHEMA

ENTITLED

CYTOTOXIC ACTIVITIES AND MOLECULAR TARGETS OF  
ATRACTYLODIN AND BETA-EUDESOL IN  
CHOLANGIOCARCINOMA

was approved as partial fulfillment of the requirements for  
the degree of Doctor of Philosophy in Bioclinical Sciences

on November 29, 2017

Advisor



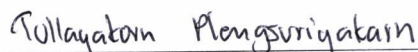
(Professor Kesara Na-Bangchang, Ph.D.)

Co-Advisor



(Assistant Professor Wanna Chaijaroenkul, Ph.D.)

Co-Advisor



(Assistant Professor Tullyakorn Plengsuriyakarn, Ph.D.)

Co-Advisor



(Mayuri Tarasuk, Ph.D.)

Co-Advisor



(Phunuch Muhamad, Ph.D.)

Dean



(Associate Professor Kamal Kumar Pawa, M.D.)

Dissertation Title	CYTOTOXIC ACTIVITIES AND MOLECULAR TARGETS OF ATRACTYLODIN AND BETA-EUDESOL IN CHOLANGIOCARCINOMA
Author	Mr. Vivek Bhakta Mathema
Degree	Doctor of Philosophy (Bioclinical Sciences)
Department/ Faculty/ University	Drug Discovery and Development, Chulabhorn International College of Medicine, Thammasat University
Dissertation Advisor	Prof. Kesara Na-Bangchang, Ph.D
Academic Year	2017

## ABSTRACT

Cholangiocarcinoma (CCA) is a progressively fatal form of cancer which generally occurs due to malignant transformation of hepatic biliary cholangiocytes. Several countries including Thailand, Cambodia, and Laos have been reported to for the high prevalence of CCA and are in desperate need for development of more effective chemotherapnautics for treatment of this cancer. Although the exact factors underlying genesis of CCA remains unclear, conditions including cirrhosis, liver fluke infection, intrahepatic biliary stones, and virus-linked hepatitis are considered as risk factors associated with CCA. The lack of in-depth molecular studies for identification and subsequent obstruction of potential molecular targets to prevent cancer growth has remained as a major impediment in CCA research. The study was primarily focused on *in vitro* anticancer potentials of naturally occurring sesquiterpenoid present in rhizomes of *Atractylodes lancea* (Thunb) DC., namely atractylodin and  $\beta$ -eudesmol for their cytotoxicity and mode of action at molecular level on CCA-associated cell line (CL-6). The normal human embryonic fibroblast (OUMS) was taken as control cell line for

cytotoxicity evaluation. The effects of these compounds on crucial cell signaling pathways associated with cell survival, proliferation and cytoprotective activity in CL-6 cells were investigated. In particular, the suppressive effects of the compounds on cell signaling cascades associated with JAK-STAT and NF- $\kappa$ B pathways were explored. Similarly, the effects of the compounds on production of cytoprotective enzymes, namely NAD(P) H-quinone oxidoreductase, and heme oxygenase-1 were investigated. Results indicated that atractylodin and  $\beta$ -eudesmol treatment exhibited selective cytotoxicity towards CL-6 as compared to OUMS cells. The compound treatment suppressed colony forming ability of CL-6 cells. Results from fluorescence microscopy indicated that both compounds induced nuclear fragmentation in CL-6 cells. The compound pretreatment decreased wound healing ability of CL-6 cells in the presence or absence of cytokine stimulation. Results from western blot analysis indicated that the compounds were able to suppress STAT1/3 phosphorylation, NF- $\kappa$ B activation, and expression of cytoprotective enzymes. Real-time PCR analysis indicated that the compounds suppressed mRNA expression of multiple genes associated with cytoprotection, cell proliferation, and STAT1/3 activation. Taken together, results suggested that atractylodin and  $\beta$ -eudesmol exerted growth inhibitory activities on CL-6 cells which might have been linked to its inhibitory effect on STAT1/3 phosphorylation, NF- $\kappa$ B activation, and cytoprotective enzyme production. The research outcomes contribute to the field of CCA research and may serve as a vital resource for future drug development to treat CCA.

**Keywords:** *Atractylodens lancea* (Thunb) DC., atractylodin,  $\beta$ -eudesmol, cholangiocarcinoma

## ACKNOWLEDGEMENTS

I would like to express my sincere gratitude to several people who provided generous support and valuable guidance throughout my doctoral studies at Chulabhorn International College of Medicine, Thammasat University. First, I would like to present my deepest appreciation and sincere gratitude to my advisor, Professor Dr. Kesara Nangchang, for her generous support, guidance and patience all the way through my academic and dissertation process. Her knowledge, planning, and supervision were immensely beneficial to my learning experience.

I am very thankful and would like to extend my appreciation to Associate Professor Dr. Wanna Chaijaroenkul, Assistant Professor Dr. Tulayakorn Plengsuriyakarn, Dr. Mayuri Tarasuk, Dr. Kanyarat Boonprasert and department staff, who provided essential academic inspiration and devoted their valuable time and efforts to maintain the quality of this research. I truly appreciate their genuine care and professionalism towards helping me conduct my studies.

Also, my special thanks to Dr. Saranyoo Ponnikorn and Mr. Pongsakorn Martviset for their generous support and guidance during my experimental studies. Several instructors provided me opportunities to gain knowledge from their real experience and offered their generous support and encouragement to complete my study. Without their combined assistance, the completion of this dissertation would have been impossible.

I would also like to thank my colleagues Mr. Kanawut Kotawang, Ms. Siriprapa Warathumpitak and Mr. Author Navarro who have shared their knowledge and offered genuine help during my research. Last but not the least, I would like to express my greatest thanks and appreciation to my parents and sister. Their unconditional encouragement, inspiration, affection and support has helped me move forward with my academic life and complete my doctorate degree.

Mr. Vivek Bhakta Mathema

## TABLE OF CONTENTS

	Page
ABSTRACT	(1)
ACKNOWLEDGEMENT	(3)
TABLE OF CONTENTS	(4)
LIST OF TABLES	(13)
LIST OF FIGURES	(14)
LIST OF ABBREVIATIONS	(19)
CHAPTER 1 INTRODUCTION	1
1.1 Introduction	1
1.2 Significance of research	3
CHAPTER 2 REVIEW OF LITERATURE	4
2.1 Background information	4
2.2 Epidemiology of cholangiocarcinoma	5
2.3 Anatomical classification of cholangiocarcinoma	8
2.4 Risk factors relating to cholangiocarcinoma	9
2.5 Pathogenesis of cholangiocarcinoma	9
2.6 Role of cytoprotective enzymes in malignancy and drug resistance	17
2.7 Current biomarkers in cholangiocarcinoma	22
2.8 Epigenetic aspects of cholangiocarcinoma	24



3.1 General objectives	39
3.2 Specific objectives	39

4.1	Cell line and reagents	40
4.1.1	Cell lines	40
4.1.2	Reagents	40
4.2	Cytotoxicity testing	41
4.2.1	Cell culture	41
4.2.2	Cell viability assay	41
4.3	Molecular signaling pathways	42
4.3.1	JAK-STAT pathway	42
4.3.1.1	Cell culture	43
4.3.1.2	Brightfield inverted microscopy	43
4.3.1.3	Fluorescence microscopy	43

4.3.1.4 Colony forming assay	44
4.3.1.5 Wound healing assay	44
4.3.1.6 RNA extraction and real time PCR analysis	45
4.3.1.7 Western blotting analysis	47
4.3.2 NF- $\kappa$ B pathway	48
4.3.2.1 Cell culture	48
4.3.2.2 Cell viability assay	48
4.3.2.3 Western blotting analysis	49
4.3.3 Heme oxygenase-1 and NAD(P)H quinone oxidoreductase 1	49
4.3.3.1 Cell culture	50
4.3.3.2 Florescence microscopy	50
4.3.3.3 Colony forming assay	51
4.3.3.4 Wound healing assay	51
4.3.3.5 RNA extraction and real time PCR analysis	51
4.3.3.6 Western blotting analysis	52
4.4 Statistical analysis	53
CHAPTER 5 RESULTS	54
5.1 Anti-cholangiocarcinoma effect of atractylodin	54
5.1.1 Cytotoxicity of atractylodin in cholangiocarcinoma cells	54
5.1.2 Morphological evidence of atractylodin-induced cell death in cholangiocarcinoma cells	55
5.1.3 Evaluation of atractylodin treatment on colony forming ability of cholangiocarcinoma cells	55
5.1.4 Evaluation of atractylodin treatment on wound healing ability of cholangiocarcinoma cells	59
5.1.5 Evaluation of atractylodin treatment on the production of heme oxygenase-1 in cholangiocarcinoma cells	62

5.1.6 Evaluation of atractylodin treatment on the production of NQO1 in cholangiocarcinoma cells	62
5.1.7 Evaluation of cytokine induced STAT1 3 phosphorylation	
5.1.7 Evaluation of cytokine induced STAT1/3 phosphorylation in cholangiocarcinoma cells	65
5.1.8 Effect of atractylodin treatment on cytokine induced STAT1/3 phosphorylation in cholangiocarcinoma cells	65
5.1.9 Effect of nifuroxazide treatment on cytokine induced STAT1.3 phosphorylation in cholangiocarcinoma cells	68
5.1.10 Evaluation of atractylodin treatment on aggregate expression of major NF- $\kappa$ B proteins in cholangiocarcinoma cells	70
5.1.11 Evaluation of the cytokine-induced IkBA degradation in cholangiocarcinoma cells	73
5.1.12 Effect of atractylodin treatment on cytokine-induced IkB $\alpha$ degradation in cholangiocarcinoma cells	73
5.1.13 Effect of MG132 treatment on cytokine-induced IkB $\alpha$ degradation in cholangiocarcinoma cells	76
5.1.14 Evaluation of atractylodin treatment on ICAM-1 and iNOS mRNA expression in cholangiocarcinoma cells	78
5.1.15 Evaluation of atractylodin treatment on mRNA expression of tumor associated genes in cholangiocarcinoma cells	78
5.2 Anti-cholangiocarcinoma effect of $\beta$ -eudesmol	82
5.2.1 Cytotoxicity of $\beta$ -eudesmol treatment in cholangiocarcinoma cells	82
5.2.2 Morphological evidence of $\beta$ -eudesmol -induced cell death in cholangiocarcinoma cells	84
5.2.3 Evaluation of $\beta$ -eudesmol treatment on colony forming ability of cholangiocarcinoma cells	87

5.2.4 Evaluation of $\beta$ -eudesmol treatment on wound healing ability of cholangiocarcinoma cells	90
5.2.5 Evaluation of $\beta$ -eudesmol treatment on production of heme oxygenase-1 in cholangiocarcinoma cells	92
5.2.6 Evaluation of $\beta$ -eudesmol treatment on the production of NQO1 in cholangiocarcinoma cells	92
5.2.7 Effect of $\beta$ -eudesmol on cytokine induced STAT1/3 phosphorylation in cholangiocarcinoma cells	95
5.2.8 Evaluation of $\beta$ -eudesmol treatment on aggregate expression of major NF- $\kappa$ B proteins in cholangiocarcinoma cells.	97
5.2.9 Effect of $\beta$ -eudesmol on cytokine induced I $\kappa$ B $\alpha$ degradation in cholangiocarcinoma cells	100
5.2.10 Evaluation of $\beta$ -eudesmol treatment on ICAM-1 and iNOS mRNA expression in cholangiocarcinoma cells	102
5.2.11 Evaluation of $\beta$ -eudesmol treatment on multiple tumor-associated genes in cholangiocarcinoma cells	104
5.2.12 Effect of SnCl <sub>2</sub> and $\beta$ -eudesmol treatment on colony forming ability of cholangiocarcinoma cells	106
5.2.13 Effect of SnCl <sub>2</sub> and $\beta$ -eudesmol treatment of wound healing ability of cholangiocarcinoma cells	106
5.2.14 Effect of SnCl <sub>2</sub> treatment on heme oxygenase-1 expression in cholangiocarcinoma cells	109
5.2.15 Effect of SnCl <sub>2</sub> treatment on nuclear morphology of $\beta$ -eudesmol -treated cholangiocarcinoma cells	113
5.2.16 Effect of SnCl <sub>2</sub> treatment on $\beta$ -eudesmol-induced cell death of cholangiocarcinoma cells	114
5.2.17 Effect of SnCl <sub>2</sub> treatment on $\beta$ -eudesmol-induced suppression of HO-1 mRNA expression in cholangiocarcinoma cells	114

5.2.18 Evaluation of Zinc protoporphyrin IX treatment on cell viability of cholangiocarcinoma cells	117
5.2.19 Evaluation of Zinc protoporphyrin IX treatment on HO-1 expression in cholangiocarcinoma cells	118
5.2.20 Evaluation of Zinc protoporphyrin IX treatment on heme oxygenase-1 mRNA expression in cholangiocarcinoma cells	118
5.2.21 Effect of $\beta$ -eudesmol treatment on nuclear morphology of cytokine-stimulated cholangiocarcinoma cells	121
5.2.22 Comparison of colony forming inhibitory effect between atractrylodin and $\beta$ -eudesmol against cholangiocarcinoma cells	122
5.2.23 Comparison of wound healing inhibitory effect between atractrylodin and $\beta$ -eudesmol against cholangiocarcinoma cells	122
5.2.24 Summarized effect of atractrylodin and $\beta$ -eudesmol on Heme oxygenase-1 expression in cholangiocarcinoma cells	125
5.2.25 Summarized effect of atractrylodin and $\beta$ -eudesmol on NQO1 expression in cholangiocarcinoma cells	125
5.2.26 Summarized effect of atractrylodin and $\beta$ -eudesmol on STAT1 and STAT3 activation in cholangiocarcinoma cells	125
5.2.27 Summarized effect of atractrylodin and $\beta$ -eudesmol on aggregate NF- $\kappa$ B expression in cholangiocarcinoma cells	126
5.2.28 Summarized effect of atractrylodin and $\beta$ -eudesmol on aggregate NF- $\kappa$ B expression in cytokine stimulated cholangiocarcinoma cells	131

5.2.29 Summarized effect of atractylodin and $\beta$ -eudesmol on I $\kappa$ B $\alpha$ degradation in cytokine stimulated cholangiocarcinoma cells	131
5.2.30 Summarized effect of atractylodin and $\beta$ -eudesmol on relative mRNA expression of major tumor associated genes in cholangiocarcinoma cells	134
5.2.31 Summarized effect of atractylodin and $\beta$ -eudesmol on relative mRNA expression of STAT-associated genes in cholangiocarcinoma cells	134
CHAPTER 6 DISCUSSION	137
6.1 Cytotoxicity evaluation of atractylodin and $\beta$ -eudesmol in cholangiorarcinoma cells	137
6.2 Effect of atractylodin and $\beta$ -eudesmol induced cytotoxicity cell culture and nuclear morphology of cholangiocarcinoma cells	137
6.3 Anti-proliferative effect of atractylodin and $\beta$ -eudesmol in cholangiocarcinoma cells	138
6.4 Effect of atractylodin and $\beta$ -eudesmol on <i>in vitro</i> wound healing ability of cholangiocarcinoma cells	139
6.5 Effect of atractylodin and $\beta$ -eudesmol on mRNA expression in cholangiocarcinoma cells cells	140
6.6 Inhibitory effect of atractylodin and $\beta$ -eudesmol on HO-1 production in cholangiocarcinoma cells	141
6.7 Inhibitory effect of atractylodin and $\beta$ -eudesmol on NQO1 production in cholangiocarcinoma cells	142
6.8 Effect of atractylodin and $\beta$ -eudesmol on JAK-STAT pathway activation in cholangiocarcinoam cells	143
6.9 Effect of atractylodin and $\beta$ -eudesmol on NF- $\kappa$ B pathway activation in cholangiocarcinoma cells	144

6.10 Effects of SnCl <sub>2</sub> -induced HO-1 expression in $\beta$ -eudesmol-treated cholangiocarcinoma cells	147
6.11 Effects of Zinc(II) Protoporphyrin IX on HO-1 expression in cholangiocarcinoma cells	148
CHAPTER 7 CONCLUSIONS AND RECOMMENDATIONS	149
7.1 Anti-cholangiocarcinoma effect of atractylodin	149
7.2 Anti-cholangiocarcinoma effect of $\beta$ -eudesmol	150
REFERENCES	152
APENDICES	168
APPENDIX A	168
APPENDIX B	171
APPENDIX C	173
APPENDIX D	174
APPENDIX E	175
APPENDIX F	176
APPENDIX G	177
APPENDIX H	178
APPENDIX I	180
APPENDIX J	182
APPENDIX K	184
APPENDIX L	186
APPENDIX M	188
APPENDIX N	190
APPENDIX O	191
APPENDIX P	192
APPENDIX Q	194

APPENDIX R	195
APPENDIX S	196
APPENDIX T	197
APPENDIX U	198
APPENDIX V	199
 BIOGRAPHY	 200





## LIST OF TABLES

Tables	Page
2.1 Summary of potential biomarkers used in cholangiocarcinoma study	23
2.2 List of well known plants-derived anti-cancer drugs	30
2.3 Some known biological activities of atractylodin and $\beta$ -eudesmol	34
4.1 List of forward and reverse primers used for amplification of genes using real-time PCR	46
5.1 $IC_{50}$ and SI values for atractylodin	54
5.2 $IC_{50}$ and SI values for $\beta$ -eudesmol	82
5.3 $IC_{50}$ values for specific pathway inhibitors	83

## LIST OF FIGURES

Figures	Page
2.1 Worldwide incidence of cholangiocarcinoma. The data reflecting occurrence of cholangiocarcinoma for period of 1977 to 2007	6
2.2 Distribution and prevalence of <i>Opisthorchis viverrini</i> infection and cholangiocarcinoma incident in Thailand	7
2.3 Anatomical classification of cholangiocarcinoma	8
2.4 Schematic overview of JAK-STAT pathway in cell survival and proliferation	11
2.5 Schematics of mechanism for involvement of STAT3 in cancer	12
2.6 Schematic overview of the NF-KappaB family pathway	13
2.7 Schematic overview of the involvement of NF-κB in cancer	14
2.8 Schematic overview of multiple factors potentially resulting in genesis of cholangiocarcinoma	16
2.9 Up-regulation of expression of NQO1 and HO-1 regulated by Keap1/Nrf2/ARE pathway	18
2.10 Involvement of heme oxygenase-1 in lungs cancer metastasis	19
2.11 Involvement of NAD(P)H quinone dehydrogenase 1 in breast cancer metastasis	20
2.12 Current strategy for diagnosis and possible treatment of cholangiocarcinoma using surgical interventions	26
2.13 Overall schematic for anti-cholangiocarcinoma activity evaluation of evaluation of atractylodin and β-eudesmol in cholangiocarcinoma cells	28
2.14. Chemical structure of atractylodin, atractylenolide III, β-eudesmol and hinesol	33
2.15 Schematic overview of molecular pathway leading to apoptosis	37

5.1 Chemical structure of atractylodin and effect of atractylodin treatment on cholangiocarcinoma and OUMS cell culture morphology	56
5.2 Effect of atractylodin on nuclear morphology of cholangiocarcinoma cells	57
5.3 Effect of atractylodin on colony forming ability of cholangiocarcinoma cells	58
5.4 Effect of atractylodin on wound healing ability of cholangiocarcinoma cells	60
5.5 Effect of nifuroxazide on wound healing ability of cholangiocarcinoma cells	61
5.6 Inhibitory effect of atractylodin on HO-1 expression in cholangiocarcinoma cells	63
5.7 Inhibitory effect of atractylodin on NQO1 expression in cholangiocarcinoma cells	64
5.8 Evaluation of cytokine-induced STAT1/3 activation in cholangiocarcinoma cells	66
5.9 Effect of atractylodin on cytokine-induced STAT1/3 activation in cholangiocarcinoma cells	67
5.10 Effect of nifuroxazide on cytokine-induced STAT1/3 activation in cholangiocarcinoma cells	69
5.11 Effect of atractylodin on aggregate expression of major NF- $\kappa$ B proteins in cholangiocarcinoma cells	71
5.12 Effect of atractylodin on aggregate expression of major NF- $\kappa$ B proteins in cytokine stimulated cholangiocarcinoma cells	72
5.13 Effect of cytokine stimulation on I $\kappa$ B $\alpha$ degradation in cholangiocarcinoma cells	74
5.14 Effect of atractylodin on I $\kappa$ B $\alpha$ degradation in cytokine stimulated cholangiocarcinoma cells	75
5.15 Effect of MG132 on I $\kappa$ B $\alpha$ degradation in cytokine stimulated cholangiocarcinoma cells	77
5.16 Effect of atractylodin on ICAM-1 and iNOS mRNA expression in cytokine stimulated cholangiocarcinoma cells	79

5.17 Effect of nifuroxazide on ICAM-1 and iNOS mRNA expression in cytokine stimulated cholangiocarcinoma cells	80
5.18 Effect of atractylodin on mRNA expression of tumor associated genes in cholangiocarcinoma cells	81
5.19 Chemical structure of $\beta$ -eudesmol and the effect of $\beta$ -eudesmol on culture morphology of cholangiocarcinoma and OUMS cells	85
5.20 Effect of $\beta$ -eudesmol on nuclear morphology of cholangiocarcinoma cells	86
5.21 Effect of $\beta$ -eudesmol on colony forming ability of cholangiocarcinoma cells	88
5.22 Effect of nifuroxazide and 5-flurouracil on colony forming ability of cholangiocarcinoma cells	89
5.23 Effect of $\beta$ -eudesmol on wound healing ability of cholangiocarcinoma cells	91
5.24 Effect of $\beta$ -eudesmol on HO-1 expression in cholangiocarcinoma cells	93
5.25 Effect of $\beta$ -eudesmol on NQO1 expression in cholangiocarcinoma cells	94
5.26 Effect of $\beta$ -eudesmol on cytokine-induced STAT1/3 activation cholangiocarcinoma cells	96
5.27 Effect of $\beta$ -eudesmol on aggregate expression of major NF- $\kappa$ B protein in cholangiocarcinoma cells	98
5.28 Effect of $\beta$ -eudesmol on aggregate expression of major NF- $\kappa$ B proteins in cytokine stimulated cholangiocarcinoma cells	99
5.29 Effect of $\beta$ -eudesmol on cytokine-stimulated degradation of I $\kappa$ B $\alpha$ in cholangiocarcinoma cells	101
5.30 Effect of $\beta$ -eudesmol on ICAM-1 and iNOS mRNA expression in cytokine stimulated cholangiocarcinoma cells	103
5.31 Effect of $\beta$ -eudesmol on mRNA expression of tumor-associated genes in cholangiopcarcinoma cells	105

5.32 Effect of SnCl <sub>2</sub> on colony forming ability of β-eudesmol-treated cholangiocarcinoma cells	107
5.33 Effect of SnCl <sub>2</sub> on wound healing ability of β-eudesmol-treated cholangiocarcinoma cells	108
5.34 Effect of SnCl <sub>2</sub> on expression of HO-1 in cholangiocarcinoma cells	110
5.35 Time-dependent expression of HO-1 in β-eudesmol-treated cholangiocarcinoma cells	111
5.36 Effect of SnCl <sub>2</sub> treatment on HO-1 expression in β-eudesmol-treated cholangiocarcinoma cells	112
5.37 Effect of SnCl <sub>2</sub> on nuclear morphology of β-eudesmol-treated cholangiocarcinoma cells	113
5.38 Effect of SnCl <sub>2</sub> on β-eudesmol-induced cell death of cholangiocarcinoma cells	115
5.39 Effect of SnCl <sub>2</sub> on HO-1 mRNA expression in β-eudesmol-treated cholangiocarcinoma cells	116
5.40 Effect of Zinc protoporphyrin IX on viability of cholangiocarcinoma cells	117
5.41 Effect of Zinc protoporphyrin IX on HO-1 expression in cholangiocarcinoma cells	119
5.42 Effect of Zinc protoporphyrin IX on HO-1 mRNA expression in cholangiocarcinoma cells	120
5.43 Effect of β-eudesmol and nifuroxazide on nuclear morphology of cytokine stimulated cholangiocarcinoma cells	121
5.44 Summary of the effect of atractylodin and β-eudesmol on colony forming ability of cholangiocarcinoma cells	123
5.45 Summary of the effect of atractylodin and β-eudesmol on wound healing ability of cholangiocarcinoma cells	124
5.46 Summary of the effect of atractylodin and β-eudesmol on heme oxygenase-1 expression in cholangiocarcinoma cells	127

5.47 Summary of the effect of atraction and $\beta$ -eudesmol on NQO1 expression in cholangiocarcinoma cells	126
5.48 Summary of the effect of atraction and $\beta$ -eudesmol on STAT1 and STAT3 activation in cholangiocarcinoma cells	129
5.49 Summary of the effect of atraction and $\beta$ -eudesmol on major NF- $\kappa$ B protein expression in cholangiocarcinoma cells	130
5.50 Summary of the effect of atraction and $\beta$ -eudesmol on major NF- $\kappa$ B protein expression in cholangiocarcinoma cells	132
5.51 Summary of the effect of atraction and $\beta$ -eudesmol on I $\kappa$ B $\alpha$ degradation in cytokine stimulated cholangiocarcinoma cells	133
5.52 Summary of the effect of atraction and $\beta$ -eudesmol on relative mRNA expression of major tumor associated genes expression in cholangiocarcinoma cells	135
5.54 Summary of the effect of atraction and $\beta$ -eudesmol on relative mRNA expression of major tumor associated genes expression in cholangiocarcinoma cells	136

## LIST OF ABBREVIATIONS

Symbols/Abbreviations	Terms
5-FU	5- flurouracil
ANOVA	One-way analysis of variance
ARE	Anti-oxidant response element
ATRIII	Atractylenolide III
CA19-9	Carbohydrate antigen 19-9
CCA	Cholangiocarcinoma
cDNA	Complementary DNA
CHIP	Chromatin immune precipitation
CK	Cytokeratins
CK-19	Cytokeratin-19
COX-2	Cyclooxygenase-2
CT scan	Computerized tomography scan
DAPI	4',6-diamidino-2-phenylindole
dCCA	distal cholangiocarcinoma
DMSO	Dimethyl sulfoxide
EGFR	Epidermal growth factor receptor
ELISA	Enzyme linked immune sorbent assay
EMSA	Electro mobility shift assay
FISH	Fluorescence <i>in situ</i> hybridization
GAPDH	Glyceraldehydes 3-phosphate dehydrogenase

HDAC	Histone deacetylase
HCC	Hepatocellular carcinoma
HDGF	Hepatoma-derived growth factor
HO-1	Hemo oxygenase -1
iCCA	intrahepatic cholangiocarcinoma
IKK	I $\kappa$ B kinase
IL-6	Interleukin-6
IFN- $\gamma$	Interferon- $\gamma$
ICAM-1	Intercellular adhesion molecule 1
iNOS	Inducible nitric oxide synthase
I $\kappa$ B	Inhibitory of kappa-B
JAK-STAT	Janus kinase/signal transducers and activators
MAPK	Mitogen-activated protein kinase
MMP	Matrix metalloproteinases
MS-PCR	Methylation specific- polymerase chain reaction
MTT	3-(4,5-Dimethylthiazol-2-yl)-2,5-Diphenyltetrazolium Br
NF- $\kappa$ B	Nuclear Factor-Kappa B
NO	Nitric oxide
NQO1	NAD(P)H-quinone oxidoreductase of transcription
NRF2	NFE2L2 nuclear factor, erythroid 2 like 2
pCCA	Perihilar cholangiocarcinoma
PSC	Primary sclerosing cholangitis



SSP411	Spermatogenesis associated 20
TGF	Tumor growth factor
TNF	Tumor necrosis factor
VEGF	Vascular endothelial growth factor
WHO	World health organization
ZN(II)PPIX	Protoporphyrin IX zinc(II)



## CHAPTER 1

### INTRODUCTION

#### 1.1 Introduction

Cholangiocarcinoma (CCA) is basically the cancer originating from malignant transformation of epithelial cells lining the hepatic biliary tree which commonly involves cholangiocytes. CCA has been accounted for almost 15% of all hepatobiliary-related malignancies. The cancer is fairly complicated to diagnose during early stages and is known to exhibit dismal prognosis. Second to the hepatic cancer, CCA is becoming increasingly common form of liver-associated cancer with rising incidence worldwide. CCA has high fatality rate with less than 5% of those the acquiring advanced stages of the cancer live on up to five years (1, 2). CCA is a multifactorial disease of which its pathogenesis remains unclear. Primary sclerosing cholangitis (PSC), congenital intrahepatic biliary stones, fibropolycystic hepatic disease, cirrhosis, viral hepatitis, and liver fluke infection are considered high risk factors for CCA. CCA is progressively fatal unless the malignant tumor is resected during early stages of the disease. However, absence of early and specific diagnostic methods and lack of effective therapeutic agents are major bottlenecks facing the treatment of CCA (3). Recently, there has been a stark rise in studies related to CCA and much effort has also been put on to investigate the immunology associated with this cancer for establishment of the links between CCA and host immunity (4). In this context, the growing occurrences of CCA and lack of proper medication strategies has created a pressing demand for more research and development of drugs for effective chemotherapeutic interventions against CCA (5). In addition, genesis and metastasis of CCA implicates multifaceted molecular events which have not been clearly described and thus demands more experimental data for better understanding the significance of such pathways in preventing disease progression.

In this research, cytotoxicity and underlying molecular objectives of the two purified bioactive compounds evidently found in *Atractylodes lancea* (Thumb.) DC., namely atractylodin and  $\beta$ -eudesmol have been investigated utilizing suitable *in vitro* experimental fashions for CCA. Implementation of plant extracts and isolates has remained the predominant aid for drug development. The flora belonging to genus *Atractylodes* have been shown to include several bioactive additives with medicinal values. The results of these plant-derived bioactive compounds on vital signaling pathways related to cellular survival, proliferation and oncogenesis had been investigated. Likewise, the proteins and related pathways liable for anti-oxidative and cytoprotective effects of both compounds had been investigated. In addition, the consequences of those compounds had been examined based mainly on expression or activation of genes associated with cell proliferation and tumorigenesis. Universal, results obtained from the systematic and in-intensity molecular studies could be beneficial to generate crucial records to beautify our modern knowledge of the disorder therefore allowing the capability drug discovery and development for CCA.

## 1.2 Significance of research

CCA is a progressively lethal form of biliary track cancer with very limited and rather inefficient options for therapeutic interventions. In general, the overall significance of the research includes identification of candidate compounds that may hold therapeutic potentials against CCA. In particular, this study focused on *in vitro* analysis which included cytotoxicity and underlying molecular targets of action of atractylodin and  $\beta$ -eudesmol on human CCA-associated cell lines. This would certainly helps generate significant insights on the oncology behind CCA and may assisted in identifying potential molecular targets to devise effective strategy for future drug development against CCA using these compounds.

The research group was led by our academic institution comprising well-experienced faculty in molecular biology, pharmacology, and oncology that are required for comprehensive and efficient research on cell culture, cancer biology, immunological assays, molecular biology and biochemical analysis. The direct benefit of the research would be the expansion of our knowledge regarding current understanding of CCA-associated molecular pathways and the mechanism by which investigational anti-cancer compounds may prevent the cancer progression. Lastly, the research with a significant outcome will personally benefit me as a Ph.D. scholar by enabling me to fulfill my partial requirement criteria for completion of doctoral degree dissertation in Bioclinical Sciences under the rules and regulations of Thammasat University.

## CHAPTER 2

### REVIEW OF LITERATURE

#### 2.1 Background information

Cancer is considered as second most leading cause of death worldwide. Both modern and enthnotraditionally used medicines to treat or alleviate several types of cancer are derived from natural plant products. Throughout the recorded history of medicine, plant products have been shown to be valuable sources of novel anti-cancer drug. Natural anti-cancer properties of such floral resources also forms the foundation for modern pharmaceuticals. However still merely 10-15% of the approximately 250,000 higher plants have ever been studied for bioactive compounds (6). Some important benefit of using plant-derived drugs is their natural origins which seems to favor the human body with none or few side-effects and also the efficacy of the crude-form of the drugs through existing ethnopharmacological knowledge. CCA is a progressively fatal adenocarcinoma of bile duct that shows very less response to traditionally used anti-cancer drugs including 5-FU (7). Thus, search and discovery of new plant-derived bioactive compounds with significant growth inhibitory effect on CCA seems to be an urgent requirement of today. In this literature review we briefly summarize the overall importance of ethnopharamcology in cancer research. We also review the current known use of plant-derived drugs against CCA. Similarly, we will briefly discuss on both *in vivo* and *in vitro* study models used to study this cancer.

## 2.2 Epidemiology of cholangiocarcinoma

CCA is a progressively fatal and rare form of adenocarcinoma which generally originates from the epithelial cells covering the biliary channel which normally involves cholangiocytes. It is the probably the most common primary form of liver-associated neoplasm following hepatocellular carcinoma (HCC) that represents less than 5% of all gastrointestinal malignancies (8-10). It is believed that around 10-20% of hepatobiliary-related deaths are due to CCA (10, 11). The CCA is eventually lethal with 95% mortality rates for patients bearing advance stages of the cancer for around five years (1, 2). Lack of CCA-specific diagnosis procedure and complexity surrounding the nature of this disease makes it difficult to timely diagnose and apply surgical intervention (3). The incidence of CCA-associated cases in United States of America is one or two per million which is equivalent to 3,500 new cases annually (12). Incidents of CCA is recorded to be highest in parts of Asia namely Laos and Northeastern Thailand (13). A study indicated highest recorded worldwide incident of CCA (Figure 2.1) in Northeastern Thailand in the period between 1977 and 2007 (14). Epidemiological data based on gender as reported by a different survey suggests that the cases of CCA are comparatively more in men belonging to age group 60-70 as relative to the women of identical age group (11). However, it is arguable that the observed incidents of the disease is simply due to real increase in CCA cases or advancement in diagnosis techniques for CCA. Likely, recently published study regarding the prevalence of *Opisthorchis viverrini* infection and CCA incident within Thailand (Figure 2.2) suggest that the *O. viverrini* is a high risk factor for the development of this cancer. In addition, the high incident of CCA in *O. viverrini* risk areas are also the regions with prevalence of its intermediate host, a snail belong to the genus *Bithynia* (15).

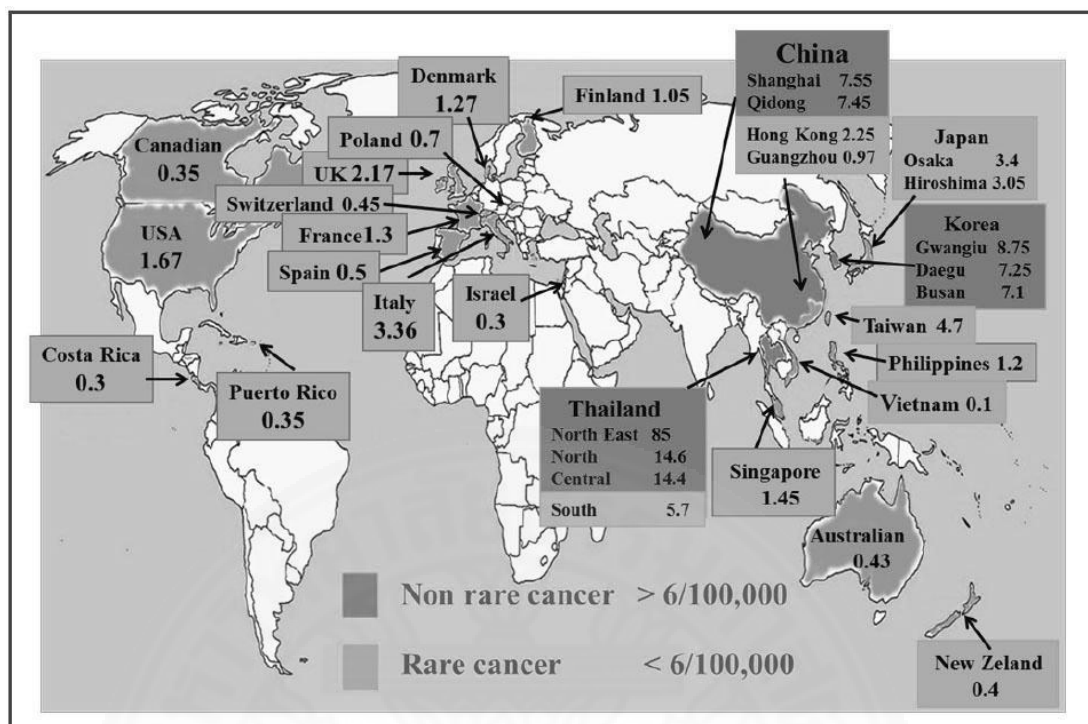


**Figure 2.1** Worldwide incidence of cholangiocarcinoma. The data reflecting occurrence of cholangiocarcinoma for period of 1977 to 2007 (14).

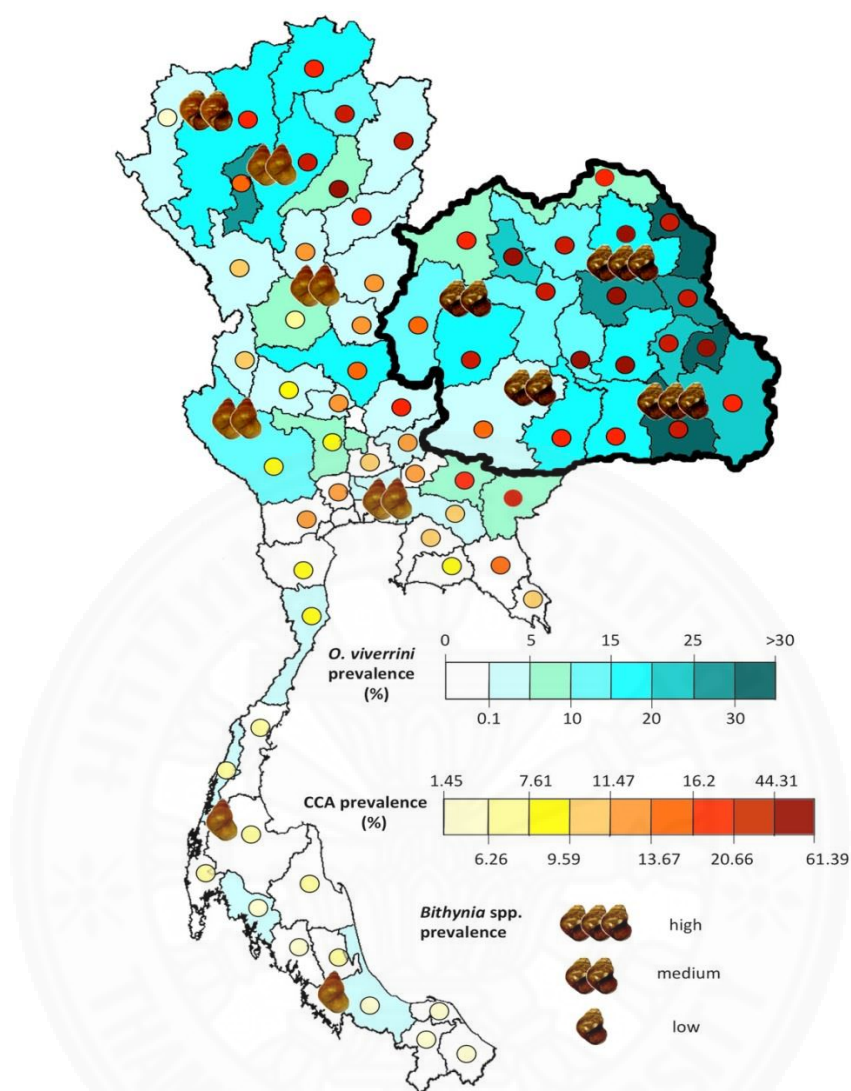


**Figure 2.2** Distribution and prevalence of *Opisthorchis viverrini* infection and cholangiocarcinoma incident in Thailand (15).



### 2.3 Anatomical classification of cholangiocarcinoma

Anatomically the CCA can be characterized as perihilar CCA (pCCA), distal CCA (dCCA), and intrahepatic CCA (iCCA) based on the site of the malignant tumor (Marrero, 2014). The pCCAs can develop from areas within the secondary bile ducts and sections above the position of origins of cystic ducts. The dCCA can arise from sites located between hepatopancreatic ampulla and cystic duct origins. The iCCA can be classifiable as the adenocarcinoma originating from intrahepatic bile duct which then spreads all the way through biliary tract and may also generate intrahepatic lesions (Figure 2.3). The terms dCCA and pCCA are often literally denoted as extrahepatic CCA (4).

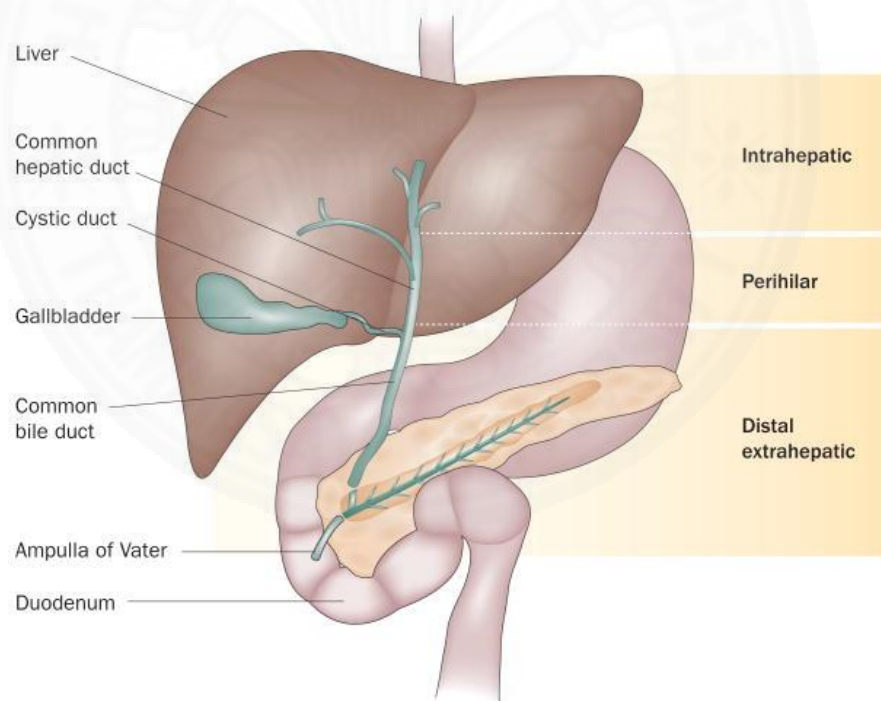


**Figure 2.3** Anatomical classification of cholangiocarcinoma (3).

## 2.4 Risk factors relating to cholangiocarcinoma

The genesis of CCA in majority of cases are of unknown etiology. Nonetheless, several risk factors have been established that are linked to increased incidents of CCA. The factors including congenital fibropolycystic hepatic disease, PSC, intrahepatic biliary stones, liver fluke infection, cirrhosis and viral Hepatitis are considered as risk factors related to development of CCA. Specifically, apart from parasite infection of bile duct, the PSC is thought to be a prevalent risk factors predisposition towards getting CCA with lifetime prevalency around 10% among PSC patients (16). Likely, the infection of liver by hepatic flukes, particularly, *Opisthorchis viverrini* and *Clonorchis sinensis* due to consumption of raw and undercooked fish is common in Southeast Asia. Particularly, *O. viverrini* is considered as a major risk for CCA development as regions with high incidents of its CCA are the often the same region endemic to *O. viverrini* infection in Thailand. These conditions are seen as high risk factors for CCA as these parasites accumulate mainly in the bile duct of the hosts causing chronic inflammation leading to cancer (17). Similarly, long-term exposure to nitrosamines, dioxin, and nitroxyl group containing chemicals are also suggested to be a considerable risk factors for the cancer (4, 18).

## 2.5 Pathogenesis of cholangiocarcinoma

The cytological events leading to genesis of CCA is barely understood but are known to be significantly influenced by chronic biliary inflammation (cholangitis), associated with bile flow obstruction (cholestasis). The chronic inflammation conditions along with the risk factors considerably amplifies the susceptibility towards growth of CCA. Furthermore, these inflammatory conditions may stimulate irregular and abnormal cell growth that can undermine activities of DNA mismatch repair genes/proteins and promote variations in the regulation of tumor suppressor genes and proto-oncogenes. It has been know that CCA cells have highly up-regulated MAPK

activities and are known to activate anti-apoptotic protein of the BCL-2 family, which promotes CCA cell survival. The cell survival pathways and tumor-associated proteins such as Janus kinase/signal transducers and activators of transcription (JAK/STAT) pathway and tumor growth factors (TGFs) are also suggested to abnormally up-regulated in CCA-linked cell lines respectively (19). Basically, the JAK-STAT signaling cascade is triggered by binding of the JAK-STAT receptors with cytokine ligand which causes receptor phosphorylation and activation of STAT transcriptional factors that regulate expression of several genes (Figure 2.4). There are some known inhibitors of the pathways including the chemicals such as nifuroxazide and 5,15-DPP that are known to block STAT and taken as positive controls in experiments involving inhibition of JAK-STAT signaling cascade (20).

A brief schematic overview (Figure 2.5) of the involvement of a prominent member of JAK-STAT pathway, namely STAT3 involves implication of this transcriptional factor activation and its interaction with multiple signaling pathways to induce cell survival and proliferation (21). Aberrant STAT3 activation can result in induction of anti-apoptotic genes such as BCL2, c-Myc and BCL-XL promoting persistent growth. Likely, the STAT3 activation can also result in increased expression of angiogenesis promoting factors such as VEGF and MMPs. The cross-talk between STAT3 and NF- $\kappa$ B are known to promote cell proliferation and abrogate apoptosis. Recently, IL6/STAT are also appearing to be involved in maintenance of cancer stem cells. In addition, the aberrant activation of glycoprotein coupled receptors (GPCR) and receptor tyrosine kinase (RTK) are also suggested to promote abnormal upregulation of JAK-STAT pathway leading to malignant transformation of cells.

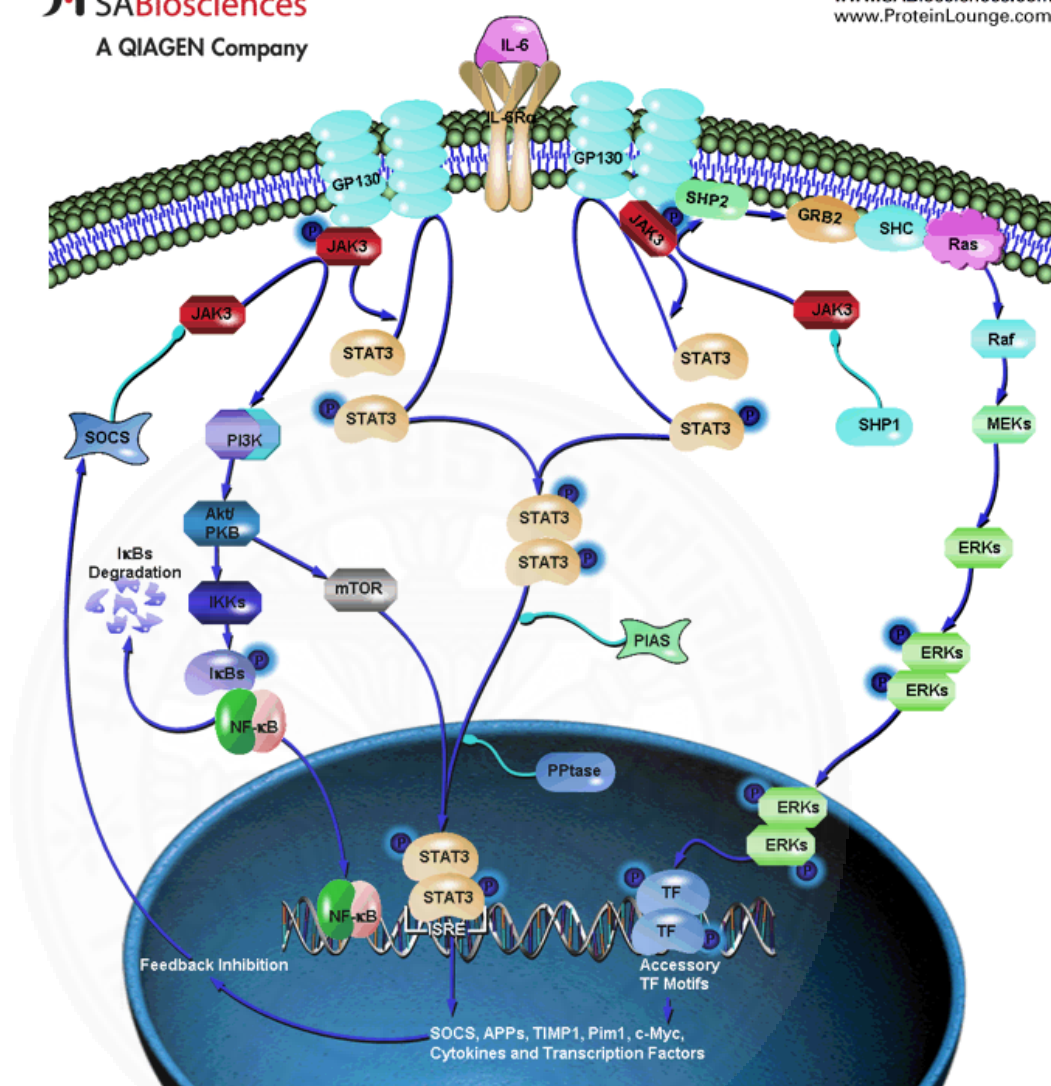


**Figure 2.4** Schematic overview of JAK-STAT pathway in cell survival and proliferation (Quagens© 2017).

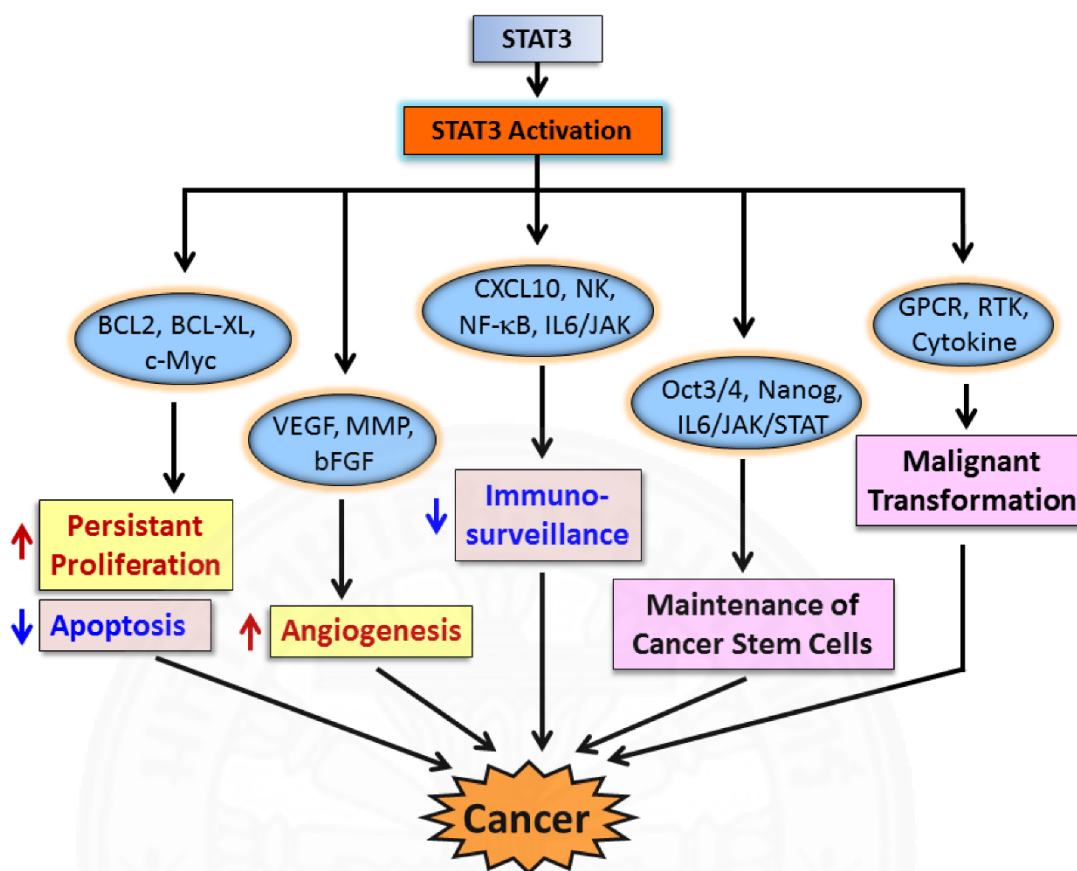


**Figure 2.5** Schematics of mechanism for involvement of STAT3 in cancer

Similar, critical  $\kappa$ B transcriptional factor-dependent signaling cascade, namely, nuclear factor-kappaB (NF- $\kappa$ B) pathway which are central to cell proliferation and inflammation (Figure 2.6), are abnormally altered in CCA promoting tumorigenesis (22). These NF- $\kappa$ B family of transcriptional factor proteins include homo- or hetero-dimer of transcriptional factor proteins such as p50, p52, p65, c-Rel and RelB which are regulated by a class of inhibitory of kappa-B (I $\kappa$ B) and I $\kappa$ B kinase (IKK) proteins (23). There are several known inhibitors of the NF- $\kappa$ B pathways including 2-[6-(4-Chlorophenoxy)hexyl]-1-cyano-3-pyridin-4-ylguanidine and Gliotoxin that are known to block NF- $\kappa$ B activity and are often taken as positive controls in experiments involving inhibition of NF- $\kappa$ B signaling cascade (24).



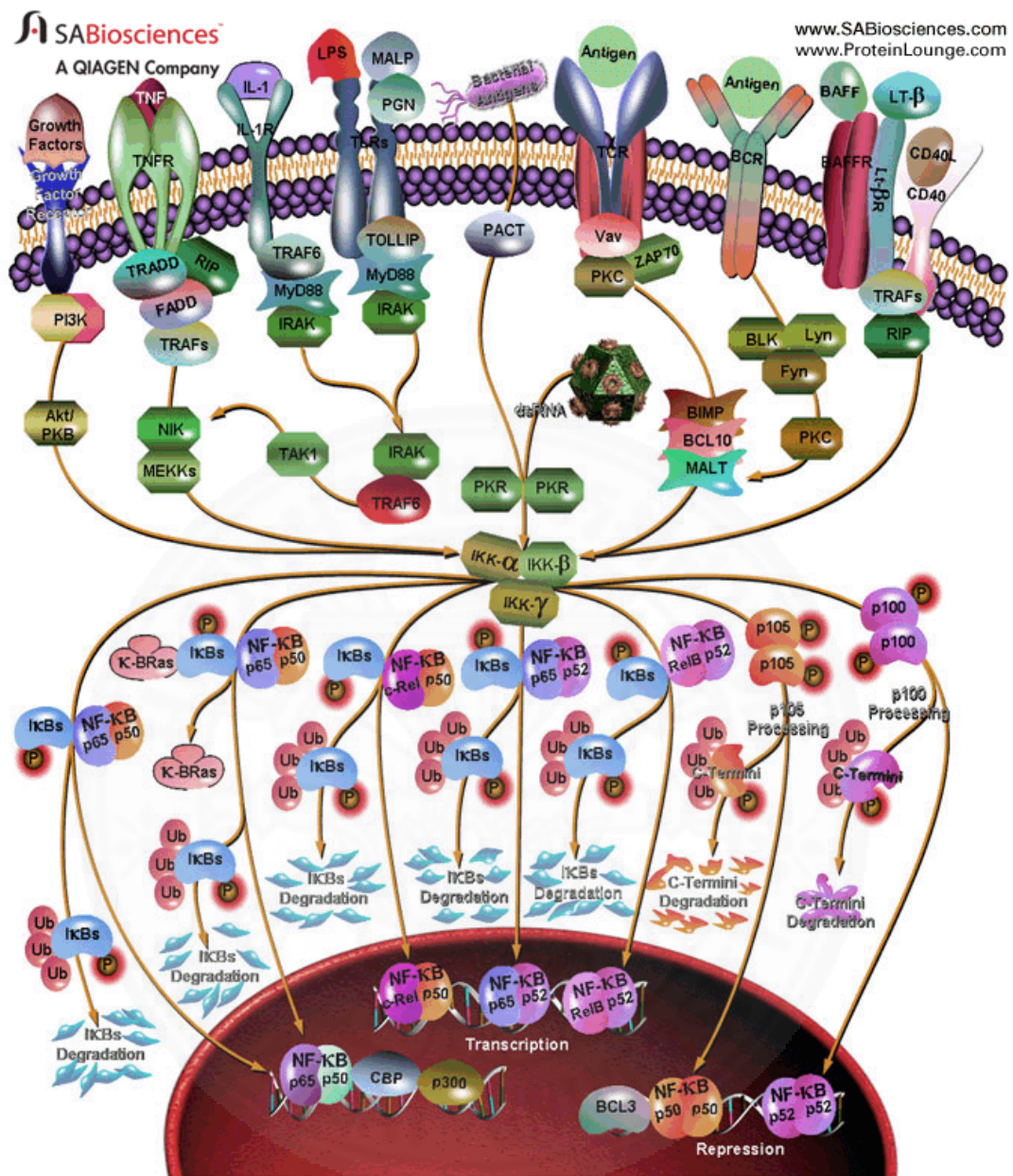


**Figure 2.6** Schematic overview of the NF-KappaB family pathway (Qiagen© 2017).

In a brief overview, the role of NF- $\kappa$ B pathways in cancer can be summarized by the following flow chart (Figure 2.7). The complex nature and diversity of NF- $\kappa$ B transcription factors makes it interact with various signaling modules and has wide range of functionality to assist cell survival and proliferation. The NF- $\kappa$ B pathways can interact with pathways enhancement for telomerase regeneration to promote immortality. NF- $\kappa$ B such as P65 can induce production of TNFs and IL-1 induces chronic inflammation that are known to assist cellular transformation. Activation of NF- $\kappa$ B pathways has direct influence on production of angiogenic growth factors such as VEGF and IL-8 that can promote blood vessels formation for tumor growth. Likely, the MCL-1, ICAM-1 and VCAM-1 are known promoters of metastasis in various cancers and are under significant influence of NF- $\kappa$ B activation. Likely, influence of NF- $\kappa$ B pathways on iNOS, COX2, cyclins and Bcl proteins production collectively indicates widespread involvement of of NF- $\kappa$ B transcription factors in cancer cell survival and proliferation.

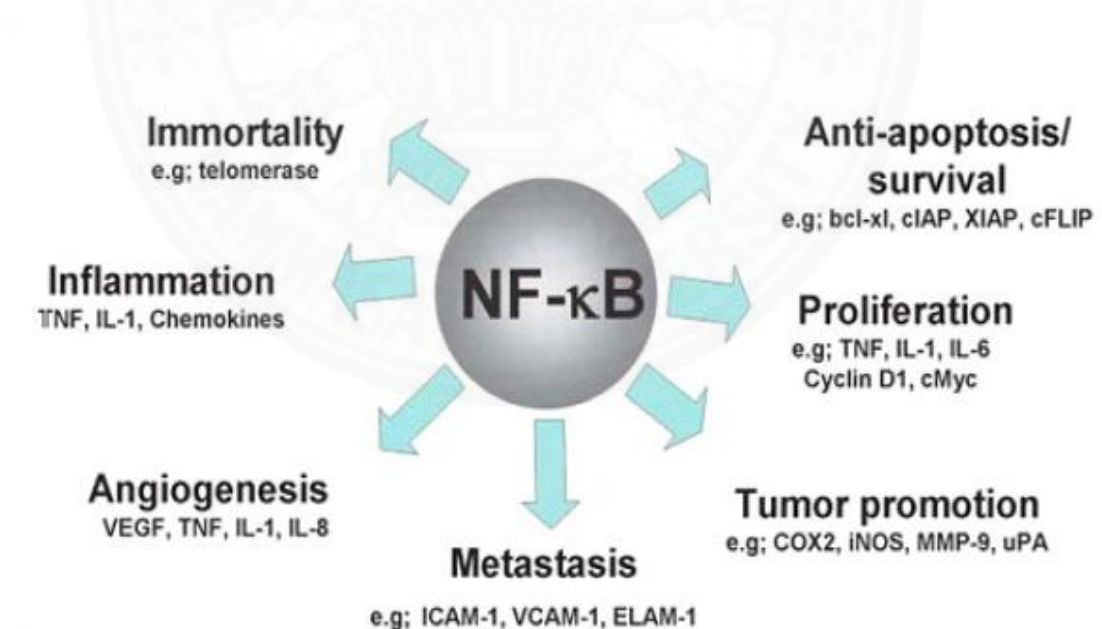


**Figure 2.7** Schametic overview of the involvement of NF- $\kappa$ B in cancer

Likely the CCA-associated cells have enhanced secretion of matrix metalloproteinases (MMP) which assists metastasis of these cancer cells. Similarly the production of cyclooxygenase-2 (COX-2), nitric oxide (NO) produced by inducible nitric oxide synthase (iNOS), and epidermal growth factor receptor (EGFR) are also enhanced significantly. Pro-inflammatory cytokine interleukin (IL-6), is also reported to play crucial role in CCA. The chronic inflammatory environment in bile duct or the CCA cells itself are known to maintain elevated levels of IL-6 that in turn promote the survival and other oncological aspects of cholangiocarcinogenic process (25-27). These effector proteins are generally under the control of major signaling module including NF- $\kappa$ B and JAK-STAT signaling pathways. Thus, study of these pathways in CCA research is crucial for generating effective therapeutic drugs.

The Figure 2.8 summarizes typical series of events that can lead to development of cholangiocarcinoma. Genesis of CCA involves several complex steps with multiple different factors forcing chronic stress on hepatic biliary cholangiocytes. The external and internal cellular stress often appears as chronic hepatobiliary inflammation with involvement of critical mediators of inflammation such as IL-6 and NF- $\kappa$ B. The CCA-associated risk factors may include exogenous certain liver-fluke infection, nitrosamine, viral hepatitis and *H. pylori* infection. Similarly, the reactive free radicles and oxidizing species can cause substantial damage to genomic DNA and enhance genetic susceptibility to oncogenic mutations that can ultimately result in malignant transformation of cholangiocytes.



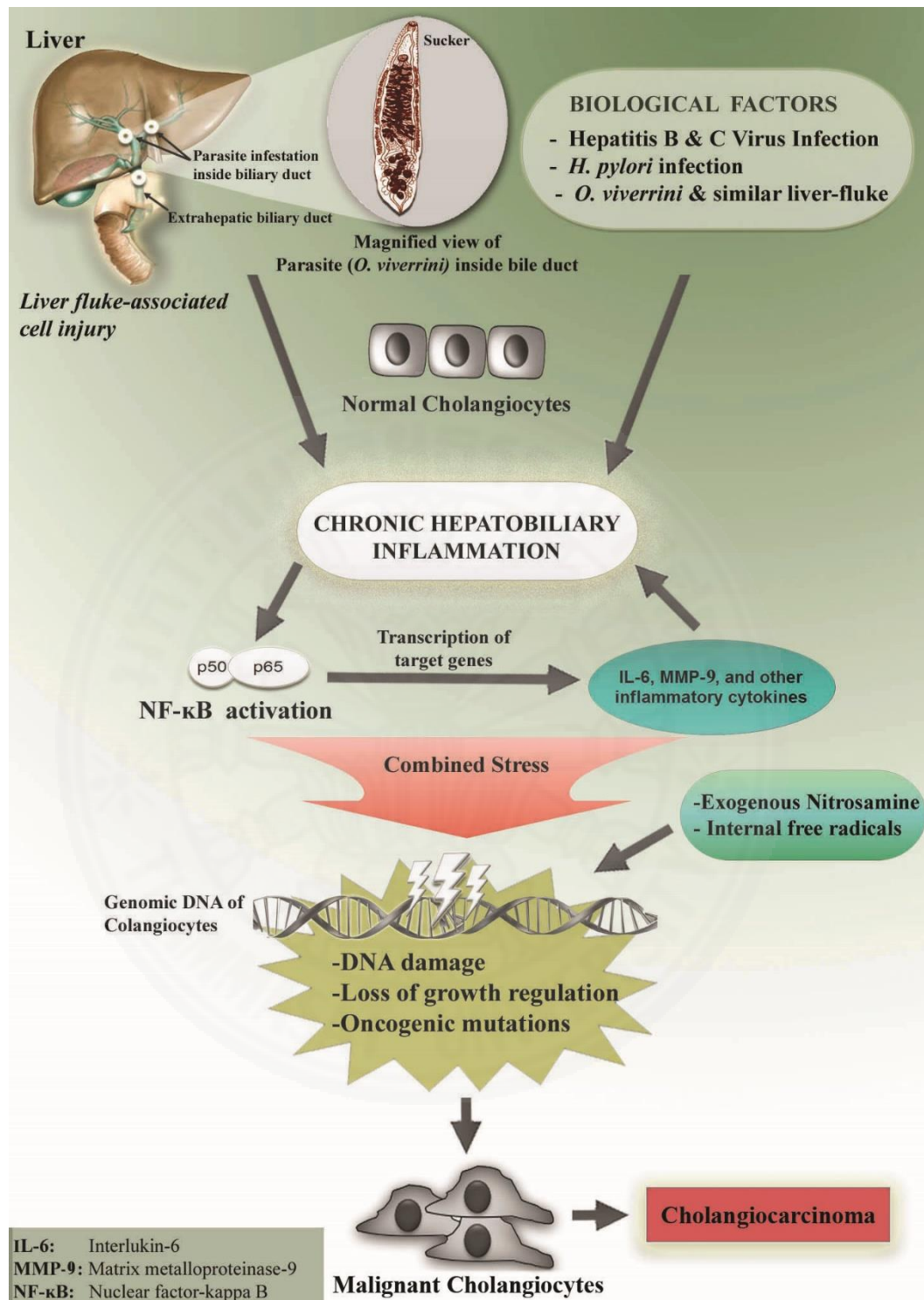


**Figure 2.8** Schematic overview of multiple factors potentially resulting in genesis of cholangiocarcinoma (28)

## 2.6 Role of cytoprotective enzymes in malignancy and drug resistance

Alterations in expression of ROS neutralizing enzymes are often linked to changes in tumor sensitivity to chemotherapeutic drugs. The enzymes NAD(P)H: Quinone oxidoreductase (NQO1) is an oxidoreductase enzyme regulated by the Keap1/Nrf2/ARE pathway and play key role in ubiquinone and vitamin E quinone metabolism(29). Heme oxygenase -1 (HO-1) is another enzyme involved in rate-limiting reaction of heme catabolism. Both of these enzymes are majorly under the influence of Keap1/Nrf2/Anti-oxidant responsive element (ARE) pathway and are expressed as a part of ARE-associated proteins (30, 31). These ARE-associated enzymes function as cytoprotective enzymes and are found to assist survival of cancer cells by abrogating the ROS-dependent cellular stress (Figure 2.9).

Previous literatures have suggested that altered expression of NQO1 and HO-1 have been correlated with CCA, thus making it a significant target for chemotherapeutics (29, 32). A study suggests that anti-cancer drugs such as menadione and  $\beta$ -lapachone used against breast cancer can have their sensitivity significantly depleted on patients with altered genomics and unregulated levels of NQO1 at transcriptome levels(33). Similarly, reports have indicated the Nrf2 and HO-1 forms an axis for cancer cell cancer growth and chemoresistance that strongly correlates with tumour progression, aggressiveness, resistance to therapy, and poor prognosis in patients with breast cancer and leukemia (34). The aberrant unregulated expression of HO-1 has been reported to exert anti-apoptotic effects on acute myeloid leukemia (AML) cells which probably suppresses P53 activity or neutralizes ROS to abrogate cell death (35). Some known inhibitors of the pathways including the chemicals such as (-)-Schisandrin B and that are known to block Nrf2 and taken as positive controls in experiments involving inhibition of Keap1/Nrf2/ARE signaling cascade (36).

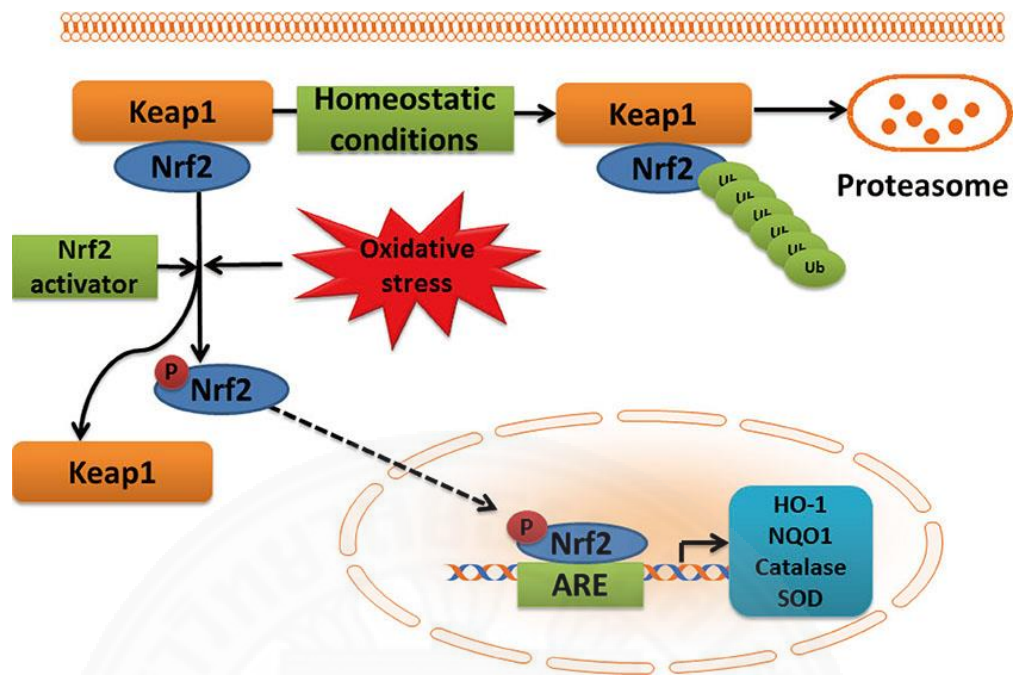


**Figure 2.9** Up-regulation of expression of NQO1 and HO-1 regulated by Keap1/Nrf2/ARE pathway (30)

Involvement of HO-1 in cancer progression *via* assisting lung metastasis has been reported in recent research (Figure 2.10) involving cancer progression of human fibrosarcoma cells (37). In brief, upon loss of attachment during metastatic progression, the activating transcription factor 4 (ATF4) were able to induce HO-1 *via* transcription factor Nrf2. Coordination with the cytoprotective enzymes protected malignantly transformed cells against apoptosis following matrix detachment and also promoted tumor metastatic activity.

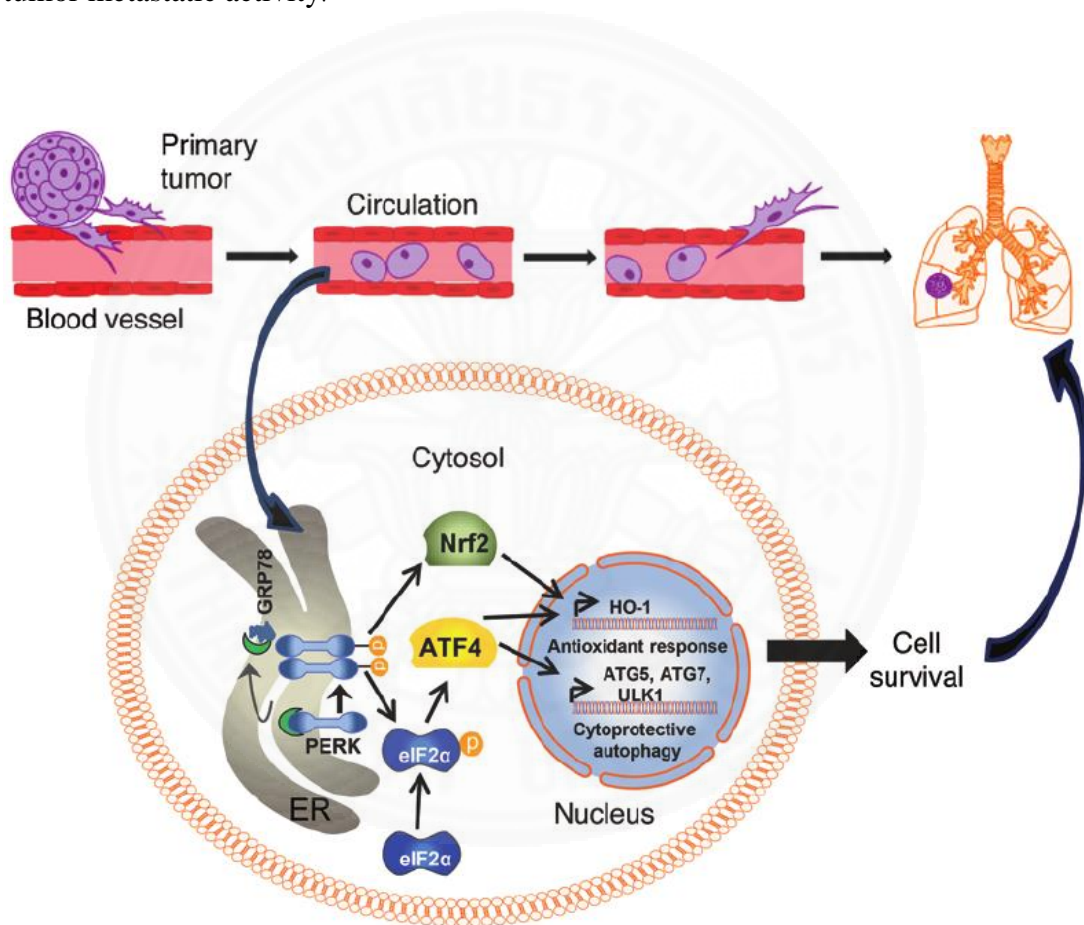


**Figure 2.10** Involvement of heme oxygenase -1 in lungs cancer metastasis (37)

The NQO1 are reported to be starkly elevated in solid tumors. Recently published study (Figure 2.11) indicates that cytoprotective enzyme NQO1 has been reported to assist metastatic activity during epithelial-to-mesenchymal transition in breast cancer cell lines (38). The metastatic activity was decreased by implementation of investigational compound  $\beta$ -lapachone which potentially inhibited NQO1 expression and Akt/mTOR pathway. Thus, this example indicates active role of NQO1 in cancer progression

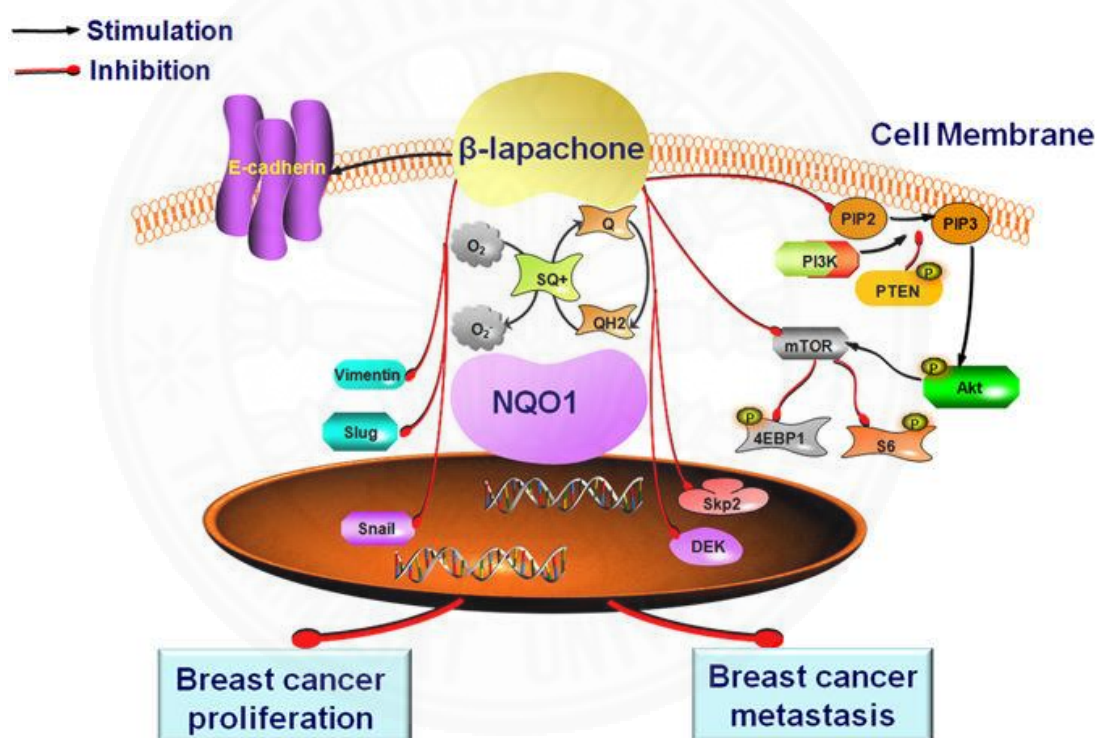


**Figure 2.11** Involvement of NAD(P)H quinone dehydrogenase 1 in breast cancer metastasis (38)



Taken together, the tumorigenesis of CCA is known to involve altered expression of cytoprotective enzymes such as NQO1 and HO-1 and abnormally up-regulated critical molecular signaling cascade including JAK-STAT and NF- $\kappa$ B pathways that are central to proliferation, metastasis, angiogenesis and inhibition of apoptosis of these cancerous cells (39, 40). The exploration of chemical compounds that can selectively inhibit these pathways may have significant inhibitory effect on survival, growth and proliferation of the cancer cells. The pathways and their terminal gene products including the enzymatic activities of such genes play vital role in assisting tumorigenesis. In this context, the growth inducing activities of secretory proteins and cytokines such as interleukins, tumor growth factors and enzymatic activities of enzymes such as NQO1 should also be investigated. On doing so, it will help achieve understanding of the full insights of the signaling cascade and possible targets for the inhibition of selective pathways. The commercial availability of selective pathway inhibitors such as (-)-Schisandrin B, gliotoxin, and nifuroxazide for Keap/Nrf2/ARE, NF- $\kappa$ B, and JAK-STAT pathway respectively, provides us with precise analysis of the selected signaling module with test compounds along with these inhibitors as positive control. Thus, analysis of signaling pathways with reference to standard positive control and investigational compounds or combination of compounds can provide in-depth effect of the test samples on the molecular signaling pathways. Hence, the data generated undoubtedly will help in understanding more about CCA.

## 2.7 Current biomarkers in cholangiocarcinoma

Diagnosis of CCA during early stage has remained fairly difficult. Cases under initial phases of this cancer are usually asymptomatic and exhibit non-specific symptoms such as cachexia, fatigue, and abdominal pain (3). The victims of CCA are often diagnosed only during late stages of the cancer where surgical options such as tumor resection is a non-viable option to treat the cancer leading to increased mortality rates (41). Lack of sensitive early diagnosis procedure and inadequate chemotherapeutic are major hurdles in preventing CCA-linked deaths. CA19-9 and carcinoembryonic antigen are few potent serum-based biomarkers which have shown encouraging results for timely diagnosis of the cancer (42, 43). Unfortunately, these markers tend to exhibit lower sensitivity and are unable to distinguish between benign and malignant form of biliary tumors (41). In this context, CA19-9 is known to have sensitivity of up to 80% in diagnosing extrahepatic CCA (44). Furthermore, for the patients with PSC, evaluation of serum CA19-9 levels and cytological assays of liver tissues were combined studied for a more selective test for development of disease (45). Likely, the cytohistological studies combined with inflorescence techniques such as fluorescence *in situ* hybridization has shown the presence of polysomy in chromosome 3 and 7 in patients with PSC presents a substantial risk for increased susceptibility to developing iCCA. In this context, recently, the fluorescence *in situ* hybridization assay is being recommended as a reliable test in predicting genetic predisposition towards CCA to PSC patients (46). The cytokeratins (CK) signifies a crucial class of proteins that assist formation of cytoskeleton of several cell types. Approximately 20 different forms of CKs are now documented and particularly the CK-19, expressed by epithelium tissues of biliary tract is known to be closely related to development of CCA (47). In addition, the CK-19 is suggested as a biomarker having specificity towards iCCA and may have tends to show utility to differentiate between iCCA from HCC (43, 48). A brief summary of the potential biomarkes for CCA research is given in Table 2.1.

**Table 2.1** Summary of potential biomarkers used in cholangiocarcinoma study (28)

Biomarkers	Description	Reference
Carbohydrate antigen 19-9 (CA19-9)	Serum marker commonly used in clinical practice	Patel et al. 2000
Carcinoembryonic antigen	Serum marker associated with hepatic cancer	Patel et al. 2000
Cytokeratin-19 (CK-19)	Protein associated with cytoskeleton	Stroescu et al. 2006
Fascin	Actin cross-linking protein monomer	Ruys et al. 2014
Hepatoma-derived growth factor (HDGF)	Factor associated with cell mobility and adhesion	Han et al. 2013
CD133 and Oct3/4	Surface receptor and transcription factor, respectively	Thana et al. 2013
Mucins	Heavily glycosylated protein produced by epithelial cells	Ruys et al. 2014
Metalloproteinase-7	Associated with breakdown of extracellular matrix and also promote metastasis of tumor cells	Lee et al. 2014
Spermatogenesis associated 20 (SSP411)	Protein found in serum and also associated with hepatic abnormalities	Shen et al. 2012



## 2.8. Epigenetic aspects of cholangiocarcinoma

Current advancement in molecular techniques have allowed study of molecular pathogenesis highlighted in terms of epigenetic alterations *via* evaluating histone deacetylation and promoter region hypermethylation. The hypermethylation of promoter regions alters and prevents corresponding gene transcription and hypomethylation can abnormally up-regulate the gene expression respectively. Thus, methylation state of proto-oncogenes can have significant effect on cell survival and tumorigenesis (49). Likely, histones are proteins that complexes with DNA to produce nucleosomes. Various post-translational modifications like acetylation, methylation, and phosphorylation of histones can have considerable effects in gene expression. Several genes associated with proliferation and tumorigenesis have shown to contain altered histone modification leading to overexpression of tumor inducer genes including those that promote cell invasion and inflammation (50). Currently, techniques such as microarray, methylation-specific PCR (MS-PCR), and chromatin immunoprecipitation (ChIP) can be applied to study these methylation and histone modifications associated with tumorigenesis.

## 2.9. Current treatment approaches for treatment of cholangiocarcinoma

Several strategies for the treatment of the CCA exist mainly based on surgical resection and combined chemo-radiotherapy. Standard anti-cancer drugs including 5-fluorouracil (5-FU) are known to be inefficient against CCA. Even the modern and more expensive anti-cancer drugs such as doxorubicin, cisplatin and gemcitabine have discouraging outcome for several cases of advance CCA. Therefore, currently available effective therapeutic strategy is mainly based on surgical removal of the tumor at early stage of CCA. The two major clinical CCA phenotypes are mass-forming intrahepatic tumors and large ductal tumors. Within the ductal CCA, liver hilum lesions are most frequent (51). The emerging tools for improved diagnosis including enhanced histological imaging, laparoscopy and computerized tomography (CT) scan are significantly diagnosis and systemic therapies for improvement in survival of CCA patients. In addition, combined chemotherapy and radiotherapy therapies are used for the treatment of the CCA but treatment outcome is less promising depending upon stage of the disease, patients history and clinical facilities.

The systematic flowchart (Figure 2.12) summarizes a current strategy for diagnosis and possible treatment of CCA using surgical intervention. Thus, in this context, in absence of a single effective therapeutic approach it becomes essential to search for reliable chemotherapeutic drugs that can timely prevent the disease and save lives. Since, Thailand is in the frontline of the CCA-associated fatalities with high recorded incidents of this cancer, it becomes contextual to focus on research and drug development to treat CCA. Taken together, identification of potential candidate compounds and detailed investigation for its specific therapeutic potential for drug development will definitely be a crucial step in CCA research.

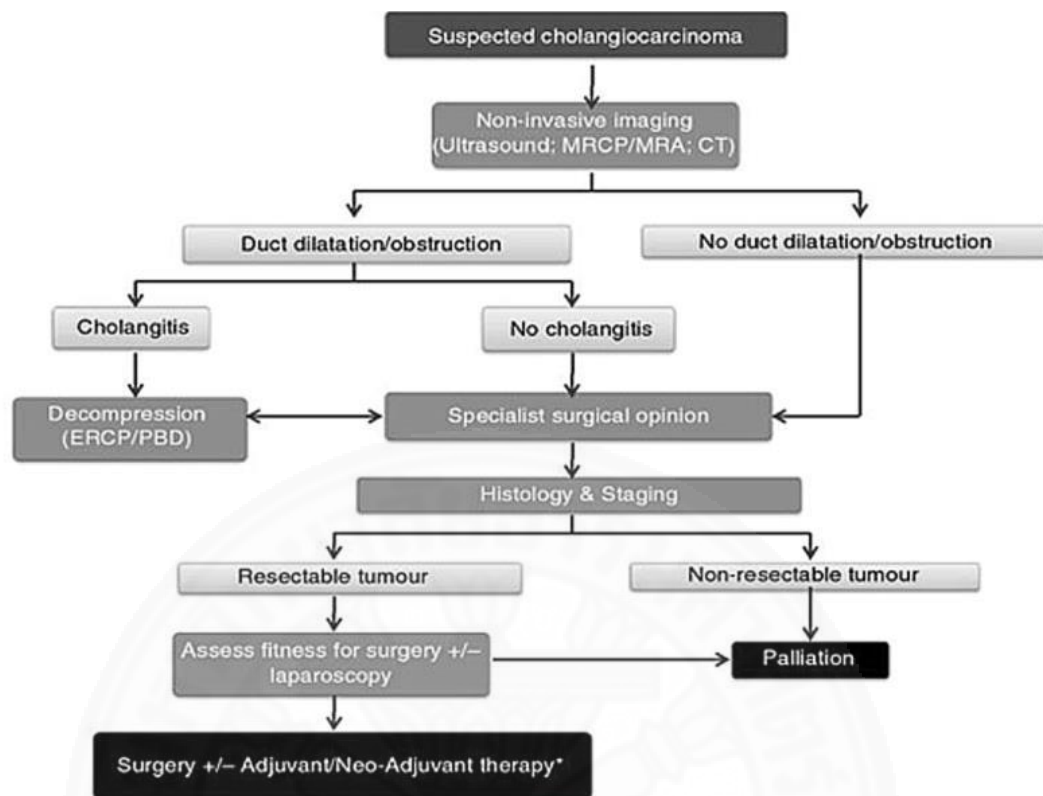


**Figure 2.12** Current strategy for diagnosis and possible treatment of cholangiocarcinoma using surgical interventions (52).

## 2.10 Conceptual framework for the choice of experimentation

In order to achieve the desired objectives of *in vitro* anti-CCA study, a number of sequential and systematic experimentation should be designed. The experiments should involve effect of treatment on both morphological observable phenotypic characteristics and mechanistic target protein and gene analysis. Hence, the set of experiments thus include studies that explore morphological, cytotoxicological, molecular studies. In brief, the experiments such as standard MTT assay provides quantitative analysis of the compound induced cytotoxicity. Similarly, the light microscopy provides morphological status of overall cell culture. The nuclear fluorescence staining helps to observe the effect of compounds on nuclear morphology for traits of apoptosis or cell death. The anti-proliferative effect is accessed through colony forming assay which is critical to study regenerative effect of cells after compound treatment under various condition. In addition, the simplistic approach to study *in vitro* cell migration is achieved through wound healing assay. In context to mechanistic study, the effect exerted by study compounds on protein expression or phosphorylation of major cell signaling mediators and enzymes is evaluated through western blotting. The target pathways include JAK-STAT 1/3 pathway, Major NF- $\kappa$ B pathway protein expression and cytoprotective enzyme including HO-1 and NRO1. Similarly, for transactional-level studies involving mRNAs, the relative expression of multiple target genes associated with these pathways will be investigated using real-time PCR. Thus, the following flowchart (Figure 2.13) provides a comprehensive summary of the conceptual framework of the studies being conducted to evaluate the anti-cancer potentials and underlying molecular mechanism of atracylodin and  $\beta$  eudesmol in cholangiocarcinoma cells.

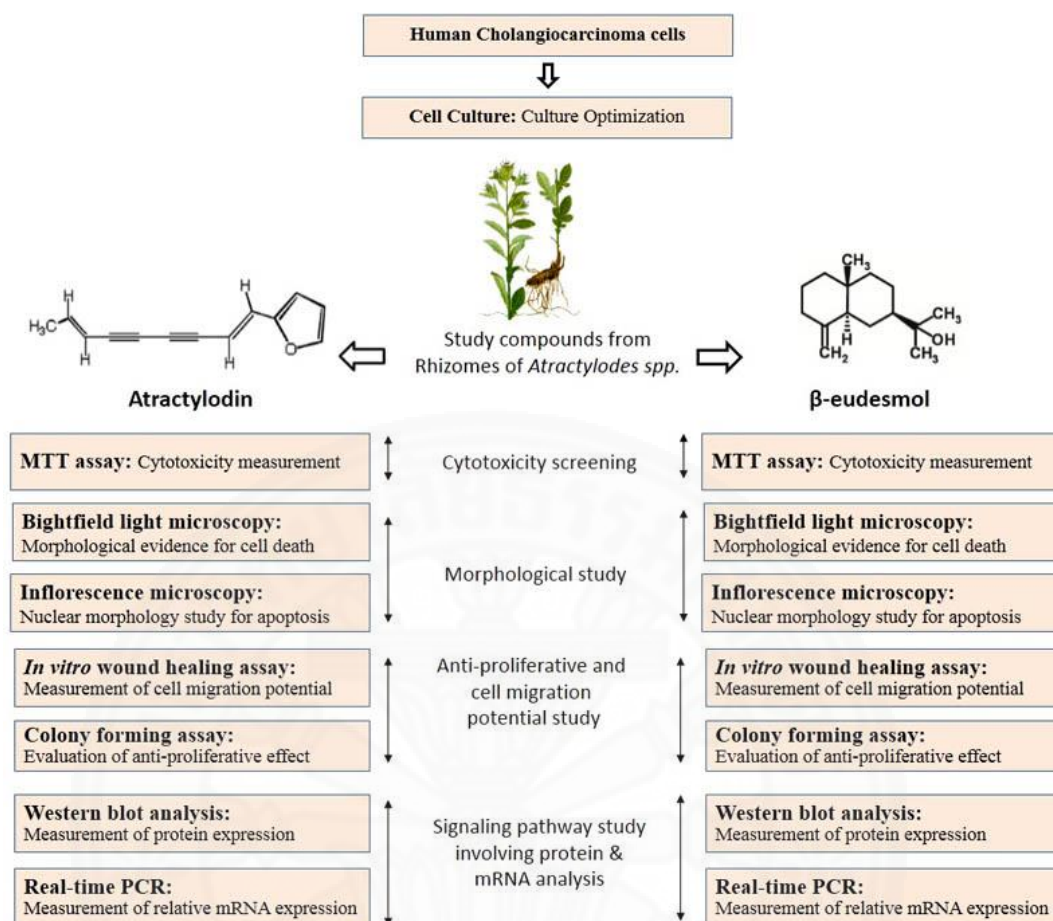


**Figure 2.13** Overall schematic for anti-cholangiocarcinoma activity evaluation of atractylodin and β-eudesmol in cholangiocarcinoma cells

## 2.11 Ethnopharmacology for cancer treatment

Herbal plants have been ethno medicinally used throughout history for treatment of multiple diseases and abnormalities. Before the arrival of modern pharmaceutical-based drugs the main source of medication was crude extracts from natural herbs and medicinal plants. Ethno-pharmacology which refers to the scientific study of ethnic groups and their use of drugs has played a vital role in our community for maintaining valuable information and exchange of medicinal plant resources. In fact, traditional medicine is believed to have their foundation led on ethno medicine systems which includes the Ayurveda and Siddha of India, Jamu of Indonesia, Ying and Yan principles of Chinese herbal medicines, Unani system of middle- and far East-Asian regions and many others (53). Even though it's the age of modern medicine, the plant-based natural products have remained as a major resource for production of drugs by pharmaceutical industry. Till date, around 80 % of all modern medicines discovered and at least partially derived from medicinal herbs and around 20% of commercially available are solely plant derived drugs (54). Out of 252 drugs classified under basic and essential medicine by the world health organization (WHO), around 11% are plant-derived drugs and a majority of the synthetic drugs derived from the natural precursors (55). For instance, few noteworthy drugs obtained from plants are quinidine from *Cinchona spp.*, digoxin from *Digitalis spp.*, atropine from *Atropa belladonna*, morphine from *Papaver somniferum*, and vincristine from *Catharanthus roseus*. In addition, it is estimated that over 60% of anti-cancer and anti-infectious medicines already available on the market or undergoing phase-3 clinical trials are of plant origin (56). The table (Table 2.2) below shows lists of some plant-derived anti-cancer drugs and their sources.

**Table 2.2** List of well known plants-derived anti-cancer drugs

S.N	Plant derived anti-cancer drugs	Mode of action	Source plant
1	Camptothecin	DNA enzyme topoisomerase I inhibitor	<i>Camptotheca acuminata</i>
2	Docetaxel and Paclitaxel	Chemotherapy medication (breast, prostate cancer)	<i>Taxus brevifolia</i>
3	Elliptinium (Celiptium)	Interchelating anti-cancer agents	<i>Bleekeria vitensis</i>
4	Flavoptridol	Angiogenesis inhibitors	<i>Dysoxylum binectariferum</i>
5	Ingenol mebutate (Picato™)	Anti-cancer, apoptosis-inducer	<i>Euphorbia peplus</i>
6	Parthinolide	Anti-cancer and apoptosis inducer	<i>Tanacetum parthenium</i>
7	Podophyllotoxin	Anti-cancer, cyto-static	<i>Podophyllum peltatum</i>
8	Podophyllotoxins	Topoisomerase inhibitors	<i>Podophyllum peltatum</i>
9	Sulforaphane	HDAC inhibitors	Cruciferous vegetable
10	Teniposide (Vumon™)	Anti-neoplastic drugs.	<i>Berberidaceae spp.</i>
11	Thymoquinone	Reactive oxygen species inducer	<i>Nigella sativa</i>
12	Topotecan	Topoisomerase inhibitor	<i>Camptotheca Spp.</i>
13	Vincristine	Anti-mitotic	<i>Catharanthus rosea</i>

## 2.12 Natural products for their use in cancer treatment

Cancer has become a global health problem threatening lives of millions of individuals. A scientific study has predicted that between the year 2000-2020, the overall cancer-related cases is estimated to grow more than 70% in the developing countries and around 30% in the developed countries (57). Even though there has been medical breakthrough in clinical therapies and synthetic drug design for treatment of cancer, the majority of anti-cancer medicines are still based on plant-derived drugs. A report suggests that over 3000 floral species have been actively used to treat variety of cancer including leukemia, melanoma, prostate, and other form of cancers (58). Thus, study and evaluation of phytochemicals and anti-cancer activities of such locally available medicinal plants becomes essential for discovery and potential use of the plant resource for cancer treatment including CCA.

## 2.13 Ethnobotanical resources for treatment of cholangiocarcinoma

The indigenous knowledge of plants is scientifically and culturally very significant. The long history and several evidences of use of folkloric medicines to treat cancer clearly indicate the importance of ethno pharmacological in CCA research. Several indigenous medicinal flora have been traditionally used for alleviating the effects of CCA which includes the crude extracts from *Tripterygium wilfordii*, *Atractylodes lancea* (Thunb) DC, and *Zingiber officinale* Roscoe. In addition, extracts from the *Curcuma longa* Linn. and Thai traditional folk medicinal formulations such as Prasa-Pras-Yhai have been used to heal CCA and other liver diseases (59). In particular, the extracts of *A. lancea* has been found to be effective against cell lines associated with CCA and human gastrointestinal cancer cell lines namely, BGC-823 and SGC-7901 cells (60). In a separate report, the extract from *A. lancea* was found to be highly efficient against CCA cell line CL-6 with  $IC_{50} 32.1 \pm 3.72 \mu\text{g/ml}$ , indicating the therapeutic



potential of this medicinal plant to treat CCA(61). Thus, in-depth investigation of such botanical resources for identification and development of bioactive compounds for potential drugs development to treat CCA cannot be undermined.

#### **2.14 Modern medicines and candidate chemicals for cholangiocarcinoma**

Today the modern medicines are focused on development of drugs that can target specific molecular pathways for preventing cancer. The identification of specific constituent and use of purified components for targeted toxicity against cancer cell is the prime focus of drug development in CCA research. Previous research indicates that a bioactive component, capsaicin, found in fruits of flora with genus *Capsicum*, has anti-cancer activity by inhibiting cell migration and metastasis of CCA cells. Similarly, *luteolin*, is an another example of flavonoid present in several flora that has been found to exhibit apoptotic effect and cell cycle arrest in human CCA KKU-M156 cells (62). In particular, the dried rhizomes of *A. lancea* has been particularly known for its ethno medicinal uses in Chinese as ‘Cang Zhu’, Japan as ‘So-jutsu’ and Thailand as ‘Khod-Kha-Mao’ for suppression of inflammation and tumor activities (63). The extracts have been found to be rich in components such as atractylodin,  $\beta$ -eudesmol, hinesol, and atractylenolide III (Figure 2.14) that are known to be bioactive against CCA (Table 2.3).

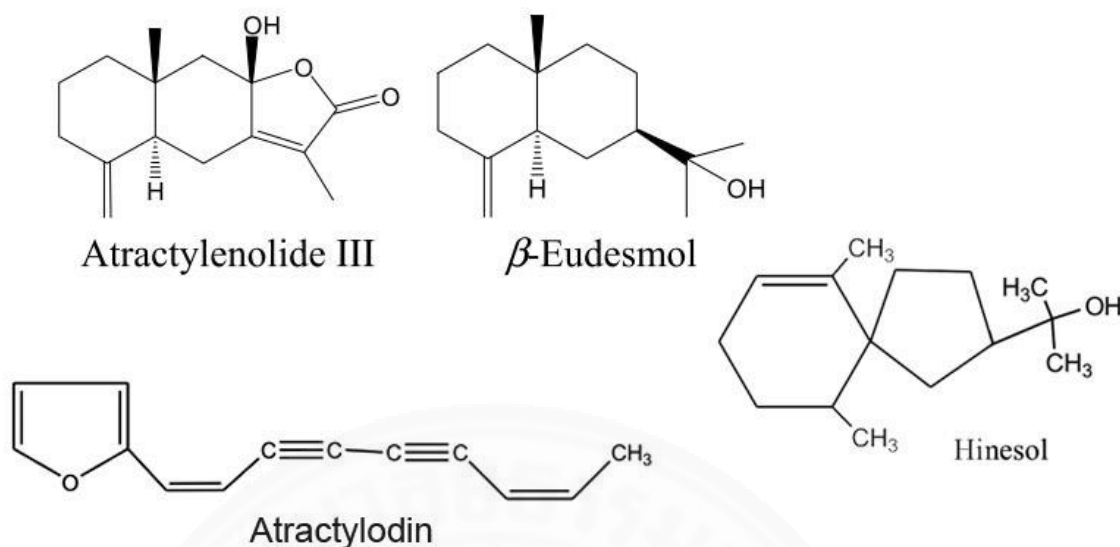


**Figure 2.14** Chemical structure of atractylodin, atractylenolide III, β-eudesmol and hinesol (64).

In addition, reports indicate that several of these constituents have cytoprotective and gastroprotective activity on murine neural cells (65). Similarly, some of these compounds presents promising prospects for their potential pharmacological activities in cardiovascular system and also as an anti-inflammatory agent (66). Since the standard anticancer drug 5-FU seems to have less efficacy against CCA, the studies concentrated on identification, purification and detailed knowledge of such unique bioactive chemicals may hold huge potential for a therapeutic drug and are vital to CCA research. Hence, our prime focus is on bioactive components present in *A. lancea*, namely the two sesquiterpenoid atractylodin and beta-eudesmol, which have been screened for potential anti-CCA activity but the in-depth mechanism underlying the effect is barely understood.

**Table 2.3** Some known biological activities of atractylodin and  $\beta$ -eudesmol

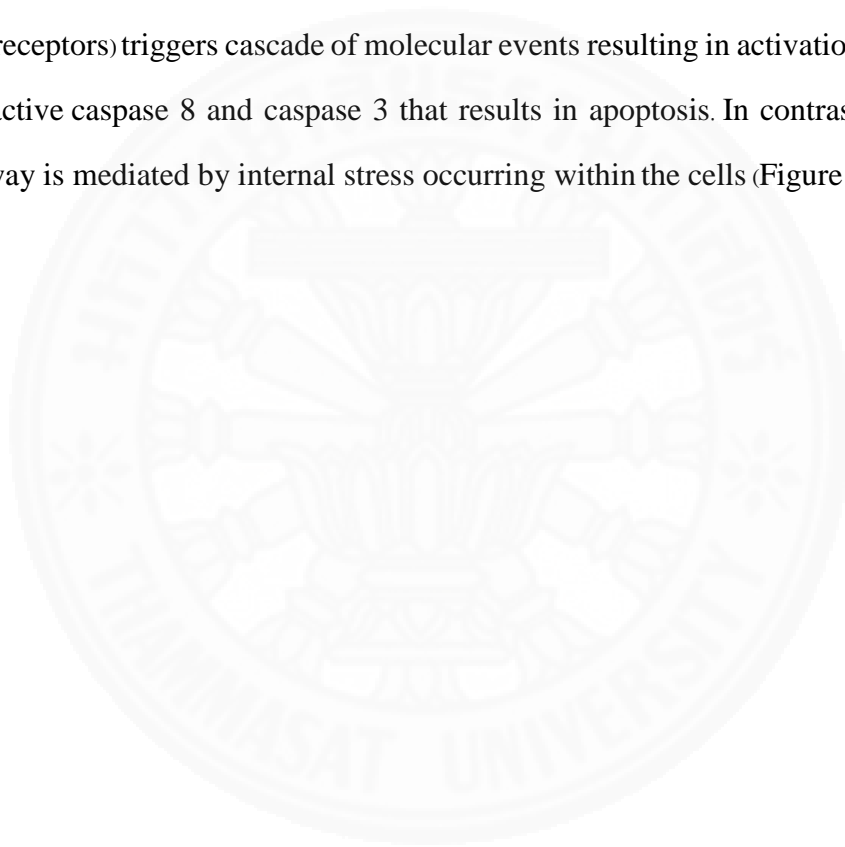
Biological Activity	Experimental Model	Significance	Active components	References
Anti-bacterial activity	<i>In vitro</i> , Bacterial culture	Anti-bacterial properties against <i>Escherichia coli</i> , <i>Staphylococcus aureus</i>	Atractylodin	(67)
Pharmacological activity of gastro intestinal track	<i>In vivo</i> , Gastric emptying stimulated by N <sup>G</sup> -nitro-L-arginine in rats	Aqueous extract improved the delayed gastric emptying	Atractylodin	(68)
Insecticidal and repellent activities	<i>In vitro</i> & <i>In vivo</i>	Potential insecticidal and repellent activities against the insect <i>Tribolium castaneum</i>	Atractylodin	(69)
Pharmacology activity on obesity/ fat reduction	<i>In vivo</i> , High-fat diet-induced obesity mice model	Atractylodin from <i>A. lancea</i> showed the highest lipase inhibitory activity	Atractylodin	(70)
Insecticidal activities	<i>In vivo</i> , tests on insects	Significant insecticidal effect against <i>Drosophila melanogaster</i> by <i>Hinesol</i> and $\beta$ -eudesmol	$\beta$ -eudesmol	(71)
Anti-cancer activity	<i>In vitro</i> , Human leukemia cell line	Inhibitory effect on growth of leukemia-associated HL-60 cells	$\beta$ -eudesmol	(72)
Anti-tumor activity	<i>In vitro</i> , inhibition of blood vessels formation	Inhibitory effect on porcine brain microvascular endothelial cells and HUVEC cells	$\beta$ -eudesmol	(73)

## 2.15 Models for study of cholangiocarcinoma

CCA research requires investigation of the disease is molecular, cellular, tissue and organ levels for better understanding of the disease and identification of potential therapeutic targets. For this, selection and use of both *in vitro* and *in vivo* models are crucial. The *in vitro* models for CCA are generally primary culture of the transformed cholangiocytes from patients and bile duct-derive cells which includes MMNK1, M055 and M214 (74). Likely, a well-established cell line human cholangiocarcinoma (CL-6), human bile duct epithelial carcinoma cell line (HuCCTA-1) and closely associated hepatocarcinoma cell line (Hep-G2) has been utilize to study several molecular mechanism and cellular physiology of CCA (75). Even though the *in vitro* models provide a suitable platform for the molecular studies, the actual response of these cells and a near-perfect microenvironment is hard to reproduce in this system. Thus, the *in vivo* models utilizing immune compromised laboratory balb/c nude mice in xenograft models provide a nearest microenvironment substitution for the CCA cells (76). The most common wild-type and specific gene knockout mouse models such of C57BL/6 and Balb/6 type mice have been used to study the disease (77). Recently, the C57BL/6 mice model has also been used to investigate IL-33 facilitated oncogene-induced CCA development in these mice model. The experimental production of CCA was achieved through transposon transfection system coupled with transduction of constitutively active AKT (myr-AKT) and Yes-associated protein through intrabiliary instillation in the C57BL/6 mice (78). Likely, Syrian golden hamsters infected with *O. viverrini* and treated with N-nitrosodimethylamine have been used for study of *in vivo* screening of anti-cancer drugs (79). Thus, study of both *in vivo* and *in vitro* models can help provide vital knowledge to devising proper strategy for therapeutic drug development against CCA.

## 2.16 Stress-induced apoptosis and cell death

Majority of modern drugs specifically target apoptotic pathways selective to cancer cells. Apoptosis is programmed cell death which can be both intrinsic and extrinsic in nature. The hallmarks of apoptosis included cell shrinkage, formation of membrane-bound apoptotic bodies and induction of phagocytosis by neighboring cells (80). During extrinsic pathway of apoptosis, the ligand binding to death receptors (e.g: FAS receptors) triggers cascade of molecular events resulting in activations procaspases into active caspase 8 and caspase 3 that results in apoptosis. In contrast, the intrinsic pathway is mediated by internal stress occurring within the cells (Figure 2.15).



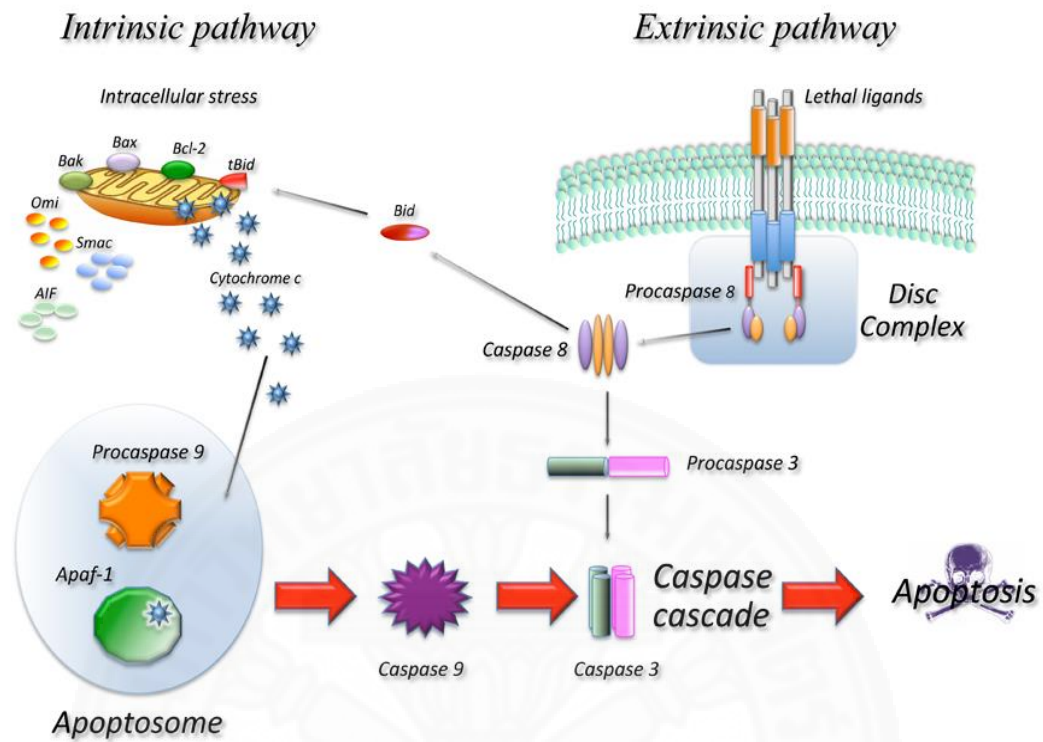


**Figure 2.15** Schematic overview of molecular pathway leading to apoptosis (81)

These stresses can be either induced by cellular senescence, chemicals, infections and toxins, which may not require cell-cell receptors (81). Here, the stress triggers suppression of production of anti-apoptotic proteins (e.g. bcl-2, bcl-x) and induced expression of pro-apoptotic proteins (e.g. bax). This subsequently leads to release of cytochrome C from mitochondria which results in formation of apoptosomes, activation of caspase 9 from its procaspase form and ultimately activates caspase 3 resulting in cell death (81, 82). In contrary, the up-regulation or constitutive activation of signaling cascade including JAK-STAT and NF- $\kappa$ B pathways tend to alleviate the cellular stress and abrogate apoptosis of cancer cells (22, 83). In addition, the NQO1 and HO-1 are also known to act as anti-oxidant and neutralizing the ROS-induced activation of intrinsic apoptotic pathways which in turn assists cancer cell survival and promote malignancy (30, 31). Thus understanding these crucial molecular step is essential for anti-cancer drug development research.

## CHAPTER 3

### OBJECTIVES

#### 3.1 General objective

The overall objective of this research was to investigate anticancer effects of the naturally occurring sesquiterpenoids in rhizomes of *A. lancea* namely, atractylodin and  $\beta$ -eudesmol on CCA cells.

#### 3.2 Specific objectives

- 3.2.1 To access the cytotoxicity of atractylodin and  $\beta$ -eudesmol on CCA cells.
- 3.2.2 To evaluate the effects of atractylodin and  $\beta$ -eudesmol on major cell survival and proliferation associated molecular mechanisms, particularly the JAK-STAT and NF- $\kappa$ B cell signaling pathways
- 3.2.3 To access the effects of atractylodin and  $\beta$ -eudesmol on the expression of major cytoprotective enzymes mainly focusing on heme oxygenase-1 and NAD(P)H quinone oxidoreductase 1.



## **CHAPTER 4**

### **RESEARCH METHODOLOGY**

#### **4.1 Cell lines and reagents**

##### **4.1.1 Cell lines**

The human CCA cell line CL-6 was originally isolated and developed from tumor tissues of a CCA patient at Sriraj Hospital (Mahidol University, Thailand) and was provided as a kind gift to our laboratory for CCA research. Human embryonic fibroblast cell line (OUMS) was purchased from Japanese Collection of Research Bioresources (JCRB) cell bank (Osaka, Japan)

##### **4.1.2 Reagents**

Atractylodin and  $\beta$ -eudesmol were purchased from Wako Pure Chemical Industries (Osaka, Japan). 5-FU, 4',6-diamidino-2-phenylindole (DAPI), 3-(4,5-dimethyl-2-thiazoyl)-2,5-diphenyl-2H-tetrazolium bromide (MTT), paraformaldehyde, and nifuroxazide were purchased from Sigma Chemical Co. Ltd. (St. Louis, MO, USA). Human IL-6 was obtained from Cell Signaling (Danvers, MA, USA). Primary and secondary antibodies against HO-1, STAT3, and phospho-STAT3 (Tyr705) were purchased from Abcam (Cambridge, UK). Dimethyl sulfoxide (DMSO), BCIP/NBT, RIPA lysis buffer, and mammalian protease inhibitor cocktail were purchased from Amresco (Solon, OH, USA). Detergent compatible (DC) protein assay kit, iCycler iQ Real Time Polymerase chain reaction (PCR) system and ZOE™ Fluorescent Cell Imager were purchased from Bio-Rad (Richmond, CA, USA). Reagents used for cell culture including Roswell Park Memorial Institute (RPMI)-1640, Dulbecco's Modified Eagle's Medium (DMEM), fetal bovine serum (FBS),

HEPES buffer, Trypsin-EDTA (0.25%) and Antibiotic-Antimycotic (100×) containing 10,000 U/ml of penicillin, 10,000 µg/mL of streptomycin, and 25 µg/mL of amphotericin B were purchased from Gibco BRL Life Technologies (Grand Island, NY, USA). Primo Vert Inverted Microscope was purchased from Carl Zeiss (Munich, Germany). Varioskan™ flash multimode microplate reader was purchased from ThermoFisher Scientific (Waltham, MA USA).

## **4.2 Cytotoxicity testing**

Anticancer effect of chemicals/drugs are mainly evaluated by its selective cytotoxicity towards transformed cells. The chemicals with high selectivity index (SI) towards the cancer cells as compared to the normal cells are considered good candidate compounds. The standard cell viability assay was used in the experiment to determine the cytotoxicity of test compounds on various cell lines.

### **4.2.1 Cell culture**

CL-6 cells were cultured in complete RPMI media supplemented with 10% FBS, 12.5 mM, HEPES (pH 7.3) and 1× Antibiotic-Antimycotic (Appendix C, D). The OUMS cells were cultured in complete DMEM media consisting of 10% heat inactivated FBS (Appendix B), 12.5 mM HEPES (pH 7.3), and 1× Antibiotic-Antimycotic. Both cells were maintained under an atmosphere of 5% CO<sub>2</sub> at 37°C. The cells were subcultured every 3-4 days using 0.25% Trypsin-EDTA.

### **4.2.2 Cell viability assay for atractylodin and β-eudesmol**

The standard colorimetric MTT metabolic activity assay was used to determine cell viability with minor modifications (Appendix E). Briefly, CL-6 or OUMS cells were seeded ( $1.0 \times 10^4$  cells/well) onto a 96-well plate and pre-incubated at 37 °C for 24 h. This was followed by treatment of cells to varying concentrations (Appendix

A) of atractylodin,  $\beta$ -eudesmol, 5-FU (positive control) or culture medium alone (negative control) for additional 48 h. After removing the supernatant, each well was washed twice with PBS. The culture medium (100  $\mu$ l) and 20  $\mu$ l of MTT solution (5 mg/ml in PBS) were added and further incubation for additional 4 h. The supernatant was discarded, resultant formazan crystals were dissolved in 100  $\mu$ l of DMSO and the absorbance intensity was measured at 570 nm using Varioskan™ microplate reader. The cytotoxicity experiment was repeated three times, triplicate each. Cell viability in terms of its corresponding half maximal inhibitory concentration ( $IC_{50}$ ) values was calculated using CalcuSyn v2.11 software (Biosoft, Cambridge, UK). The selectivity index (SI) was determined as follows:

$$\text{Selectivity Index (SI)} = \frac{IC_{50} \text{ of test compound in CCA cells}}{IC_{50} \text{ of test compound in OUMS cells}}$$

### 4.3 Molecular signaling pathways

Study of the effect of test compounds on molecular signaling pathways is essential to understand the targets of action of these compounds at molecular level and to deduce the potential molecular target of these chemicals in signaling cascade. In this context, several molecular analysis techniques were applied to investigate the effects of AT and BE on crucial signaling pathways that are generally associated with survival and proliferation of the cancer cells.

#### 4.3.1 JAK-STAT pathway

The JAK-STAT pathway is a crucial signaling cascade which transmits ligand-mediated extracellular signal to the nucleus *via* STAT transcription factor which results in transcription and expression of several genes associated with proliferation, oncogenesis, and apoptosis. In several cancer cells, these pathways involving mainly STAT1, and STAT3 are abnormally unregulated, resulting in

uncontrolled growth. Thus, *in vitro* study of this pathway is undoubtedly crucial for the CCA research.

#### **4.3.1.1 Cell culture**

CL-6 cells were cultured in complete RPMI media (Appendix C, D). In brief, the RPMI media was supplemented with 10% heat inactivated FBS (Appendix B), 12.5 mM, HEPES (pH 7.3) and 1× Antibiotic-Antimycotic. Cells were maintained under an atmosphere of 5% CO<sub>2</sub> at 37°C. The cells were subcultured every 3-4 days following trypsinization with 0.25% Trypsin-EDTA.

#### **4.3.1.2 Brightfield inverted microscopy**

Standard brightfield microscopy technique was used to study cell culture morphology. The brightfield microscopy was used to view and image the cell culture morphology. Briefly, cells in the presence or absence of treatment were observed at specific time point under brightfield inverted microscope and series of images were taken at different time points to access cell culture morphology. All images are representative of three independent experiments.

#### **4.3.1.3 Fluorescence Microscopy**

Standard DAPI staining method was used for fluorescent nuclear staining (Appendix H). The procedure was carried out as previously described with minor modification (84). In brief, CL-6 cells ( $0.6 \times 10^5$ /well) were seeded onto a 24 well plate and incubated overnight. The cells were washed with PBS and incubated with culture media containing atractylodin,  $\beta$ -eudesmol or nifuroxazide (positive control) in presence or absence of IL-6 stimulation. After 24 h incubation, cells were washed with PBS, fixed using 4% paraformaldehyde (Appendix A) and stained with DAPI (400 nM in PBS). Fluorescent images of stained nuclei were immediately visualized using ZOE™ Fluorescent Cell Imager. Cells with fragmented or

abnormally condensed nuclei were regarded as apoptotic cells. All images are representative of three independent experiments.

#### **4.3.1.4 Colony formation assay**

Standard colony formation assay was performed to access antiproliferative effect of AL and BE on CL-6 cells (Appendix F). The procedure was carried out as previously described with minor modifications (85). In brief, after 24 h of treatment of atractylodin,  $\beta$ -eudesmol or nifuroxazide, the cells were collected following trypsinization. The CL-6 cells (300 cells/well) were seeded onto a 6-well plate and further incubated for additional 10-12 days. Culture medium was refreshed every third day. Once the colonies (>50 cells) appeared, the cells were fixed with absolute methanol and stained with Diff-Quik™ methylene blue solution. The stained colonies were washed with PBS and counted under microscope. The results are representative of three independent experiments.

#### **4.3.1.5 Wound healing assay**

The experiment (Appendix G) was conducted according to the previously described method with minor modifications (19). CL-6 cells ( $1 \times 10^5$  per well) were seeded onto a 24-well plate and were grown in RPMI complete medium supplemented with 5% fetal calf serum until the cells became confluent. A scratch wound was made with a sterile 200  $\mu$ l pipette tip. The cultures were washed with PBS to remove any detached cells and treated with media containing atractylodin,  $\beta$ -eudesmol, or nifuroxazide without cytokine stimulation. At 0 and 24 h, series of images were acquired using inverted microscope and the inhibitory effect (% of control) on cell migration was estimated. The closing of scratched wound which represents the migration process, was determined by analyzing the image for wound closure along the length of scratch using ImageJ software (NIH, Maryland, USA). The results are representative of three independent experiments.

#### **4.3.1.6 RNA extraction and real time PCR analysis**

The real time PCR analysis was performed to access relative mRNA expression of the target genes. Total RNA was extracted from CL-6 cells using Trizol reagent according to the manufacturer's instructions (Appendix P). The NanoDrop was used to calculate RNA and DNA concentrations (Appendix Q). RQ1 RNase-Free DNase (Promega, WI, USA) was used to remove any residual genomic DNA (Appendix R). Total RNA (1 µg) was reverse transcribed to single-stranded cDNA by using SuperScript™ III Reverse Transcriptase cDNA construction kit following manufacturer's instruction (Appendix S). Real-time PCR was carried out using specific primers for the target genes (Table 4.1).

**Table 4.1** List of forward and reverse primers used for amplification of genes by real-time PCR

No.	Gene	Primer sequence (5'-3')	Amplicon size (bp)
1	GAPDH	Forward: TCAACGGATTTGGTCGTATT Reverse: CTGTGGTCATGAGTCCTTCC	508
2	HO-1	Forward: CTGACCCATGACACCAAGGAC Reverse: AAAGCCCTACAGCAACTGTCTG	196
3	ICAM-1	Forward: ATGCCCAGACATCTGTGTCC Reverse: GGGGTCTCTATGCCCAACAA	112
4	Inos	Forward: TTCAGTATCACAACCTCAGCAAG Reverse: TGGACCTGCAAGTTAAAATCCC	207
5	NRF-2	Forward: GGC GTTAGAAAGCATCCTTCC Reverse: GCAGAGGGCACACTCAAAGT	202
6	NQO1	Forward: GAAGAGCACTGATCGTACTGGC Reverse: GGATACTGAAAGTTCGCAGGG	196
7	MCL-1	Forward: TGCTTCGGAAACTGGACATCA Reverse: TAGCCACAAAGGCACCAAAAG	135
8	MMP9	Forward: GTACCGCTATGGTTACACTCG Reverse: GGCAGGGACAGTTGCTTCT	97
9	VEGF-A	Forward: AGGGCAGAATCATCACGAAGT Reverse: AGGGTCTCGATTGGATGGCA	75

Primers were used to determine relative fold of expression of the target genes. HO-1= heme oxygenase-1, ICAM-1 = intracellular adhesion molecule-1, Inos = inducible nitric oxide synthase, NRF-2 = nuclear receptor factor-2, NQO1 = NAD(P)H quinone dehydrogenase 1, MCL-1 = induced myeloid leukemia cell differentiation protein, MMP-9 = Matrix metalloproteinase-9, and VEGF-A = vascular endothelial growth factor-A.

The real-time PCR was performed using iTaq™ Universal SYBR® Green Supermix following manufacturer's instructions (Appendix T). Relative fold of mRNA expression was analyzed using  $2^{-\Delta\Delta C_t}$  method (Appendix U) and GAPDH gene was taken as internal control. The real time PCR was performed using the following conditions: denaturation at 95 °C for 5 min and amplification by cycling 40 times at 95 °C for 30 s and 60 °C for 45 s. The experiment was repeated three times in triplicate and data are represented as mean  $\pm$  SEM values.

Relative gene expression =  $2^{-\Delta\Delta C_t}$

Where,  $\Delta\Delta C_t = \Delta C_t$  test sample –  $\Delta C_t$  calibrator sample

$\Delta C_t = C_t$  target –  $C_t$  reference

$C_t$  represents cycle threshold for given gene

#### 4.3.1.7 Western blotting analysis

Western blot technique was used to evaluate protein expression and phosphorylation (Appendix I-O). The procedure was carried out as previously described with minor modifications (86). Briefly, CL-6 cells were washed with PBS, harvested and lysed in RIPA buffer containing protease inhibitor cocktail. Protein concentration was determined using DC protein assay kit following manufacturer's instructions (Appendix J). Equal amounts of protein (50 µg/lane) were subjected to sodium dodecyl sulfate-polyacrylamide (SDS) gel electrophoresis and transferred to a nitrocellulose membrane. After blocking with 5% BSA in TBS at room temperature for 1 h, membranes were incubated overnight at 4°C with appropriate dilution of the P-STAT1 (Tyr 701), P-STAT3 (Tyr 705), STAT1, STAT3, and  $\beta$ -actin primary antibody. Membranes were washed extensively with 0.1% Tween-20 in TBS and incubated with alkaline phosphatase (AP)-conjugate secondary antibody at 25 °C for 1 h. Bands corresponding to the antibodies were developed using AP-conjugated secondary antibody and AP chromogen (BCIP/NBT) system (Amresco, USA). The



densitometric analysis of the protein bands were performed using GelQuant.NET analysis software (Biochem Lab Solutions, CA, USA). Data are expressed as densitometric values (mean  $\pm$  SD) values of protein expression normalized to loading control. The results are representative of three independent experiments.

### **4.3.2 NF- $\kappa$ B pathway**

NF- $\kappa$ B is a major transcriptional regulatory pathway responsible for wide range of cellular activities including survival, proliferation, and oncogenesis. Important members of NF- $\kappa$ B family include homo or hetero dimer of p50, p52, p65, c-Rel, and RelB. The NF- $\kappa$ B pathway are frequently altered in cancer cells and usually play crucial role in malignancy and survival of transformed cells.

#### **4.3.2.1 Cell culture**

CL-6 cells were cultured in complete RPMI media supplemented with 10% heat inactivated FBS (Appendix B), 12.5 mM, HEPES (pH 7.3) and 1 $\times$  Antibiotic-Antimycotic. Cells were maintained under an atmosphere of 5% CO<sub>2</sub> at 37°C. The cells were subcultured every 3-4 days following trypsinization with 0.25% Trypsin-EDTA.

#### **4.3.2.2 Cell viability assay**

The standard colorimetric MTT metabolic activity assay was used to determine cell viability with minor modifications (Appendix E). Briefly, CL-6 cells were seeded ( $1.0 \times 10^4$  cells/well) onto a 96-well plate and pre-incubated at 37 °C for 24 h. This was followed by treatment of cells with varying concentrations of MG132 (positive control) or culture medium alone (negative control) for additional 48 h. The experiment was repeated three times in triplicate. Cell viability in terms of its corresponding half maximal inhibitory concentration (IC<sub>50</sub>) value was calculated using CalcuSyn v2.11 software.

#### 4.3.2.3 Western blotting analysis

Western blot analysis was used to determine protein expression and phosphorylation (Appendix I-O). The procedure was carried out as previously described with minor modifications (86). Briefly, CL-6 cells were washed with PBS, harvested and lysed in RIPA buffer containing protease inhibitor cocktail (Appendix I). Protein concentration was determined using DC protein assay kit following manufacturer's instructions (Appendix J). Equal amounts of protein (50 µg/lane) were subjected to sodium dodecyl sulfate-polyacrylamide (SDS) gel electrophoresis and transferred to a nitrocellulose membrane. After blocking with 5% BSA in TBS at room temperature for 1 h, membranes were incubated overnight at 4°C with appropriate dilution of the p65 (RelA), RelB, c-Rel, NF-κB1 (p105) and NF-κB2 (p100), IκBα, and β-actin primary antibody. Membranes were washed extensively with 0.1% Tween-20 in TBS and incubated with alkaline phosphatase (AP)-conjugate secondary antibody at room temperature for 1 h. Bands corresponding to the antibodies were developed using AP-conjugated secondary antibody and AP chromogen (BCIP/NBT) system (Amresco, USA). The densitometric analysis of the protein bands were performed using GelQuant.NET analysis software (Biochem Lab Solutions, CA, USA). Data are expressed as densitometric values (mean ± SD) of protein expression normalized to loading control. The results are representative of three independent experiments.

#### 4.3.3 Heme oxygenase-1 and NAD(P)H quinone oxidoreductase 1

Heme oxygenase-1 (HO-1) is a critical cytoprotective enzyme known to promote anti-apoptotic activities and chemotherapeutic resistance in several types of tumor cells (87, 88). NQO1 is an obligatory two-electron reductase that catalyzes the reduction of quinone substrate. NQO1 has been found to be abnormally up-regulated in several human cancer including breast, lung, colon, and pancreatic cancers. The intracellular

enzyme NQO1 has been known to stabilize several growth proteins including NF- $\kappa$ B family proteins by inhibiting their proteasomal degradation and hence suppressing apoptosis.

#### **4.3.3.1 Cell culture**

CL-6 cells were cultured in complete RPMI media supplemented with 10% heat inactivated FBS (Appendix B), 12.5 mM, HEPES (pH 7.3) and 1 $\times$  Antibiotic-Antimycotic. Cells were maintained under an atmosphere of 5% CO<sub>2</sub> at 37°C. The cells were subcultured every 3-4 days following trypsinization with 0.25% Trypsin-EDTA.

#### **4.3.3.2 Fluorescence Microscopy**

Standard DAPI staining method (Appendix H) was used as previously described with minor modifications (84). In brief, CL-6 cells (0.6  $\times$  10<sup>5</sup>/well) were seeded onto a 24-well plate and incubated overnight. The cells were washed with PBS and incubated with media containing atractylodin,  $\beta$ -eudesmol, SnCl<sub>2</sub>, or Zn(II)PPIX (Appendix A). After 24 h incubation, cells were washed with PBS, fixed using 4% paraformaldehyde (Appendix A) and stained with DAPI (400 nM in PBS). Fluorescent images of stained nuclei were visualized using ZOETM<sup>TM</sup> Fluorescent Cell Imager (Bio-Rad, CA, USA). Cells with fragmented or abnormally condensed nuclei were regarded as apoptotic cells. All images are representative of three independent experiments.

#### 4.3.3.3 Colony formation assay

Colony formation assay was performed (Appendix F) as previously described with minor modifications (85). In brief, after 24 h treatment of atractylodin,  $\beta$ -eudesmol,  $\text{SnCl}_2$  or media alone, CL-6 cells were collected following trypsinization. The CL-6 cells (300 cells/well) were seeded onto a 6-well plates and further incubated for additional 10-12 days. Culture medium was refreshed every third day. Once the colonies ( $>50$  cells) appeared, the cells were fixed with absolute methanol and stained with Diff-Quik<sup>TM</sup> methylene blue solution. The stained colonies were washed with PBS and counted under microscope. The results are representative of three independent experiments.

#### 4.3.3.4 Wound healing assay

The experiment was conducted (Appendix G) according to previously described method with minor modifications (19). CL-6 cells ( $1 \times 10^5$  per well) were seeded onto a 24-well plate and were grown in RPMI complete medium supplemented with 5% fetal calf serum until the cells became confluent. A scratch wound was made with a sterile 200  $\mu\text{l}$  pipette tip. The cultures were washed with PBS to remove any detached cells and treated with media containing atractylodin,  $\beta$ -eudesmol, or  $\text{SnCl}_2$  with or without cytokine stimulation. At 0 and 24 h, series of images were acquired using inverted microscope and the inhibitory effect (% of control) on cell migration was estimated. The closing of scratched wound which represents the migration process, was determined by analyzing the image for wound closure along the length of scratch using ImageJ software (NIH, Maryland, USA). The results are representative of three independent experiments.

#### 4.3.3.5 RNA extraction and real time PCR analysis

Total RNA was extracted (Appendix P) from cells using Trizol™ reagent (Invitrogen, CA, USA) according to the manufacturer's instructions. The NanoDrop was used to calculate RNA and DNA concentrations (Appendix Q). RQ1 RNase-Free DNase was used to remove any residual genomic DNA (Appendix R). One microgram of total RNA was measured and reverse transcribed to single-stranded cDNA by using SuperScript™ III Reverse Transcriptase cDNA construction kit (Appendix S) following manufacturer's instruction (ThermoScientific, MA USA). Real-time PCR analysis was carried out using specific primers for target genes (Table 4.1). Relative fold of mRNA expression was analyzed using  $2^{-\Delta\Delta C_t}$  method (Appendix U) and GAPDH gene was taken as internal control. The real-time PCR was performed using iTaq™ Universal SYBR® Green Supermix (Appendix T) under following conditions: denaturation at 95 °C for 5 min and amplification by cycling 40 times at 95 °C for 30 s and 60 °C for 45 s. The experiment was repeated three times in triplicate and data are represented as mean  $\pm$ SEM values.

Relative gene expression  $= 2^{-\Delta\Delta C_t}$

Where,  $\Delta\Delta C_t = \Delta C_t$  test sample –  $\Delta C_t$  calibrator sample

$\Delta C_t = C_t$  target –  $C_t$  reference

$C_t$  represents cycle threshold for given gene

#### 4.3.3.6 Western blot analysis

Western blot technique was used to evaluate protein expression and phosphorylation (Appendix I-O). The procedure was carried out as previously described method with minor modifications (86). Briefly, CL-6 cells were washed with PBS, harvested and lysed in RIPA buffer containing protease inhibitor cocktail (Appendix I). Protein concentration was determined using DC protein assay kit following manufacturer's instructions (Appendix J). Equal amounts of protein (50

µg/lane) were subjected to sodium dodecyl sulfate-polyacrylamide (SDS) gel electrophoresis and transferred to a nitrocellulose membrane. After blocking with 5% BSA in TBS at room temperature for 1 h, membranes were incubated overnight at 4°C with appropriate dilution of the HO-1, NQO1, and β-actin primary antibody. Membranes were washed extensively with 0.1% Tween-20 in TBS and incubated with alkaline phosphatase (AP)-conjugate secondary antibody at room temperature for 1 h. Bands corresponding to the antibodies were developed using AP-conjugated secondary antibody and AP chromogen (BCIP/NBT) system (Amresco, USA). The densitometric analysis of the protein bands were conducted using GelQuant.NET analysis software (Biochem Lab Solutions, CA, USA). Data are expressed as densitometric values (mean±SD) of protein expression normalized to loading control. The results are representative of three independent experiments.

#### 4.4. Statistical analysis

The statistical analyses were performed using GraphPad Prism 5 (GraphPad Software Inc., CA, USA). Comparison of quantitative variables were performed using SPSS with independent t-test wherever appropriate. Qualitative variables are represented as number and percentage values. Quantitative variables are presented as mean±SD or mean±SEM. Statistical significant difference was set at values.  $p < 0.05$  for all test performed.

## CHAPTER 5

### RESULTS

#### 5.1 Anticholangiocarcinoma activity of atractylodin

##### 5.1.1 Cytotoxicity of atractylodin in cholangiocarcinoma cells

Atractylodin exhibited promising cytotoxic activity against CL-6 cells with  $IC_{50}$  of  $221.25 \pm 11.42$  (mean  $\pm$  SEM)  $\mu$ M. Potency of activity exhibited by atractylodin was about 3-fold of the standard drug 5-FU ( $IC_{50}$  of  $670.06 \pm 28.44$   $\mu$ M). Interestingly, the atractylodin treatment was less toxic to normal control cell line OUMS compared with 5-FU with observed  $IC_{50}$  values of  $2.45 \pm 6.91$  and  $1,010.44 \pm 8.73$   $\mu$ M, respectively. The corresponding selectivity index (SI) values for atractylodin and 5-FU on CL-6 were 1.6 and 1.5, respectively. The  $IC_{50}$  and SI values of atractylodin and 5-FU are presented in Table 5.1.

**TABLE 5.1 The  $IC_{50}$  and SI values for atractylodin.**

No.	Cell Line	Compound	$IC_{50} \pm SEM$ ( $\mu$ M)	Median $\pm$ Range ( $\mu$ M)	Inter Quartile Range ( $\mu$ M)	Specificity Index (SI)
1	CL-6	Atractylodin	$221.25 \pm 11.42$	$216.77 \pm 21.56$	10.79	1.6
		5-Flurouracil	$680.06 \pm 18.44$	$687.75 \pm 34.72$	17.36	1.5
2	OUMS	Atractylodin	$352.45 \pm 6.91$	$351.04 \pm 13.66$	6.83	1.0
		5-Flurouracil	$1010.44 \pm 8.73$	$1013.13 \pm 16.71$	8.36	1.0

Data are represented as values of three independent experiments done in triplicate.  $IC_{50}$  = Half maximal inhibitory concentration ( $IC_{50}$ ); SI= selectivity index.

### **5.1.2 Morphological evidence of atracylodin-induced cell death in cholangiocarcinoma cells**

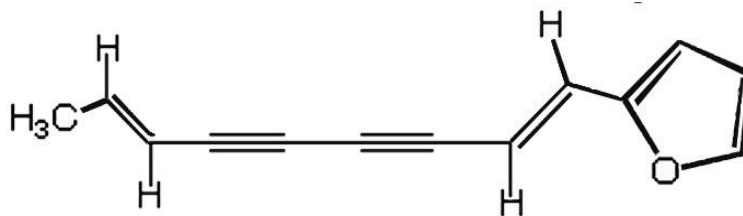
Morphological examination under light microscopy indicated concentration-dependent cytotoxicity of atracylodin on CL-6 cell growth. Atracylodin treatment at concentration of 250  $\mu$ M led to distorted morphology of CL-6 cells with visible signs of cell debris and floating dead cells. Concentrations of atracylodin above 250  $\mu$ M caused clearly noticeable cell death with extensive cell debris as compared to untreated control (Figure 5.1). In contrast, the observable cytotoxic effect on the OUMS cells was relatively less prominent as compared to CL-6 cells for similar concentrations of atracylodin treatment. Even at the concentrations above 250  $\mu$ M, only slight visible signs of cell death were observed in OUMS cell culture (Figure 5.1). The results indicated selective toxicity of atracylodin on CL-6 cells.

### **5.1.3 Evaluation of atracylodin treatment on colony forming ability of cholangiocarcinoma cells**

The colony forming ability is a measure of proliferative potential of cells to form colony from a single cell and is measured in term of colony forming unit (CFU). Results from colony formation assay indicated that in absence of atracylodin, CL-6 cells were able to extensively proliferate by forming large number of CFUs. In contrast, atracylodin treatment resulted in concentration-dependent inhibition on colony forming ability of CL-6 cells. Atracyldoin concentrations above 50  $\mu$ M caused stark and significant ( $p = 0.001$ ) decline in CFU (Figure 5.3) formation ability. In addition to the culture morphology, the effect of compound treatment on nuclear degradation for signs of visible traits of apoptosis was investigated using fluroscent staining. The results from DAPI staining indicated that CL-6 cell culture in the absence of atrsctylodin treatment resulted in healthy growth as reflected by its sound nuclear morphology at 0 and 24 h post-incuation condition (Figure 5.2). In contrast, cells treated with atracylodin treatment clearly displayed substancial amount of growth inhibition and visual traits of nuclear degradation at 24 h post incubation (Figure 5.2).



(A)



(B)

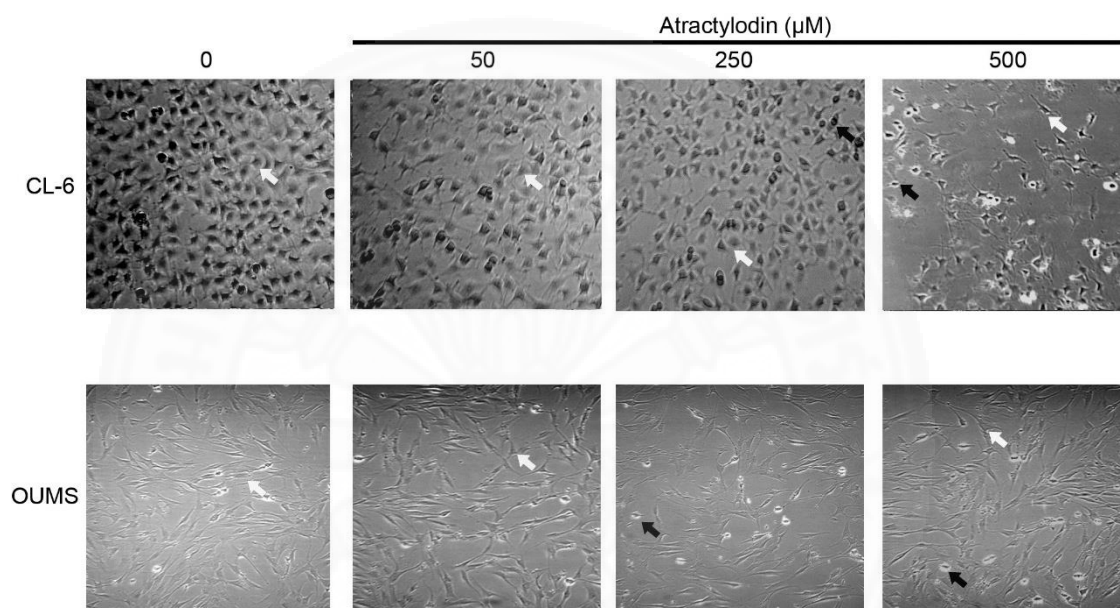


**Figure 5.1** Chemical structure of atractylodin and effect of atractylodin on CL-6 and OUMS cells morphology. (A) Chemical structure of atractylodin. (B) CL-6 or OUMS cells were treated with indicated concentrations of atractylodin. After 24 h, cell morphology was examined under the light microscopy. The images shown are representative of three independent experiments. *White arrow* indicates live cells. *Dark arrow* indicates dead cells.

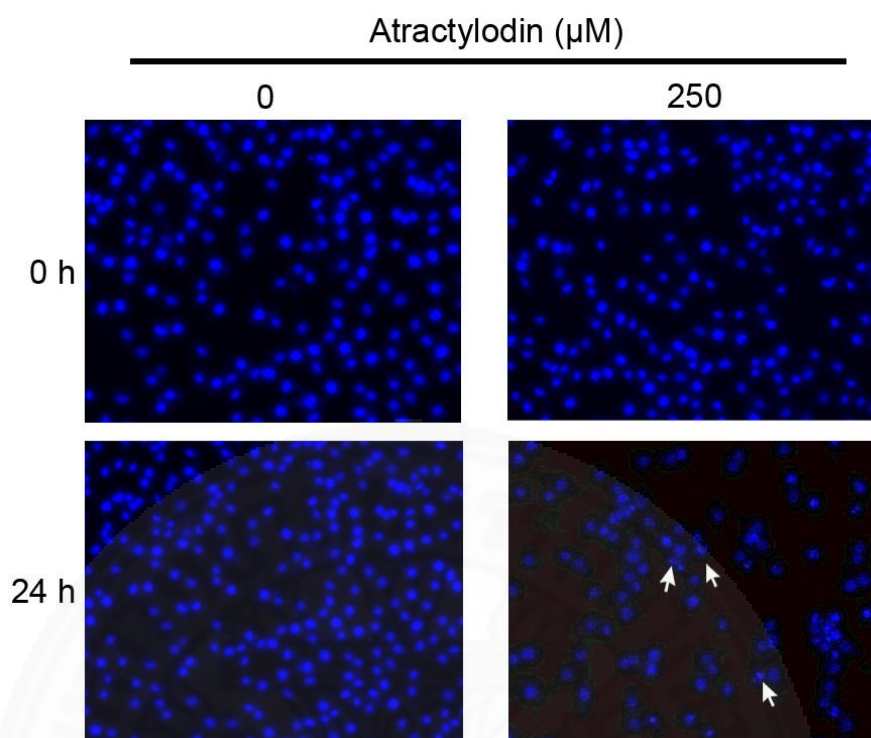


**Figure 5.2** Effect of atractylodin on nuclear morphology of CL-6 cells. The cells were allowed to grow overnight in the presence or absence of atractylodin (250  $\mu\text{M}$ ). The cells were fixed using paraformaldehyde and stained using DAPI at 0 and 24 h time point to visualize nuclear morphology for signs of apoptosis. All images are representative of three independent experiments. *White arrow* indicates the cells with signs of degenerative nucleus.

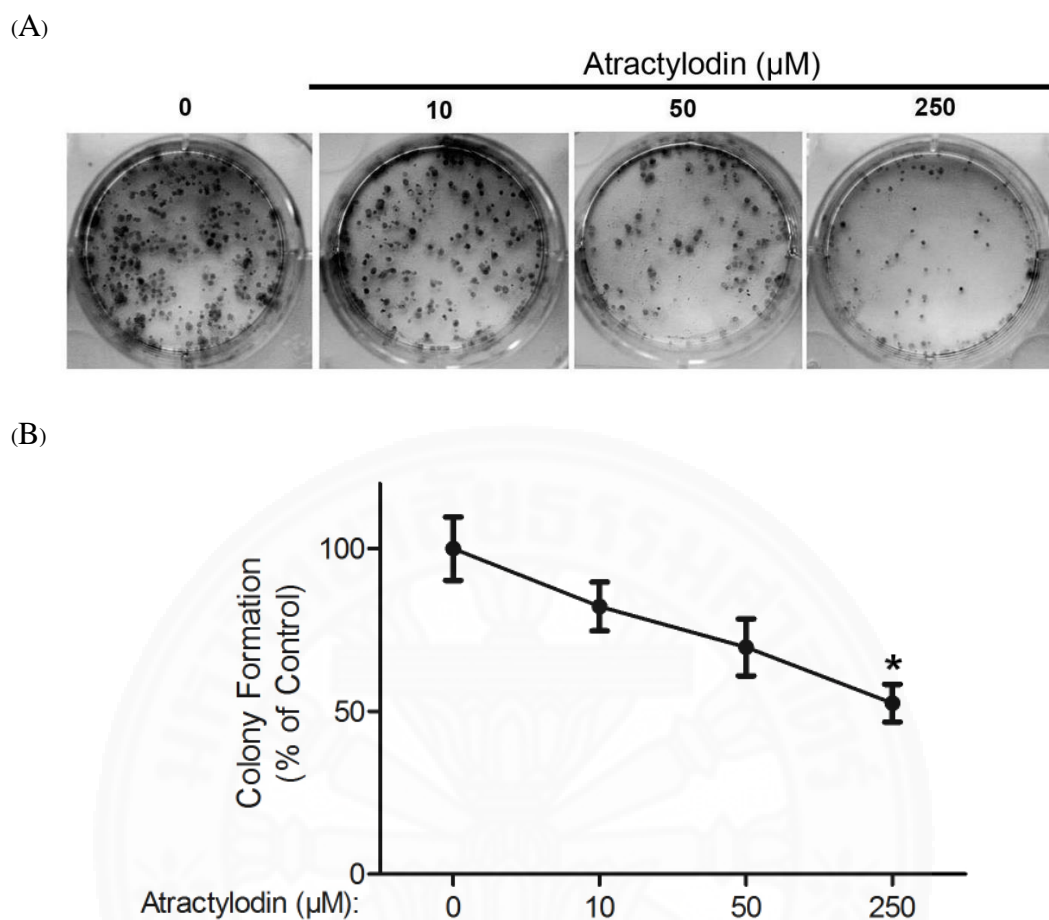


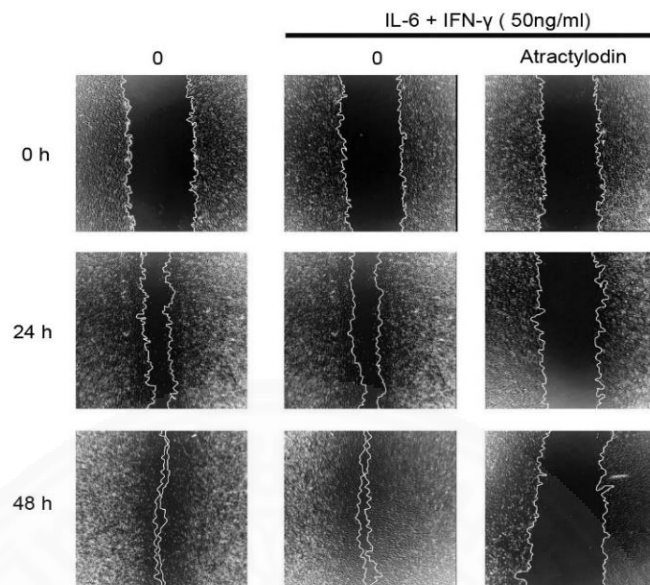
**Figure 5.3** Effect of atractylodin on colony forming ability of the CL-6 cells. After 24 h of treatment of indicated concentrations of atractylodin the CL-6 cells were collected after trypsinization, seeded (300 cells/well) into a 6-well plate and further incubated for additional 6-10 days. When the colonies appeared with at least 50 cells, the cells were fixed using ethanol and stained with methylene blue to visualize the colonies. (A) Effect of atractylodin on colony formation of CL-6 cells, and (B) Line chart representing the effect of atractylodin on colony formation as percentage of control. Data are presented as mean $\pm$ SD and are representative of three independent experiments. \* $p < 0.05$  vs untreated control.

#### **5.1.4 Evaluation of atractylodin treatment on wound healing ability of cholangiocarcinoma cells**

Results from wound healing assay indicated promising ability of atractylodin to suppress the *in vitro* wound healing ability of CL-6 cells. The absence of atractylodin or cytokine treatment resulted in rapid wound closure in CL-6 cells within 48 h of incubation. In the absence of atractylodin treatment, relatively similar extent of wound closure was observed in both cytokine stimulated and unstimulated cells for the respective time period of 24 and 48 h. Atractylodin (250  $\mu$ M) treatment on the other hand, significantly ( $p=0.001$ ) depleted the wound healing ability and even slightly widened the initial wound area at 48 h of incubation (Figure 5.4). The corresponding bar graph representing wound closure relative to untreated control clearly indicated significant ( $p=0.001$ ) suppression of wound closure at 24 and 48 h by atractylodin as compared to both cytokine treated and untreated control groups (Figure 5.4).

The ability of nifuroxazide, a known selective inhibitor of STAT1/3 activation, to exert wound healing effect on CL-6 cells was investigated under similar conditions. The results indicated that nifuroxazide significantly ( $p=0.001$ ) suppressed wound healing ability of CL-6 cells at both 24 h and 48 h (Figure 5.5).

(A)



(B)

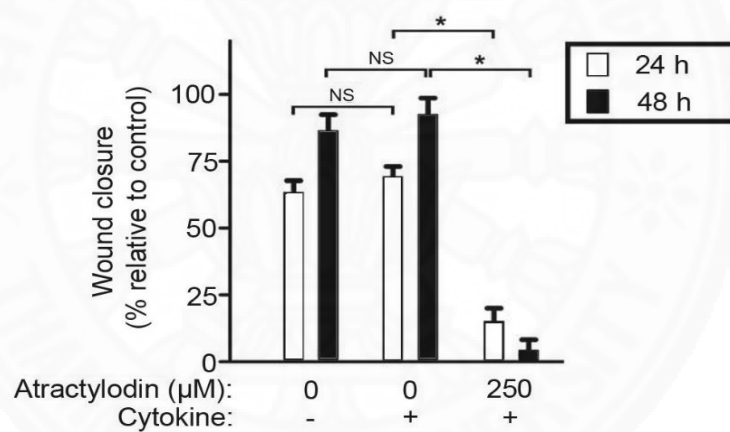
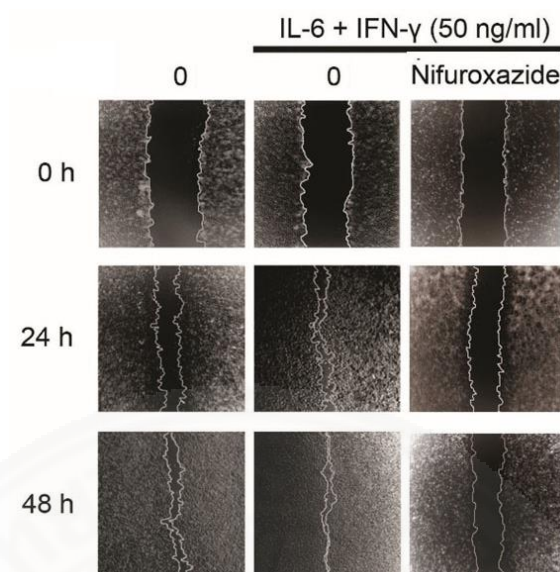


**Figure 5.4** Effect of atractylodin on wound healing ability of CL-6 cells. The cells were cultured in a 24-well plate and at near confluency, serum starved for 18 h, followed by creation of wound and subsequent treatment with media alone, media containing cytokine mixture (50 ng/mL IL-6 and 50 ng/mL IFN- $\gamma$ ) along with atractylodin (250  $\mu$ M) for further 48 h. Wound closure was measured at 0, 24 and 48 h. (A) Effect of atractylodin on wound healing. (B) Bar diagram representing the effect of atractylodin on wound healing ability. Data are presented as mean $\pm$ SD values and are representative of three independent experiments. \* $p < 0.05$ . IL-6 = Interlukin-6, IFN- $\gamma$  = Interferon- $\gamma$ , NS = non-significant.

(A)



(B)

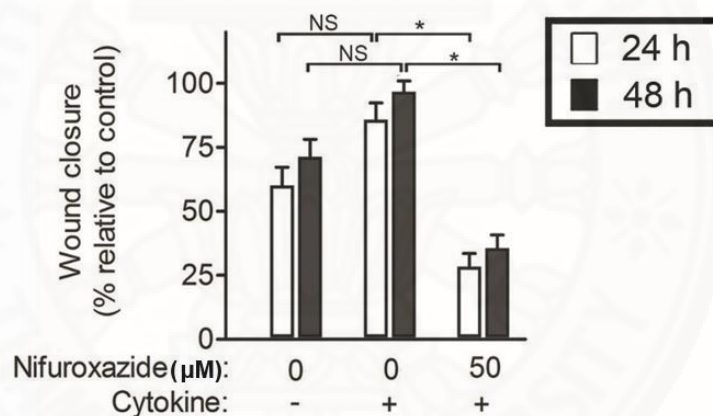


**Figure 5.5** Effect of nifuroxazide on wound healing ability of CL-6 cells. The cells were cultured in a 24-well plate and at near confluency, serum starved for 18 h, followed by creation of wound and subsequent treatment of media alone, and media containing cytokines (50 ng/mL IL-6 and 50 ng/mL IFN- $\gamma$ ) along with nifuroxazide (50  $\mu$ M) for 48 h. Wound closure was measured at 0, 24 and 48 h. (A) Effect of nifuroxazide on wound healing. (B) Bar diagram representing the effect of nifuroxazide on wound healing. Data are presented as mean $\pm$ SD and are representative of three independent experiments. \* $p$  < 0.05. IL-6 = Interlukin-6, IFN- $\gamma$  = Interferon- $\gamma$ , NS = non-significant..



### **5.1.5 Evaluation of atractylodin treatment on the production of heme oxygenase-1 in cholangiocarcinoma cells**

The expression of HO-1 is essential for maintaining cytoprotective activity of cells. Results from western blot analysis revealed considerable amount of baseline expression of HO-1 enzyme in CL-6 cells (Figure 5.6). The inhibitory effect of atractylodin treatment on HO-1 expression was subtle within 6 h of treatment. In contrast, immunoblot analysis and corresponding densitometry bar chart indicated that atractylodin treatment significantly suppressed the production of HO-1 enzyme at 12 h ( $p=0.006$ ) and 24 h ( $p=0.0003$ ) post treatment as compared to untreated control (Figure 5.6).

### **5.1.6 Evaluation of atractylodin treatment on the production of NQO1 in cholangiocarcinoma cells**

The expression of NQO1 is an important cytoprotective activity of cells. Results from western blot analysis revealed considerable amount of baseline expression of NQO1 enzyme in CL-6 cells (Figure 5.7). The inhibitory effect of atractylodin treatment on NQO1 expression was barely noticeable within 6 h of treatment. In contrast, immunoblot analysis and corresponding densitometric bar chart indicates that atractylodin treatment significantly inhibited ( $p=0.001$ ) the expression of NQO1 enzyme at 24 h post treatment as compared to untreated control (Figure 5.7). The effect of atractylodin on NQO1 was non-significant ( $p=0.631$ ) at time period before 24 h in CL-6 cells.

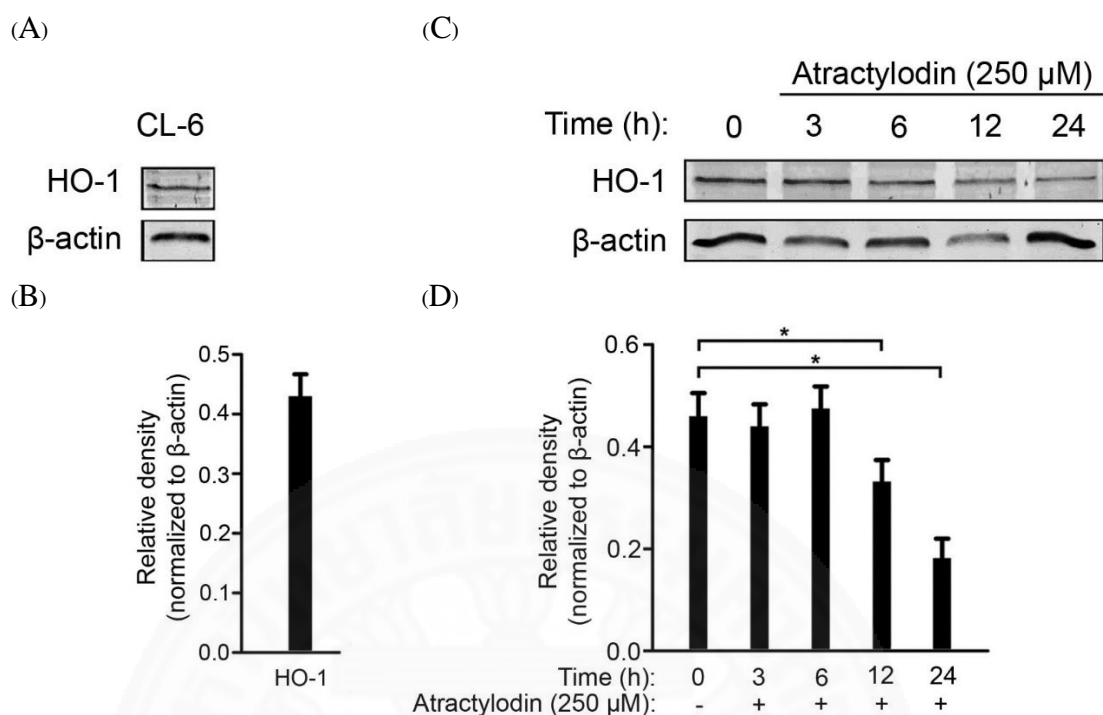


**Figure 5.6** Inhibitory effect of atractylodin on HO-1 expression in CL-6 cells. The cells were serum starved for overnight, pretreated with designated concentrations of atractylodin for 0-24 h. Whole cell extracts were prepared and 50  $\mu$ l aliquots of cell lysates were subjected to western blotting for HO-1 protein expression.  $\beta$ -actin was taken as loading control. (A) Baseline expression of HO-1 in CL-6 cells. (B) Graph representing means $\pm$ SD of three independent experiments for densitometric values of baseline HO-1 expression normalized to  $\beta$ -actin. (C) Effect of atractylodin treatment on HO-1 expression in CL-6 cells. (D) Graph representing the mean $\pm$ SD of three independent experiments for densitometric values of HO-1 protein expression normalized to  $\beta$ -actin. \* $p < 0.05$  vs untreated control. HO-1 = Heme oxygenase-1.



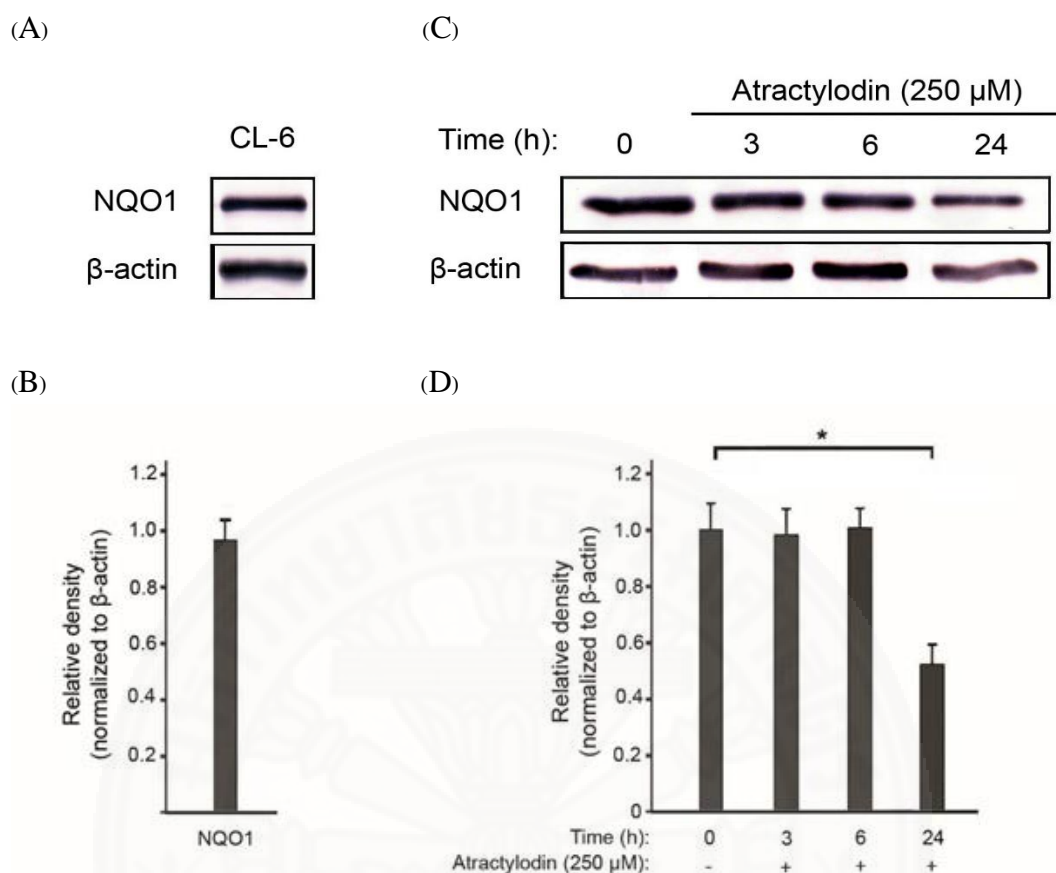


**Figure 5.7** Inhibitory effect of atractylodin on NQO1 expression in CL-6 cells. The cells were serum starved for overnight, pretreated with designated concentrations of atractylodin for 0-24 h. Whole cell extracts were prepared and 50  $\mu$ l aliquots of cell lysates were subjected to western blotting for NQO1 protein expression.  $\beta$ -actin was taken as loading control. (A) Baseline expression of HO-1 in CL-6 cells. (B) Graph representing the mean $\pm$ SD of three independent experiments for densitometric values of baseline NQO1 expression normalized to  $\beta$ -actin. (C) Effect of atractylodin treatment on NQO1 production in CL-6 cells. (D) Graph representing the mean $\pm$ SD of three independent experiments for densitometric values of protein expression normalized to  $\beta$ -actin. \* $p < 0.05$  vs untreated control. NQO1 = NAD(P)H Quinone dehydrogenase 1.

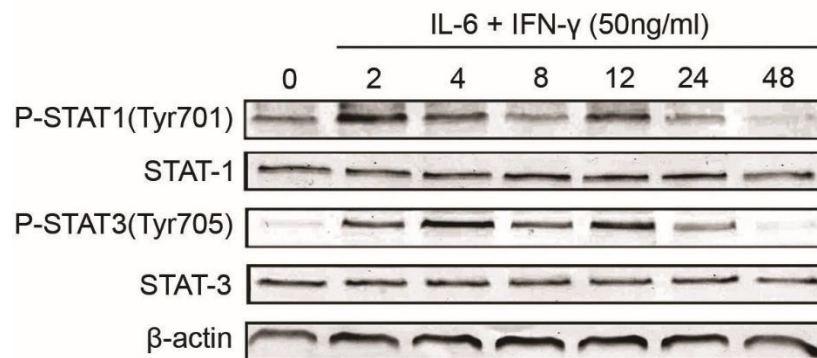
### **5.1.7 Evaluation of cytokine induced STAT1/3 phosphorylation in cholangiocarcinoma cells**

Cytokine stimulation induced STAT1/3 activation in the CL-6 cells. IFN- $\gamma$  and IL-6 (50 ng/ml each), respectively, was used to stimulate STAT1 and STAT3 activation *via* phosphorylation in CL-6 cells. The results from immunoblots and corresponding densitometric analysis indicated that CL-6 cells produced maximal activation of both STAT1 ( $p=0.001$ ) and STAT3 ( $p=0.011$ ) proteins through STAT stimulation of phosphorylation at approximately 4 h after cytokine treatment. In the absence of cytokine stimulation, the cells displayed little or no baseline level of STAT1/3 activation. Cytokine treatment had no effect on expression levels of total STAT1/3 expression. Similarly, cytokine stimulation exhibited no effect on total expression of  $\beta$ -actin taken as loading control (Figure 5.8).

### **5.1.8 Effect of atractylodin treatment on cytokine induced STAT1/3 phosphorylation in cholangiocarcinoma cells**

Atractylodin showed potential for concentration-dependent suppression of STAT1/3 activation in the CL-6 cells. Pretreatment of CL-6 cells with 0-500  $\mu$ M of atractylodin for 2 h and further stimulation with cytokine mixture for 4 h resulted in suppression of both STAT1 and STAT3 phosphorylation in a concentration-dependent manner. Densitometric analysis of protein expression normalized with corresponding STAT proteins expression indicated that atractylodin at concentrations higher than 50  $\mu$ M had significant inhibitory effect on activation of both STAT1 ( $p=0.005$ ) and STAT3 ( $p=0.001$ ) as compared to cytokine-treated control. In the absence of cytokine stimulation, little or no baseline level of STAT1/3 phosphorylation occurred. Atractylodin treatment had insignificant effect on the expression levels of total STAT1/3 or  $\beta$ -actin in CL-6 cells (Figure 5.9).

(A)



(B)

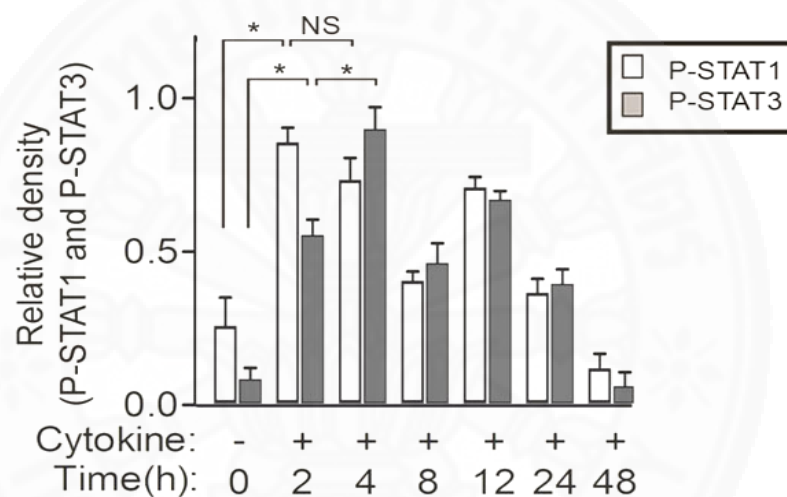
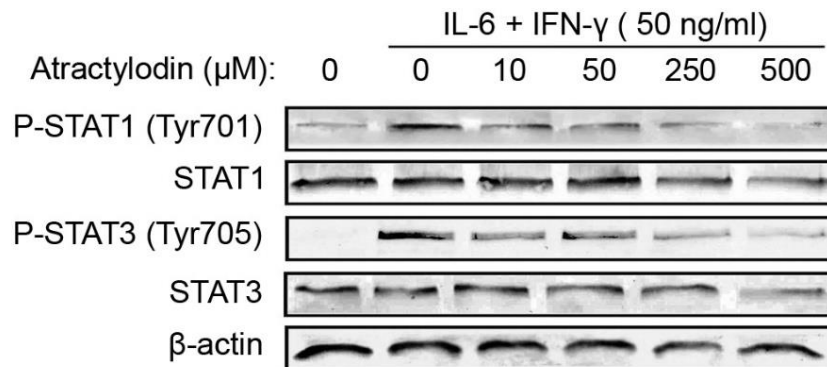


**Figure 5.8** Evaluation of cytokine-induced STAT1/3 activation in CL-6 cells. The cells were serum starved overnight and stimulated with cytokines (50 ng/mL IL-6 and 50 ng/mL IFN- $\gamma$ ) cytokines for 0-48 h. Whole cell extracts were prepared and 50  $\mu$ L aliquots were subjected to western blotting for accessing relative expression levels of STAT1 and STAT3 phosphorylation.  $\beta$ -actin was taken as loading control. (A) Representative immunoblots for expression of STAT1, STAT3, P-STAT1, P-STAT3, and  $\beta$ -actin in CL-6 cells. (B) Bar chart representing the mean $\pm$ SD values of three independent experiments for densitometric values of protein expression ratios (P-STAT/STAT) of the levels of phosphorylated proteins to its corresponding total protein level.  $*p<0.05$ .

(A)



(B)

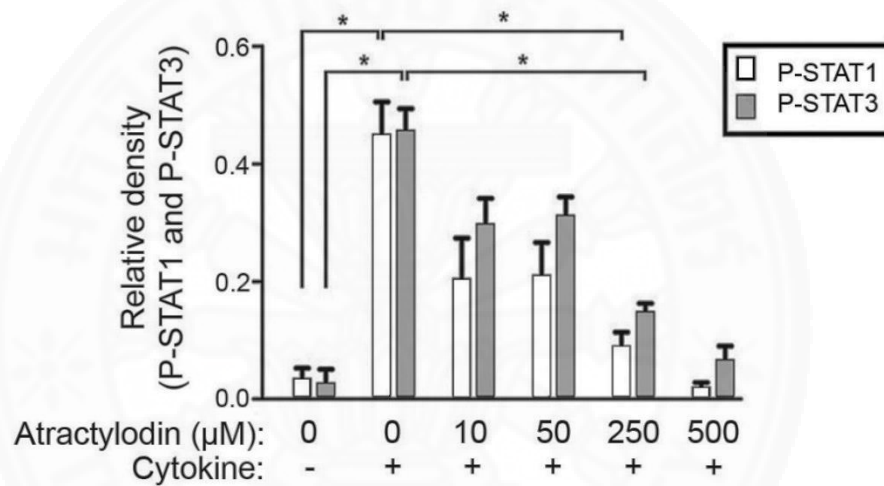


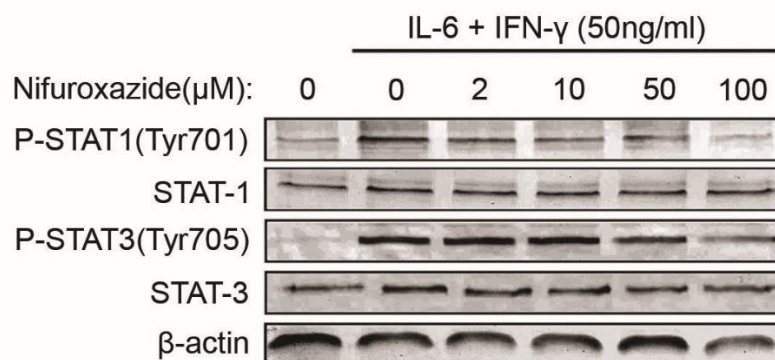
**Figure 5.9** Effect of atractylodin on cytokine-induced STAT1/3 activation in CL-6 cells.

The cells were serum starved overnight and pretreated with indicated concentrations of atractylodin for 2 h and further stimulated with cytokines (50 ng/mL IL-6 and 50 ng/mL IFN- $\gamma$ ) for 4 h. Whole cell extracts were prepared and 50  $\mu$ L aliquots were subjected to western blotting for accessing relative expression levels of STAT1 and STAT3 phosphorylation.  $\beta$ -actin was taken as loading control. (A) Representative immunoblots for expression of STAT1, STAT3, P-STAT1, P-STAT3, and  $\beta$ -actin in CL-6 cells. (B) Bar chart representing the mean $\pm$ SD of three independent experiments for densitometric values of protein expression ratios (P-STAT/STAT) of the levels of phosphorylated proteins to its corresponding total protein level.  $*p < 0.05$ .

### **5.1.9 Effect of nifuroxazide treatment on cytokine induced STAT1/3 phosphorylation in cholangiocarcinoma cells**

Nifuroxazide is a known inhibitor of STAT activation and displayed expected results inhibitory effect on STAT phosphorylation in CL-6 cells. Pretreatment of CL-6 cells with 0-100  $\mu$ M of nifuroxazide for 2 h and further stimulation with cytokine mixture for 4 h resulted in suppression of both STAT1 and STAT3 phosphorylation in a concentration-dependent manner. Densitometric analysis for immunoblots indicated that inhibitory effect was relatively more intense and significant ( $p=0.0001$ ) at the concentrations above 50  $\mu$ M compared to the similar concentration of atractylodin treatment in CL-6 cells. Treatment with nifuroxazide had no significant effect on the expression levels of total STAT1/3 or  $\beta$ -actin (Figure 5.10).

(A)



(B)

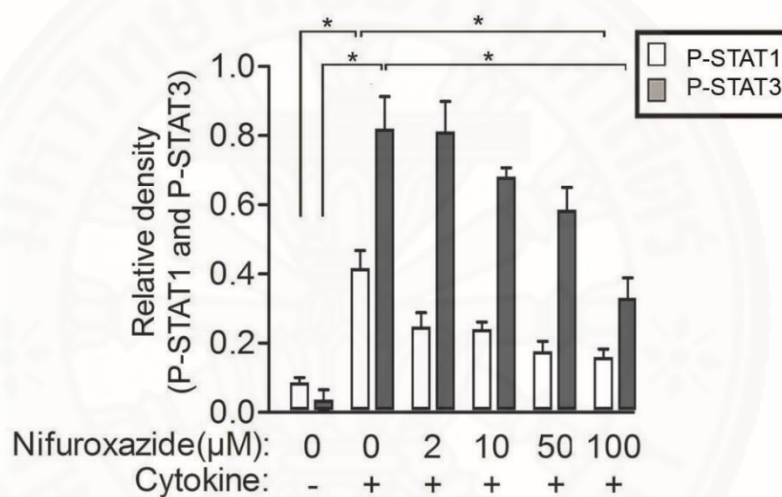


**Figure 5.10** Effect of nifuroxazide on cytokine-induced STAT1/3 activation in CL-6 cells. The cells were serum starved overnight and pretreated with designated concentrations of nifuroxazide for 2 h and further stimulated with cytokines (50 ng/mL IL-6 and 50 ng/mL IFN- $\gamma$ ) for 4 h. Whole cell extracts were prepared and 50  $\mu$ L aliquots were subjected to western blotting for accessing relative expression levels of STAT1 and STAT3 phosphorylation.  $\beta$ -actin was taken as loading control. (A) Representative immunoblots for expression of STAT1, STAT3, P-STAT1, P-STAT3 and  $\beta$ -actin in CL-6 cells. (B) Bar chart representing the mean $\pm$ SD of three independent experiments for densitometric values of protein expression ratios (P-STAT/STAT) of the levels of phosphorylated

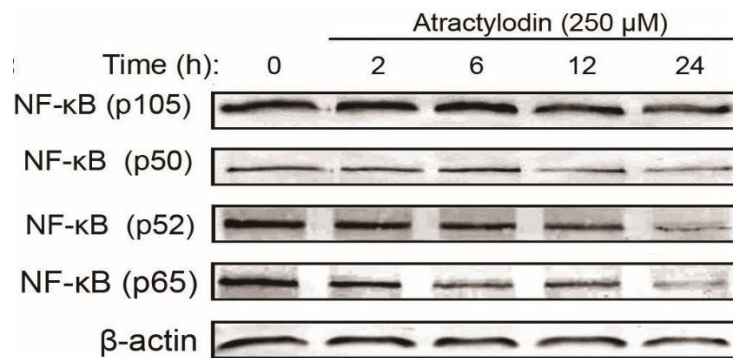
### 5.1.10 Evaluation of atracylodin treatment on aggregate expression of major NF- $\kappa$ B proteins in cholangiocarcinoma cells

Atracylodin exhibited promising potential for suppression of aggregate NF- $\kappa$ B proteins expression in CL-6 cells. CL-6 cells were treated with atracylodin (250  $\mu$ M) for 0-24 h and total cell lysates were collected at various time points and analyzed for the collective expression of key NF- $\kappa$ B proteins. Results from western blot analysis indicated that atracylodin treatment significantly downregulated the expression of key NF- $\kappa$ B proteins, particularly at 24 h for p50 ( $p=0.0001$ ), p52 ( $p=0.0032$ ) and p65 ( $p=0.0001$ ) in a time-dependent manner (Figure 5.11). The effect observed on the expression levels of p105 was however, only moderate. Atracylodin treatment had no effect on the expression levels of  $\beta$ -actin taken as loading control (Figure 5.11).

Similarly, the concentration-dependent effect of atracylodin on the expression of NF- $\kappa$ B protein was evaluated in the absence or presence of cytokine stimulation (Figure 5.12). IFN- $\gamma$  and IL-6 (50 ng/mL each), respectively, were used to stimulate STAT1 and STAT3 activation *via* phosphorylation in CL-6 cells. The CL-6 cells were pretreated with 0-500  $\mu$ M of atracylodin for 2 h and further stimulated with cytokine mixture for 4 h. Interestingly, results from western blot analysis showed that cytokine stimulation had little or no effect on the aggregate expression levels of NF- $\kappa$ B proteins ( $p \geq 0.38$ ). However, atracylodin treatment moderately downregulated the expression of all these key NF- $\kappa$ B proteins (*i.e.* NF- $\kappa$ B p105, p50, p52, and p65) as compared to untreated control. Pretreatment with atracylodin at concentrations higher or equal to 250  $\mu$ M produced significant inhibitory effect on the aggregate expression of NF- $\kappa$ B p105 ( $p=0.036$ ), p50 ( $p=0.006$ ), p52 ( $p=0.031$ ) and p65 ( $p=0.021$ ). Treatment with atracylodin had no significant effect on the expression of  $\beta$ -actin taken as loading control (Figure 5.12).



(A)



(B)

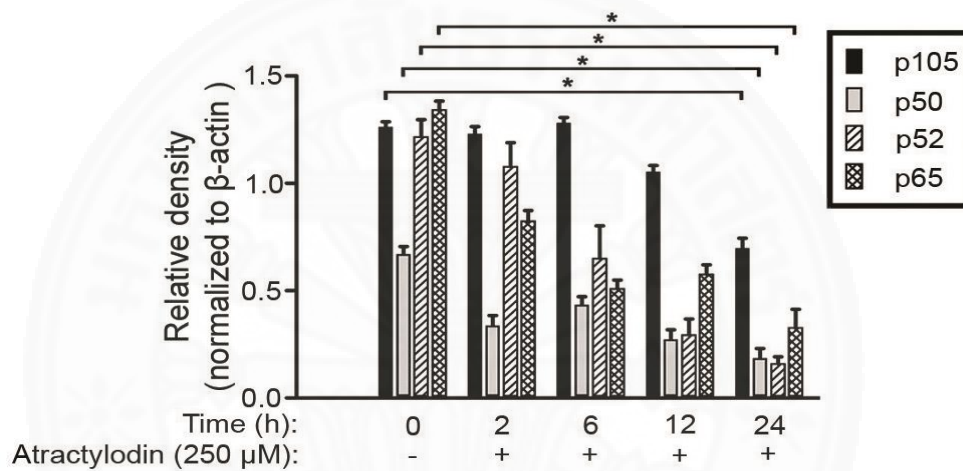
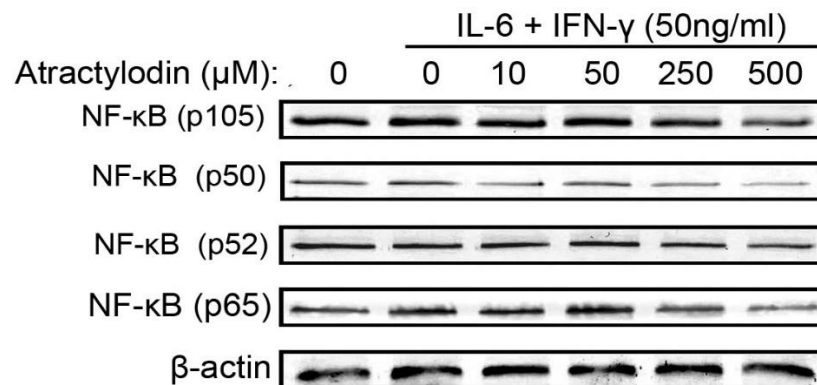


**Figure 5.11** Effect of atractylodin on aggregate expression of major NF-κB proteins in CL-6 cells. The cells were serum starved overnight and pretreated with designated concentrations of atractylodin for 0-24 h. Whole cell extracts were prepared and 50 μL aliquots were subjected to western blotting for accessing total expression levels of NF-κB p105, p50, p52, and p65. β-actin was taken as loading control. (A) Representative immunoblots for expression of NF-κB p105, p50, p52 and p65, and β-actin in CL-6 cells. (B) Bar chart representing the mean ± SD values of three independent experiments for densitometric values of protein expression normalized to β-actin.  $p < 0.05$  vs untreated control.



(A)



(B)

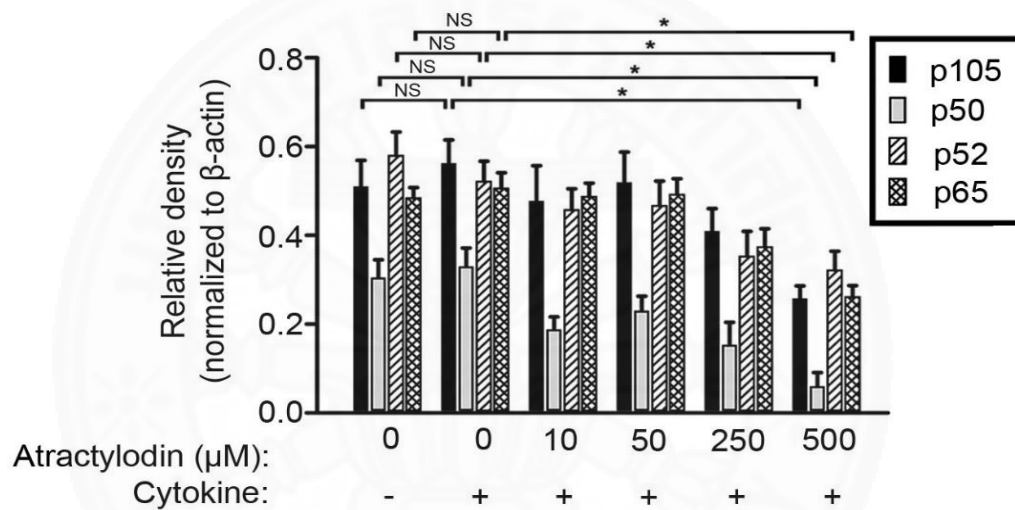


**Figure 5.12** Effect of atractylodin on aggregate expression of major NF-κB proteins in cytokine stimulated CL-6 cells. The cells were serum starved overnight and pretreated with designated concentrations of atractylodin for 2 h and further stimulated with cytokines (50 ng/mL IL-6 and 50 ng/mL IFN-γ) for 4 h. Whole cell extracts were prepared and 50 μL aliquots were subjected to western blotting for accessing total expression levels of NF-κB p105, p50, p52 and p65. β-actin was taken as loading control. (A) Representative immunoblots for expression of NF-κB p105, p50, p52 and p65, and β-actin in CL-6 cells. (B) Bar chart representing the mean±SD of three independent experiments for densitometric values of protein expression normalized to β-actin. \* $p < 0.05$  vs untreated control, NS = non-significant.

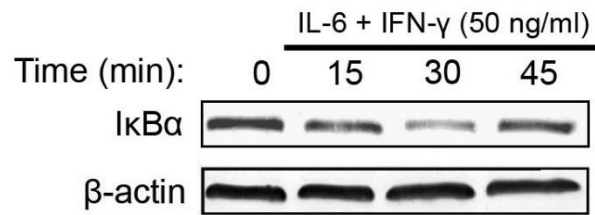
#### **5.1.11 Evaluation of the cytokine-induced I $\kappa$ B $\alpha$ degradation in cholangiocarcinoma cells**

Cytokine stimulation results in rapid phosphorylation-induced degradation of I $\kappa$ B $\alpha$  thus leading to activation of NF- $\kappa$ B transcription factor. CL-6 cells were stimulated with 50 ng/mL IL-6 and 50 ng/mL IFN- $\gamma$ . Total proteins were collected at 0, 15, 30 and 45 mins to access total I $\kappa$ B $\alpha$  expression. Results from immunoblots and corresponding densitometric analysis revealed rapid degradation of I $\kappa$ B $\alpha$  starting at 15 min and peaked at around 30 mins post-stimulation ( $p=0.002$ ) in the CL-6 cells as compared to baseline levels. The I $\kappa$ B $\alpha$  returned to its baseline levels within 45 mins ( $p = 0.317$ ) post stimulation (Figure 5.13). The cytokine stimulation had no effect on total expression of  $\beta$ -actin taken as loading control (Figure 5.13).

#### **5.1.12 Effect of atractylodin treatment on cytokine-induced I $\kappa$ B $\alpha$ degradation in cholangiocarcinoma cells**

Atractylodin treatment displayed promising suppressive effect on cytokine-induced I $\kappa$ B $\alpha$  degradation. CL-6 cells were pre-treated with atractylodin (250  $\mu$ M) for 2 h and further stimulated with 50 ng/mL IL-6 and 50 ng/mL IFN- $\gamma$  for 45 min. Total proteins were collected at 0, 15, 30 and 45 mins to access total I $\kappa$ B $\alpha$  expression. Results from immunoblots and corresponding densitometric analysis suggested that atractylodin-suppressed degradation of I $\kappa$ B $\alpha$ , which was normally achieved within 15-30 min post stimulation (Figure 5.13, 5.14). The reduction in I $\kappa$ B $\alpha$  degradation at 30 min had no significant effect ( $p=0.533$ ) and was almost comparable to baseline levels of I $\kappa$ B $\alpha$  indicating considerable suppressive effect of atractylodin on I $\kappa$ B $\alpha$  degradation. The atractylodin treatment had no significant effect on total expression of  $\beta$ -actin taken as loading control (Figure 5.14).

(A)



(B)

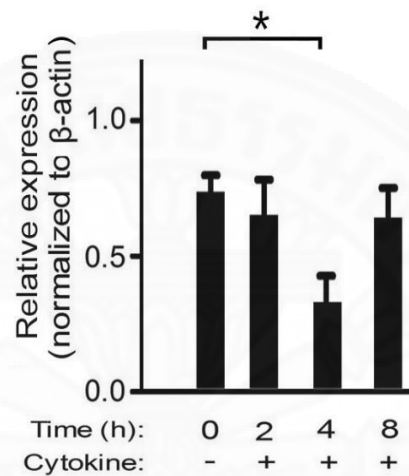
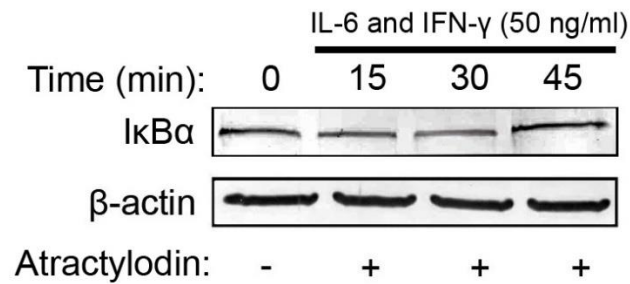


**Figure 5.13** Effect of cytokine stimulation on IkBα degradation in CL-6 cells. The cells were serum starved overnight and stimulated with cytokines (50 ng/mL IL-6 and 50 ng/mL IFN-γ) for designated time points. Whole cell extracts were prepared and 50 μL aliquots were subjected to western blotting for accessing total expression levels of IkBα. β-actin was taken as loading control. (A) Representative immunoblots for expression of IkBα and β-actin in CL-6 cells. (B) Bar chart representing the mean±SD of three independent experiments for densitometric values of protein expression normalized to β-actin. \* $p < 0.05$  vs untreated control.

(A)



(B)

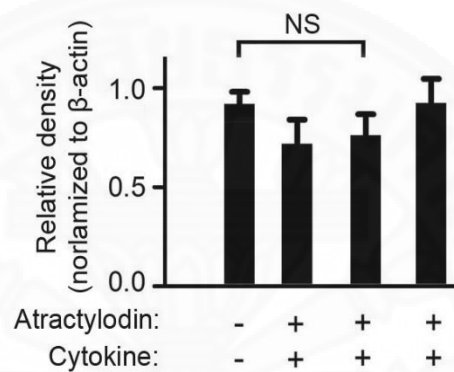
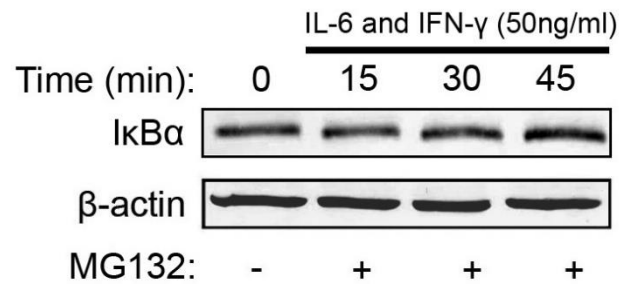


**Figure 5.14** Effect of atracyclodin on IkBα degradation in cytokine stimulated CL-6 cells. The cells were serum starved overnight and pretreated with atracyclodin (250 μM) for 2 h and further stimulated with cytokines (50 ng/mL IL-6 and 50 ng/mL IFN-γ) for designated time points. Whole cell extracts were prepared and 50 μL aliquots were subjected to western blotting for accessing total expression levels of IkBα. β-actin was taken as loading control. (A) Representative immunoblots for expression of IkBα and β-actin in CL-6 cells. (B) Bar chart representing the mean±SD of three independent experiments for densitometric values of protein expression normalized to β-actin. NS = non-significant.

### 5.1.13 Effect of MG132 treatment on cytokine-induced I $\kappa$ B $\alpha$ degradation in cholangiocarcinoma cells

MG132 is a known inhibitor of NF- $\kappa$ B activation through inhibition of proteasome-mediated degradation of I $\kappa$ B $\alpha$ . CL-6 cells were pre-treated with MG132 (25  $\mu$ M) for 2 h and further stimulated with IFN- $\gamma$  and IL-6 (50 ng/ml each) for 45 min. Total proteins were collected at 0, 15, 30 and 45 min to access total I $\kappa$ B $\alpha$  expression. As expected, results from western blots and corresponding densitometric analysis suggested that MG132 inhibited degradation of I $\kappa$ B $\alpha$ , which was normally achieved within 15-30 mins post-stimulation (Figure 5.13, 5.15). The inhibition of I $\kappa$ B $\alpha$  degradation at 15-30 min was clearly non-significant ( $p=0.644$ ) and equitable to baseline levels of I $\kappa$ B $\alpha$  expression indicating strong inhibitory effect of MG132 on I $\kappa$ B $\alpha$  degradation in CL-6 cells. The MG132 treatment had no effect on total expression of  $\beta$ -actin taken as loading control (Figure 5.15).

(A)



(B)

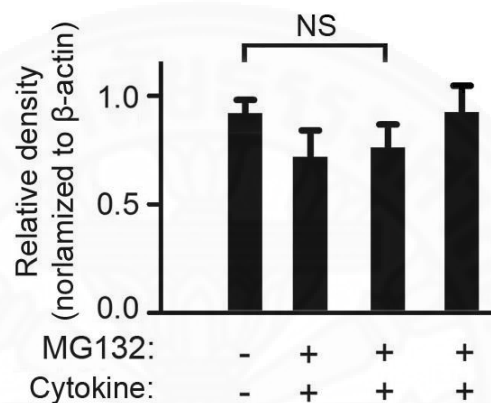


**Figure 5.15** Effect of MG132 on IkBα degradation in cytokine stimulated CL-6 cells. The cells were serum starved overnight and pretreated with MG132 (25 μM) for 2 h and further stimulated with cytokines (IFN-γ and IL-6, 50 ng/mL each) for designated time points. Whole cell extracts were prepared and 50 μL aliquots were subjected to western blotting for accessing total expression levels of IkBα. β-actin was taken as loading control. (A) Representative immunoblots for expression of IkBα and β-actin in CL-6 cells. (B) Bar chart representing the mean±SD of three independent experiments for densitometric values of protein expression normalized to β-actin. NS = non-significant.

#### **5.1.14 Evaluation of atracylodin treatment on ICAM-1 and iNOS mRNA expression in cholangiocarcinoma cells**

ICAM1 and iNOS are generally associated with STAT activation and are induced by various cytokines including IL-6. Atracylodin exhibited promising suppressive effect on mRNA expression of both ICAM-1 and iNOS in CL-6 cells.

CL-6 cells were pretreated with atracylodin (250  $\mu$ M) for 2 h and further stimulated with IFN- $\gamma$  and IL-6 (50 ng/ml each) for additional 4 h. Total RNA was extracted, converted to cDNA and analyzed for relative mRNA expression of target gene. The GAPDH was taken as internal control gene. Results from real time PCR indicates that cytokine stimulation significantly increased ICAM-1 ( $p=0.02$ ) and iNOS ( $p=0.027$ ) mRNA expression in CL-6 cells. In contrast, atracylodin pretreatment resulted in suppression of both ICAM-1 ( $p=0.0036$ ) and iNOS ( $p=0.0012$ ) mRNA expression in cytokine-stimulated CL-6 cells (Figure 5.16). In addition, the effect of nifuroxazide, a known STAT1/3 selective inhibitor, was also evaluated for its inhibitory effect on ICAM-1 and iNOS mRNA expression. As expected, nifuroxazide pretreatment resulted in significant suppression of both ICAM-1 ( $p=0.0077$ ) and iNOS ( $p=0.0012$ ) mRNA expression in cytokine-stimulated CL-6 cells (Figure 5.17).

#### **5.1.15 Evaluation of atracylodin treatment on mRNA expression of tumor associated genes in cholangiocarcinoma cells**

Atracylodin exhibited promising suppressive effect on mRNA expression of major tumor associated genes, namely VEGF-A and MCL-1 in CL-6 cells. The CL-6 cells were cultured for 24 h in the presence or absence of atracylodin (250  $\mu$ M) and total mRNA was extracted, converted to cDNA for relative gene expression using Real-time PCR assay. Atracylodin treatment significantly decreased mRNA expression of VEGF-A ( $p=0.015$ ) and MCL-1 ( $p=0.037$ ) in CL-6 cells (Figure 5.18). The GAPDH was taken as internal control gene.

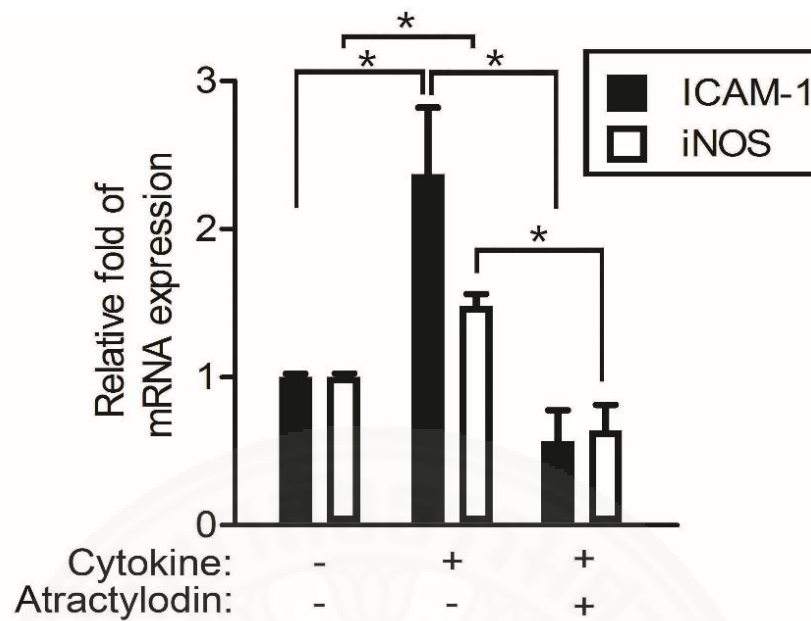


**Figure 5.16** Effect of atractylodin on ICAM-1 and iNOS mRNA expression in cytokine stimulated CL-6 cells. The cells were cultured in a 6-well plate and pretreated with atractylodin (250  $\mu$ M) for 2 h and stimulated with interleukin-6 (50 ng/mL) for further 4 h. Total RNA was extracted and converted to cDNA. Real time PCR as conducted to access relative expression of ICAM and iNOS mRNA. GAPDH was taken as internal control. Bar chart represents relative expression of ICAM and iNOS mRNA expression normalized to GAPDH. All data are expressed as mean $\pm$ SEM and are representative of three independent experiments. \* $p$ <0.05. ICAM-1= intercellular adhesion molecule 1; iNOS = inducible nitric oxide synthase, GAPDH = glyceraldehyde 3-phosphate dehydrogenase.



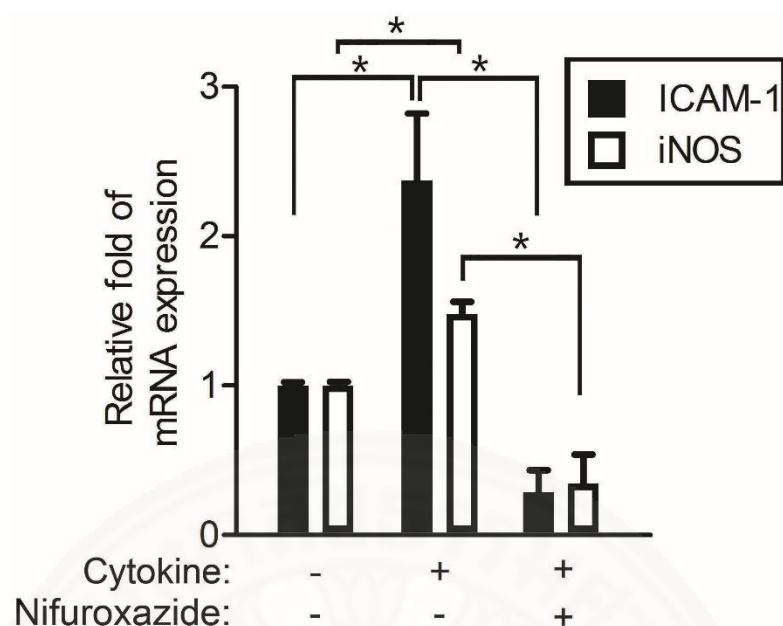


**Figure 5.17** Effect of nifuroxazide on ICAM-1 and iNOS mRNA expression in cytokine stimulated CL-6 cells. The cells were cultured in a 6-well plate and pretreated with nifuroxazide (50  $\mu$ M) for 2 h and stimulated with interleukin-6 (50 ng/mL) for further 4 h. Total RNA was extracted and converted to cDNA. Real time PCR as conducted to access relative expression of ICAM and iNOS mRNA. GAPDH was taken as internal control. Bar chart represents relative expression of ICAM and iNOS mRNA expression normalized to GAPDH. All data are expressed as mean $\pm$ SEM values and are representative of three independent experiments.  $p < 0.05$ . ICAM-1= intercellular adhesion molecule 1, iNOS= inducible nitric oxide synthase, GAPDH = glyceraldehyde 3-phosphate dehydrogenase.

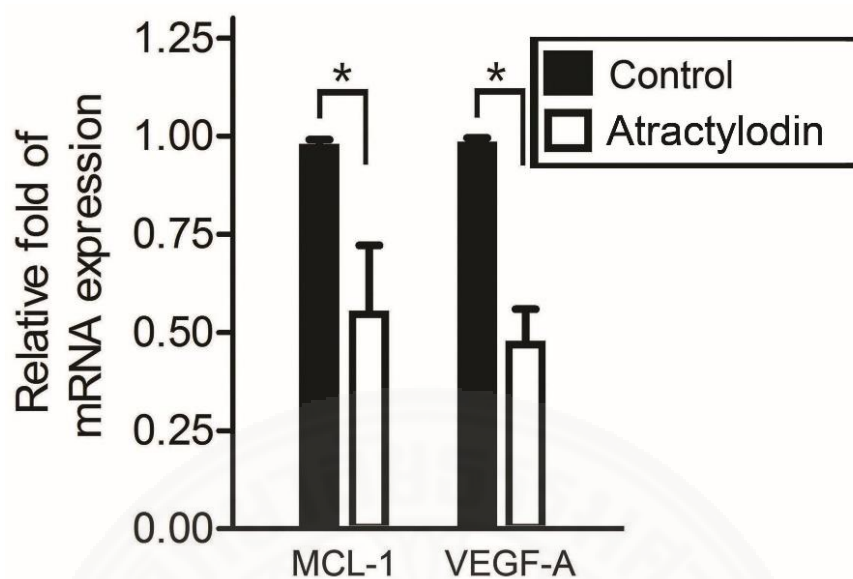


**Figure 5.18** Effect of atractylodin treatment on mRNA expression of tumor associated genes in CL-6 cells. The cells were cultured in a 6-well plate and treated with atractylodin (250  $\mu$ M) for 24 h. Total RNA was extracted and converted to cDNA. Real time PCR was conducted to access relative expression of MCL-1 and VEGF-A. GAPDH was taken as internal control. Bar chart represents relative expression of indicated genes normalized to GADPH. All data are expressed as mean $\pm$ SEM values and are representative of three independent experiments.  $p < 0.05$ . MCL-1= induced myeloid leukemia cell differentiation protein, VEGF-A= vascular endothelial growth factor A, GAPDH= glyceraldehyde 3-phosphate dehydrogenase.

## 5.2 Anti-cholangiocarcinoma effect of $\beta$ -eudesmol

### 5.2.1 Cytotoxicity of $\beta$ -eudesmol in cholangiocarcinoma cells

The  $\beta$ -eudesmol exhibited promising cytotoxic activity against CL-6 cells with  $IC_{50}$  of  $166.75 \pm 3.69$  (mean $\pm$ SEM)  $\mu$ M. Potency of activity exhibited by  $\beta$ -eudesmol was about 3-fold of the standard drug 5-FU ( $IC_{50}$  of  $670.06 \pm 28.44$   $\mu$ M). Interestingly, the  $\beta$ -eudesmol treatment was relatively less toxic to normal control cell line OUMS with observed  $IC_{50}$  values for  $\beta$ -eudesmol and 5-FU of  $240.01 \pm 16.54$   $\mu$ M and  $1,010.44 \pm 8.73$   $\mu$ M respectively. The selectivity index (SI) values for  $\beta$ -eudesmol and 5-FU on CL-6 cells were 1.5 and 1.5 respectively. The  $IC_{50}$  and SI values for  $\beta$ -eudesmol and 5-FU are presented in Table 5.2.

**TABLE 5.2**  $IC_{50}$  and SI values for  $\beta$ -eudesmol

No.	Cell Line	Compound	$IC_{50} \pm SEM$ ( $\mu$ M)	Median $\pm$ Range ( $\mu$ M)	Inter Quartile Range	Specificity Index (SI)
<b>1</b>	CL-6	$\beta$ -eudesmol	$166.75 \pm 3.69$	$169.92 \pm 7.33$	3.68	1.5
		5-Flurouracil	$680.06 \pm 18.44$	$687.75 \pm 34.72$	17.36	1.5
<b>2</b>	OUMS	$\beta$ -eudesmol	$240.01 \pm 16.54$	$231 \pm 32.21$	16.15	1.0
		5-Flurouracil	$1010.44 \pm 8.73$	$1013.13 \pm 16.71$	8.36	1.0

Data are represented as mean $\pm$ SEM values of three independent experiments done in triplicate.  $IC_{50}$ =Half maximal inhibitory concentration; SI= selectivity index.

In addition to atractylodin and  $\beta$ -eudesmol, as a supplementary observation, the cytotoxicity against CL-6 cells of specific pathway or enzyme inhibitors used in our experiments was also investigated. The high  $IC_{50}$  concentration of inhibitors required for obtaining half of maximum growth indicates strong survival capability of CL-6 cells. The results for cytotoxicity of pathway inhibitors are summarized in Table 5.3.

**TABLE 5.3  $IC_{50}$  values for specific pathway inhibitors**

No.	Cell Line	Compound	$IC_{50} \pm SEM$ ( $\mu M$ )	Median $\pm$ Range ( $\mu M$ )	Inter Quartile Range	Target Pathway
1	CL-6	Nifuroxazide	$49.17 \pm 2.78$	$48.04 \pm 5.51$	2.76	JAK-STAT
2	CL-6	ZN(II)PPIX	$130.32 \pm 3.14$	$132.22 \pm 5.71$	2.86	HO-1
3	CL-6	MG132	$22.34 \pm 2.23$	$22.97 \pm 5.56$	2.77	NF- $\kappa$ B

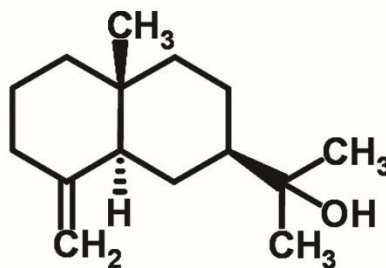
Data are representative of three independent experiments done in triplicate. Half maximal inhibitory concentration ( $IC_{50}$ ). HO-1 = Heme oxygenase-1; ZN(II)PPIX=Zinc protoporphyrin IX.

### **5.2.2 Morphological evidence of $\beta$ -eudesmol-induced cell death in cholangiocarcinoma cells**

Results from light microscopy for morphological investigation indicated concentration-dependent cytotoxicity of  $\beta$ -eudesmol on CL-6 cell growth.  $\beta$ -eudesmol treatment at concentration of 180  $\mu$ M led to distorted morphology of the CL-6 cells with visible signs of cell debris and floating dead cells. Concentrations of  $\beta$ -eudesmol above 180  $\mu$ M caused clearly noticeable cell death with extensive cell debris in  $\beta$ -eudesmol-treated cells as compared to untreated control (Figure 5.19). In contrast, the observable cytotoxic effect on the OUMS cell was relatively less prominent as compared to CL-6 cells for similar concentrations of  $\beta$ -eudesmol. Even at  $\beta$ -eudesmol concentrations above 180  $\mu$ M only minor visible signs of cell death in OUMS cell culture was observed (Figure 5.19). The results indicated selective cytotoxicity of  $\beta$ -eudesmol towards CL-6 cells.

In order to investigate the effect of  $\beta$ -eudesmol treatment on nuclear integrity for visible traits of apoptosis, the fluorescent staining was employed to assess nuclear morphology. To obtain contrasting visual effects of  $\beta$ -eudesmol treatment on nuclear morphology, the cells were treated with approximate  $IC_{50}$  values for  $\beta$ -eudesmol. The results from DAPI staining indicated that CL-6 cell culture in absence of  $\beta$ -eudesmol treatment resulted in normal growth as revealed by its sound nuclear morphology at 0 and 24 h post-incubation condition (Figure 5.20). In contrast, cells treated with  $\beta$ -eudesmol noticeably displayed substantial amount of growth inhibition and signs of nuclear degradation at 24 h post incubation (Figure 5.20).

(A)



(B)

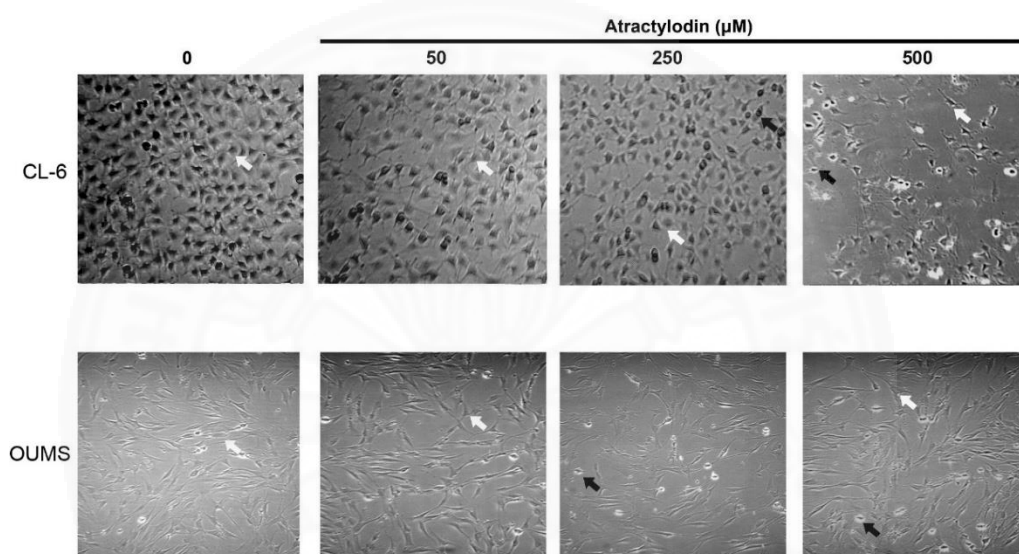


**Figure 5.19** Chemical structure of  $\beta$ -eudesmol and the effect of  $\beta$ -eudesmol treatment on CL-6 and OUMS cells. (A) Chemical structure of  $\beta$ -eudesmol. (B) CL-6 or OUMS cells were treated with designated concentrations of  $\beta$ -eudesmol. After 24 h, cell morphology was examined under the light microscopy. The images shown are representative of three independent experiments. White arrow indicates live cells. Dark arrow indicates dead cells.

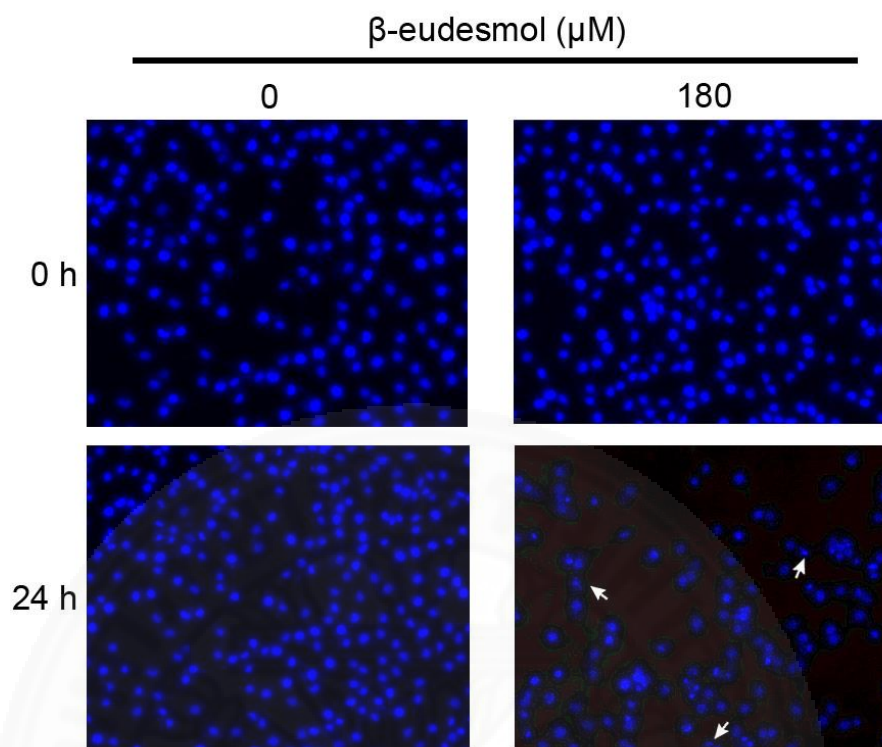


**Figure 5.20** Effect of  $\beta$ -eudesmol on nuclear morphology of CL-6 cells. The cells were allowed to grow overnight in the presence or absence of  $\beta$ -eudesmol (180  $\mu$ M) treatment. The cells were fixed using paraformaldehyde and stained using DAPI at 0 and 24 h time point to visualize nuclear morphology for signs of apoptosis. All images are representative of three different experiments. *White arrow* indicates the cells with signs of degenerative nucleus.

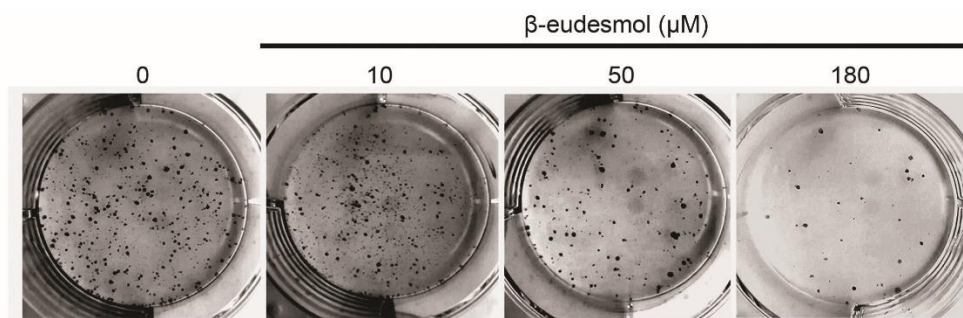
### 5.2.3 Evaluation of $\beta$ -eudesmol treatment on colony forming ability of cholangiocarcinoma cells

The colony forming potential measures regenerative ability of a single cell to form colony and is measured in term of CFU. Results from colony formation assay indicated that in the absence of  $\beta$ -eudesmol treatment, CL-6 cells underwent unhindered proliferation by forming large number of CFUs. In contrast,  $\beta$ -eudesmol treatment above 10  $\mu$ M resulted in significant ( $p=0.002$ ) concentration-dependent inhibition on colony forming ability of CL-6 cells as compared to control.  $\beta$ -eudesmol at the concentrations above 50  $\mu$ M markedly decreased CFU of CL-6 cells (Figure 5.21).

Additionally, in order to compare the effect of other standard drug to  $\beta$ -eudesmol, the effects of 5-FU and nifuroxazide on colony forming ability of CL-6 cells were also investigated. The results indicated that for the corresponding  $IC_{50}$  concentrations, along with  $\beta$ -eudesmol, the 5-FU ( $p=0.006$ ) and nifuroxazide ( $p=0.003$ ) both significantly inhibited the colony forming ability of CL-6 cells as compared untreated control (Figure 5.22). Interestingly,  $\beta$ -eudesmol was considerably more efficient ( $p=0.0001$ ) in inhibiting CFU of CL-6 as compared to 5-FU and nifuroxazide.



(A)



(B)

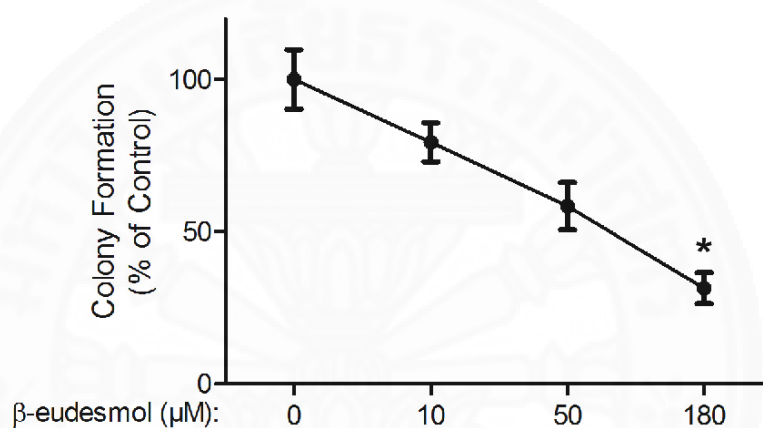
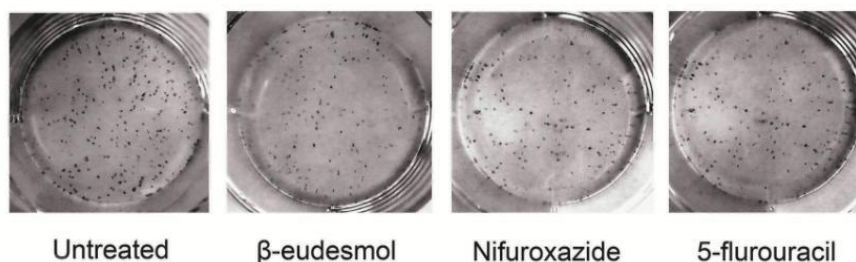


**Figure 5.21** Effect of  $\beta$ -eudesmol on colony forming ability of CL-6 cells. After 24 h of treatment of indicated concentrations of  $\beta$ -eudesmol the CL-6 cells were collected after trypsinization, seeded (300 cells/well) in a 6-well plate and further incubated for additional 6-10 days. When the colonies appeared with at least 50 cells, the cells were fixed with ethanol then stained with methylene blue to visualize the colonies. (A) Effect of  $\beta$ -eudesmol on colony formation in CL-6 cells. (B) Line chart representing the effect of  $\beta$ -eudesmol on colony formation as percentage of control. Data are presented as mean  $\pm$  SD and are representative of three independent experiments.  $*p < 0.05$  vs untreated control.

(A)



(B)

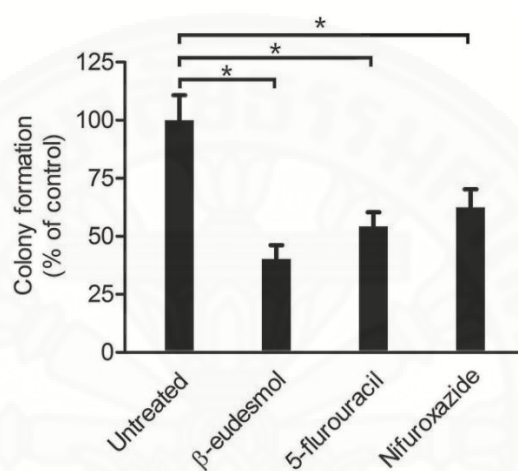
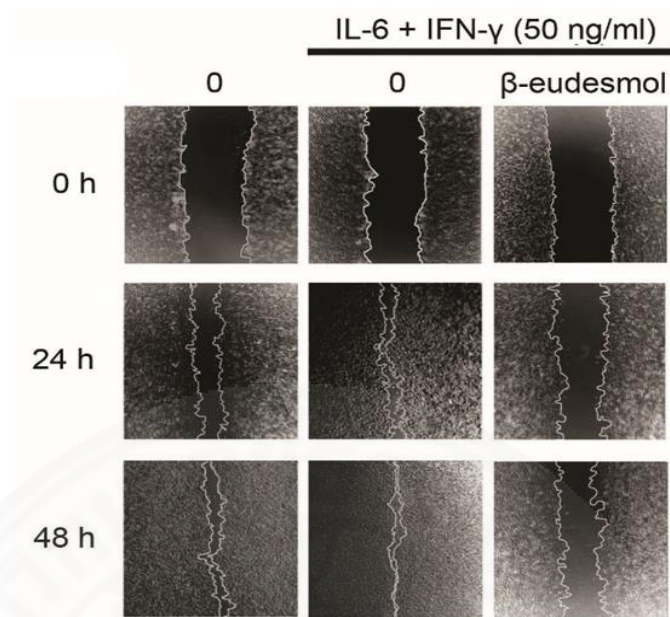


**Figure 5.22** Effect of nifuroxazide and 5-fluorouracil on colony forming ability of CL-6 cells. After 24 h of treatment of  $\beta$ -eudesmol (180  $\mu$ M), nifuroxazide (50  $\mu$ M) or 5-fluorouracil (700  $\mu$ M), the CL-6 cells were collected after trypsinization, seeded (300 cells/well) onto a 6-well plate and further incubated for additional 6-10 days. CL-6 cells were seeded (300 cells/well) onto a 6-well plate. When the colonies appeared with at least 50 cells, the cells were fixed with ethanol then stained with methylene blue to visualize the colonies. (A) Effect of  $\beta$ -eudesmol (180  $\mu$ M), nifuroxazide (50  $\mu$ M), or 5-fluorouracil (700  $\mu$ M) on colony formation in CL-6 cells. (B) Line chart representing the effect of corresponding compounds on colony formation as percentage of control.  $*p < 0.05$  vs untreated control. Data are presented as mean  $\pm$  SD and are representative of three independent experiments.

#### 5.2.4 Evaluation of $\beta$ -eudesmol treatment on wound healing ability of cholangiocarcinoma cells

Wound healing assay enables *in vitro* study of direction cell migration potential. Results from wound healing assay indicated promising ability of  $\beta$ -eudesmol to suppress the *in vitro* wound healing ability of CL-6 cells. IL-6 and IFN- $\gamma$  (50 ng/ml each) were used to stimulate the CL-6 cells. The absence of  $\beta$ -eudesmol or cytokine treatment resulted in rapid wound closure in CL-6 cells within 48 h of incubation. In the absence of  $\beta$ -eudesmol treatment, relatively similar and non significant ( $p=0.163$ ) extent of wound closure was observed in both cytokine stimulated and unstimulated cells for the respective time period of 24 and 48 h. In contrary,  $\beta$ -eudesmol (180  $\mu$ M) pretreatment significantly decreased the wound healing ability at 24 ( $p =0.001$ ) and 48 h ( $p =0.001$ ) of incubation (Figure 5.23). The corresponding bar chart representing wound closure relative to untreated control clearly suggested significant inhibitory effect of  $\beta$ -eudesmol on wound closure as compared to both cytokine treated and untreated control groups (Figure 5.23).

(A)



(B)

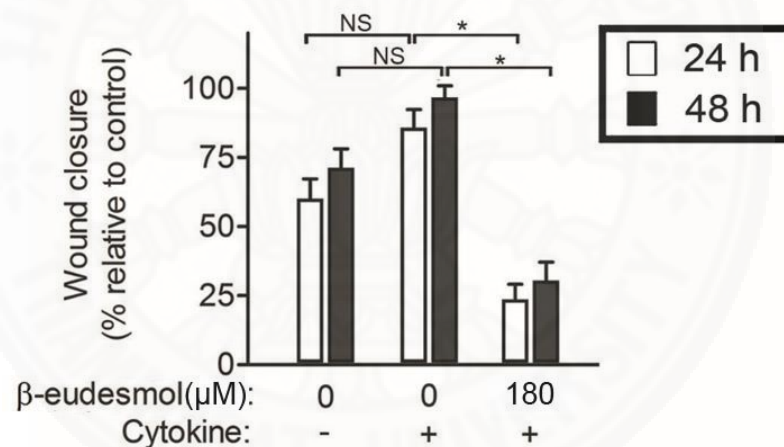


**Figure 5.23** Effect of  $\beta$ -eudesmol on wound healing ability of CL-6 cells. The cells were cultured in 24 well plate and at near confluency, serum starved for 18 h, followed by creation of wound and subsequent treatment of media alone, media containing cytokines (50 ng/mL IL-6 and 50 ng/mL IFN- $\gamma$ ) along with  $\beta$ -eudesmol (180  $\mu$ M) for 48 h. Wound closure was measured at 0, 24 and 48 h. (A) Effect of  $\beta$ -eudesmol on wound healing. (B) Bar diagram representing the effect of  $\beta$ -eudesmol on wound healing. Data are presented as mean $\pm$ SD and are representative of three independent experiments. \* $p$  < 0.05. IL-6 = Interlukin-6, IFN- $\gamma$  = Interferon- $\gamma$ , NS= non-significant.

### 5.2.5 Evaluation of $\beta$ -eudesmol treatment on production of heme oxygenase-1 in cholangiocarcinoma cells

The expression of cytoprotective enzyme such as HO-1 is vital for maintaining cytoprotective activity of cells. Results from western blot analysis revealed considerable amount of baseline expression of HO-1 enzyme in CL-6 cells (Figure 5.24). The inhibitory effect of  $\beta$ -eudesmol treatment on HO-1 expression was minimal but significant ( $p=0.01$ ) from 6 h of treatment. In contrast, western blot analysis and corresponding densitometry bar chart indicated that  $\beta$ -eudesmol treatment significantly inhibited ( $p=0.0001$ ) the production of HO-1 enzyme at 24 h post treatment as compared to untreated control (Figure 5.24).

### 5.2.6 Evaluation of $\beta$ -eudesmol treatment on the production of NQO1 in cholangiocarcinoma cells

The expression of NQO1 is an important cytoprotective activity of cells. Results from western blot analysis revealed considerable amount of baseline expression of NQO1 enzyme in CL-6 cells (Figure 5.25). The inhibitory effect of  $\beta$ -eudesmol (180  $\mu$ M) treatment was hardly noticeable and non significant ( $p=0.081$ ) compared to control within 6 h of treatment. However, immunoblot analysis and corresponding densitometric bar chart indicated significant inhibition ( $p=0.001$ ) of NQO1 enzyme production by  $\beta$ -eudesmol treatment at 24 h post treatment as compared to untreated control (Figure 5.25).

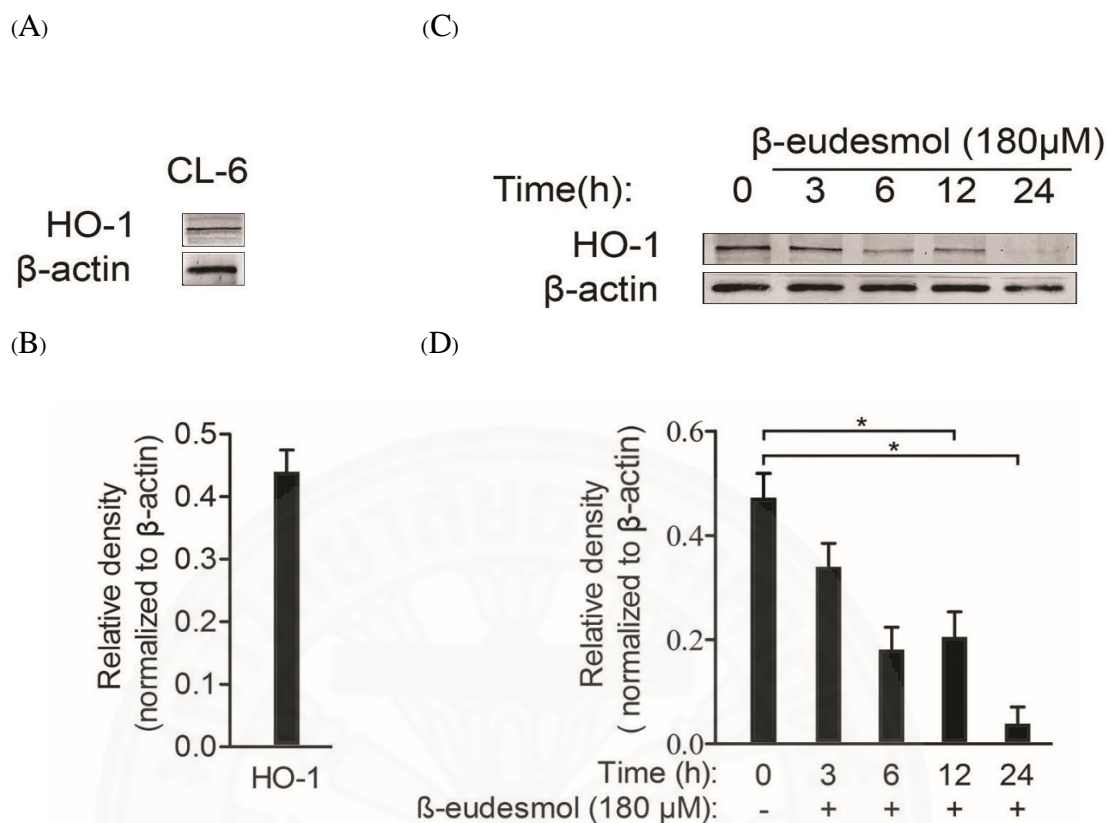


**Figure 5.24** Effect of  $\beta$ -eudesmol on HO-1 expression in CL-6 cells. The cells were serum starved for overnight, pretreated with designated concentrations of  $\beta$ -eudesmol for 0-24 h. Whole cell extracts were prepared and 50  $\mu$ L aliquots of cell lysates were subjected to western blotting for HO-1 protein expression.  $\beta$ -actin was taken as loading control. (A) Baseline expression of HO-1 in CL-6 cells. (B) Graph representing the mean $\pm$ SD of three independent experiments for densitometric values of baseline HO-1 expression normalized to  $\beta$ -actin. (C) Effect of  $\beta$ -eudesmol treatment on HO-1 production in CL-6 cells. (D) Graph representing the mean $\pm$ SD of three independent experiments for densitometric values of protein expression normalized to  $\beta$ -actin. \* $p < 0.05$  vs untreated control. HO-1 = Heme oxygenase-1.

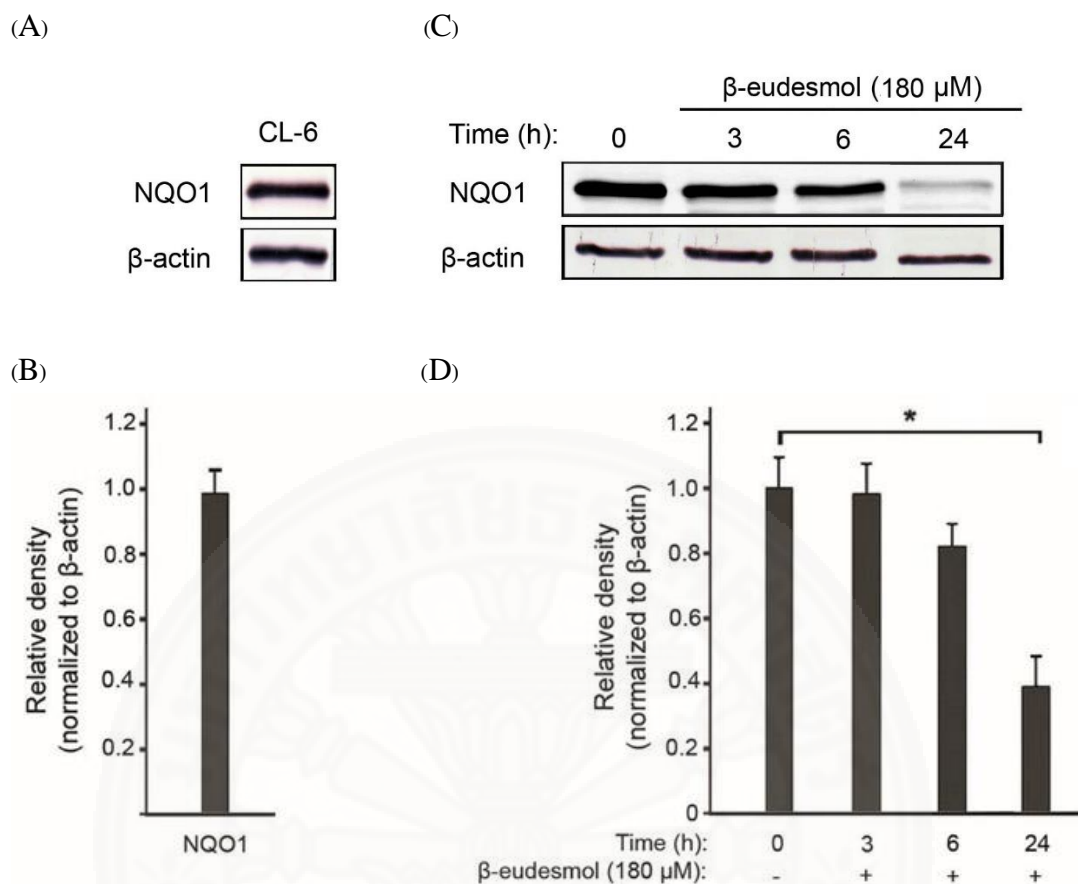


**Figure 5.25** Effect of  $\beta$ -eudesmol on NQO1 expression in CL-6 cells. The cells were serum starved for overnight, pretreated with designated concentrations of  $\beta$ -eudesmol for 0-24 h. Whole cell extracts were prepared and 50  $\mu$ L aliquots of cell lysates were subjected to western blotting for NQO1 protein expression.  $\beta$ -actin was taken as loading control. (A) Baseline expression of NQO1 in CL-6 cells. (B) Graph representing the mean $\pm$ SD of three independent experiments for densitometric values of baseline NQO1 expression normalized to  $\beta$ -actin. (C) Effect of atractylodin treatment on NQO1 production in CL-6 cells. (D) Graph representing the mean $\pm$ SD of three independent experiments for densitometric values of protein expression normalized to  $\beta$ -actin. \* $p$ <0.05 vs untreated control. NQO1 = NAD(P)H Quinone dehydrogenase 1.

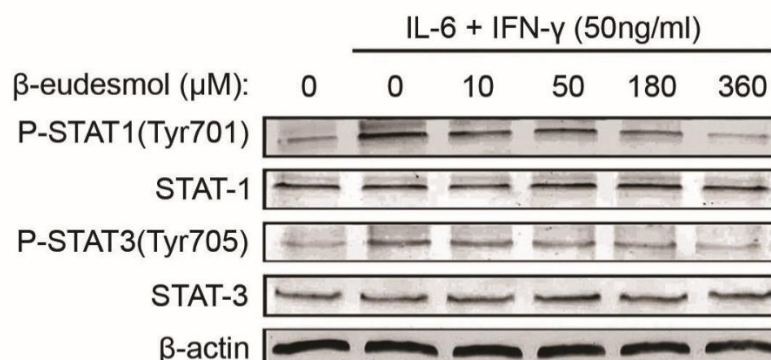


### **5.2.7 Effect of $\beta$ -eudesmol on cytokine induced STAT1/3 phosphorylation in cholangiocarcinoma cells**

$\beta$ -eudesmol exhibited promising potential for concentration-dependent suppression of STAT1/3 activation in CL-6 cells. Pretreatment of CL-6 cells with 0-360  $\mu$ M of  $\beta$ -eudesmol for 2 h followed by stimulation with cytokine mixture for additional 4 h resulted in suppression of both STAT1 and STAT3 phosphorylation in a concentration-dependent manner (Figure 5.26). Immunoblots and corresponding densitometric analysis of protein expression suggested that  $\beta$ -eudesmol at concentrations higher than 50  $\mu$ M produced significant inhibitory effect on activation of both STAT1 ( $p=0.002$ ) and STAT3 ( $p=0.0045$ ) as compared to cytokine-treated control. In the absence of cytokine stimulation, little or no baseline level of STAT1/3 phosphorylation occurred.  $\beta$ -eudesmol treatment had no effect on the aggregate expression of STAT1, STAT3, or  $\beta$ -actin in CL-6 cells (Figure 5.26).



(A)



(B)

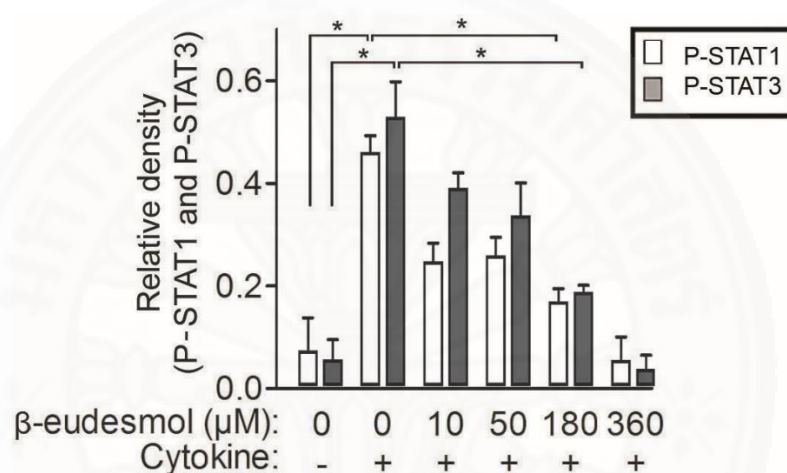


**Figure 5.26** Effect of  $\beta$ -eudesmol on cytokine-induced STAT1/3 activation in CL-6 cells.

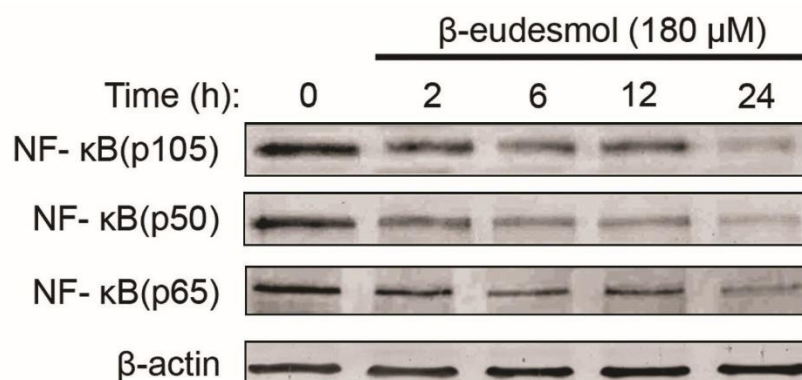
The cells were serum starved overnight and pretreated with indicated concentration of  $\beta$ -eudesmol for 2 h and further stimulated with cytokines (50 ng/mL IL-6 and 50 ng/mL IFN- $\gamma$ ) for 4 h. Whole cell extracts were prepared and 50  $\mu$ L aliquots were subjected to western blotting for accessing relative expression levels of STAT1 and STAT3 phosphorylation.  $\beta$ -actin was taken as loading control. (A) Representative immunoblots for expression of STAT1, STAT3, P-STAT1, P-STAT3, and  $\beta$ -actin in CL-6 cells. (B) Bar chart representing the mean  $\pm$  SD of three independent experiments for densitometric values of protein expression ratios (P-STAT/STAT) of the levels of phosphorylated proteins to its corresponding total protein level.  $*p < 0.05$ . IL-6 = Interlukin-6, IFN- $\gamma$  = Interferon- $\gamma$ .

### 5.2.8 Evaluation of $\beta$ -eudesmol treatment on aggregate expression of major NF- $\kappa$ B proteins in cholangiocarcinoma cells

$\beta$ -eudesmol showed considerable potential for suppression of aggregate NF- $\kappa$ B proteins expression in CL-6 cells. The cells were treated with 180  $\mu$ M of  $\beta$ -eudesmol for 0-24 h and total cell lysates were collected at various time points and analyzed for the expression of key NF- $\kappa$ B proteins. Results from immunoblots and corresponding densitometric analysis indicated that  $\beta$ -eudesmol treatment significantly decreased the expression of key NF- $\kappa$ B proteins at 24 h, particularly, p105 ( $p=0.0001$ ), p50 ( $p=0.0046$ ), and p65 ( $p=0.0001$ ), in a time-dependent manner (Figure 5.27).  $\beta$ -eudesmol treatment had no effect observable effect on expression levels of  $\beta$ -actin taken as loading control (Figure 5.27).

Similarly, the concentration-dependent effect of  $\beta$ -eudesmol treatment on the expression of NF- $\kappa$ B protein was analyzed in the absence or presence of cytokine stimulation (Figure 5.28). IFN- $\gamma$  and IL-6 (50 ng/ml each) was respectively, used to induce STAT1 and STAT3 activation *via* phosphorylation in CL-6 cells. CL-6 cells were pretreated with 0-360  $\mu$ M of  $\beta$ -eudesmol for 2 h and further stimulated with cytokine mixture for 4 h. Remarkably, results from immunoblot analysis showed that cytokine stimulation had no significant effect ( $p \geq 0.268$ ) on the aggregate expression levels of major NF- $\kappa$ B proteins. However,  $\beta$ -eudesmol treatment moderately downregulated the expression of all key NF- $\kappa$ B proteins (*i.e.* NF- $\kappa$ B p105, p50, and p65) as compared to untreated control. Pretreatment with  $\beta$ -eudesmol at concentrations 180  $\mu$ M resulted in marked decline in expression of all NF- $\kappa$ B p105 ( $p=0.027$ ), p50 ( $p=0.028$ ), and p65 ( $p=0.002$ ) proteins under investigation as compared to untreated control. Treatment with  $\beta$ -eudesmol had no significant effect on expression of  $\beta$ -actin taken as loading control (Figure 5.28).

(A)



(B)

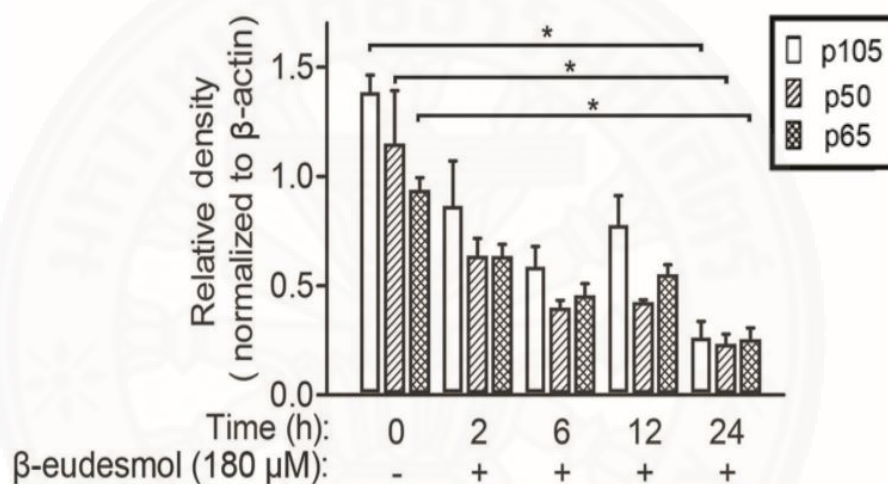
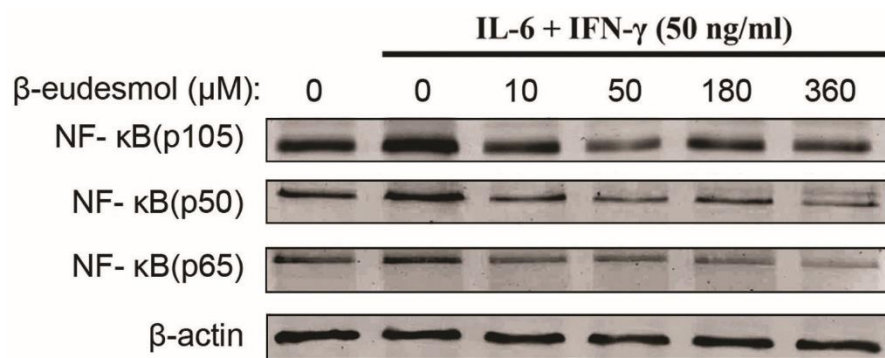


**Figure 5.27** Effect of  $\beta$ -eudesmol on aggregate expression of major NF- $\kappa$ B protein in CL-6 cells. The cells were serum starved overnight and pretreated with designated concentrations of  $\beta$ -eudesmol for 0-24 h. Whole cell extracts were prepared and 50  $\mu$ L aliquots were subjected to western blotting for accessing total expression levels of NF- $\kappa$ B p105, p50, p52, and p65.  $\beta$ -actin was taken as loading control. (A) Representative immunoblots for expression of NF- $\kappa$ B p105, p50, p65 and  $\beta$ -actin in CL-6 cells. (B) Bar chart representing the mean $\pm$ SD of three independent experiments for densitometric values of protein expression normalized to  $\beta$ -actin.  $*p < 0.05$  vs untreated control.

(A)



(B)

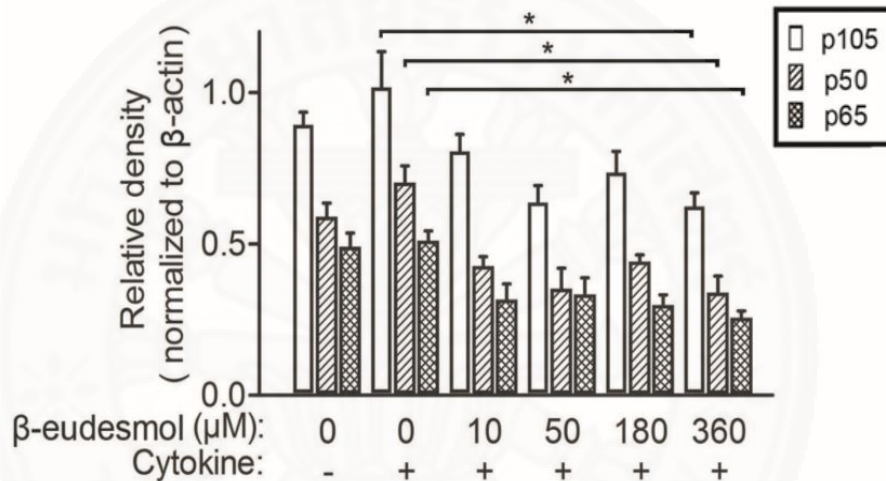
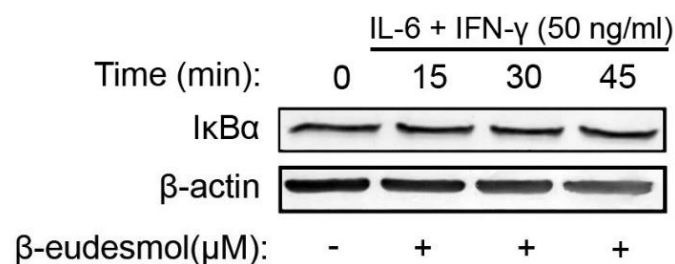


**Figure 5.28** Effect of  $\beta$ -eudesmol on aggregate expression of major NF- $\kappa$ B proteins in cytokine stimulated CL-6 cells. The cells were serum starved overnight and pretreated with designated concentrations of  $\beta$ -eudesmol for 2 h and further stimulated with cytokines (50 ng/mL IL-6 and 50 ng/mL IFN- $\gamma$ ) for 4 h. Whole cell extracts were prepared and 50  $\mu$ L aliquots were subjected to western blotting for accessing total expression levels of NF- $\kappa$ B p105, p50 and p65.  $\beta$ -actin was taken as loading control. (A) Representative immunoblots for expression of NF- $\kappa$ B p105, p50, p65, and  $\beta$ -actin in CL-6 cells. (B) Bar chart representing the mean  $\pm$  SD of three independent experiments for densitometric values of protein expression normalized to  $\beta$ -actin.  $*p < 0.05$  vs untreated control. NS = non-significant. IL-6 = Interlukin-6, IFN- $\gamma$  = Interferon- $\gamma$ .

### 5.2.9 Effect of $\beta$ -eudesmol on cytokine induced I $\kappa$ B $\alpha$ degradation in cholangiocarcinoma cells

$\beta$ -eudesmol exhibited promising inhibitory effect on cytokine-induced I $\kappa$ B $\alpha$  degradation in CL-6 cells. The cells were pre-treated with  $\beta$ -eudesmol (180  $\mu$ M) for 2 h and further stimulated with IFN- $\gamma$  and IL-6 (50 ng/ml each) for 45 mins. Whole cell lysates were collected at 0, 15, 30 and 45 min to access total I $\kappa$ B $\alpha$  expression. Results from immunoblots and corresponding densitometric analysis indicated that  $\beta$ -eudesmol-suppressed degradation of I $\kappa$ B $\alpha$ , which was normally achieved within 15-30 min post stimulation (Figure 5.29). The decrease in I $\kappa$ B $\alpha$ , degradation at 30 min was non significant ( $p=0.463$ ) and suppressed almost equal to baseline levels of I $\kappa$ B $\alpha$  suggesting considerable inhibitory effect of  $\beta$ -eudesmol on I $\kappa$ B $\alpha$  degradation. The suppression of I $\kappa$ B $\alpha$  degradation was clearly noticeable as compared to the normally achieved levels of I $\kappa$ B $\alpha$  degradation by cytokine stimulation at similar time points (Figure 5.13). The  $\beta$ -eudesmol treatment had no effect on total expression of  $\beta$ -actin taken as loading control (Figure 5.29).

(A)



(B)

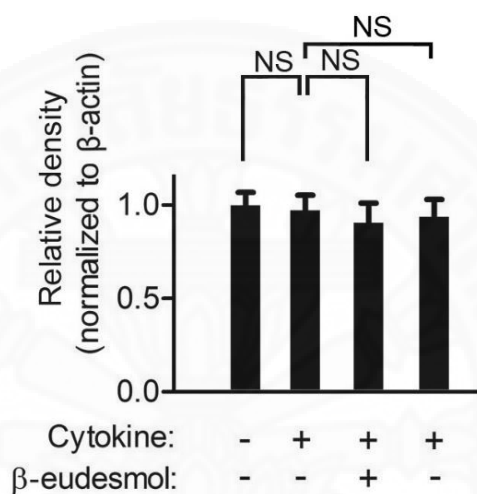


**Figure 5.29** Effect of  $\beta$ -eudesmol on cytokine-stimulated degradation of IkB $\alpha$  in CL-6 cells. The cells were serum starved overnight and stimulated with cytokines (50 ng/mL IL-6 and 50 ng/mL IFN- $\gamma$ ) for designated time points. Whole cell extracts were prepared and 50  $\mu$ L aliquots were subjected to western blotting for accessing total expression levels of IkB $\alpha$ .  $\beta$ -actin was taken as loading control. (A) Representative immunoblots for expression of IkB $\alpha$  and  $\beta$ -actin in CL-6 cells. (B) Bar chart representing the mean $\pm$ SD of three independent experiments for densitometric values of protein expression normalized to  $\beta$ -actin.  $*p < 0.05$  vs untreated control. IL-6 = Interlukin-6, IFN- $\gamma$  = Interferon- $\gamma$ .

#### **5.2.10 Evaluation of $\beta$ -eudesmol treatment on ICAM-1 and iNOS mRNA expression in cholangiocarcinoma cells**

ICAM1 and iNOS are known to be associated with STAT activation and are induced by several cytokines including IL-6.  $\beta$ -eudesmol showed promising inhibitory effect on mRNA expression of both ICAM-1 and iNOS in CL-6 cells. CL-6 cells were pretreated with  $\beta$ -eudesmol (180  $\mu$ M) for 2 h, followed by IFN- $\gamma$  and IL-6 (50 ng/ml each) stimulation for additional 4 h. Total RNA was extracted, converted to cDNA and relative expression of target genes were evaluated. The GAPDH expression was taken as internal control gene. Results from real time PCR suggested that cytokine stimulation significantly increased ICAM-1 ( $p=0.02$ ) and iNOS ( $p=0.027$ ) mRNA expression in CL-6 cells. In contrast, atracylodin pretreatment significantly suppressed ICAM-1 ( $p=0.005$ ) and iNOS ( $p=0.006$ ) mRNA expression in cytokine-stimulated CL-6 cells (Figure 5.30).



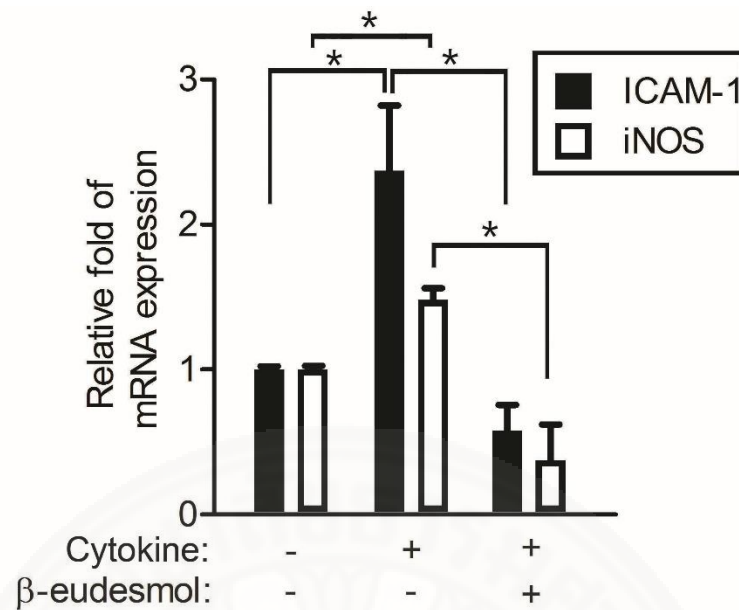


**Figure 5.30** Effect of  $\beta$ -eudesmol on ICAM-1 and iNOS mRNA expression in cytokine stimulated CL-6 cells. The cells were cultured in six-well plate and pretreated with  $\beta$ -eudesmol (180  $\mu$ M) for 2 h and stimulated with interleukin-6 (50 ng/mL) for further 4 h. Total RNA was extracted and converted to cDNA. Real time PCR analysis was performed to access relative expression of ICAM and iNOS mRNA. GAPDH was taken as internal control. Bar chart represents relative expression of ICAM and iNOS mRNA expression normalized to GAPDH. All data are expressed as mean $\pm$ SEM values and are representative of three independent experiments.  $p < 0.05$ . ICAM-1 = intercellular adhesion molecule 1, iNOS = inducible nitric oxide synthase, GAPDH = glyceraldehyde 3-phosphate dehydrogenase.



### 5.2.11 Evaluation of $\beta$ -eudesmol treatment on multiple tumor-associated genes in cholangiocarcinoma cells

$\beta$ -eudesmol showed remarkable potential of suppressing mRNA expression of multiple genes associated with tumorigenesis, *i.e.*, MCL-1, HO-1, MMP-9, NQO1, NRF2, and VEGF-A. CL-6 cells were cultured 24 h in presence of absence of  $\beta$ -eudesmol and total mRNA was extracted, converted to cDNA for relative gene expression. The GAPDH mRNA expression was taken as internal control. Results from real time PCR indicated that CL-6 cells expressed considerable baseline levels of target genes.  $\beta$ -eudesmol treatment significantly decreased mRNA expression of VEGF-A ( $p=0.022$ ), MCL-1 ( $p=0.041$ ), HO-1 ( $p=0.022$ ), MMP-9 ( $p=0.022$ ), NQO1 ( $p=0.0047$ ), and NRF2 ( $p=0.0042$ ) in CL-6 cells (Figure 5.31). The GAPDH was taken as internal control gene.

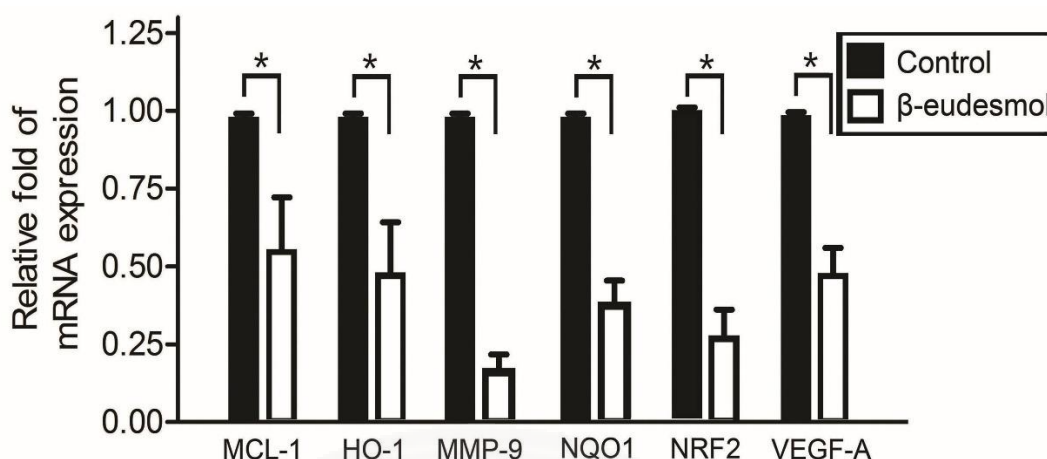


**Figure 5.31** Effect of  $\beta$ -eudesmol on mRNA expression of tumor-associated genes in CL-6 cells. The cells were cultured in six-well plate and treated with  $\beta$ -eudesmol (180  $\mu$ M) for 24 h. Total RNA was extracted and converted to cDNA. Real time PCR analysis was performed to access relative expression of MCL-1, HO-1, MMP9, NQO1, NRF2, and VEGF-A mRNA. GAPDH was taken as internal control. Bar chart represents relative expression of indicated genes normalized to GAPDH. All data are expressed as mean $\pm$ SEM values and are representative of three independent experiments.  $p < 0.05$ . MCL-1 = induced myeloid leukemia cell differentiation protein, HO-1 = heme oxygenase-1, MMP9 = matrix metalloproteinase-9, NQO1 = NAD(P)H quinone dehydrogenase-1, NRF2 = Nuclear factor (erythroid-derived 2)-like 2; VEGF-A = vascular endothelial growth factor A, GAPDH = glyceraldehyde 3-phosphate dehydrogenase.

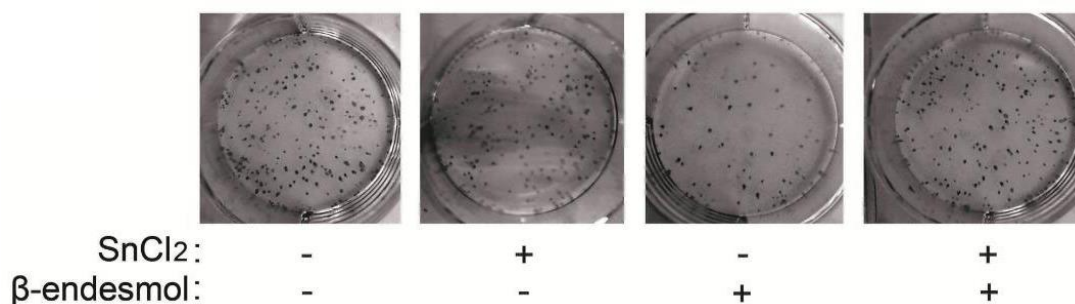
#### **5.2.12 Effect of SnCl<sub>2</sub> and $\beta$ -eudesmol treatment on colony forming ability of cholangiocarcinoma cells**

SnCl<sub>2</sub> is an inducer of the HO-1 enzyme and is known to promote cell survival by assisting HO-1 production. Results indicated that  $\beta$ -eudesmol treatment alone significantly decreased ( $p = 0.007$ ) the colony forming ability of CL-6 cells. The observed colony formation and corresponding bar chart showed that SnCl<sub>2</sub> treatment alone had no significant effect ( $p = 0.596$ ) on colony forming ability of CL-6 cells. Interestingly, SnCl<sub>2</sub> cotreatment significantly ( $p = 0.002$ ) restored the loss of colony forming capacity induced by  $\beta$ -eudesmol in CL-6 cells (Figure 5.32).

#### **5.2.13 Effect of SnCl<sub>2</sub> and $\beta$ -eudesmol treatment of wound healing ability of cholangiocarcinoma cells**

Interestingly, combined treatment of SnCl<sub>2</sub> and  $\beta$ -eudesmol significantly increased colony forming ability of the CL-6 cells. Similarly, SnCl<sub>2</sub> treatment alone had no significant ( $p = 0.182$ ) effect on wound healing ability of CL-6 cells. The observed wound closure and corresponding bar chart indicated that  $\beta$ -eudesmol treatment alone significantly ( $p = 0.0013$ ) reduced wound healing ability of CL-6 cells. As expected, combined treatment of SnCl<sub>2</sub> and  $\beta$ -eudesmol significantly ( $p = 0.007$ ) increased wound healing ability of CL-6 cells (Figure 5.33). The results indicated that SnCl<sub>2</sub> cotreatment ameliorated the loss of wound healing capacity induced by  $\beta$ -eudesmol in CL-6 cells (Figure 5.33).

(A)



(B)

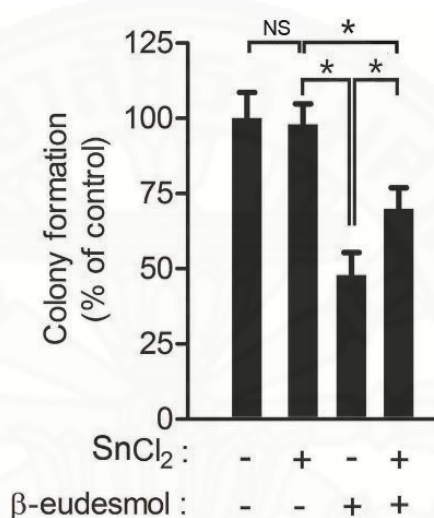
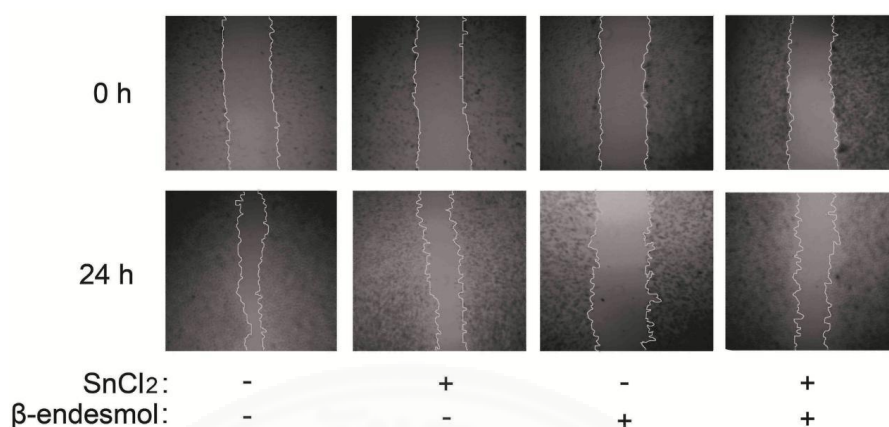


**Figure 5.32** Effect of SnCl<sub>2</sub> on colony forming ability of β-eudesmol-treated CL-6 cells. The cells were treated with β-eudesmol (180 μM), SnCl<sub>2</sub> (10 μM) or both for 24 h. The CL-6 cells were collected after trypsinization, seeded (300 cells/well) onto a 6-well plate and further incubated for additional 6-10 days. When the colonies appeared with at least 50 cells, the cells were fixed using ethanol and stained with methylene blue to visualize the colonies. (A) Representative figure showing colony forming ability of CL-6 cells. (B) Bar chart representing effect of β-eudesmol (180 μM), SnCl<sub>2</sub> (10 μM) or combined treatment on colony forming ability of CL-6 cells. All images shown are representative of three independent experiments. Data are expressed as mean±SD and are representative of three independent experiments. \**p*<0.05 vs untreated control. NS = non-significant.

(A)



(B)

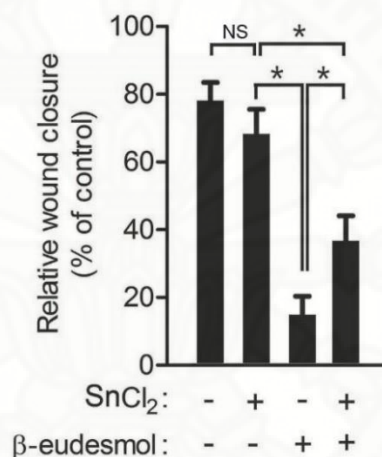
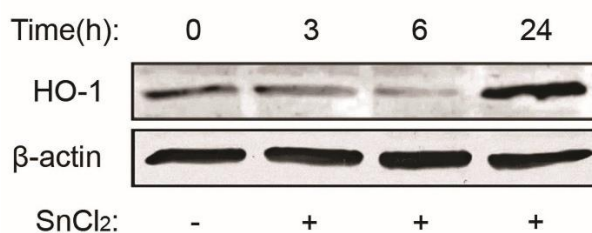


**Figure 5.33** Effect of SnCl<sub>2</sub> on wound healing ability of β-eudesmol-treated CL-6 cells. The cells were cultured in 24 well plate and at near confluency, cells were serum starved for 18 h, followed by creation of wound and subsequent treatment of β-eudesmol (180 μM), SnCl<sub>2</sub> (10 μM) on CL-6 cells. Wound closure was measured at 0 and 24 h. (A) Effect of β-eudesmol, SnCl<sub>2</sub> or both on wound healing ability of CL-6 cells. (B) Bar chart representing effect of β-eudesmol, SnCl<sub>2</sub>, or combined treatment on wound healing ability of CL-6 cells. All images shown are representative of three independent experiments. Data are expressed as mean±SD and are representative of three independent experiments. \**p*<0.05 vs untreated control. NS = non-significant.

#### 5.2.14 Effect of SnCl<sub>2</sub> treatment on heme oxygenase-1 expression in cholangiocarcinoma cells

The HO-1 expression is a crucial cytoprotective enzyme for survival and proliferation of multiple cancer cells. In order to specifically determine the role of HO-1 in CL-6, the effect HO-1 expression in the presence or absence of SnCl<sub>2</sub> and its cotreatment with  $\beta$ -eudesmol were investigated. Results from western blot analysis showed that CL-6 cells expressed considerable baseline levels of HO-1 expression in CL-6 cells (Figure 5.34). The treatment of SnCl<sub>2</sub> (10  $\mu$ M) induced significant level ( $p=0.008$ ) of HO-1 expression within 24 h of treatment as compared to the baseline level of HO-1 expression in CL-6 cells (Figure 5.34). In contrast, during same time interval, independent experiment involving the treatment of  $\beta$ -eudesmol treatment alone significantly decreased ( $p=0.0004$ ) the expression of HO-1 protein compared to untreated control (Figure 5.35). The western blots and corresponding densitometric bar chart showed that  $\beta$ -eudesmol-induced inhibition of HO-1 expression was prominent at 24 h post treatment (Figure 5.35). Interestingly, the combined treatment of SnCl<sub>2</sub> and  $\beta$ -eudesmol considerably abolished ( $p=0.0018$ ) the effect of  $\beta$ -eudesmol-induced suppression of HO-1 expression in CL-6 cells. The immuoblots and corresponding barchart clearly indicated that  $\beta$ -eudesmol-induced depletion in HO-1 expression at 24 h time interval was significantly resotred by SnCl<sub>2</sub> cotreatment in CL-6 cells (Figure 5.36).

(A)



(B)

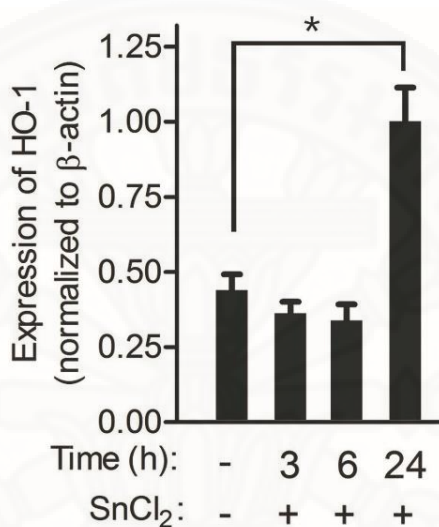
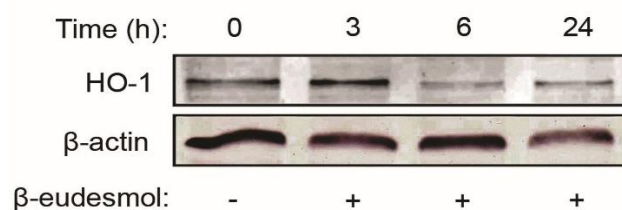


**Figure 5.34** Effect of SnCl<sub>2</sub> treatment on expression of HO-1 in CL-6 cells. The cells were stimulated with SnCl<sub>2</sub> (10 μM) for 0-24 h. Whole cell extracts were prepared for designated time points and 50 μL aliquots were subjected to western blotting for accessing total expression levels of HO-1 enzyme. β-actin was taken as loading control. (A) Representative Immunoblots for expression of HO-1 and β-actin in CL-6 cells. (B) Bar chart representing the mean±SD of three independent experiments for densitometric values of HO-1 protein expression normalized to β-actin. \**p*<0.05 vs untreated control. HO-1 = heme oxygenase-1.

(A)



(B)

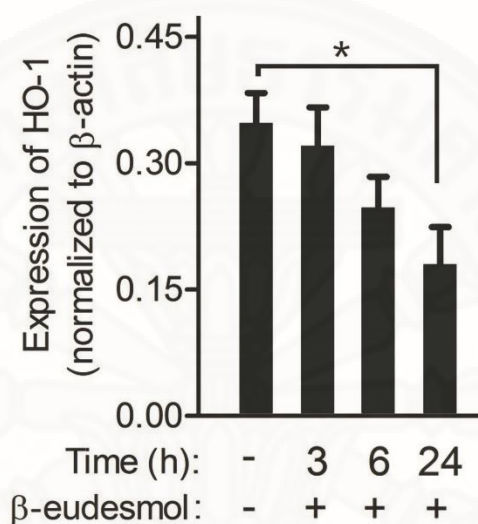
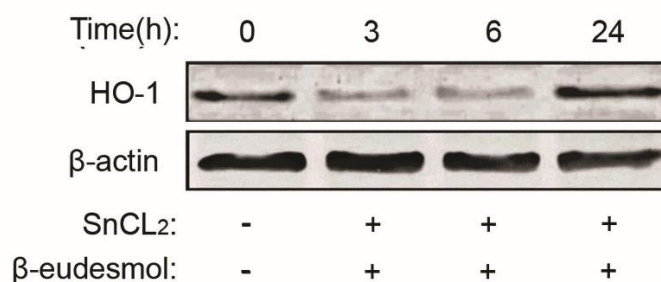


**Figure 5.35** Time-dependent expression of HO-1 expression in β-eudesmol-treated CL-6 cells. The cells were treated with β-eudesmol (180 μM) for 0-24 h. Whole cell extracts were prepared for designated time points and 50 μL aliquots were subjected to western blotting for accessing total expression levels of HO-1 enzyme. β-actin was taken as loading control. (A) Representative immunoblots for expression of HO-1 and β-actin in CL-6 cells. (B) Bar chart representing the mean ± SD of three independent experiments for densitometric values of HO-1 protein expression normalized to β-actin. \* $p < 0.05$  vs untreated control. HO-1 = heme oxygenase-1.



(A)



(B)

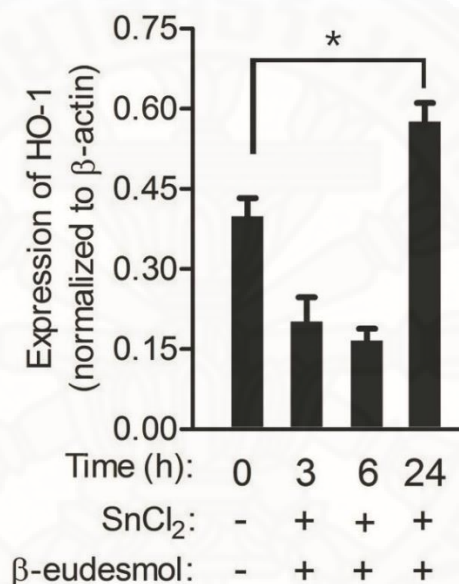


**Figure 5.36** Effect of SnCl<sub>2</sub> treatment on HO-1 expression in  $\beta$ -eudesmol-treated CL-6 cells. The cells were co-treated with  $\beta$ -eudesmol (180  $\mu$ M) and SnCl<sub>2</sub> (10  $\mu$ M) for 0-24 h. Whole cell extracts were prepared for designated time points and 50  $\mu$ L aliquots were subjected to western blotting for accessing total expression levels of HO-1 enzyme.  $\beta$ -actin was taken as loading control. (A) Representative immunoblots for expression of HO-1 and  $\beta$ -actin in CL-6 cells. (B) Bar chart representing the means  $\pm$  SD of three independent experiments for densitometric values of HO-1 protein expression normalized to  $\beta$ -actin. \* $p < 0.05$  vs untreated control. HO-1 = heme oxygenase-1.

### 5.2.15 Effect of SnCl<sub>2</sub> treatment on nuclear morphology of $\beta$ -eudesmol-treated cholangiocarcinoma cells

The DAPI staining is a well-established method for studying the nuclear morphology of cells. Results from DAPI staining and cytotoxicity assay indicated that SnCl<sub>2</sub> treatment alone had little or no effect on nuclear morphology of CL-6 cells (Figure 5.37). The nuclear morphology of untreated or SnCl<sub>2</sub>-treated cells exhibited healthy nuclear morphology.  $\beta$ -eudesmol treatment induced nuclear defragmentation with noticeable signs of apoptosis in CL-6 cells within 24 h treatment. In contrast, SnCl<sub>2</sub> and  $\beta$ -eudesmol cotreatment considerably decreased the nuclear defragmentation and ameliorated the noticeable signs of apoptosis caused by  $\beta$ -eudesmol treatment in CL-6 cells (Figure 5.37).

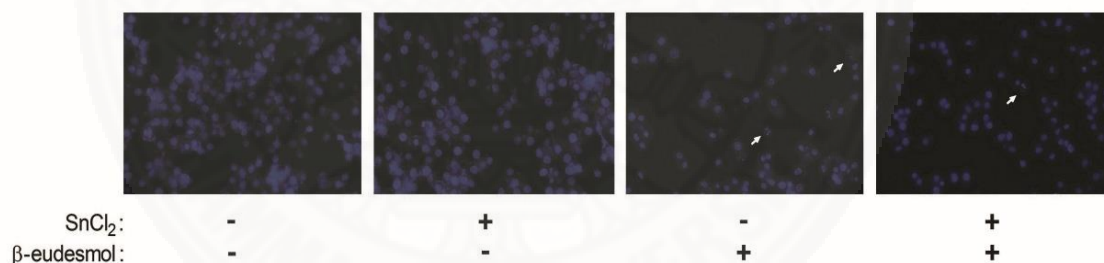


**Figure 5.37** Effect of SnCl<sub>2</sub> on nuclear morphology of  $\beta$ -eudesmol-treated CL-6 cells. Fluorescence microscopy of DAPI-stained CL-6 cells treated with  $\beta$ -eudesmol (180  $\mu$ M), SnCl<sub>2</sub> (10  $\mu$ M), or both for 24 h. White arrowhead represents apoptotic cells. All images are representative of three independent experiments.

### **5.2.16 Effect of SnCl<sub>2</sub> treatment on $\beta$ -eudesmol-induced cell death of cholangiocarcinoma cells**

The MTT viability is a standard method for studying the effects in cell viability under chemical treatment. Since the SnCl<sub>2</sub> treatment was able to alleviate the inhibitory effects of  $\beta$ -eudesmol on HO-1 production, the viability tests was conducted to access its effect on cell survival. Results from viability assay indicated that SnCl<sub>2</sub> treatment alone had no significant effect ( $p=0.091$ ) on cell viability compared to the control within 24 h or treatment (Figure 5.38). In contrast,  $\beta$ -eudesmol treatment significantly decreased ( $p=0.017$ ) cell viability by approximately 40% compared to untreated CL-6 cells within the same time interval. As expected, the SnCl<sub>2</sub> and  $\beta$ -eudesmol cotreatment significantly decreased ( $p=0.017$ ) the cell death thus ameliorating the  $\beta$ -eudesmol-induced cytotoxicity in CL-6 cells (Figure 5.38).

### **5.2.17 Effect of SnCl<sub>2</sub> treatment on $\beta$ -eudesmol-induced suppression of HO-1 mRNA expression in cholangiocarcinoma cells**

In order to investigate the effect of SnCl<sub>2</sub> and  $\beta$ -eudesmol cotreatment on HO-1 transcription, real time PCR was conducted to access HO-1 mRNA expression. Results from real-time PCR indicated that SnCl<sub>2</sub> treatment alone significantly increased ( $p=0.037$ ) HO-1 mRNA expression by approximately 2.3 folds compared to baseline level in CL-6 cells. In contrast,  $\beta$ -eudesmol treatment alone significantly decreased ( $p=0.0293$ ) the HO-1 mRNA expression below the baseline levels. However,  $\beta$ -eudesmol-induced reduction of HO-1 mRNA expression was significantly ( $p=0.0323$ ) alleviated by combined treatment of SnCl<sub>2</sub> and  $\beta$ -eudesmol in CL-6 cells (Figure 5.39).

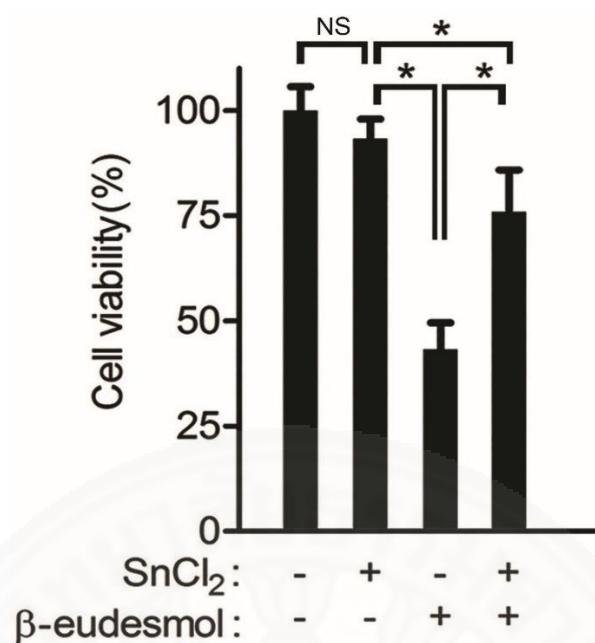


**Figure 5.38** Effect of SnCl<sub>2</sub> treatment on β-eudesmol-induced cell death of CL-6 cells.

Bar chart representing MTT viability assay of CL-6 cells treated with β-eudesmol (180 μM), SnCl<sub>2</sub> (10 μM), or combined treatment for 24 h. All data are expressed as mean±SD and are representative of three independent experiments.  $p < 0.05$ . NS = non-significant.

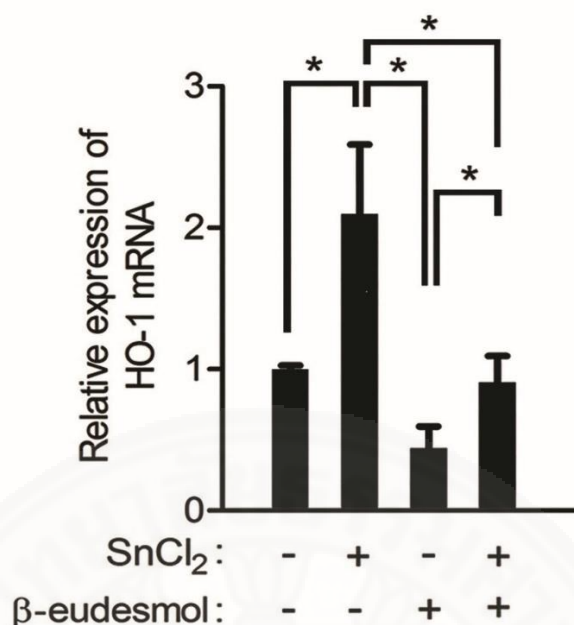


**Figure 5.39** Effect of SnCl<sub>2</sub> on HO-1 mRNA expression in β-eudesmol-treated CL-6 cells. The cells were cultured in six-well plate and treated with β-eudesmol (180 μM), SnCl<sub>2</sub> (10 μM), or both for 24 h. Total RNA was extracted and converted to cDNA. Real time PCR analysis was performed to access relative expression of HO-1 mRNA. GAPDH was taken as internal control. Bar chart represents relative expression of HO-1 mRNA expression normalized to GAPDH. All data are expressed as mean±SD values and are representative of three independent experiments.  $p < 0.05$ . GAPDH = glyceraldehyde 3-phosphate dehydrogenase, HO-1 = heme oxygenase -1.

### 5.2.18 Evaluation of Zinc protoporphyrin IX treatment on cell viability of cholangiocarcinoma cells

The effect of ZN(II)PPIX on cell viability within 24 h of treatment was evaluated using standard MTT assay. The CL-6 cells were treated with 0-130  $\mu\text{M}$  of ZN(II)PPIX and viability was studied. The results indicate that ZN(II)PPIX was able to induce dose-dependent cytotoxicity on CL-6 cells (Figure 5.40). Treatment of ZN(II)PPIX below 65  $\mu\text{M}$  had no significant ( $p=0.083$ ) effect on cell viability. As clearly noticeable from bar chart, the treatment of ZN(II)PPIX at 65  $\mu\text{M}$  ( $p=0.02$ ) and 130  $\mu\text{M}$  ( $p=0.017$ ) had significant cytotoxicity on CL-6 (Figure 5.40).

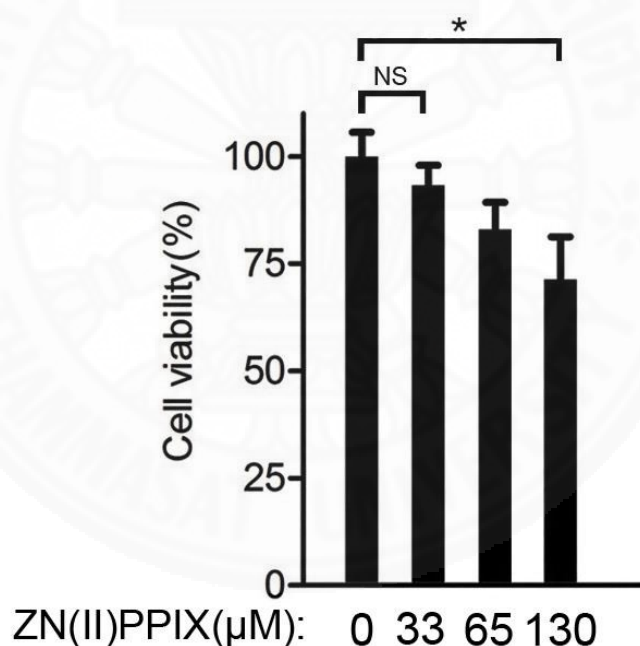


**Figure 5.40** Effect of Zinc protoporphyrin IX on viability of CL-6 cells. Bar chart representing MTT viability assay of CL-6 cells treated with indicated concentrations of ZN(II)PPIX for 24 h. All data are expressed as mean $\pm$ SD values and are representative of three independent experiments.  $p^*<0.05$ , NS = non-significant. ZN(II)PPIX, Zinc protoporphyrin IX.

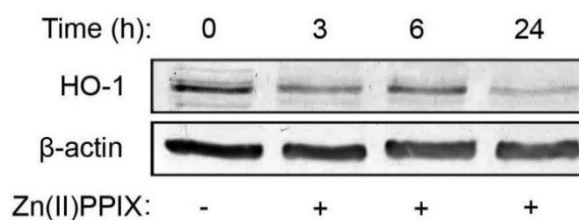
### **5.2.19 Evaluation of Zinc protoporphyrin IX treatment on HO-1 expression in cholangiocarcinoma cells**

ZN(II)PPIX is a known selective inhibitor of HO-1. In order to further evaluate the specific role of HO-1 in overall cell survival, the effect of ZN(II)PPIX was evaluated in CL-6 cells. The results from western blot analysis and corresponding densitometric bar chart revealed considerable amount of baseline expression of HO-1 enzyme in CL-6. The inhibitory effect of ZN(II)PPIX treatment was non-significant within 6 h of treatment in CL-6 cells. In contrast, ZN(II)PPIX treatment significantly suppressed ( $p<0.05$ ) the expression of HO-1 enzyme at 24 h post treatment as compared to untreated control (Figure 5.41).

### **5.2.20 Evaluation of Zinc protoporphyrin IX treatment on heme oxygenase-1 mRNA expression in cholangiocarcinoma cells**

The results from real time PCR analysis indicated that CL-6 cells exhibited considerable amount of baseline HO-1 expression. As expected, ZN(II)PPIX treatment at 24 h exhibited significant suppressive effect ( $p=0.028$ ) on HO-1 mRNA expression in CL-6 cells at 24 h with reference to the GAPDH mRNA expression taken as internal control (Figure 5.42).

(A)



(B)

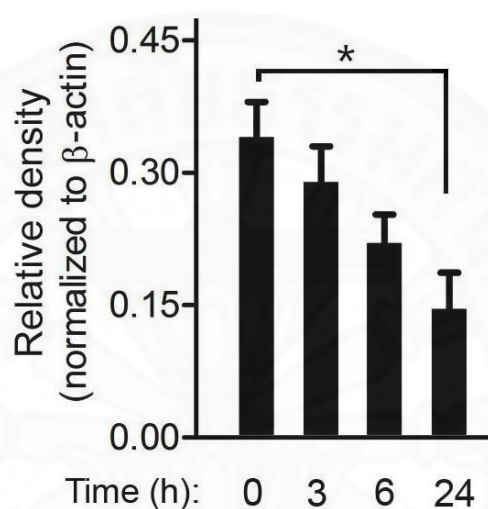


**Figure 5.41** Effect of Zinc protoporphyrin IX on HO-1 expression in CL-6 cells. The cells were stimulated with ZN(II)PPIX (130  $\mu$ M) for 0-24 h. Whole cell extracts were prepared for designated time points and 50  $\mu$ L aliquots were subjected to western blotting for accessing total expression levels of HO-1 enzyme.  $\beta$ -actin was taken as loading control. (A) Representative immunoblots for expression of HO-1 and  $\beta$ -actin in CL-6 cells. (B) Bar chart representing the mean $\pm$ SD value of three independent experiments for densitometric values of HO-1 protein expression normalized to  $\beta$ -actin.  $*p < 0.05$  vs untreated control. HO-1 = heme oxygenase-1. ZN(II)PPIX = Zinc protoporphyrin IX.



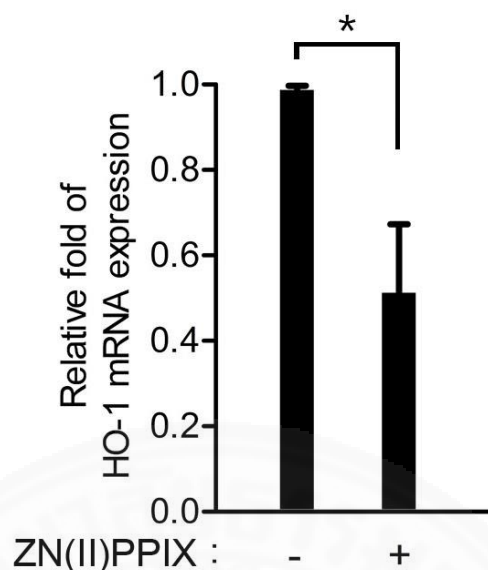


**Figure 5.42** Effect of Zinc protoporphyrin IX treatment on HO-1 mRNA expression in CL-6 cells. The cells were cultured in a 6-well plate and treated with ZN(II)PPIX (130  $\mu$ M) for 24 h. Total RNA was extracted and converted to cDNA. Real time PCR analysis was performed to access relative expression of HO-1 mRNA. GAPDH was taken as internal control. Bar chart represents relative expression of HO-1 mRNA expression normalized to GAPDH. All data are expressed as mean $\pm$ SD values and are representative of three independent experiments.  $p^*<0.05$ . GAPDH = glyceraldehyde 3-phosphate dehydrogenase, HO-1= heme oxygenase -1.

### 5.2.21 Effect of $\beta$ -eudesmol treatment on nuclear morphology of cytokine stimulated cholangiocarcinoma cells

As a supplementary investigation, the effect of  $\beta$ -eudesmol on nuclear morphology of cytokine-induced CL-6 cells was investigated for visible traits of apoptosis using DPAI-based fluorescent staining. The CL-6 cells in the presence or absence of cytokine stimulation exhibited healthy growth based on their normal nuclear morphology (Figure 5.43). In contrast, the  $\beta$ -eudesmol or nifuroxazide treated cells displayed substantial amount of nuclear defragmentation.

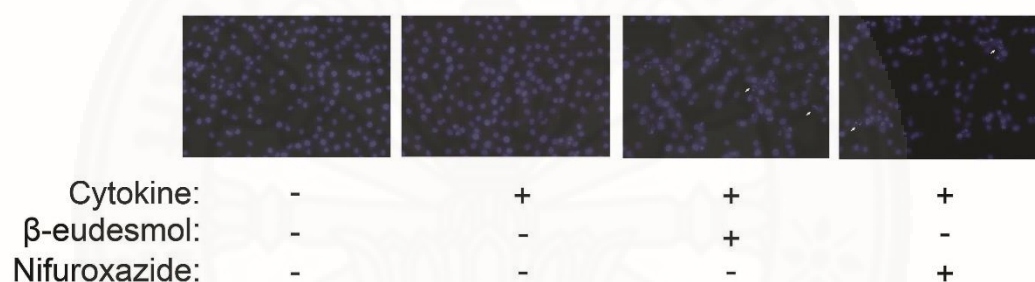


**Figure 5.43** Effects of  $\beta$ -eudesmol and nifuroxazide on nuclear morphology of cytokine stimulated cholangiocarcinoma cells. CL-6 cells were pretreated with  $\beta$ -eudesmol (180  $\mu$ M) or nifuroxazide (50  $\mu$ M) for 2 h and further stimulated with cytokine (50 ng/ml) for 24 h. This followed by DAPI fluorescence microscopy for nuclear staining. White arrowhead represents apoptotic cells. All images are representative of three independent experiments.

### **5.2.22 Comparison of colony forming inhibitory effect between atractylodin and $\beta$ -eudesmol against cholangiocarcinoma cells**

Based on results of colony forming assay from section 5.1.3 and 5.2.3, the data analysis using independent t-test with one-tailed hypothesis and level of significance set at  $p < 0.05$  indicate that overall proliferative capacity of CL-6 cells upon atractylodin and  $\beta$ -eudesmol treatment was  $52.63 \pm 5.82\%$  and  $35.97 \pm 5.1\%$  compared to untreated control, respectively. The  $\beta$ -eudesmol significantly reduced number of colony forming units ( $p=0.011$ ) compared to atractylodin (Figure 5.44). The results indicated that  $\beta$ -eudesmol is more potent for anti-proliferative activity than atractylodin.

### **5.2.23 Comparison of wound healing inhibitory effect between atractylodin and $\beta$ -eudesmol against cholangiocarcinoma cells**

Based on results of wound healing assay in section 5.1.4 and 5.2.4, data analysis using independent t-test with two-tailed hypothesis and level of significance set at  $p < 0.05$  indicated that there was no significant difference between cytokine stimulated and unstimulated control on wound healing effect at 24 h ( $p=0.231$ ) and 48 h ( $p=0.163$ ) post-stimulation in CL-6 cells.

The overall wound healing activity of CL-6 cells upon atractylodin treatment at 24 h and 48 h was  $22.50 \pm 4.27\%$  and  $8.40 \pm 3.73\%$  of control, respectively. Similarly, the  $\beta$ -eudesmol exhibited wound healing activity of CL-6 cells  $25.6 \pm 3.06\%$  and  $30.33 \pm 4.04\%$  at 24 h and 48 h as compared to untreated control, respectively. Comparing the results using one-tailed analysis between atractylodin and  $\beta$ -eudesmol on tendency of the compounds to suppress wound healing ability compared to percentage of control suggested that the atractylodin exhibited stronger suppression of wound healing ability ( $p=0.001$ ) in CL-6 cells at 48 h post stimulation as compared to  $\beta$ -eudesmol.

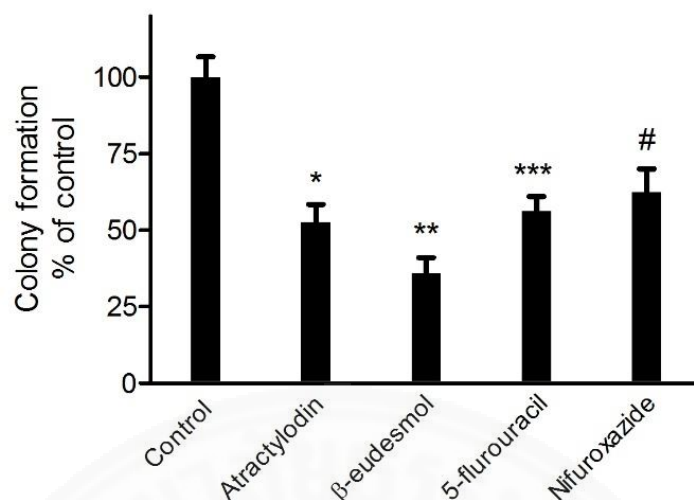


**Figure 5.44** Summary of the effect of atractylodin and β-eudesmol on colong formation ability of CL-6 cells. The inhibitory effect of atractylodin (250 μM), β-eudesmol (180 μM) along with standard compounds 5-flurouracil (700 μM) and nifuroxazide (50 μM) on colony forming ability of CL-6 expressed in terms of percentage of untreated control. All data are expressed as mean±SD values and are representative of three independent experiments. \* $p < 0.05$ , \*\*  $p < 0.05$ , \*\*\*  $p < 0.05$ , ##  $p < 0.05$ .

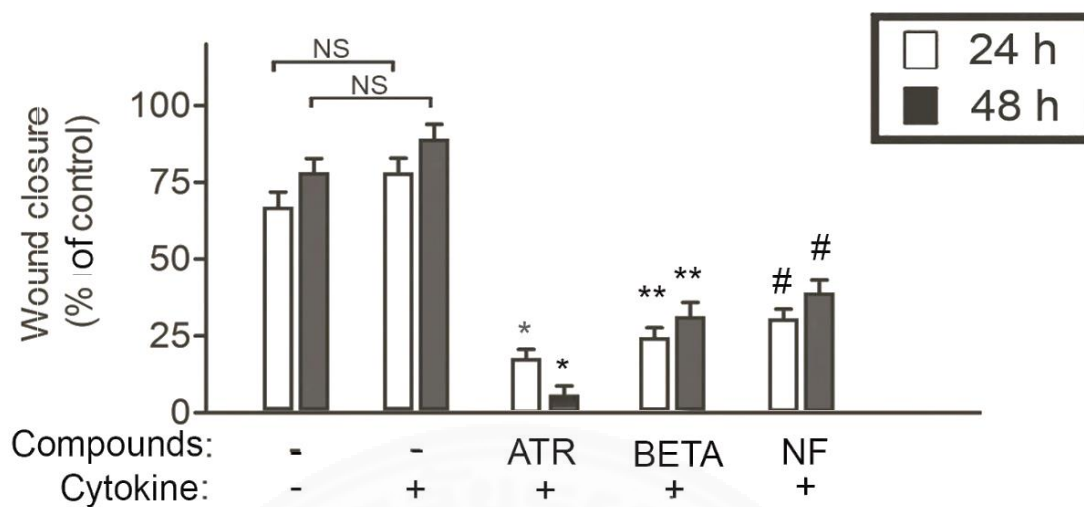


**Figure 5.45** Summary of the effect of atractylodin and  $\beta$ -eudesmol on wound healing ability of CL-6 cells. The inhibitory effect of atractylodin (250  $\mu$ M),  $\beta$ -eudesmol (180  $\mu$ M) along with nifuroxazide (50  $\mu$ M) on wound closure of CL-6 expressed in terms of percentage of cytokine stimulated control. All data are expressed as mean $\pm$ SD values and are representative of three independent experiments. \* $p < 0.05$ , \*\*  $p < 0.05$ .

#### **5.2.24 Summarized effect of atractylodin and $\beta$ -eudesmol on Heme oxygenase-1 expression in cholangiocarcinoma cells**

Based on western blot results of section 5.1.5 and 5.2.5, the protein expressions of HO-1 treated by atractylodin and  $\beta$ -eudesmol were  $37.49 \pm 5.73\%$  and  $10.81 \pm 4.21\%$  of control, respectively. The results indicated that  $\beta$ -eudesmol significantly reduced HO-1 protein expression compared to atractylodin ( $p=0.001$ ) (Figure 5.46).

#### **5.2.25 Summarized effect of atractylodin and $\beta$ -eudesmol on NQO1 expression in cholangiocarcinoma cells**

Based on the results of section 5.1.6 and 5.2.6, the protein expression of NQO1 treated by atractylodin and  $\beta$ -eudesmol was  $51.94 \pm 6.04\%$  and  $41.34 \pm 8.55\%$  of control, respectively. There was no statistically significant difference among these compound on the NQO1 protein expression ( $p=0.162$ ) (Figure 5.47).

#### **5.2.26 Summarized effect of atractylodin and $\beta$ -eudesmol on STAT1 and STAT3 activation in cholangiocarcinoma cells**

Based on the results of section 5.1.8 and 5.2.7, the STAT1 protein expressions of atractylodin and  $\beta$ -eudesmol were  $21.89 \pm 5.30\%$  and  $33.32 \pm 6.08\%$  of control, respectively. The result analysis using independent t-test with two-tailed hypothesis and level of significance set at  $p < 0.05$  indicated that there was no difference of STAT1 activation between these two compounds ( $p=0.059$ ) (Figure 5.48, A). Similarly, for STAT3 phosphorylation (Figure 5.48, B), the effect of atractylodin and  $\beta$ -eudesmol on STAT3 activation had no statistical difference ( $30.68 \pm 4.9\%$  vs  $29.64 \pm 4.69\%$  of control, respectively).

### 5.2.27 Summarized effect of atractylodin and $\beta$ -eudesmol on aggregate NF- $\kappa$ B expression in CL-6 cells.

Based on the results of atractylodin and  $\beta$ -eudesmol on NF- $\kappa$ B protein expressions were shown in section 5.1.10 and 5.2.8. The protein expressions of NF- $\kappa$ B p105 at 24 h treatment with atractylodin and  $\beta$ -eudesmol were  $57.87 \pm 4.39\%$  and  $19.64 \pm 4.75\%$  of control, respectively (Figure 5.49 A). The corresponding values of NF- $\kappa$ B p50 were  $31.72 \pm 4.67\%$  and  $16.77 \pm 4.03\%$  of control, respectively (Figure 5.49 B). While, the proteins expression of NF- $\kappa$ B p65 were  $23.12 \pm 6.07\%$  and  $26.18 \pm 6.31\%$  of control, respectively (Figure 5.49 C). Result analysis using independent t-test with one-tailed hypothesis and level of significance set at  $p < 0.05$  indicated that suppressive effect of  $\beta$ -eudesmol was significantly stronger than atractylodin for suppression of aggregate expression of NF- $\kappa$ B p105 ( $p=0.001$ ) and p50 ( $p=0.018$ ) in CL-6 cells. In contrast, atractylodin compared to  $\beta$ -eudesmol had no significance ( $p=0.596$ ) on aggregate expression of NF- $\kappa$ B p65 in CL-6 cells. The results overall indicate both atractylodin and  $\beta$ -eudesmol are promising candidate compound for their inhibitory effect on aggregate expression of major NF- $\kappa$ B phosphorylation in CL-6 cells.

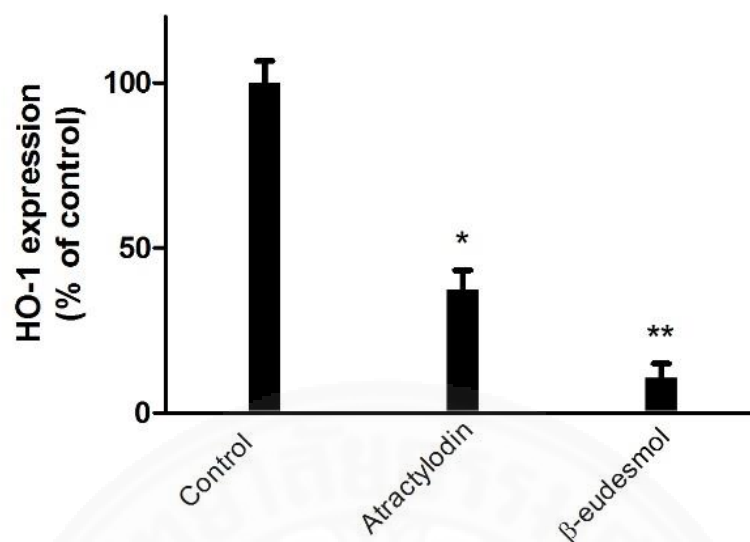


**Figure 5.46** Summary of the effect of atractylodin and β-eudesmol on heme oxygenase-1 expression in CL-6 cells. The inhibitory effect of 24 h treatment of atractylodin (250 μM) or β-eudesmol (180 μM) on heme oxygenase-1 expression in CL-6 cells expressed in terms of percentage of control. All data are expressed as mean±SD values and are representative of three independent experiments. \* $p<0.05$ , \*\*  $p<0.05$ . HO-1= heme oxygenase-1



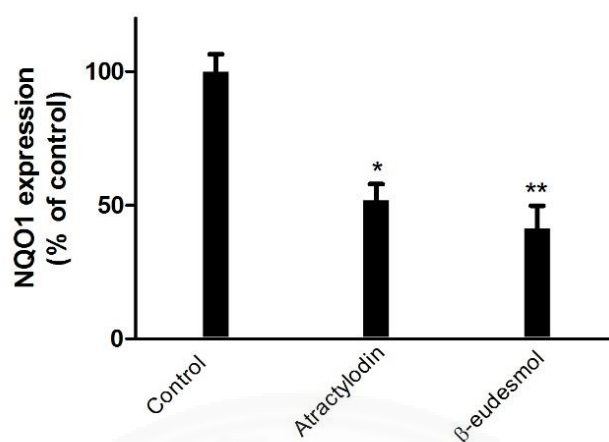


**Figure 5.47** Summary of the effect of atractylodin and  $\beta$ -eudesmol on heme oxygenase-1 expression in CL-6 cells. The inhibitory effect of 24 h treatment of atractylodin (250  $\mu$ M) or  $\beta$ -eudesmol (180  $\mu$ M) on NQO1 expression in CL-6 cells expressed in terms of percentage of control. All data are expressed as mean $\pm$ SD values and are representative of three independent experiments. \* $p<0.05$ , \*\* $p<0.05$ .

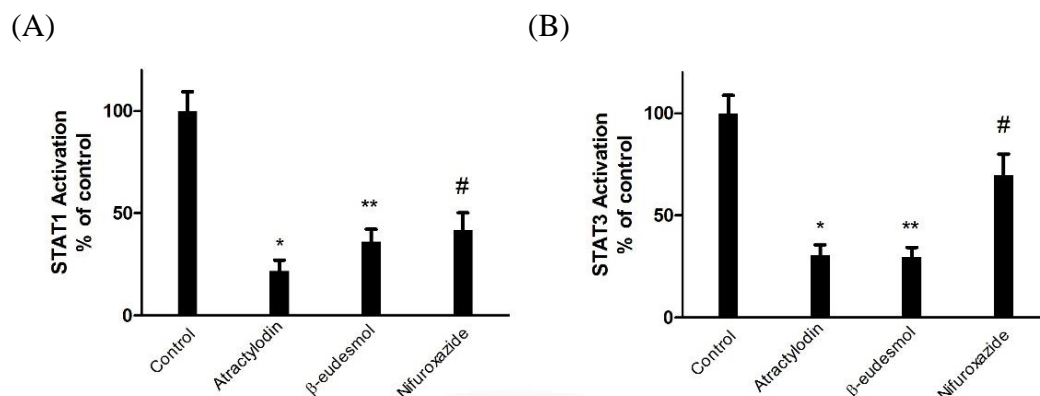


**Figure 5.48** Summary of the effect of atractylodin and β-eudesmol on STAT1 and STAT3 activation in CL-6 cells. The inhibitory effect of atractylodin (250 μM), β-eudesmol (180 μM) along with nifuroxazide (50 μM) 2h pre-treatment on (A) Stat1 and (B) STAT3 activation *via* phosphorylation on CL-6 cells at 4h post-cytokine stimulation expressed in terms of percentage of cytokine stimulated control. All data are expressed as mean±SD values and are representative of three independent experiments. \* $p < 0.05$ , \*\*  $p < 0.05$ .

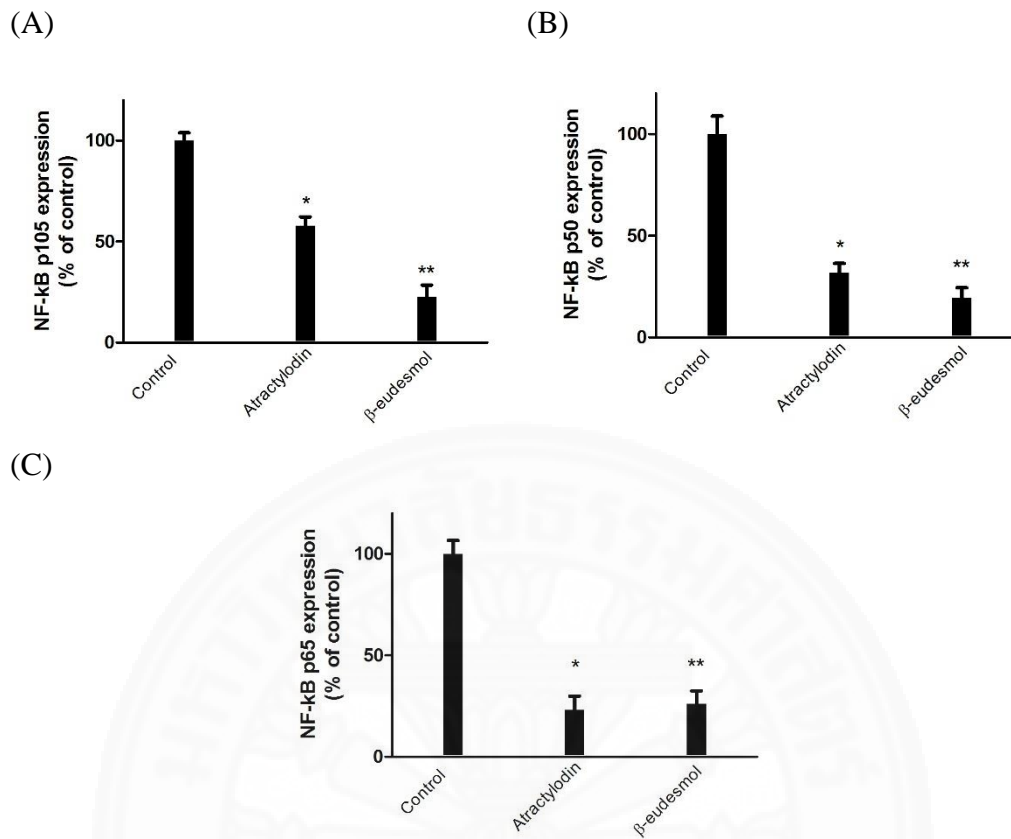


**Figure 5.49** Summary of the effect of atracylodin and β-eudesmol on major NF-κB protein expression in CL-6 cells. The inhibitory effect of atracylodin (250 μM) or β-eudesmol (180 μM) on aggregate expression of NF-κB (A) p105, (B) p50 and (C) p65 at 24 h post-treatment in CL-6 cells expressed in terms of percentage of cytokine stimulated control. All data are expressed as mean±SD values and are representative of three independent experiments. \* $p < 0.05$ , \*\*  $p < 0.01$ .

### 5.2.28 Summarized effect of atractylodin and $\beta$ -eudesmol on aggregate NF- $\kappa$ B expression in cytokine stimulated cholangiocarcinoma cells

Based on western blot results of section 5.1.10 and 5.2.8, the result analysis using independent t-test with two-tailed hypothesis and level of significance set at  $p < 0.05$  indicated that there was no significant ( $p \geq 0.1$ ) difference on aggregate expression of p105, p50 and p65 in presence or absence of cytokine stimulation. The protein expressions of NF- $\kappa$ B p105 at 4 h post stimulation of atractylodin ( $71.61 \pm 11.32\%$  of control) and  $\beta$ -eudesmol ( $67.31 \pm 8.1\%$  of control) were not statistically significant ( $p=0.625$ ). The protein expressions of NF- $\kappa$ B p50 of atractylodin and  $\beta$ -eudesmol were also not statistically different ( $53.31 \pm 10.05\%$  and  $65.60 \pm 7.14\%$  of control, respectively;  $p=0.167$ ). Similarly, there was no significant difference in protein expressions of NF- $\kappa$ B p65 among atractylodin and  $\beta$ -eudesmol ( $73.21 \pm 9.60\%$  vs  $58.35 \pm 6.55\%$  of control, respectively;  $p=0.1$ ) (Figure 5.49 A, B, C).

### 5.2.29 Summarized effect of atractylodin and $\beta$ -eudesmol on I $\kappa$ B $\alpha$ degradation in cytokine stimulated cholangiocarcinoma cells

Based on results in section 5.1.11 and 5.2.9, the data analysis using independent t-test with two-tailed hypothesis and level of significance set at  $p < 0.05$  indicated that the cytokine stimulation significantly ( $39.48 \pm 9.91\%$  of control,  $p=0.0014$ ) caused maximum I $\kappa$ B $\alpha$  degradation at 30 min post stimulation in cytokine stimulated CL6 cells. The I $\kappa$ B $\alpha$  protein expressions induced by atractylodin and  $\beta$ -eudesmol were  $89.01 \pm 11.34\%$  and  $90.04 \pm 7.28\%$  of control, respectively (Figure 5.51). There was no statistical difference of I $\kappa$ B $\alpha$  expressions among these two compounds ( $p \geq 0.1$ ). The results overall indicate both atractylodin and  $\beta$ -eudesmol as promising candidate compound for their ability to cytokine stimulated I $\kappa$ B $\alpha$  degradation and thus suppress activation of NF- $\kappa$ B in CL-6 cells.

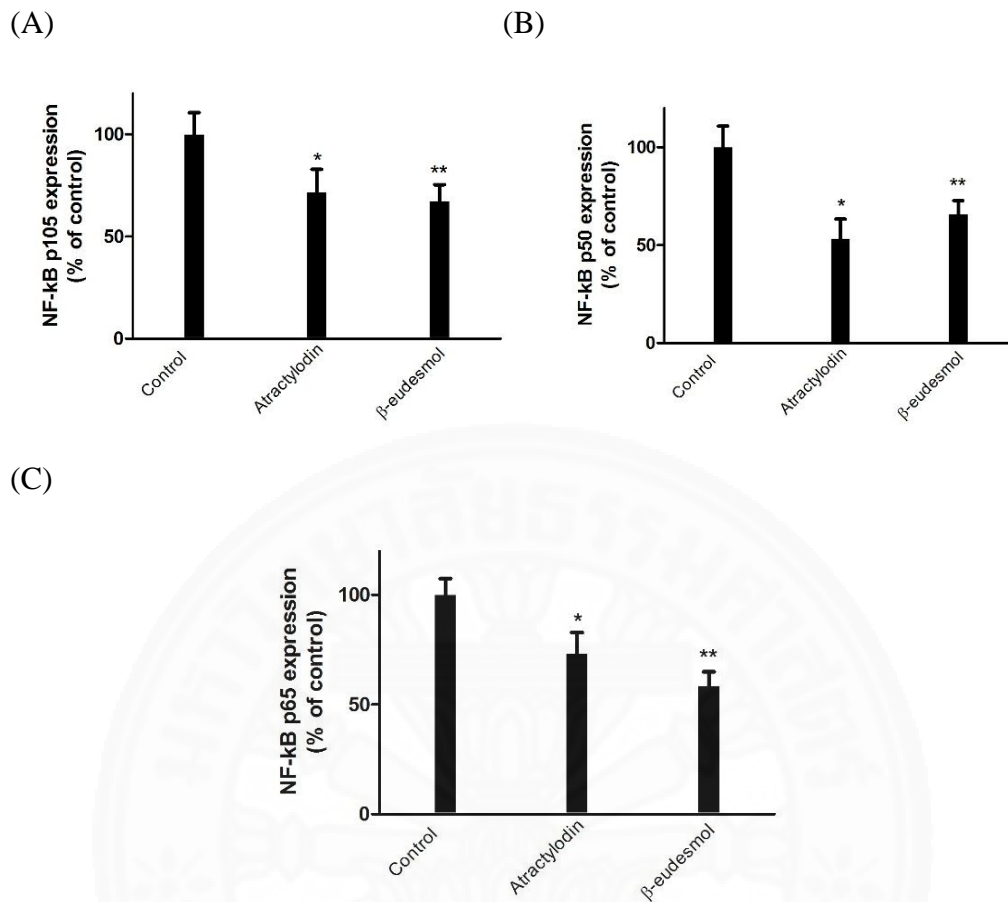


**Figure 5.50** Summary of the effect of atractylodin and β-eudesmol on major NF-κB protein expression in CL-6 cells. The inhibitory effect of 2h pre-treatment of atractylodin (250 μM) or β-eudesmol (180 μM) on aggregate expression of NF-κB (A) p105, (B) p50 and (C) p65 at 4h post- cytokine stimulated CL-6 cells expressed in terms of percentage of cytokine stimulated control. All data are expressed as mean±SD values and are representative of three independent experiments. \* $p < 0.05$ , \*\*  $p < 0.05$ .

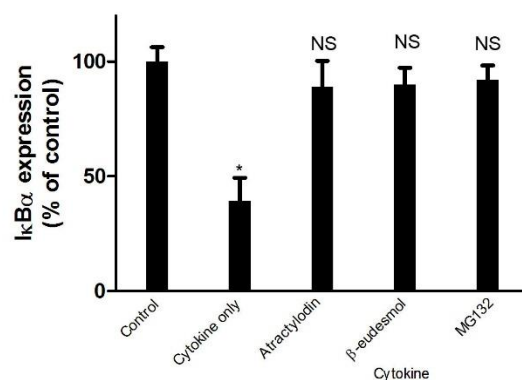


**Figure 5.51** Summary of the effect of atractylodin and  $\beta$ -eudesmol on IkB $\alpha$  degradation in cytokine stimulated CL-6 cells. The inhibitory effect of atractylodin (250  $\mu$ M),  $\beta$ -eudesmol (180  $\mu$ M) and MG132 (25  $\mu$ M) on IkB $\alpha$  degradation at 30 min post cytokine stimulation in CL-6 cells expressed in terms of percentage of control. All data are expressed as mean $\pm$ SD values and are representative of three independent experiments. \* $p < 0.05$ , NS= non significant.

### **5.2.30 Summarized effect of atractylodin and $\beta$ -eudesmol on relative mRNA expression of major tumor associated genes in CL-6 cells.**

Briefly, based on real time PCR assay results of section 5.1.14 and 5.2.11, the VEGF-A mRNA expressions of CL-6 cells at 24 h after treated with atractylodin and  $\beta$ -eudesmol were  $45.66 \pm 11.80\%$  and  $53.84 \pm 9.93\%$  of control, respectively. There was no difference of VEGF-A mRNA expression among these two compounds ( $p=0.446$ ). The similar results were observed in MCL-1 mRNA expression. There was no statistically significant difference of MCL-1 mRNA expression between atractylodin and  $\beta$ -eudesmol ( $52.96 \pm 16.3\%$  vs.  $53.48 \pm 14.62\%$  of control, respectively;  $p=0.969$ ). The results overall indicate both atractylodin and  $\beta$ -eudesmol are promising candidate compound for their inhibitory effect on mRNA expression of VEGF-A and MCL-1 in CL-6 cells.

### **5.2.31 Summarized effect of atractylodin and $\beta$ -eudesmol on relative mRNA expression of STAT associated genes in cholangiocarcinoma cells.**

Based on real time PCR assay results of section 5.1.15 and 5.2.10, the relative ICAM-1 mRNA expression of CL-6 cells after 24 h treated with atractylodin and  $\beta$ -eudesmol were  $29.65 \pm 11.30\%$  and  $23.63 \pm 7.13\%$  of control, respectively. The corresponding values of iNOS mRNA expressions were  $46.58 \pm 15.68\%$  and  $25.69 \pm 16.59\%$  of control, respectively. There were no statistically significant difference of ICAM-1 ( $p=0.446$ ) and iNOS ( $p \geq 0.13$ ) mRNA expressions among these two compounds. The results overall indicate both atractylodin and  $\beta$ -eudesmol are promising candidate compound for their inhibitory effect on mRNA expression of ICAM-1 and iNOS in CL-6 cells.

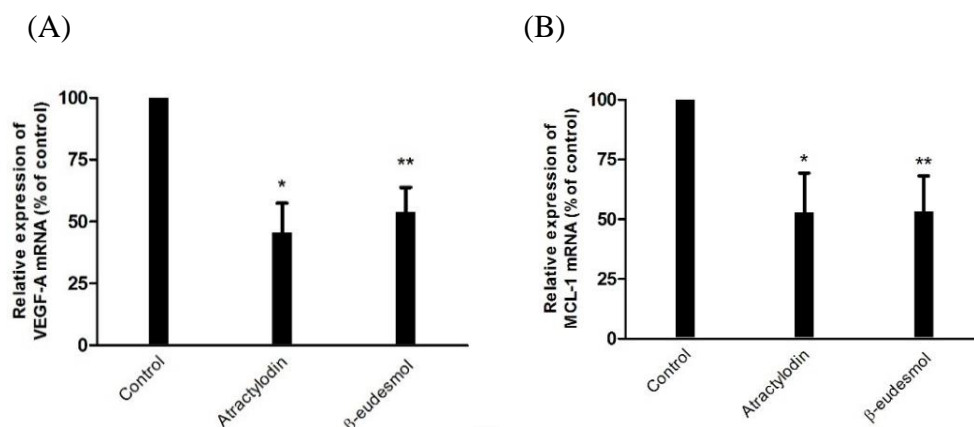


**Figure 5.52** Summary of the effect of atractylodin and β-eudesmol on relative mRNA expression of major tumor associated genes expression in CL-6 cells. The inhibitory effect of 24 h treatment of atractylodin (250 μM) or β-eudesmol (180 μM) on relative mRNA expression of (A) VEGF-A and (B) MCL-1 in CL-6 cells expressed in terms of percentage of control. All data are expressed as mean±SEM values and are representative of three independent experiments. \* $p < 0.05$ , \*\* $p < 0.05$ . VEGF-A = vascular endothelial growth factor-A; MCL-1 = induced myeloid leukemia cell differentiation protein



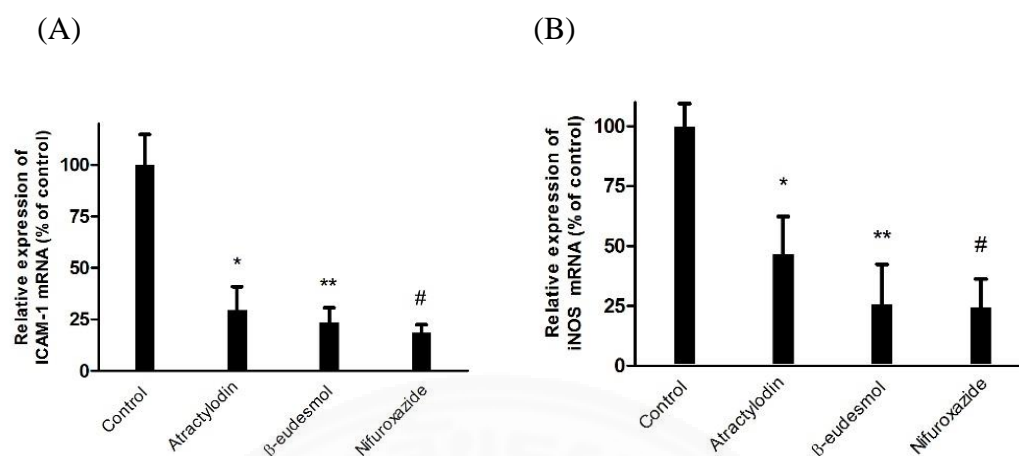


**Figure 5.53** Summary of the effect of atractylodin and  $\beta$ -eudesmol on relative mRNA expression of major tumor associated genes expression in CL-6 cells. The inhibitory effect of 24 h treatment of atractylodin (250  $\mu$ M),  $\beta$ -eudesmol (180  $\mu$ M) and nifuroxazide (50  $\mu$ M) on relative mRNA expression of (A) ICAM-1 and (B) iNOS in CL-6 cells expressed in terms of percentage of cytokine-stimulated control. All data are expressed as mean $\pm$ SEM values and are representative of three independent experiments. \* $p < 0.05$ , \*\*  $p < 0.05$ . ICAM-1 = intracellular adhesion molecule-1, iNOS = inducible nitric oxide synthase.

## **CHAPTER 6**

### **DISCUSSION**

#### **6.1 Cytotoxicity evaluation of atractylodin and $\beta$ -eudesmol in cholangiocarcinoma cells**

Previous studies have indicated that CCA-associated cell lines are highly resistant to conventional anticancer drugs such as 5-FU with reported  $IC_{50}$  of greater than 800  $\mu$ M (89). Such drug resistance can present serious chemotherapeutic obstacle in treatment of CCA. Results from the present study suggested that cytotoxicity activity of atractylodin and  $\beta$ -eudesmol was selective towards CL-6 cells with potency of about 2-3 times of 5-FU. The observed cytotoxicity of atractylodin and  $\beta$ -eudesmol towards CL-6 is qualitatively consistent with results from other research for anticancer effect of this compound on several human cancers including human cervical carcinoma cells (90). The selectivity and relatively low  $IC_{50}$  ( $<300 \mu$ M) of atractylodin and  $\beta$ -eudesmol provided possibilities for further in-depth investigation of these compounds on underlying potential molecular mechanism for observed cytotoxicity in CL-6 cells.

#### **6.2 Effect of atractylodin and $\beta$ -eudesmol induced cytotoxicity in cell culture and nuclear morphology of cholangiocarcinoma cells**

Morphological examination of both CL-6 and OUMS cells following exposure to atractylodin treatment under the light microscopy supported selective dose-dependent inhibitory effect of the compound on cancer cells. Late phase of apoptosis and subsequent cell death is characterized by a series of typical morphological features such as loss of adhesion, distorted morphology, cell shrinkage, fragmentation and increased amount of cell debris in culture (80). Prominent signs of cell debris and floating dead cells following atractylodin or  $\beta$ -eudesmol exposure in CL-6 cell culture

as compared to OUMS culture indicated stress-induced cell death in cancer cells. Nuclear fluorescent staining such as DAPI have been frequently used to visually evaluate nuclear morphology of apoptotic cells including human cervical cancer cells (91). The apoptotic cells displays distorted and fragmented nuclear morphology as a hallmark of programmed cell death. Thus, the observed nuclear defragmentation by  $\beta$ -eudesmol or atractylodin treatment provides strong visual indication of compound-induced apoptosis in CL-6 cells. In addition, the inhibitory effect of the study compounds on cytoprotective enzyme such as HO-1 and NQO1 production and suppression of JAK-STAT and NF- $\kappa$ B pathway activation can be collectively linked to the observed cytotoxicity.

### **6.3 Anti-proliferative effect of atractylodin and $\beta$ -eudesmol in cholangiocarcinoma cells**

Colony forming assay is a well-established techniques used for *in vitro* evaluation of cell proliferation potentials of cancer cells. Pathways such as JAK/STAT and NF- $\kappa$ B are known to be actively involved in cell proliferations (19, 85). Thus, clonogenic assay can be used to determine effects of cytotoxic agents on inhibition of cell reproducibility after treatment with cytotoxic agents (92, 93). Previous report has indicated that STAT1/3 inhibitor nifuroxazide was able induce concentration-dependent inhibition of colony forming ability in breast cancer associated cell line (85). Atractylodin or  $\beta$ -eudesmol treatment was able to exhibit concentration-dependent inhibitory effect on colony forming ability of CL-6 cells. The effect was comparable with inhibition of CFU achieved by nifuroxazide and 5-FU treatment. Both atractylodin and  $\beta$ -eudesmol for their corresponding IC<sub>50</sub> concentration significantly suppressed CFU formation compared to untreated control. However,  $\beta$ -eudesmol treatment compared to atractylodin exhibited higher suppression of colony forming ability in CL6 cells for their corresponding IC<sub>50</sub> concentrations. Thus, the results provides a direct phenotypic evidence of the antiproliferative activity of the compounds treatment in CL-6 cells. In

addition, the results also suggest that observed antiproliferative activity may be associated with ability of the study compounds to suppress cytoprotective enzyme, NF- $\kappa$ B activation and JAK-STAT pathway.

#### **6.4 Effect of atractylodin and $\beta$ -eudesmol on *in vitro* wound healing ability of cholangiocarcinoma cells**

Several classes of cytokine including IL-6 and IFN- $\gamma$  are known to be inducers of cell migration (94-96). In particular, rapid cell migration is a distinct feature of cancer cells which helps promote metastasis (97). Previous study in CCA-related cell lines has reported association between cytokine-induced *in vitro* cell migration and STAT1/3 activation (19). In particular, IL-6 has been a prominent inducer of metastasis through activation of IL-6/STAT3 signaling in human CCA (98). Likewise, NF- $\kappa$ B can also be activated through IL-6 signaling and are reported to be essential for epithelial-mesenchymal transition during metastasis breast cancer progression (99). Based on results of the present study, the inability of cytokine stimulation to noticeably affect the wound healing ability of CL-6 cells may perhaps be due to the collective effect of aberrant activation of multiple signaling module associated with cell proliferation in CL-6 cells. However, atractylodin or  $\beta$ -eudesmol exposure resulted in significant depletion of wound closure ability in CL-6 cell. Atractylodin compared to  $\beta$ -eudesmol was comparatively stronger on suppression of wound healing ability of CL-6 cells at 48 h post stimulation. Similarly, the atractylodin exhibited relatively stronger effect on wound healing ability as compared to nifuroxazide in CL-6 cells. This may well be linked to the inhibitory effect of the compound on JAK-STAT activation. Overall, both atractylodin and  $\beta$ -eudesmol exhibited promising inhibitory effect on wound closure of CL-6 cells. In addition, the suppression of NF- $\kappa$ B activation and cytoprotective enzyme production may have also collectively contributed to the loss of wound healing ability of CL-6 cells.

## 6.5 Effect of atractylodin and $\beta$ -eudesmol on mRNA expression in cholangiocarcinoma cells

Phosphorylation-mediated activation of STAT transcription factors subsequently triggers induction of target gene amplification. In particular, the STAT3 activation is predominantly known to induce genes assisting epithelial-mesenchymal transition and metastasis in breast cancer cells (99). Intercellular cell adhesion molecule-1 (ICAM-1) and inducible nitric oxide synthase (iNOS) are frequently involved in JAK-STAT associated tumorigenesis and inflammation, respectively. Such association between metastatic progression and STAT3 associated gene induction has been well characterized in both *in vivo* and *in vitro* models for oncological studies (19, 100). In addition, aberrantly elevated serum levels of ICAM-1 has even been studied for its use as a potential discriminatory diagnostic marker for CCA patients (101). Similarly, chronic and up regulated levels of iNOS expression has been detected using immunohistochemistry in biliary epithelium biopsies of CCA patients conferring to continual inflammatory microenvironment maintenance for cancer progression (102). Therefore, the observed atractylodin or  $\beta$ -eudesmol pretreatment-induced suppression of ICAM-1 and iNOS mRNA expression in cytokine-stimulated CL-6 cells could be related with inhibitory effect of the study compounds on JAK-STAT activation. The suppressive effect on target gene expression was comparable to inhibition achieved by nifuroxazide on similar condition suggesting promising inhibitory effect of the study compounds on JAK/STAT activation.

Angiogenesis is crucial for tumor growth as well as for metastasis. Tumor cells proactively produce angiogenic factors such as vascular endothelial growth factor (VEGF) that act on receptors of endothelial cells to induce new blood vessels (103). Likewise, myeloid cell leukemia-1 (MCL-1) is a critical factor involved in increased drug resistance, cell survival and metastasis in plethora of tumors including breast cancer and cholangiocarcinoma (104, 105). Both VEGF-A and MCL-1 transcription can

be influenced by major cell survival and proliferation pathways. Therefore, ability of atractylodin or  $\beta$ -eudesmol to suppress VEGF and MCL-1 mRNA expression indicated wide range tumor suppression ability in CL-6 cells. Nonetheless, the noticeable inhibitory effect of  $\beta$ -eudesmol on additional genes including MMP9, Nrf2, HO-1 and NQO1 involved in tumor metastasis, tumor invasion and cytoprotection has demonstrated remarkable therapeutic potentials of the compound for further investigation.

### **6.6 Inhibitory effect of atractylodin and $\beta$ -eudesmol on HO-1 production in cholangiocarcinoma cells**

Tumorigenesis and metastasis generally involve increased expression of cytoprotective and cell survival-associated genes. In general, cytoprotective enzymes like HO-1 play a critical role in maintaining cellular homeostasis and has significant cytoprotective effect (106). However, cancer cells tend to have elevated metabolism and are exposed to generation of unusually high levels of reactive oxygen species (ROS) that can impact DNA, lipids, and proteins (34). Thus, to counteract such cellular stress and to maintain physiologically tolerable levels of ROS, the cancer cells often induce activation of a key regulator of redox-sensitive transcription factor, nuclear factor erythroid 2 p45-related factor 2 (Nrf2) which triggers production of HO-1 (34, 107). The HO-1 enzyme has been shown to be up-regulated and promote tumor growth and metastasis (88). In addition, it has been reported to enhance chemotherapy resistance in breast cancer cells and assist survival of renal cancer cells through modulation of autophagy- and apoptosis-regulating proteins (87, 108). Our present study showed substantial baseline level of HO-1 expression and its production inhibition by both atractylodin and  $\beta$ -eudesmol. Even though the effect of  $\beta$ -eudesmol compared to atractylodin was relatively stronger for suppression of HO-1 expression both compounds exhibited promising inhibitory potentials for suppression of HO-1

production. Thus the observed cytotoxicity on compound treatment may be linked to reduction of cytoprotective enzyme resulting in decreased survival of CL-6 cells.

### **6.7 Inhibitory effect of atractylodin and $\beta$ -eudesmol on NQO1 production in cholangiocarcinoma cells**

NQO1 is a ubiquitous cytosolic enzyme that catalyzes the reduction of quinone substrates. Expression of the enzyme is regulated by the Keap1-Nrf2 pathway, both in normal condition and during oxidative stress conditions (109). Numerous studies have indicated aberrant upregulation of NQO1 in cancers such as breast cancer, pancreatic cancer, colorectal cancer, and cholangiocarcinoma. The high expression of NQO1 has been reported to be associated with poor prognosis in serous ovarian carcinoma and pancreatic cancer (110). A report has suggested increased susceptibility of cancer cells towards chemotherapeutic agents such as gemcitabine and doxorubicin upon suppression of NQO1 production in CCA associated cells (111). During our study, we observed strong baseline expression of NQO1 in CL-6 cells which may be required for maintaining cellular homeostasis of these metabolically hyperactive cancer cells. Atractylodin and  $\beta$ -eudesmol treatment exhibited similar levels of suppression on NQO1 enzyme production in CL-6 cells. The inhibition of NQO1 enzyme production by atractylodin or  $\beta$ -eudesmol treatment in CL-6 cells may have thus contributed to overall cytotoxicity observed in CL-6 cells. However, the in detailed effectiveness in redox enzymatic activity of NQO1 can be an interesting topic for further research. Thus, our present study indicates considerable inhibitory effect of atractylodin or  $\beta$ -eudesmol on NQO1 production in CL-6.



## 6.8 Effect of atractylodin and $\beta$ -eudesmol on JAK/STAT pathway activation in cholangiocarcinoma cells

The JAK/STAT pathway has essential role in cell survival and proliferation. STAT3 is a key transcription factor (TF) in JAK/STAT pathway which is known to promote cell growth and migration. IL-6 and IFN- $\gamma$  can induce receptor-mediated site-specific phosphorylation of STAT3 and STAT1 at Tyr705 and Tyr701, respectively. This subsequently triggers its dimerization, nuclear translocation, recognition, and binding at STAT-specific DNA binding elements (23, 112). More specifically, the STAT3 activation subsequently leads to transcription of various STAT3 promoter-associated genes such as ICAM1, c-myc, survivin, and others that assist cell survival and proliferation (113). Similarly, IFN- $\gamma$ -induced phosphorylation of STAT1 consequently leads to transcription of genes that are usually considered as a tumor suppressor such as bcl-2, caspase-1, and bak (114). However, there is a growing evidence that correlates aberrant STAT1 activation with increased tumor progression in multiple types of cancer (19, 115). STAT3-linked signaling module are reported to be frequently altered in cancer cells to facilitate uncontrolled cell growth resulting in tumorigenesis and metastasis (100, 116). STAT3 is often considered to be a prominent transcription factor associated with oncogenic driver and promoter of malignancy in several cancers. It is recently being considered as one of the most promising new targets for cancer therapies (117, 118). Likewise, STAT1 is suggested to be involved in up-regulation of DNA repair pathways in breast cancer leading to radiotherapy and chemotherapy resistance (119-121). In addition, irregular presence and/or activation states of STAT1 has been reported in number of human tumors (114). Nonetheless, human STAT1 mutations and their implication in cancers have not been well understood. Hence, in contrast to normal cells where the STAT1/3 expression is only transient and strictly regulated, the cancer cells are often known to exhibit aberrant activation of STAT1/3 (118, 121). Both atractylodin and  $\beta$ -eudesmol displayed similar levels of suppression on



STAT1/3 activation. In contrast, atractylodin displayed relatively stronger suppressive effect on STAT1 phosphorylation as compared to nifuroxazide in CL-6 cells. Atractylodin and  $\beta$ -eudesmol both displayed relatively stronger suppressive effect on STAT3 phosphorylation as compared to nifuroxazide in CL-6. Overall, the observed inhibitory effects of atractylodin and  $\beta$ -eudesmol on STAT1/3 phosphorylation may have produced suppressive effect on overall JAK-STAT signaling cascade, leading to loss of cell viability in CL-6 cells. The inhibitory effect of atractylodin and  $\beta$ -eudesmol on STAT1/3 phosphorylation observed during our present study was comparable to effect displayed by known STAT1/3 selective inhibitor nifuroxazide which indicates considerable suppressive potency of atractylodin and  $\beta$ -eudesmol treatment on STAT1/3 activation. In addition, reduced colony forming ability has also been reported to be associated with inhibition of STAT3 activation in hepatic cancer cells (122). In this context, the observed concentration-dependent inhibition of CFU in CL-6 cells may also be linked to suppression of STAT activity by study compounds.

### **6.9 Effect of atractylodin and $\beta$ -eudesmol on NF- $\kappa$ B pathway activation in cholangiocarcinoma cells**

The NF- $\kappa$ B signaling cascade has essential role in cell proliferation, inflammation and innate immunity (123, 124). NF- $\kappa$ B transcription factors consists of complex variety of homo and hetero dimers of p65 (RelA), RelB, c-Rel, NF- $\kappa$ B1 (p105) and NF- $\kappa$ B2 (p100). The pre-forms NF- $\kappa$ B1 and NF- $\kappa$ B2 undergo proteolytic processing to produce p50 and p52, respectively (125). In normal stage, the NF- $\kappa$ B retains in cytosol as an inactive complex of NF- $\kappa$ B and I $\kappa$ B $\alpha$ . However, activation of NF- $\kappa$ B then requires rapid phosphorylation and ubiquitination of I $\kappa$ B $\alpha$ , which subsequently frees and enables NF- $\kappa$ B transcription factor to translocate into nucleus and activate  $\kappa$ B-associated promoter sites. Thus, accessing allowing I $\kappa$ B $\alpha$  degradation provides indirect measurement of NF- $\kappa$ B activation (126). Altered or aberrantly up-regulated expression of key NF- $\kappa$ B proteins, namely, p65, p50, or p52 have been observed in plethora of

cancers (127-130). In particular, aberrant expression and activation of p65 and p52 is widely reported in several forms of CCA and hepatocellular carcinomas (22, 131). NF- $\kappa$ B is among the key drivers of both acute and chronic inflammatory response which assists cancer progression (124, 132). A separate report suggests the synergistic interaction between STAT3 and NF- $\kappa$ B p65 in enhancement of gastric cancer cell migration and tissue invasion (133). IL-6 is a known enhancer of NF- $\kappa$ B pathway modulation. IFN- $\gamma$  has comparatively restrictive but supportive effects on NF- $\kappa$ B-mediated signaling (134, 135). In our current study, the observed dose- and time-dependent inhibition of key NF- $\kappa$ B proteins expression by atractylodin and  $\beta$ -eudesmol treatment in CL-6 cells suggested wide spectrum down regulatory activity of the study compounds on NF- $\kappa$ B signaling cascade. Remarkably, the cytokine stimulation did not significantly affected total baseline aggregate expression of NF- $\kappa$ B indicating unregulated expression of NF- $\kappa$ B independent of cytokine stimulation. Chemical-induced down-regulation of the p65 NF- $\kappa$ B protein has previously been used to investigate the collective inhibitory effect of various chemicals on NF- $\kappa$ B expression in hepatic cancer cells (136). Interestingly, baseline level of the p100 NF- $\kappa$ B protein was undetectable, which may be due to the altered or abnormally high levels of phosphorylation-dependent ubiquitination and processing of p100 protein in CL-6 cells. This can often be possible due to constitutional activation of non-canonical p52/RelB pathway with complex implication of NF- $\kappa$ B-inducing kinase and inhibitor of NF- $\kappa$ B kinase  $\alpha$  in cancer cells (137, 138). However, the underlying mechanism was beyond the scope of our current investigation. The consistent baseline expression and transient I $\kappa$ B $\alpha$  degradation within 45 min of cytokine stimulation suggests considerably non-constitutive activation of major NF- $\kappa$ B transcription factors in CL-6 cells. Atractylodin and  $\beta$ -eudesmol induced inhibitory activity on key NF- $\kappa$ B proteins downregulation and I $\kappa$ B $\alpha$  degradation may have at least in part contributed to the observed cytotoxicity in CL-6 cells. Interestingly, suppressive effect of  $\beta$ -eudesmol was relatively stronger than atractylodin for suppression of aggregate expression of NF- $\kappa$ B p105 and p50 in CL-6

cells at 24 h post treatment. However, both compounds exhibited similar levels of major NF- $\kappa$ B proteins inhibitions during cytokine stimulated condition. In addition, the ability of both atracylodin and  $\beta$ -eudesmol to suppress IL-6 induced I $\kappa$ B $\alpha$  degradation provides a strong indication of the inhibitory role of study compounds on NF- $\kappa$ B activation.

Studies have shown that MG132 is a specific, potent cell-permeable proteasome inhibitor and a well-known inhibitor of NF- $\kappa$ B pathway (139). Our observed high resistance of CL-6 against MG-132 directed cell death (IC<sub>50</sub> >20  $\mu$ M) indicates strong chemoresistative nature of CL-6 cells against proteasome-mediated apoptosis which is a frequent occurrence in cholangiocarcinoma and pancreatic cancers. These chemoresistant cancer cells have been reported to develop novel mechanism directed against the proteasome inhibitor including MG132 (140, 141). In this context, the suppressive effect exhibited by atracylodin and  $\beta$ -eudesmol on I $\kappa$ B $\alpha$  degradation being able to be comparable to the inhibition achieved by standard MG132 suggests promising potentials of the compounds on NF- $\kappa$ B pathway.

Both STAT and NF- $\kappa$ B transcriptional factors are known to promote directional cell migration, proliferation, and tissue invasion in various tumors (142, 143). Studies investigating crosstalk between STAT and NF- $\kappa$ B have indicated STAT3 and NF- $\kappa$ B crosstalk and collaboration in progression of gastric, colon, and liver cancers *via* expression of pro-proliferative, anti-apoptotic, and immune response gene. The cytokines such as IL-6 induced in tumor microenvironment results in induction of STAT3 activation in malignant cells (144). For instance, molecular cross-talk between the STAT3 and NF- $\kappa$ B signaling cascade has been reported to promote head and neck squamous cell Carcinoma through epidermal growth factor receptor-independent mechanisms (145). Nonetheless, the observed inhibitory effect of atracylodin and  $\beta$ -eudesmol on STAT1/3 phosphorylation as well as I $\kappa$ B $\alpha$  degradation suggests wide spectrum suppressive activity of the study compound that could potentially disrupt any existing cross-talk between the STAT and NF- $\kappa$ B signaling pathways. This may have

collectively contributed to the observed cytotoxicity of atractylodin and  $\beta$ -eudesmol treated CL-6 cells. However, these complex interactions often involve physical interaction between these transcriptional factors at gene promoters/enhancers level which is beyond the current scope of our study. In summary, our collective results from western blots suggested that atractylodin and  $\beta$ -eudesmol exerted promising inhibitory effect on these crucial cell survival and proliferation pathways in CL-6 cells.

#### **6.10 Effects of SnCl<sub>2</sub>-induced HO-1 expression in $\beta$ -eudesmol-treated cholangiocarcinoma cells**

Expression of HO-1 can be effectively induced by stannous chloride (SnCl<sub>2</sub>) stimulation (87, 88). Previous reports have indicated that SnCl<sub>2</sub> treatment (<20  $\mu$ M) was able to induce noticeable amounts of HO-1 in the course of 24 h in CCA associated cell lines (32). Likewise, previous study has shown that HO-1 gene knock down promotes apoptosis, enhances autophagy and makes breast cancer cells more susceptible towards chemotherapeutic agents (108). Interestingly, in our present study, SnCl<sub>2</sub> stimulation alone had no significant effect on colony forming and wound healing ability of CL-6 cells. This might be due to aberrant activation of multiple growth-associated pathways in CL-6 cells. However, the observed improvement achieved in colony forming, wound healing and cell viability of CL-6 during cotreatment of SnCl<sub>2</sub> and  $\beta$ -eudesmol indicated that HO-1 specifically had important role in cell survival and alleviates the cytotoxicity effect of  $\beta$ -eudesmol in CL-6 cells. Likewise, significant increment in SnCl<sub>2</sub>-induced HO-1 mRNA and protein expression was observed in CL-6 cells. The SnCl<sub>2</sub> noticeably induced the HO-1 expression within 24 h of treatment which is agreement with previous report (32). Thus, the ability of SnCl<sub>2</sub> to replenish  $\beta$ -eudesmol-induced reduction of HO-1 mRNA and protein expression might be linked to observed improvement in wound closure, nuclear defragmentation, and cell death of CL-6 cells.

### **6.11 Effects of Zinc(II) Protoporphyrin IX on HO-1 expression in cholangiocarcinoma cells**

ZN(II)PPIX is a known selective HO-1 inhibitor and exerts antitumor effects in various cancer cells. The compound has been previously reported to enhance chemotherapeutic susceptibility of hepatoma cells to cisplatin (146). ZN(II)PPIX has also been reported to exert anticancer effect by suppressing  $\beta$ -catenin protein expression in human ovarian carcinoma cells (147). Thus, as a supplementary information, the specific effect of ZN(II)PPIX treatment on HO-1 expression in CL-6 cells was observed in the present study. Interestingly the observed inhibitory effect of ZN(II)PPIX on HO-1 mRNA and protein expression suggested crucial role of HO-1 expression in CL-6 cells. The observed dose-dependent inhibition and  $IC_{50}$  value ( $<150 \mu M$ ) indicated that inhibition of HO-1 had substantial role in growth inhibition and viability of CL-6 cells. Taken together, the ZN(II)PPIX-induced suppression of HO-1 expression and considerable loss of cell viability suggested that targeting HO-1 production alone could have substantial effect on CL-6 cell viability. Thus, the corollary of this observation might explain the ability of atracylodin or  $\beta$ -eudemsol to effectively exert cytotoxic effect on CL-6 cells.

## CHAPTER 7

### CONCLUSIONS AND RECOMMENDATION

#### 7.1 Anti-cholangiocarcinoma effect of atractylodin

The CCA-associated cell line CL-6 provided a suitable *in vitro* model for testing the cytotoxic effect of atractylodin. The compound was relatively more cytotoxic towards CL-6 with  $IC_{50} < 300 \mu M$ , which is quite remarkable for highly drug resistant cancer of this type. Based on the morphological, antiproliferative and cell migration evaluation, atractylodin tended to show promising potentials to inhibit cell proliferation and migration of cancer cells. In particular, the ability of atractylodin to inhibit STAT1/3 phosphorylation suggested its potential to suppress JAK-STAT pathway. Likewise, the suppression of NF- $\kappa$ B activation *via* inhibition of I $\kappa$ B $\alpha$  degradation and overall downregulatory effect of atractylodin on major NF- $\kappa$ B suggested its ability to suppress NF- $\kappa$ B signaling pathway. In addition, the inhibitory effect exerted by atractylodin on production of crucial cytoprotective enzymes such as HO-1 and mRNA expression of metastasis-associated genes including ICAM-1, VEGF-A and MCL-1 opens up promising new avenues to explore its therapeutic potentials in CCA research. However, the in-depth molecular pathway analysis requires multiple additional experiments such as promoter activation analysis and study of potential epigenetic effect. Likewise, the current study does not investigate effect of atractylodin on other major pathways including PI3K-Akt and MAPKs pathways which might have significant role in cell survival. Due to limited availability and high cost of both compounds, the effect of atractylodin in animal model was not investigated. Future studies involving additional pathways, epigenetic evaluation, and *in vivo* experimentation are recommended to further explore the therapeutic potentials of atractylodin in CCA research.

## 7.2 Anti-cholangiocarcinoma effect of $\beta$ -eudesmol

Based on the observed inhibitory effect of  $\beta$ -eudesmol on CCA-associated cell line CL-6, the cytotoxic effect was considered to be remarkable with observed  $IC_{50} < 200 \mu M$ . This is quite noteworthy since CCA cells has exhibited high resistance to anticancer drugs such as 5-FU ( $IC_{50} > 1,000 \mu M$ ). The results from morphological, antiproliferative and cell migration assays suggested promising inhibitory effect of  $\beta$ -eudesmol on proliferation and migration of CCA cells. In particular, the observed suppressive effect of  $\beta$ -eudesmol on STAT1/3 phosphorylation suggested its ability to down-regulate JAK-STAT pathway. Similarly, the down-regulation of aggregate NF- $\kappa$ B protein expression and suppression of NF- $\kappa$ B activation by inhibiting I $\kappa$ B $\alpha$  degradation suggested its ability to suppress NF- $\kappa$ B signaling cascade. Likewise, the suppressive effect exerted by  $\beta$ -eudesmol on mRNA and protein expression of critical cytoprotective enzymes HO-1 tended to have considerably contributed to the overall cytotoxicity in CL-6 cells. The ability of  $\beta$ -eudesmol to exert wide spectrum inhibitory effect on mRNA expression of cell survival, tumorigenesis, and metastasis-associated genes such as MMP-9, VEGF-A, MCL-1, NQO1, NRF2, ICAM-1, VEGF-A, and MCL-1 indicated promising therapeutic potentials of the compound in CCA research. Nonetheless, additional in-depth molecular experiments involving epigenetic effect, promoter activity analysis and effect on enzyme cytoprotective activity are needed for future studies. Similarly, the present investigation does not focus on the effect of  $\beta$ -eudesmol on other major pathways including MAPKs, TRAIL, and PI3K-Akt signaling pathways which might have substantial role in survival cancer cells. The study did not include *in vivo* model to investigate the effect of  $\beta$ -eudesmol due to obtainability and cost of pure compounds. Current investigations have provided fruitful insights and promising anti-CCA potentials of  $\beta$ -eudesmol. It is highly recommended to conduct future in-depth studies

to explore further anticancer properties of  $\beta$ -eudesmol involving additional signaling pathways, epigenetic effect, and *in vivo* animal models.





## REFERENCES

1. Oh SW, Yoon YS, Shin SA. Effects of excess weight on cancer incidences depending on cancer sites and histologic findings among men: Korea National Health Insurance Corporation Study. *J Clin Oncol*. 2005 Jul 20;23(21):4742-54. PubMed PMID: 16034050.
2. Ustundag Y, Bayraktar Y. Cholangiocarcinoma: a compact review of the literature. *World J Gastroenterol*. 2008 Nov 14;14(42):6458-66. PubMed PMID: 19030196. PMCID: 2773330.
3. Blechacz B, Komuta M, Roskams T, Gores GJ. Clinical diagnosis and staging of cholangiocarcinoma. *Nat Rev Gastroenterol Hepatol*. 2011 Sep;8(9):512-22. PubMed PMID: 21808282. PMCID: 3331791.
4. Razumilava N, Gores GJ. Classification, diagnosis, and management of cholangiocarcinoma. *Clin Gastroenterol Hepatol*. 2013 Jan;11(1):13-21 e1; quiz e3-4. PubMed PMID: 22982100. PMCID: 3596004.
5. Ruys AT, Groot Koerkamp B, Wiggers JK, Klumpen HJ, ten Kate FJ, van Gulik TM. Prognostic biomarkers in patients with resected cholangiocarcinoma: a systematic review and meta-analysis. *Ann Surg Oncol*. 2014 Feb;21(2):487-500. PubMed PMID: 24081803.
6. Amin A, Gali-Muhtasib H, Ocker M, Schneider-Stock R. Overview of major classes of plant-derived anticancer drugs. *Int J Biomed Sci*. 2009 Mar;5(1):1-11. PubMed PMID: 23675107. PMCID: 3614754.
7. Namwat N, Amimanan P, Loilome W, Jearanaikoon P., Sripan B, Bhudhisawasdi V, et al. Characterization of 5-Fluorouracil-Resistant Cholangio-carcinoma Cell Lines. *Chemotherapy*. 2008;54:9.
8. Patel T. Cholangiocarcinoma. *Nat Clin Pract Gastroenterol Hepatol*. 2006 Jan;3(1):33-42. PubMed PMID: 16397610.
9. Gatto M, Bragazzi MC, Semeraro R, Napoli C, Gentile R, Torrice A, et al. Cholangiocarcinoma: update and future perspectives. *Dig Liver Dis*. 2010 Apr;42(4):253-60. PubMed PMID: 20097142.
10. Gores GJ. Cholangiocarcinoma: current concepts and insights. *Hepatology*. 2003 May;37(5):961-9. PubMed PMID: 12717374.

11. Shaib Y, El-Serag HB. The epidemiology of cholangiocarcinoma. *Semin Liver Dis.* 2004 May;24(2):115-25. PubMed PMID: 15192785.
12. Anderson CD, Pinson CW, Berlin J, Chari RS. Diagnosis and treatment of cholangiocarcinoma. *Oncologist.* 2004;9(1):43-57. PubMed PMID: 14755014.
13. Sripan B, Pairojkul C. Cholangiocarcinoma: lessons from Thailand. *Curr Opin Gastroenterol.* 2008 May;24(3):349-56. PubMed PMID: 18408464. PMCID: 4130346.
14. Bragazzi MC, Cardinale V, Carpio G, Venere R, Semeraro R, Gentile R, et al. Cholangiocarcinoma: Epidemiology and risk factors. *Translational Gastrointestinal Cancer.* 2012;1(1):12.
15. Pinlaor S, Onsurathum S, Boonmars T, Pinlaor P, Hongsrirach N, Chaidee A, et al. Distribution and abundance of *Opisthorchis viverrini* metacercariae in cyprinid fish in Northeastern Thailand. *Korean J Parasitol.* 2013 Dec;51(6):703-10. PubMed PMID: 24516277. PMCID: 3916461.
16. Burak K, Angulo P, Pasha TM, Egan K, Petz J, Lindor KD. Incidence and risk factors for cholangiocarcinoma in primary sclerosing cholangitis. *Am J Gastroenterol.* 2004 Mar;99(3):523-6. PubMed PMID: 15056096.
17. Haswell-Elkins MR, Sithithaworn P, Mairiang E, Elkins DB, Wongratanacheewin S, Kaewkes S, et al. Immune responsiveness and parasite-specific antibody levels in human hepatobiliary disease associated with *Opisthorchis viverrini* infection. *Clin Exp Immunol.* 1991 May;84(2):213-8. PubMed PMID: 2025950. PMCID: 1535388.
18. Tyson GL, El-Serag HB. Risk factors for cholangiocarcinoma. *Hepatology.* 2011 Jul;54(1):173-84. PubMed PMID: 21488076. PMCID: 3125451.
19. Senggunprai L, Kukongviriyapan V, Prawan A, Kukongviriyapan U. Quercetin and EGCG exhibit chemopreventive effects in cholangiocarcinoma cells via suppression of JAK/STAT signaling pathway. *Phytother Res.* 2014 Jun;28(6):841-8. PubMed PMID: 24038588.
20. Yu H, Jove R. The STATs of cancer--new molecular targets come of age. *Nat Rev Cancer.* 2004 Feb;4(2):97-105. PubMed PMID: 14964307.
21. Xiong A, Yang Z, Shen Y, Zhou J, Shen Q. Transcription Factor STAT3 as a Novel Molecular Target for Cancer Prevention. *Cancers (Basel).* 2014 Apr 16;6(2):926-57. PubMed PMID: 24743778. PMCID: 4074810.

22. Seubwai W, Wongkham C, Puapairoj A, Khuntikeo N, Pugkhem A, Hahnvajjanawong C, et al. Aberrant expression of NF-kappaB in liver fluke associated cholangiocarcinoma: implications for targeted therapy. *PLoS One*. 2014;9(8):e106056. PubMed PMID: 25170898. PMCID: 4149500.
23. Takeuchi O, Akira S. Pattern recognition receptors and inflammation. *Cell*. 2010 Mar 19;140(6):805-20. PubMed PMID: 20303872.
24. Vigushin DM, Mirsaidi N, Brooke G, Sun C, Pace P, Inman L, et al. Gliotoxin is a dual inhibitor of farnesyltransferase and geranylgeranyltransferase I with antitumor activity against breast cancer in vivo. *Med Oncol*. 2004;21(1):21-30. PubMed PMID: 15034210.
25. Malhi H, Gores GJ. Cholangiocarcinoma: modern advances in understanding a deadly old disease. *J Hepatol*. 2006 Dec;45(6):856-67. PubMed PMID: 17030071. PMCID: 1686172.
26. Fava G, Lorenzini I. Molecular pathogenesis of cholangiocarcinoma. *Int J Hepatol*. 2012;2012:630543. PubMed PMID: 21994887. PMCID: 3169310.
27. Moss SF, Blaser MJ. Mechanisms of disease: Inflammation and the origins of cancer. *Nat Clin Pract Oncol*. 2005 Feb;2(2):90-7; quiz 1 p following 113. PubMed PMID: 16264881.
28. Mathema VB, Na-Bangchang K. Current insights on cholangiocarcinoma research: a brief review. *Asian Pac J Cancer Prev*. 2015;16(4):1307-13. PubMed PMID: 25743790.
29. Buranrat B, Chau-in S, Prawan A, Puapairoj A, Zeekpudsa P, Kukongviriyapan V. NQO1 expression correlates with cholangiocarcinoma prognosis. *Asian Pac J Cancer Prev*. 2012;13 Suppl:131-6. PubMed PMID: 23480754.
30. Chen J, Zhang Z, Cai L. Diabetic cardiomyopathy and its prevention by nrf2: current status. *Diabetes Metab J*. 2014 Oct;38(5):337-45. PubMed PMID: 25349820. PMCID: 4209347.
31. Mitsuishi Y, Motohashi H, Yamamoto M. The Keap1-Nrf2 system in cancers: stress response and anabolic metabolism. *Front Oncol*. 2012;2:200. PubMed PMID: 23272301. PMCID: 3530133.
32. Kongpetch S, Kukongviriyapan V, Prawan A, Senggunprai L, Kukongviriyapan U, Buranrat B. Crucial role of heme oxygenase-1 on the sensitivity of

cholangiocarcinoma cells to chemotherapeutic agents. *PLoS One*. 2012;7(4):e34994. PubMed PMID: 22514698. PMCID: 3325916.

33. Glorieux C, Sandoval JM, Dejeans N, Ameye G, Poirrel HA, Verrax J, et al. Overexpression of NAD(P)H:quinone oxidoreductase 1 (NQO1) and genomic gain of the NQO1 locus modulates breast cancer cell sensitivity to quinones. *Life Sci*. 2016 Jan 15;145:57-65. PubMed PMID: 26687450.

34. Furfaro AL, Traverso N, Domenicotti C, Piras S, Moretta L, Marinari UM, et al. The Nrf2/HO-1 Axis in Cancer Cell Growth and Chemoresistance. *Oxid Med Cell Longev*. 2016;2016:1958174. PubMed PMID: 26697129. PMCID: 4677237.

35. Ma D, Fang Q, Li Y, Wang J, Sun J, Zhang Y, et al. Crucial role of heme oxygenase-1 in the sensitivity of acute myeloid leukemia cell line Kasumi-1 to ursolic acid. *Anticancer Drugs*. 2014 Apr;25(4):406-14. PubMed PMID: 24413389.

36. Chen P, Pang S, Yang N, Meng H, Liu J, Zhou N, et al. Beneficial effects of schisandrin B on the cardiac function in mice model of myocardial infarction. *PLoS One*. 2013;8(11):e79418. PubMed PMID: 24260217. PMCID: 3832629.

37. Dey S, Sayers CM, Verginadis, II, Lehman SL, Cheng Y, Cerniglia GJ, et al. ATF4-dependent induction of heme oxygenase 1 prevents anoikis and promotes metastasis. *J Clin Invest*. 2015 Jul 01;125(7):2592-608. PubMed PMID: 26011642. PMCID: 4563676.

38. Yang Y, Zhou X, Xu M, Piao J, Zhang Y, Lin Z, et al. beta-lapachone suppresses tumour progression by inhibiting epithelial-to-mesenchymal transition in NQO1-positive breast cancers. *Sci Rep*. 2017 Jun 02;7(1):2681. PubMed PMID: 28578385. PMCID: 5457413.

39. Yoon JH, Higuchi H, Werneburg NW, Kaufmann SH, Gores GJ. Bile acids induce cyclooxygenase-2 expression via the epidermal growth factor receptor in a human cholangiocarcinoma cell line. *Gastroenterology*. 2002 Apr;122(4):985-93. PubMed PMID: 11910351.

40. Werneburg NW, Yoon JH, Higuchi H, Gores GJ. Bile acids activate EGF receptor via a TGF-alpha-dependent mechanism in human cholangiocyte cell lines. *Am J Physiol Gastrointest Liver Physiol*. 2003 Jul;285(1):G31-6. PubMed PMID: 12606307.

41. Sriwanitchrak P, Viyanant V, Chaijaroenkul W, Srivatanakul P, Gram HR, Eursiddhichai V, et al. Proteomics analysis and evaluation of biomarkers for detection of cholangiocarcinoma. *Asian Pac J Cancer Prev*. 2011;12(6):1503-10. PubMed PMID: 22126489.
42. Patel AH, Harnois DM, Klee GG, LaRusso NF, Gores GJ. The utility of CA 19-9 in the diagnoses of cholangiocarcinoma in patients without primary sclerosing cholangitis. *Am J Gastroenterol*. 2000 Jan;95(1):204-7. PubMed PMID: 10638584.
43. Marrero JA. Biomarkers in Cholangiocarcinoma. *Clinical Liver Diseases*. 2014;3(5).
44. Tao LY, Cai L, He XD, Liu W, Qu Q. Comparison of serum tumor markers for intrahepatic cholangiocarcinoma and hepatocellular carcinoma. *Am Surg*. 2010 Nov;76(11):1210-3. PubMed PMID: 21140686.
45. Barr Fritcher EG, Voss JS, Jenkins SM, Lingineni RK, Clayton AC, Roberts LR, et al. Primary sclerosing cholangitis with equivocal cytology: fluorescence in situ hybridization and serum CA 19-9 predict risk of malignancy. *Cancer Cytopathol*. 2013 Dec;121(12):708-17. PubMed PMID: 23839915.
46. Navaneethan U, Gutierrez NG, Jegadeesan R, Venkatesh PG, Poptic E, Sanaka MR, et al. IgG4 Levels in Bile for Distinguishing IgG4-Associated Cholangiopathy from Other Biliary Disorders: A Single Blinded Pilot Study. *Clin Endosc*. 2014 Nov;47(6):555-9. PubMed PMID: 25505722. PMCID: 4260104.
47. Stroescu C, Herlea V, Dragnea A, Popescu I. The diagnostic value of cytokeratins and carcinoembryonic antigen immunostaining in differentiating hepatocellular carcinomas from intrahepatic cholangiocarcinomas. *J Gastrointest Liver Dis*. 2006 Mar;15(1):9-14. PubMed PMID: 16680226.
48. Tao J, Pu X, Jiang S. [Effect of endophytic fungal elicitors on growth and atractylodin accumulation of cell suspension cultures of *Atractylodes lancea*]. *Zhongguo Zhong Yao Za Zhi*. 2011 Jan;36(1):27-31. PubMed PMID: 21473147.
49. Sandhu DS, Shire AM, Roberts LR. Epigenetic DNA hypermethylation in cholangiocarcinoma: potential roles in pathogenesis, diagnosis and identification of treatment targets. *Liver Int*. 2008 Jan;28(1):12-27. PubMed PMID: 18031477. PMCID: 2904912.

50. Chiang NJ, Shan YS, Hung WC, Chen LT. Epigenetic regulation in the carcinogenesis of cholangiocarcinoma. *Int J Biochem Cell Biol.* 2015 Oct;67:110-4. PubMed PMID: 26100596.
51. Patel T. Cholangiocarcinoma--controversies and challenges. *Nat Rev Gastroenterol Hepatol.* 2011 Apr;8(4):189-200. PubMed PMID: 21460876. PMCID: 3888819.
52. Skipworth JR, Olde Damink SW, Imber C, Bridgewater J, Pereira SP, Malago M. Review article: surgical, neo-adjuvant and adjuvant management strategies in biliary tract cancer. *Aliment Pharmacol Ther.* 2011 Nov;34(9):1063-78. PubMed PMID: 21933219. PMCID: 3235953.
53. Kumar Bagepalli Srinivasa A, Kuruba L, Khan S, Saran GS. Antiurolithiatic activity of gokhsuradi churan, an ayurvedic formulation by in vitro method. *Adv Pharm Bull.* 2013;3(2):477-9. PubMed PMID: 24312883. PMCID: 3848215.
54. Gilani AH, Rahman AU. Trends in ethnopharmacology. *J Ethnopharmacol.* 2005 Aug 22;100(1-2):43-9. PubMed PMID: 16127805.
55. Rates SM. Plants as source of drugs. *Toxicon.* 2001 May;39(5):603-13. PubMed PMID: 11072038.
56. Shu YZ. Recent natural products based drug development: a pharmaceutical industry perspective. *J Nat Prod.* 1998 Aug;61(8):1053-71. PubMed PMID: 9722499.
57. Parkin DM. Global cancer statistics in the year 2000. *Lancet Oncol.* 2001 Sep;2(9):533-43. PubMed PMID: 11905707.
58. Lucas DM, Still PC, Perez LB, Grever MR, Kinghorn AD. Potential of plant-derived natural products in the treatment of leukemia and lymphoma. *Curr Drug Targets.* 2010 Jul;11(7):812-22. PubMed PMID: 20370646. PMCID: 2892601.
59. Plengsuriyakarn T, Viyanant V, Eursitthichai V, Picha P, Kupradinun P, Itharat A, et al. Anticancer activities against cholangiocarcinoma, toxicity and pharmacological activities of Thai medicinal plants in animal models. *BMC Complement Altern Med.* 2012;12:23. PubMed PMID: 22448640. PMCID: 3353211.
60. Zhao M, Wang Q, Ouyang Z, Han B, Wang W, Wei Y, et al. Selective fraction of *Atractylodes lancea* (Thunb.) DC. and its growth inhibitory effect on human gastric cancer cells. *Cytotechnology.* 2014 Mar;66(2):201-8. PubMed PMID: 23564282. PMCID: 3918255.



61. Mahavorasirikul W, Viyanant V, Chaijaroenkul W, Itharat A, Na-Bangchang K. Cytotoxic activity of Thai medicinal plants against human cholangiocarcinoma, laryngeal and hepatocarcinoma cells in vitro. *BMC Complement Altern Med*. 2010;10:55. PubMed PMID: 20920194. PMCID: 2956707.
62. Aneknan P, Kukongviriyapan V, Prawan A, Kongpetch S, Sripa B, Senggunprai L. Luteolin arrests cell cycling, induces apoptosis and inhibits the JAK/STAT3 pathway in human cholangiocarcinoma cells. *Asian Pac J Cancer Prev*. 2014;15(12):5071-6. PubMed PMID: 24998588.
63. Na-Bangchang K, Karbwang J. Traditional herbal medicine for the control of tropical diseases. *Trop Med Health*. 2014 Jun;42(2 Suppl):3-13. PubMed PMID: 25425945. PMCID: 4204050.
64. Murayama C, Wang CC, Michihara S, Norimoto H. Pharmacological effects of "jutsu" (*Atractylodes rhizome* and *Atractylodes lanceae rhizome*) on 1-(2,5-dimethoxy-4-iodophenyl)-2-aminopropane (DOI)-induced head twitch response in mice (I). *Molecules*. 2014;19(9):14979-86. PubMed PMID: 25237752.
65. Wang KT, Chen LG, Wu CH, Chang CC, Wang CC. Gastroprotective activity of atractylenolide III from *Atractylodes ovata* on ethanol-induced gastric ulcer in vitro and in vivo. *J Pharm Pharmacol*. 2010 Mar;62(3):381-8. PubMed PMID: 20487223.
66. Koonrunsesomboon N, Na-Bangchang K, Karbwang J. Therapeutic potential and pharmacological activities of *Atractylodes lancea* (Thunb.) DC. *Asian Pac J Trop Med*. 2014 Jun;7(6):421-8. PubMed PMID: 25066389.
67. Chen Y, Wu Y, Wang H, Gao K. A new 9-nor-atractylodin from *Atractylodes lancea* and the antibacterial activity of the atractylodin derivatives. *Fitoterapia*. 2012 Jan;83(1):199-203. PubMed PMID: 22061661.
68. Nakai Y, Kido T, Hashimoto K, Kase Y, Sakakibara I, Higuchi M, et al. Effect of the rhizomes of *Atractylodes lancea* and its constituents on the delay of gastric emptying. *J Ethnopharmacol*. 2003 Jan;84(1):51-5. PubMed PMID: 12499077.
69. Chen HP, Zheng LS, Yang K, Lei N, Geng ZF, Ma P, et al. Insecticidal and repellent activities of polyacetylenes and lactones derived from *Atractylodes lancea* rhizomes. *Chem Biodivers*. 2015 Apr;12(4):593-8. PubMed PMID: 25879503.

70. Jiao P, Tseng-Crank J, Corneliusen B, Yimam M, Hodges M, Hong M, et al. Lipase inhibition and antiobesity effect of *Atractylodes lancea*. *Planta Med.* 2014 May;80(7):577-82. PubMed PMID: 24687739.
71. Chu SS, Jiang GH, Liu ZL. Insecticidal compounds from the essential oil of Chinese medicinal herb *Atractylodes chinensis*. *Pest Manag Sci.* 2011 Oct;67(10):1253-7. PubMed PMID: 21520395.
72. Masuda Y, Kadokura T, Ishii M, Takada K, Kitajima J. Hinesol, a compound isolated from the essential oils of *Atractylodes lancea* rhizome, inhibits cell growth and induces apoptosis in human leukemia HL-60 cells. *J Nat Med.* 2015 Jul;69(3):332-9. PubMed PMID: 25833731.
73. Tsuneki H, Ma EL, Kobayashi S, Sekizaki N, Maekawa K, Sasaoka T, et al. Antiangiogenic activity of beta-eudesmol in vitro and in vivo. *Eur J Pharmacol.* 2005 Apr 11;512(2-3):105-15. PubMed PMID: 15840394.
74. Rucksaken R, Pairojkul C, Pinlaor P, Khuntikeo N, Roytrakul S, Selmi C, et al. Plasma autoantibodies against heat shock protein 70, enolase 1 and ribonuclease/angiogenin inhibitor 1 as potential biomarkers for cholangiocarcinoma. *PLoS One.* 2014;9(7):e103259. PubMed PMID: 25058392. PMCID: 4109983.
75. Srisomsap C, Sawangareetrakul P, Subhasitanont P, Panichakul T, Keeratichamroen S, Lirdprapamongkol K, et al. Proteomic analysis of cholangiocarcinoma cell line. *Proteomics.* 2004 Apr;4(4):1135-44. PubMed PMID: 15048994.
76. Huang L, Frampton G, Rao A, Zhang KS, Chen W, Lai JM, et al. Monoamine oxidase A expression is suppressed in human cholangiocarcinoma via coordinated epigenetic and IL-6-driven events. *Lab Invest.* 2012 Oct;92(10):1451-60. PubMed PMID: 22906985. PMCID: 3959781.
77. Sekiya S, Suzuki A. Intrahepatic cholangiocarcinoma can arise from Notch-mediated conversion of hepatocytes. *J Clin Invest.* 2012 Nov 1;122(11):3914-8. PubMed PMID: 23023701. PMCID: 3484442.
78. Yamada D, Rizvi S, Razumilava N, Bronk SF, Davila JJ, Champion MD, et al. IL-33 facilitates oncogene-induced cholangiocarcinoma in mice by an interleukin-6-sensitive mechanism. *Hepatology.* 2015 May;61(5):1627-42. PubMed PMID: 25580681. PMCID: 4406813.



79. Puthdee N, Vaeteewoottacharn K, Seubwai W, Wonkchalee O, Kaewkong W, Juasook A, et al. Establishment of an allo-transplantable hamster cholangiocarcinoma cell line and its application for in vivo screening of anti-cancer drugs. *Korean J Parasitol.* 2013 Dec;51(6):711-7. PubMed PMID: 24516278. PMCID: 3916462.
80. Saraste A, Pulkki K. Morphologic and biochemical hallmarks of apoptosis. *Cardiovasc Res.* 2000 Feb;45(3):528-37. PubMed PMID: 10728374.
81. Favalaro B, Allocati N, Graziano V, Di Ilio C, De Laurenzi V. Role of apoptosis in disease. *Aging (Albany NY).* 2012 May;4(5):330-49. PubMed PMID: 22683550. PMCID: 3384434.
82. Dai ZJ, Tang W, Lu WF, Gao J, Kang HF, Ma XB, et al. Antiproliferative and apoptotic effects of beta-elemene on human hepatoma HepG2 cells. *Cancer Cell Int.* 2013;13(1):27. PubMed PMID: 23496852. PMCID: 3614892.
83. Leyva-Illades D, McMillin M, Quinn M, Demorrow S. Cholangiocarcinoma pathogenesis: Role of the tumor microenvironment. *Transl Gastrointest Cancer.* 2012;1(1):71-80. PubMed PMID: 23002431. PMCID: 3448449.
84. Ebrahimi F, Gopalan V, Wahab R, Lu CT, Smith RA, Lam AK. Deregulation of miR-126 expression in colorectal cancer pathogenesis and its clinical significance. *Exp Cell Res.* 2015 Dec 10;339(2):333-41. PubMed PMID: 26455548.
85. Yang F, Hu M, Lei Q, Xia Y, Zhu Y, Song X, et al. Nifuroxazide induces apoptosis and impairs pulmonary metastasis in breast cancer model. *Cell Death Dis.* 2015;6:e1701. PubMed PMID: 25811798. PMCID: 4385941.
86. Xu Y, Zhang J, Shi W, Liu Y. Anticancer effects of 3,3'-diindolylmethane are associated with G1 arrest and mitochondria-dependent apoptosis in human nasopharyngeal carcinoma cells. *Oncol Lett.* 2013 Feb;5(2):655-62. PubMed PMID: 23420395. PMCID: 3573071.
87. Banerjee P, Basu A, Wegiel B, Otterbein LE, Mizumura K, Gasser M, et al. Heme oxygenase-1 promotes survival of renal cancer cells through modulation of apoptosis- and autophagy-regulating molecules. *J Biol Chem.* 2012 Sep 14;287(38):32113-23. PubMed PMID: 22843690. PMCID: 3442542.
88. Chau LY. Heme oxygenase-1: emerging target of cancer therapy. *J Biomed Sci.* 2015 Mar 21;22:22. PubMed PMID: 25885228. PMCID: 4380252.

89. Tepsiri N, Chaturat L, Sripa B, Namwat W, Wongkham S, Bhudhisawasdi V, et al. Drug sensitivity and drug resistance profiles of human intrahepatic cholangiocarcinoma cell lines. *World J Gastroenterol*. 2005 May 14;11(18):2748-53. PubMed PMID: 15884115. PMCID: 4305909.
90. You CX, Yang K, Wang CF, Zhang WJ, Wang Y, Han J, et al. Cytotoxic compounds isolated from *Murraya tetramera* Huang. *Molecules*. 2014 Aug 27;19(9):13225-34. PubMed PMID: 25165861.
91. Baharara J, Ramezani T, Divsalar A, Mousavi M, Seyedarabi A. Induction of Apoptosis by Green Synthesized Gold Nanoparticles Through Activation of Caspase-3 and 9 in Human Cervical Cancer Cells. *Avicenna J Med Biotechnol*. 2016 Apr-Jun;8(2):75-83. PubMed PMID: 27141266. PMCID: 4842245.
92. Franken NA, Rodermond HM, Stap J, Haveman J, van Bree C. Clonogenic assay of cells in vitro. *Nat Protoc*. 2006;1(5):2315-9. PubMed PMID: 17406473.
93. Fedr R, Pernicova Z, Slabakova E, Strakova N, Bouchal J, Grepl M, et al. Automatic cell cloning assay for determining the clonogenic capacity of cancer and cancer stem-like cells. *Cytometry A*. 2013 May;83(5):472-82. PubMed PMID: 23450810.
94. Sun W, Liu DB, Li WW, Zhang LL, Long GX, Wang JF, et al. Interleukin-6 promotes the migration and invasion of nasopharyngeal carcinoma cell lines and upregulates the expression of MMP-2 and MMP-9. *Int J Oncol*. 2014 May;44(5):1551-60. PubMed PMID: 24603891.
95. Hemeda H, Jakob M, Ludwig AK, Giebel B, Lang S, Brandau S. Interferon-gamma and tumor necrosis factor-alpha differentially affect cytokine expression and migration properties of mesenchymal stem cells. *Stem Cells Dev*. 2010 May;19(5):693-706. PubMed PMID: 20067407.
96. Lesur O, Brisebois M, Thibodeau A, Chagnon F, Lane D, Fullop T. Role of IFN-gamma and IL-2 in rat lung epithelial cell migration and apoptosis after oxidant injury. *Am J Physiol Lung Cell Mol Physiol*. 2004 Jan;286(1):L4-L14. PubMed PMID: 12922984.
97. Barouki R, Coumoul X. Cell migration and metastasis markers as targets of environmental pollutants and the Aryl hydrocarbon receptor. *Cell Adh Migr*. 2010 Jan-Mar;4(1):72-6. PubMed PMID: 20009531. PMCID: 2852561.

98. Zheng T, Hong X, Wang J, Pei T, Liang Y, Yin D, et al. Gankyrin promotes tumor growth and metastasis through activation of IL-6/STAT3 signaling in human cholangiocarcinoma. *Hepatology*. 2014 Mar;59(3):935-46. PubMed PMID: 24037855.
99. Huber MA, Azoitei N, Baumann B, Grunert S, Sommer A, Pehamberger H, et al. NF-kappaB is essential for epithelial-mesenchymal transition and metastasis in a model of breast cancer progression. *J Clin Invest*. 2004 Aug;114(4):569-81. PubMed PMID: 15314694. PMCID: 503772.
100. Jahani-Asl A, Bonni A. iNOS: a potential therapeutic target for malignant glioma. *Curr Mol Med*. 2013 Sep;13(8):1241-9. PubMed PMID: 23590833. PMCID: 4266467.
101. Janan M, Proungvitaya S, Limpai boon T, Proungvitaya T, Roytrakul S, Wongkham C, et al. Serum adhesion molecule-1 (ICAM-1) as a potential prognostic marker for cholangiocarcinoma patients. *Asian Pac J Cancer Prev*. 2012;13 Suppl:107-14. PubMed PMID: 23480771.
102. Jaiswal M, LaRusso NF, Burgart LJ, Gores GJ. Inflammatory cytokines induce DNA damage and inhibit DNA repair in cholangiocarcinoma cells by a nitric oxide-dependent mechanism. *Cancer Res*. 2000 Jan 01;60(1):184-90. PubMed PMID: 10646872.
103. Tokunaga T, Oshika Y, Abe Y, Ozeki Y, Sadahiro S, Kijima H, et al. Vascular endothelial growth factor (VEGF) mRNA isoform expression pattern is correlated with liver metastasis and poor prognosis in colon cancer. *Br J Cancer*. 1998 Mar;77(6):998-1002. PubMed PMID: 9528847. PMCID: 2150098.
104. Young AI, Law AM, Castillo L, Chong S, Cullen HD, Koehler M, et al. MCL-1 inhibition provides a new way to suppress breast cancer metastasis and increase sensitivity to dasatinib. *Breast Cancer Res*. 2016 Dec 08;18(1):125. PubMed PMID: 27931239. PMCID: 5146841.
105. Tanai M, Grambihler A, Higuchi H, Werneburg N, Bronk SF, Farrugia DJ, et al. Mcl-1 mediates tumor necrosis factor-related apoptosis-inducing ligand resistance in human cholangiocarcinoma cells. *Cancer Res*. 2004 May 15;64(10):3517-24. PubMed PMID: 15150106.
106. Maines MD. The heme oxygenase system: a regulator of second messenger gases. *Annu Rev Pharmacol Toxicol*. 1997;37:517-54. PubMed PMID: 9131263.

107. No JH, Kim YB, Song YS. Targeting nrf2 signaling to combat chemoresistance. *J Cancer Prev.* 2014 Jun;19(2):111-7. PubMed PMID: 25337579. PMCID: 4204167.
108. Zhu XF, Li W, Ma JY, Shao N, Zhang YJ, Liu RM, et al. Knockdown of heme oxygenase-1 promotes apoptosis and autophagy and enhances the cytotoxicity of doxorubicin in breast cancer cells. *Oncol Lett.* 2015 Nov;10(5):2974-80. PubMed PMID: 26722274. PMCID: 4665608.
109. Oh ET, Park HJ. Implications of NQO1 in cancer therapy. *BMB Rep.* 2015 Nov;48(11):609-17. PubMed PMID: 26424559. PMCID: 4911202.
110. Cui X, Li L, Yan G, Meng K, Lin Z, Nan Y, et al. High expression of NQO1 is associated with poor prognosis in serous ovarian carcinoma. *BMC Cancer.* 2015 Apr 09;15:244. PubMed PMID: 25885439. PMCID: 4399114.
111. Zeekpudsa P, Kukongviriyapan V, Senggunprai L, Sripa B, Prawan A. Suppression of NAD(P)H-quinone oxidoreductase 1 enhanced the susceptibility of cholangiocarcinoma cells to chemotherapeutic agents. *J Exp Clin Cancer Res.* 2014;33:11. PubMed PMID: 24460787. PMCID: 3922744.
112. Rebe C, Vegran F, Berger H, Ghiringhelli F. STAT3 activation: A key factor in tumor immunoescape. *JAKSTAT.* 2013 Jan 1;2(1):e23010. PubMed PMID: 24058791. PMCID: 3670267.
113. Li J, Piao YF, Jiang Z, Chen L, Sun HB. Silencing of signal transducer and activator of transcription 3 expression by RNA interference suppresses growth of human hepatocellular carcinoma in tumor-bearing nude mice. *World J Gastroenterol.* 2009 Jun 07;15(21):2602-8. PubMed PMID: 19496189. PMCID: 2691490.
114. Meissl K, Macho-Maschler S, Muller M, Strobl B. The good and the bad faces of STAT1 in solid tumours. *Cytokine.* 2017 Jan;89:12-20. PubMed PMID: 26631912.
115. Hix LM, Karavitis J, Khan MW, Shi YH, Khazaie K, Zhang M. Tumor STAT1 transcription factor activity enhances breast tumor growth and immune suppression mediated by myeloid-derived suppressor cells. *J Biol Chem.* 2013 Apr 26;288(17):11676-88. PubMed PMID: 23486482. PMCID: 3636858.
116. Kiu H, Nicholson SE. Biology and significance of the JAK/STAT signalling pathways. *Growth Factors.* 2012 Apr;30(2):88-106. PubMed PMID: 22339650. PMCID: 3762697.

117. Sellier H, Rebillard A, Guette C, Barre B, Coqueret O. How should we define STAT3 as an oncogene and as a potential target for therapy? *JAKSTAT*. 2013 Jul 01;2(3):e24716. PubMed PMID: 24069560. PMCID: 3772112.
118. Yu H, Lee H, Herrmann A, Buettner R, Jove R. Revisiting STAT3 signalling in cancer: new and unexpected biological functions. *Nat Rev Cancer*. 2014 Nov;14(11):736-46. PubMed PMID: 25342631.
119. Huang R, Faratian D, Sims AH, Wilson D, Thomas JS, Harrison DJ, et al. Increased STAT1 signaling in endocrine-resistant breast cancer. *PLoS One*. 2014;9(4):e94226. PubMed PMID: 24728078. PMCID: 3984130.
120. Becker M, Sommer A, Kratzschmar JR, Seidel H, Pohlenz HD, Fichtner I. Distinct gene expression patterns in a tamoxifen-sensitive human mammary carcinoma xenograft and its tamoxifen-resistant subline MaCa 3366/TAM. *Mol Cancer Ther*. 2005 Jan;4(1):151-68. PubMed PMID: 15657362.
121. Khodarev NN, Beckett M, Labay E, Darga T, Roizman B, Weichselbaum RR. STAT1 is overexpressed in tumors selected for radioresistance and confers protection from radiation in transduced sensitive cells. *Proc Natl Acad Sci U S A*. 2004 Feb 10;101(6):1714-9. PubMed PMID: 14755057. PMCID: 341831.
122. Zhao C, Wang W, Yu W, Jou D, Wang Y, Ma H, et al. A novel small molecule STAT3 inhibitor, LY5, inhibits cell viability, colony formation, and migration of colon and liver cancer cells. *Oncotarget*. 2016 Mar 15;7(11):12917-26. PubMed PMID: 26883202. PMCID: 4914331.
123. Brown M, Cohen J, Arun P, Chen Z, Van Waes C. NF-kappaB in carcinoma therapy and prevention. *Expert Opin Ther Targets*. 2008 Sep;12(9):1109-22. PubMed PMID: 18694378. PMCID: 2605706.
124. Karin M. NF-kappaB as a critical link between inflammation and cancer. *Cold Spring Harb Perspect Biol*. 2009 Nov;1(5):a000141. PubMed PMID: 20066113. PMCID: 2773649.
125. Hoesel B, Schmid JA. The complexity of NF-kappaB signaling in inflammation and cancer. *Mol Cancer*. 2013 Aug 02;12:86. PubMed PMID: 23915189. PMCID: 3750319.

126. Mathes E, O'Dea EL, Hoffmann A, Ghosh G. NF-kappaB dictates the degradation pathway of IkappaBalpha. *EMBO J*. 2008 May 07;27(9):1357-67. PubMed PMID: 18401342. PMCID: 2374849.
127. Yu Y, Wan Y, Huang C. The biological functions of NF-kappaB1 (p50) and its potential as an anti-cancer target. *Curr Cancer Drug Targets*. 2009 Jun;9(4):566-71. PubMed PMID: 19519322. PMCID: 3747820.
128. Abdel-Latif MM, O'Riordan J, Windle HJ, Carton E, Ravi N, Kelleher D, et al. NF-kappaB activation in esophageal adenocarcinoma: relationship to Barrett's metaplasia, survival, and response to neoadjuvant chemoradiotherapy. *Ann Surg*. 2004 Apr;239(4):491-500. PubMed PMID: 15024310. PMCID: 1356254.
129. Rayet B, Gelinas C. Aberrant rel/nfkb genes and activity in human cancer. *Oncogene*. 1999 Nov 22;18(49):6938-47. PubMed PMID: 10602468.
130. Nishimura D, Ishikawa H, Matsumoto K, Shibata H, Motoyoshi Y, Fukuta M, et al. DHMEQ, a novel NF-kappaB inhibitor, induces apoptosis and cell-cycle arrest in human hepatoma cells. *Int J Oncol*. 2006 Sep;29(3):713-9. PubMed PMID: 16865289.
131. Luedde T, Schwabe RF. NF-kappaB in the liver--linking injury, fibrosis and hepatocellular carcinoma. *Nat Rev Gastroenterol Hepatol*. 2011 Feb;8(2):108-18. PubMed PMID: 21293511. PMCID: 3295539.
132. Karin M, Cao Y, Greten FR, Li ZW. NF-kappaB in cancer: from innocent bystander to major culprit. *Nat Rev Cancer*. 2002 Apr;2(4):301-10. PubMed PMID: 12001991.
133. Yoon J, Cho SJ, Ko YS, Park J, Shin DH, Hwang IC, et al. A synergistic interaction between transcription factors nuclear factor-kappaB and signal transducers and activators of transcription 3 promotes gastric cancer cell migration and invasion. *BMC Gastroenterol*. 2013 Feb 12;13:29. PubMed PMID: 23402362. PMCID: 3583822.
134. Johnson C, Han Y, Hughart N, McCarra J, Alpini G, Meng F. Interleukin-6 and its receptor, key players in hepatobiliary inflammation and cancer. *Transl Gastrointest Cancer*. 2012 Apr 1;1(1):58-70. PubMed PMID: 22724089. PMCID: 3378312.
135. Harada K, Isse K, Nakanuma Y. Interferon gamma accelerates NF-kappaB activation of biliary epithelial cells induced by Toll-like receptor and ligand interaction. *J Clin Pathol*. 2006 Feb;59(2):184-90. PubMed PMID: 16443736. PMCID: 1860324.



136. Kretzmann NA, Chiela E, Matte U, Marroni N, Marroni CA. N-acetylcysteine improves antitumoural response of Interferon alpha by NF-kB downregulation in liver cancer cells. *Comp Hepatol*. 2012 Dec 04;11(1):4. PubMed PMID: 23206959. PMCID: 3539937.
137. Sun SC. The noncanonical NF-kappaB pathway. *Immunol Rev*. 2012 Mar;246(1):125-40. PubMed PMID: 22435551. PMCID: 3313452.
138. Wharry CE, Haines KM, Carroll RG, May MJ. Constitutive non-canonical NFkappaB signaling in pancreatic cancer cells. *Cancer Biol Ther*. 2009 Aug;8(16):1567-76. PubMed PMID: 19502791. PMCID: 2910422.
139. Nakajima S, Kato H, Takahashi S, Johnno H, Kitamura M. Inhibition of NF-kappaB by MG132 through ER stress-mediated induction of LAP and LIP. *FEBS Lett*. 2011 Jul 21;585(14):2249-54. PubMed PMID: 21627972.
140. Wente MN, Eibl G, Reber HA, Friess H, Buchler MW, Hines OJ. The proteasome inhibitor MG132 induces apoptosis in human pancreatic cancer cells. *Oncol Rep*. 2005 Dec;14(6):1635-8. PubMed PMID: 16273269.
141. Chong KY, Hsu CJ, Hung TH, Hu HS, Huang TT, Wang TH, et al. Wnt pathway activation and ABCB1 expression account for attenuation of proteasome inhibitor-mediated apoptosis in multidrug-resistant cancer cells. *Cancer Biol Ther*. 2015;16(1):149-59. PubMed PMID: 25590413. PMCID: 4623479.
142. Teng TS, Lin B, Manser E, Ng DC, Cao X. Stat3 promotes directional cell migration by regulating Rac1 activity via its activator betaPIX. *J Cell Sci*. 2009 Nov 15;122(Pt 22):4150-9. PubMed PMID: 19861492.
143. Phoomak C, Vaeteewoottacharn K, Sawanyawisuth K, Seubwai W, Wongkham C, Silsirivanit A, et al. Mechanistic insights of O-GlcNAcylation that promote progression of cholangiocarcinoma cells via nuclear translocation of NF-kappaB. *Sci Rep*. 2016 Jun 13;6:27853. PubMed PMID: 27290989. PMCID: 4904198.
144. Grivennikov SI, Karin M. Dangerous liaisons: STAT3 and NF-kappaB collaboration and crosstalk in cancer. *Cytokine Growth Factor Rev*. 2010 Feb;21(1):11-9. PubMed PMID: 20018552. PMCID: 2834864.
145. Squarize CH, Castilho RM, Sriuranpong V, Pinto DS, Jr., Gutkind JS. Molecular cross-talk between the NFkappaB and STAT3 signaling pathways in head

and neck squamous cell carcinoma. *Neoplasia*. 2006 Sep;8(9):733-46. PubMed PMID: 16984731. PMCID: 1584297.

146. Liu YS, Li HS, Qi DF, Zhang J, Jiang XC, Shi K, et al. Zinc protoporphyrin IX enhances chemotherapeutic response of hepatoma cells to cisplatin. *World J Gastroenterol*. 2014 Jul 14;20(26):8572-82. PubMed PMID: 25024611. PMCID: 4093706.

147. Wang S, Hannafon BN, Lind SE, Ding WQ. Zinc Protoporphyrin Suppresses beta-Catenin Protein Expression in Human Cancer Cells: The Potential Involvement of Lysosome-Mediated Degradation. *PLoS One*. 2015;10(5):e0127413. PubMed PMID: 26000787. PMCID: 4441374.

148. Nelson EA, Walker SR, Kepich A, Gashin LB, Hideshima T, Ikeda H, et al. Nifuroxazide inhibits survival of multiple myeloma cells by directly inhibiting STAT3. *Blood*. 2008 Dec 15;112(13):5095-102. PubMed PMID: 18824601. PMCID: 2597607.

149. Livak KJ, Schmittgen TD. Analysis of relative gene expression data using real-time quantitative PCR and the 2(-Delta Delta C(T)) Method. *Methods*. 2001 Dec;25(4):402-8. PubMed PMID: 11846609.



## APPENDICES

### Appendix A. Stock chemicals preparation

#### Atractylodin stock solution preparation:

- 4 mg/ml master stock solution was prepared
- 2 mg of atractylodin (M.W: 256.257) power was measured and mixed with 500  $\mu$ l of 50% ethanol to make a final concentration of 4 mg/ml solution.
- The mixture was briefly sonicated to make a clear solution and stored at -20°C.

#### $\beta$ -eudesmol stock solution preparation:

- 4 mg/ml master stock solution was prepared
- 2 mg of  $\beta$ -eudesmol (M.W: 222.372) power was measured and mixed with 500  $\mu$ l of 50% ethanol to make a final concentration of 4 mg/ml solution.
- The mixture was briefly sonicated to make a clear solution and stored at -20°C.

#### Nifuroxazide stock solution preparation:

- 10 mM of master stock was prepared
- 1.4 mg of Nifuroxazide (M.W: 275.22) power was measured and mixed with 500  $\mu$ l of 50% ethanol to make a final concentration of 10 mg/ml solution.
- The mixture was briefly sonicated to make a clear solution and stored at -20°C.

#### Protoporphyrin IX zinc(II) stock solution preparation:

- 10 mM of master stock was prepared

- 3.1 mg of Nifuroxazide (M.W: 626.03) power was measured and mixed with 500  $\mu$ l of deionized water to make a final concentration of 10 mM solution.

The mixture was briefly shaken to make a clear solution and stored at -20°C

Protoporphyrin 5-fluorouracil stock solution preparation:

- 4 mg/ml of master stock was prepared
- 2 mg of 5-fluorouracil (M.W: 130.077) power was measured and mixed with 500  $\mu$ l of 50% ethanol to make a final concentration of 4 mg/ml solution.

The mixture was briefly sonicated to make a clear solution and stored at -20°C

MG132 solution preparation:

- Ready to use 10 mM solution in DMSO

Human Interleukin-6 (Cell Signaling Cat# 8904) and  
Interferon- $\gamma$  (BioVision Cat# 7163-10)

- Arrives as lyophilized vial. Re-constitute in 1000  $\mu$ l to make 20  $\mu$ g/ml solution.
- Aliquot 20  $\mu$ l/vial and store at -20°C to -80°C

Stannous (II) chloride working solution preparation:

- Due to nature of chemical stability, only freshly prepared stannous chloride ( $\text{SnCl}_2$ ) was used during experiment.
- 10 mM working solution was prepared to minimize measuring error.
- 1.9 mg of  $\text{SnCl}_2$  (M.W: 189.62) power was measured and mixed with 50-100  $\mu$ l of 1 M HCL for obtaining clear solution.
- Final volume was made upto 1000  $\mu$ l by adding deionized water to make a final concentration of 10 mM solution.

- The mixture was briefly shaken to make a clear solution and used freshly

All stock and working solutions were further diluted using formula

$$V_1 \times S_1 = V_2 \times S_2$$

Where **V** is volume and **S** in concentration.

4% paraformaldehyde cell-fixation solution preparation protocol adopted from  
(Biotech R&D systems 2016)

- For 100 ml of 4% Formaldehyde, 80 mL of 1X PBS is added to a glass beaker on a stir plate in a ventilated hood. Heat while stirring to approximately 60 °C.
- It is made sure that the solution does not boils.
- 4 g of paraformaldehyde powder is then to the heated PBS solution.
- If powder does not immediately dissolve into solution, pH should be slowly raised by adding 1 N NaOH dropwise from a pipette until the solution clears.
- Once the paraformaldehyde is dissolved, the solution should be cooled and filtered.
- The volume is then adjusted to 100 ml by adding 1X PBS.
- pH is rechecked, and adjusted to 6.9 by adding small amounts of dilute HCl.
- The solution can be aliquoted and frozen or stored at 2-8 °C for up to one month.

**Appendix B.** Protocol for heat inactivation of Fetal Bovine Serum (FBS) adopted from Gibco Life Science (2014)

- Allow serum to acclimate at room temperature for a minimum of 10 minutes or refrigerate overnight at 2° C to 8° C.
- The serum may then be completely thawed at room temperature. Or, you may choose to proceed by thawing the serum in a water bath at 37° C. Thawing serum at temperatures above 37° C or for an extended period of time could lessen the quality of serum and possibly cause increased amounts of precipitates and/or cause a cloudy appearance to the serum. Swirl the bottles throughout the thawing process every 10-15 minutes as this will disperse the released salts and proteins uniformly.
- Prepare a water bath, if not already done so during the thawing process, that can be temperature controlled to 56° C for the heat inactivation process. There must be enough water to submerge the entire contents of all bottles.
- Fill a control bottle with water to monitor the water bath temperature. The control bottle must be identical to the bottles being heat inactivated and the temperature of the water within the control bottle should be the same as that of the thawed serum.
- Place the control bottle and serum into the 56° C water bath. Suspend a calibrated thermometer into the control bottle to monitor the temperature during the heating process. Do not allow the thermometer to touch the sides or bottom of the bottle.
- Set a timer to 30 minutes once the temperature of the control bottle has reached 56° C. Maintain this same temperature the entire duration of the process.
- Gently swirl the bottles every 3-5 minutes to make certain the serum remains uniform throughout heating. Remove the heat inactivated serum after 30 minutes and gently swirl once again.

- Allow the bottles to cool and reach room temperature.
- Store the heat inactivated serum at -20° C for future use.



### **Appendix C.** Culture media preparation for cell culture adopted from Abcam (2015)

General guideline for laboratory safety and good laboratory practice should be followed for culturing of cell lines. All cell culture must be undertaken in microbiological safety laminar airflow cabinet using aseptic technique to assure sterility.

#### **Preparation of cell growth medium**

Most cell lines can be grown using DMEM culture media or RPMI culture media supplemented with 10% Fetal Bovine Serum (FBS), 2mM glutamine and antibiotics can be added if required. RPMI complete growth medium composition. All materials should be either pre-sterile or autoclaves/filtered to maintain sterility.

Composition of RPMI complete medium for 500 mL volume

<b>Components</b>	<b>Volume</b>
RPMI	450 ml
10 % FBS	50 ml
100 X Anti-Anti (Anti-biotic solution)	5 ml
2 mM Glutamin (optional)	5 ml

Composition of DMEM complete medium for 500 ml volume

<b>Components</b>	<b>Volume</b>
DMEM	450 ml
10 % FBS	50 ml
100 X Anti-Anti (Anti-biotic solution)	5 ml
2 mM Glutamin (optional)	5 ml

**Appendix D.** Standard *in vitro* cell culture protocol adopted from Abcam (2014)

1. Remove and discard the spent cell culture media from culture flask inside laminar flow hood.
2. Wash cells using a balanced salt solution (phosphate buffered solution or PBS of approximately 2 mL). Washing solution gently added to the side of the flask opposite the attached cell layer to avoid disturbing the cell layer, and then shaking of the vessel several times.
3. Remove or discard the washing solution from the culture flask.
4. Add the pre-warmed dissociation reagent (e.g. trypsin of approximately 1 ml for T-25 flask) to the side of the flask and then gently shake the container to get the reagent completely cover the cell layer.
5. Incubate the culture vessel at room temperature for approximately 2 minutes.
6. The cells observed under the microscope for detachment and if cells are less than 90% detached, the incubation time increased for a few more minutes.
7. Add approximately 3 ml of pre-warmed RPMI complete medium and the medium is dispersed by pipetting over the cell layer surface several times.
8. Transfer the cells to a 15-mL conical tube and centrifuge then at for 5 minutes (Note: the centrifuge speed and time vary based on the cell type) and discard the supernatant.
9. Resuspend the cell in 2 in Pre-warmed culture medium and take a sample (20 uL) for counting in haemocytometer.
10. Determine the total number of cells per ml.. Pipette approximately 200 ul of cell suspension into new T-25 flask containing around 5 ml of complete growth medium. Check for the type of caps on the flask before incubation. If the caps are without filter, loosen abit for letting the gaseous exchange.
12. In case confluency of cell culture is below 60% and media turns yellow, simply exchange the growth medium and further incubate.

**Appendix E.** MTT assay for cell viability adapted from Lab (2007)

Protocol adopted for 96 well microplate assay: Each independent experiment was conducted in triplicate.

1. **Day 0:** Trypsinize T-25 culture flask of CL-6 cells and add 3 ml of complete RPMI media to trypsinized cells.
2. Centrifuge in a sterile 15 ml falcon tube at 1500 rpm for 5 min.
2. Remove media and resuspend cells to 2 ml with complete media.
3. Count the cells by using hemacytometer and calculate cells number per ml of the volume.
4. Dilute the cells ( $V_1S_1 = V_2S_2$ ) to 100,000 cells per ml (i.e.  $10^4$  cells per 100 $\mu$ l) by using complete media to dilute cells. Add 100  $\mu$ l of cells ( $10^4$  total cells) into each well of the 96-well plate and incubate overnight.
6. **Day 1:** Treat cells on next day with test compounds and standard drug (Note only media is added for the control well) to obtain desired concentration.
7. **Day 3:** (after 48 hours post-treatment): Add 20  $\mu$ l of 5 mg/ml MTT reagent (dissolved in PBS). Include one well with MTT and culture medium but no cells.
8. Shake gently to mix the MTT solution and further incubate for 3.5 hours in cell culture incubator.
9. Carefully remove the medium without disturbing the bottom layer (do not rinse with PBS).
10. Add 100  $\mu$ l of DMSO in each well for dissolving the formazan crystals. Cover plate with aluminum foil and shake with orbital shaker at 100 RPM for 10 mins.
11. Read absorbance at 590 nM using 96-well compatible spectrometer (e.g. Varioscan<sup>TM</sup> flash microplate reader).



## **Appendix F.** Protocol for Colony formation assay adopted from (148)

Protocol adopted for anti-proliferative assay using Colony formation ability of cells

1. Colony formation assay was performed as standard from of colony formation unit (CFU) measurement with minor modifications.
2. After 24-48 h of treatment, the cells are collected using trypsinization, counted (dilute 1:10X if needed before lowering down the concentration for more accuracy)
3. CL-6 cells (approximately 300 cells/well) were then seeded in six-well plates.
4. The cells are then incubated for additional 10-12 days.
5. Culture Media is exchanged every 3-4 days.
6. Once the colonies (>50 cells) appeared, the cells are fixed with absolute ethanol for 10 mins and stained with Diff-Quik® methylene blue solution for 15 min, and the number of colonies is counted under microscope.
7. Series of images is taken to document representative image for the experiment.
8. The inhibition of colonies formation is calculated using following formula:

$$\% \text{ of CFU inhibition} = \frac{(\text{Average CFU of Sample})}{(\text{Average CFU in control})} \times 100\%$$

**Appendix G.** Protocol for *in vitro* wound healing assay adopted from (19)

Protocol for *in vitro* wound healing assay. The experiment was conducted according to standard procedure of scratch tests, commonly known as wound healing assay with minor modifications.

1. CL-6 cells ( $1 \times 10^5$  per well) were seeded into a 24-well plate and were grown in RPMI complete medium supplemented with 5% fetal calf serum until the cells became confluent.
2. A scratch wound was made with a sterile 200  $\mu$ l pipette tip without destroying culture flask but only to detach cells at the area. .
3. The cultures were washed with PBS to remove any detached cells and pretreated with serum-free medium containing test sample or culture medium alone for 2 h followed by (optional, only used for STAT activation) cytokine stimulation (50 ng/ml IL-6 and 50 ng/ml IFN- $\gamma$ ) for 24-48 h.
4. At 0, 24 and 48 h, series of images were acquired using inverted microscope and the inhibitory effect (% of control) on cell migration was estimated.
5. The closing of scratched wound, which represented the migration process, was determined by analyzing the images of denuded area along the scratch using ImageJ software (NIH, Maryland, USA).
6. The wound distance was measured by dividing the area by the length of scratch and represented as percentage of wound closure compared to the untreated control.

**Appendix H.** DAPI based inflorescence Cell staining adopted from ThermoFisher Scientific Reference Library (2014)

4',6-Diamidino-2-Phenylindole, Dihydrochloride (DAPI) is a well-known nuclear and chromosome counterstain. DAPI emits blue fluorescence under UV filter upon binding to AT regions of DNA. The dye is relatively permeable and can enter the live cells at higher concentrations.

**DAPI stock preparation:**

1. Add 2 mL of deionized water (diH<sub>2</sub>O) to the entire contents of the DAPI vial to make a 14.3 mM (5 mg/mL) DAPI stock solution. (Note: DAPI has poor solubility in water, so sonicate as necessary to dissolve. The 5 mg/mL DAPI stock solution may be stored at 2–6°C for up to 6 months or at –20°C for longer periods. Cover with appropriate enclosure to avoid direct light).
2. Add 2.1 µL of the 14.3 mM DAPI stock solution to 100 µL PBS to make a 300 µM DAPI intermediate dilution. Dilute the 300 µM DAPI intermediate dilution 1:1000 in PBS as needed to make a 300 nM DAPI stain solution.

**Cell fixation using 4% Paraformaldehyde:**

1. Wash the cells two times with 1X PBS.
2. Fix the cell for 5 min using 4% paraformaldehyde (Note: use freshly prepared. whenever possible). Gently wash the cells two times with 1X PBS.

**DAPI staining:**

4. Treat each well with appropriate volume of 300 nM DAPI solution and incubate for 5-10 min at room temperature in dark.

Note: make sure that enough DAPI solution is present to completely cover the surface of culture plate.

5. Gently wash the cells several times with 1X PBS and immediately view/ image the cells under inflorescence microscope with UV filter.



**Appendix I.** Western blot sample preparation protocol adopted from Bio-Rad laboratories standard protocol for typical cell culture scenario)

**Mammalian protease inhibitor cocktail:** Contains following protease inhibitors for mammalian cell use: AEBSF, Aprotinin, E-64, Bestatin, Leupeptin and Pepstatin. Each vial can be reconstituted in 1 ml deionized water to form a 100X solution.

**RIPA cell lysis buffer:** Ready-to-use solution containing 150 mM NaCl, 1.0% IGEPAL® CA-630, 0.5% sodium deoxycholate, 0.1% SDS, 50 mM Tris, pH 8.0.

1. Place the cell culture dish in ice and wash the cells with ice-cold Tris-buffered saline (TBS).
2. Aspirate the TBS, then add ice-cold RIPA buffer (1 ml per 100 mm dish) containing 1X protease inhibitor cocktail.
3. Scrape adherent cells off the dish using a cold plastic cell scraper and gently transfer the cell suspension into a precooled microcentrifuge tube.
4. Maintain constant agitation for 30 min at 4°C.
5. If necessary, sonicate 3 times for 10-15 sec to complete cell lysis and shear DNA to reduce sample viscosity.
6. Spin at 16,000 x g for 20 min in a 4°C precooled centrifuge. Gently remove the centrifuge tube and place it on ice. Transfer the supernatant to a fresh tube, also kept on ice, and discard the pellet. Remove a small volume (10-20  $\mu$ l) of lysate to perform a protein assay. Determine the protein concentration for each cell lysate.
9. If necessary, aliquot the protein samples for long-term storage at -20°C. Repeated freeze and thaw cycles cause protein degradation and should be avoided.
10. Take 50  $\mu$ g of each sample and add an equal volume of 2x Laemmli sample buffer.

11. Boil each cell lysate in sample buffer at 95°C for 5 min. Centrifuge at 16,000 x g in a microcentrifuge for 1 min and immediately cool it on ice before use.
13. Use the samples for loading onto appropriate SDSA-PAGE gel along with suitable protein marker.



**Appendix J.** Protein concentration calculation using DC protein assay kit from Bio-Rad laboratory (2015)

The protocol is given for microplate based assay using DC protein assay (Bio-Rad™, Catalog No.#500-0116).

1. Preparation of working reagent.

Add 20 µl of reagent S to each ml of reagent A that will be needed for the run. (This working reagent A' is stable for one week even though a precipitate will form after one day. If precipitate forms, warm the solution and vortex. Do not pipet the undissolved precipitate, as this will likely plug the tip of the pipet, thereby altering the volume of reagent that is added to the sample. If samples do not contain detergent, you may simply use reagent A without adding reagent S.

2. Prepare 3-5 dilutions of a protein standard containing from 0.2 mg/ml to about 1.5 mg/ml protein. A standard curve should be prepared each time the assay is performed. For best results, the standards should always be prepared in the same buffer as the sample.

3. Pipet 5 µl of standards and samples into a clean, dry microtiter plate.

4. Add 25 µl of reagent A' or reagent A (see note from step 1) into each well.

5. Add 200 µl reagent B into each well. If microplate reader has a mixing function available, place plate in reader and let the plate mix for 5 seconds. If not, gently agitate the plate to mix the reagents. If bubbles form, pop them with a clean, dry pipet tip. Be careful to avoid cross-contamination of sample wells.

6. After 15 minutes, absorbances can be read at 750 nm. The absorbances will be stable for about 1 hour. (See Troubleshooting Guide for recommendation on using a wavelength other than 750 nm.).

### Standard calibration curve for DC protein assay

Based on the type of standard proteins used and laboratory condition, the absorbance obtained can show variation. Thus, the curve with linearity for given  $R^2$  value 0.95 is recommended for calibration.

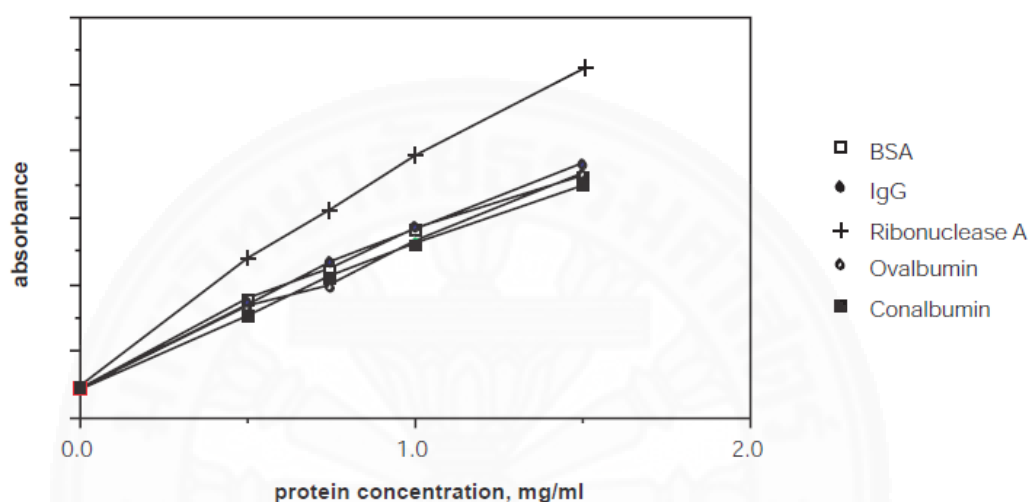


**Figure** Representation of the standard calibration curve for determination of protein using DC protein assay kit.



**Appendix K:** SDS PAGE-gel preparation protocol adopted from Bio-Rad laboratory (2015)

An intact SDS PAGE electrophoresis system should include: a tank, lid with power cables, electrode assembly, cell buffer dam, casting stands, casting frames, combs(usually 10-well or 15-well), and glass plates (thickness 0.75mm or 1.0mm or 1.5mm). (Bio-rad brand one is recommended). The SDS PAGE gel in a single electrophoresis run can be divided into stacking gel and separating gel. Stacking gel (acrylamide 5%) is poured on top of the separating gel (after solidification) and a gel comb is inserted in the stacking gel.

Thickness of the gel	Vol. of stacking gel	Vol. of separating gel
0.75mm	2ml	4ml
1.0mm	3ml	6ml
1.5mm	4ml	8ml

Volumes of stacking gel and separating gel differ according to the thickness of gel casting:

**For a 5 ml stacking gel preparation:**

H <sub>2</sub> O	2.975 ml
0.5 M Tris-HCl, pH 6.8	1.25 ml
10% (w/v) SDS	0.05 ml
Acrylamide/Bis-acrylamide (30%/0.8% w/v)	0.67 ml
10% (w/v) ammonium persulfate (AP)	0.05 ml
TEMED	0.005 ml

**For 10 ml resolving gel preparation:**

<b>Acylamide percentage</b>	<b>6%</b>	<b>8%</b>	<b>10%</b>	<b>12%</b>	<b>15%</b>
H <sub>2</sub> O	5.2ml	4.6 ml	3.8	3.2ml	2.2ml
Acrylamide/Bis-acrylamide (30%/0.8%w/v)	2ml	2.6ml	3.4ml	4ml	5ml
1.5M Tris(pH=8.8)	2.6ml	2.6ml	2.6ml	2.6ml	2.6ml
10% (w/v)SDS	0.1ml	0.1ml	0.1ml	0.1ml	0.1ml
10% (w/v) ammonium per sulfate (AP)	100μl	100μl	100μl	100μl	100μl
TEMED	10μl	10μl	10μl	10μl	10μl

Note: AP and TEMED must be added right before each us

**5X Sample buffer (loading buffer):**

10% w/v	SDS
10 mM	Dithiothreitol
20 % v/v	Glycerol
0.2 M	Tris-HCl, pH 6.8
0.05%	Bromophenolblue (w/v)

Make sure your target protein dissolved in the liquid phase, and no inappropriate ingredients present. Generally, to treat your unprepared sample, you can use sonicator, lysis buffer or both to sufficiently make your target protein released, and centrifuge to make supernatant and pellet separated.

**1x Running Buffer:**

25 mM	Tris-HCl
200 mM	Glycine
0.1% (w/v)	SDS

**Appendix L.** SDS-PAGE gel running protocol adopted from Bio-Rad laboratory  
(2015)

1. Make the SDS-PAGE gel

Separating gel preparation:

- Set the casting frames (clamp two glass plates in the casting frames) on the casting stands.
- Prepare the gel solution (as described above) in a separate small beaker. Swirl the solution gently but thoroughly.
- Pipet appropriate amount of separating gel solution (listed above) into the gap between the glass plates.
- To make the top of the separating gel be horizontal, fill in water (or isopropanol) into the gap until an overflow. Wait for 20-30min to let it gelate.

Stacking gel preparation:

- Discard the water and you can see separating gel left. Pipet in stacking gel until an overflow.
- Insert the well-forming comb without trapping air under the teeth. Wait for 20-30min to let it gelate.
- Make sure a complete gelation of the stacking gel and take out the comb. Take the glass plates out of the casting frame and set them in the cell buffer dam. Pour the running buffer (electrophoresis buffer) into the inner chamber and keep pouring after overflow until the buffer surface reaches the required level in the outer chamber.

3. Prepare the samples. Mix your samples with sample buffer (loading buffer). Heat them in boiling water for 5-10 min.
4. Load prepared samples into wells and make sure not to overflow. Don't forget loading protein marker into the first lane. Then cover the top and connect the anodes.
5. Set an appropriate volt and run the electrophoresis when everything's done.
6. As for the total running time, stop SDS-PAGE running when the downmost sign of the protein marker (if no visible sign, inquire the manufacturer) almost reaches the foot line of the glass plate. Generally, about 1 hour for a 120V voltage and a 12% separating gel. For a separating gel possessing higher percentage of acylamide, the time will be longer.

Note: Various factors affect the properties of the resulting gel. Higher concentration of ammonium persulfate and TEMED will lead to a faster gelation, on the other hand, a lower stability and elasticity. The optimal temperature for gel gelation is 23°C-25°C. Low temperature will lead to turbid, porous and inelastic gels. The pH is better to be neutral and the gelation time should be limited in 20-30 min.

**Appendix M.** Trans-Blot® Semi-Dry gel transfer protocol adopted from Bio-Rad laboratory (2015)

**Preparation of Transfer buffer**

25 mM Tris

190 mM glycine

20% methanol

Note: for proteins larger than 80 kD, we recommend that SDS be included at a final concentration of 0.1%

**Preparation of Ponceau S staining buffer**

0.2% (w/v) Ponceau S in H<sub>2</sub>O,

5% glacial acetic acid

Note: Acetic acid preparation should be done under the laminar hood.

1. Prepare transfer buffer and equilibrate acrylamide gel in buffer 20-60 minutes.
2. Cut membrane and filter paper to gel size and wet in transfer buffer 5-10 minutes.
3. Remove safety cover and prepare gel sandwich as follows:

(The sequence of sandwich is given from top to bottom)

Pre-wet filter paper

Pre-wet membrane

Equilibrated gel

Pre-wet filter paper

Note: Roll out air bubbles between layers by gently rolling a clean glass rod over the wet filter papers.

4. Secure top stainless steel cathode and safety cover.
5. Run blot. Optimized conditions will be needed for different proteins.

Mini-gel      10 V for 30 minutes or 15 V for 15 minutes.

Large gel     25 V for 30 minutes or 15 V for 60 minutes.

6. At this stage, the membranes can be temporarily stained by using Ponceau S staining buffer to visualize the transfer quality. The stain can be then removed by washing several times with distilled H<sub>2</sub>O.



**Appendix N. Immunoblotting protocol adopted from Bio-Rad laboratory (2015)****Preparation of Tris-buffered saline with Tween 20 (TBST) buffer**

20 mM Tris, pH 7.5

150 mM NaCl

0.1% Tween 20

**Preparation of blocking buffer**

5% (w/v) of bovine serum albumin (BSA) or skim milk in TBST

**Preparation of antibody diluent buffer**

1% (w/v) of bovine serum albumin (BSA) or skim milk in TBST

**Protocol for antibody treatment**

Antibody incubation

1. Briefly rinse the blot in water and stain it with Ponceau S solution to check the transfer quality.
2. Rinse off the Ponceau S stain with three washes with TBST.
3. Block in 3% BSA in TBST at room temperature for 1 h.
4. Incubate overnight in primary antibody solution against the target protein at 4°C.

Note: The antibody should be diluted in the blocking buffer according to the manufacturer's recommended ratio. Primary antibody may be applied to the blot for 1-3 h at room temperature depending on antibody quality and performance.

However, incubation overnight at 4°C is preferred for better results.

5. Rinse the blot 3-5 times for 5 min with TBST.
6. Incubate in the HRP-conjugated secondary antibody solution for 1h at RT.

Note: The antibody can be diluted using 1% skim milk in TBST.

7. Rinse the blot 3-5 times for 5 min with TBST.

**Appendix O.** Immunodetection protocol adopted from Bio-Rad laboratory (2015)**Washing Buffer**

Freshly prepared 0.1% tween-20 in TTBS

**Detection Buffer**

Normally the detection buffer is freshly prepared using following components

100 mM NaCl

100 mM Trish

50 mM MgCl<sub>2</sub>

**BCIP/NBT substrate solution:**

Ready-to-use solution containing Nitro-Blue Tetrazolium Chloride, 5-Bromo-4-Chloro-3'-Indolylphosphate p-Toluidine Salt, 5-Bromo-4-Chloro-Indolyl-Phosphatase.

1. Following the secondary antibody treatment, the membrane is washed 3 times, 5 min each with washing buffer using orbital shaker.
2. The membrane is incubated 10 mins in detection buffer
3. Finally, the detection buffer is discarded and membrane is incubated with BCIP/NBT detection substrate solution in dark.
4. Dark bands will appear in membrane within 2-20 mins of the incubation. Once, the bands development is optimum, was the membranes several times with distilled H<sub>2</sub>O water and air dry it on blotting paper.
5. Capture the chemiluminescent signals using a CCD camera-based imager.  
  
Note: The use of film is not recommended in this step because of its limited dynamic range.
6. Use commercially available gelimage analysis software (GelQuentNET image analyser) to read the band intensity of the target proteins.



**Appendix P.** Extraction of total RNA using TRIzol™ reagent from culture cells.

Total RNA extraction using TRIzol™ reagent (Sigma, USA) optimized for 6-well culture plates.

**Homogenization of culture cells**

1. Wash the cells twice by 1 ml of 1x ice-cold PBS in each well of six-well plate
2. Add 500 ul mL TRIzol® reagent per well of sample (80~95% confluency is optimum).
3. Lyse the cells directly in the culture dish by pipetting the cells up and down several times with 1000 ul micropipette to extract and homogenize samples

**Phase Separation**

4. Incubate the homogenized sample for ~5 min at room temperature to permit complete dissociation of the nucleoprotein complex (turn tube 3-5 times each minutes)
5. Add 0.1 mL of chloroform per 500 ul of TRIzol Reagent used for homogenization.  
Cap the tube securely.
6. Shake tube vigorously by hand for 15 seconds
7. Incubate for 5 minutes at room temperature
8. Centrifuge the sample at  $12,000 \times g$  for 15 minutes at 4°C.

Note: The mixture separates into a lower red phenol-chloroform phase, an interphase, and a colorless upper aqueous phase. RNA remains exclusively in the aqueous phase.

The upper aqueous phase is ~50% of the total volume.

**RNA isolation**

9. Remove the aqueous phase of the sample by angling the tube at 45° and pipetting the solution out. Avoid drawing any of the interphase or organic layer into the pipette when removing the aqueous phase.
10. Place the aqueous phase into a new tube and proceed to the RNA Isolation.
11. Add 125 µl of 100% isopropanol to the aqueous phase, per 500 µL of TRIzol® reagent used for homogenization. Turn tubes several times to mix properly.
12. Incubate at room temperature for 10 min. Centrifuge at  $12,000 \times g$  for 10 mins.

**Then Proceed to RNA wash.**

13. Remove the supernatant from the tube, leaving only the RNA pellet
14. Wash the pellet, with 500 µl of 75% ethanol (in DEPC-treated water) per 500 µl of TRIzol® reagent used in the initial homogenization. Note: The RNA can be stored in 75% ethanol at least 1 year at -20°C, or at least 1 week at 4°C.
15. Vortex the sample briefly, then centrifuge the tube at  $7500 \times g$  for 5 minutes at 4°C. Discard the wash.
16. Air dry the RNA pellet for 5–10 minutes. Do not dry the pellet by vacuum centrifuge.
17. Note: Do not allow the RNA to dry completely, because the pellet can lose solubility. Partially dissolved RNA samples have an A260/280 ratio <1.6 (best results).

**18. Proceed to RNA resuspension**

Resuspend the RNA pellet in RNase-free water (mix by gentle tapping and allow to settle mixture at bottom of tube by short spin)

19. Incubate in room temperature ~30 C for ~20-30 min.
20. Store at -20C overnight and -70C next day. The RNA can be stored for several months at -70C.

**Appendix Q.** Nanodrop DNA/RNA Quantification adopted from Thermofisher scientific (2014)

Standard Procedure

- Bring your own pipette tips and gloves to the NanoDrop machine.
- Save your data to your Z drive so that you can have it for later
- Clean the pedestal in between each run with water and a KimWipe Procedure:
- Log into the computer next to the NanoDrop machine
- On the desktop open the ND1000 program
- In the pop-up window click “Nucleic Acid” for DNA or RNA samples
- Clean the NanoDrop pedestal (the little platform where you put your sample) with a KimWipe and water.
- Load 2µl of H<sub>2</sub>O and click “Okay” then click “Blank” to calibrate it
- Where it says “Sample Type” click DNA-50 for DNA samples or RNA-40 for RNA samples
- Load 2µl of sample onto the pedestal, and click “Measure”
- After the machine analyzes it, save your data. If it is a good reading the graph will show a smooth curve. The absorbance reading at 230nm and 280nm should be about half of the reading at 260nm.
- Remember to clean the pedestal between each read.

## **Appendix R.** Protocol for removal of genomic DNA from total RNA using RQ1 DNase kit

RQ1 DNase kit for removal of genomic DNA. Product catalogue No.# M6101

### **Parts Name Size**

- M610A RQ1 RNase-Free DNase
- M199A stop solution
- M198A RQ1 DNase: 10X reaction buffer

### **DNase Treatment of RNA Samples Prior to RT-PCR**

1. Set up the DNase digestion reaction as follows:

<b>Components</b>	<b>Volume (10 µl total reaction )</b>
RNA in water or TE buffer	1–8µl
RQ1 RNase-Free DNase 10X Reaction Buffer	1µl
RQ1 RNase-Free DNase	1ul/µg of RNA
Nuclease-free water to a final volume	Makeup total 10µl

Note: Use 1 unit of RQ1 RNase-Free DNase per microgram of RNA. For smaller amounts of RNA (>1 ug), use 1 unit of RQ1 RNase-Free DNase per reaction.

2. Incubate at 37°C for 30 minutes.

Note: If analyzing RNA samples by gel electrophoresis, perform a phenol: chloroform extraction and ethanol precipitation before loading the samples on the gel because salts in the RQ1 DNase reaction buffer and Stop solution may cause aberrant migration or smearing of RNA on gels. Steps 3 and 4 may be omitted if a phenol: chloroform extraction is performed.

3. Add 1µl of RQ1 DNase Stop Solution to terminate the reaction.

4. Incubate at 65°C for 10 minutes to inactivate the DNase.

5. All or portion of, the treated RNA can be used for real time PCR.

## **Appendix S.** Protocol for cDNA synthesis from total RNA adopted for SuperScript™ VILO™ cDNA Synthesis Kit

The protocol utilized standard manufactures instructions fo SuperScript™ VILO™ cDNA Synthesis Kit (Catalogue No#: 11754-050 and 11754-250).

Product consists of 10X SuperScript™ Enzyme Mix and 5X VILO™ Reaction Mix.

The following protocol has been optimized for generating first-strand cDNA for use in two-step qRT-PCR. The reaction volume may be scaled as needed up to 100 µL.

1. For a single reaction (20 µl), combine the following components in a tube on ice. For multiple reactions, prepare a master mix without RNA.

	<b>Component</b>	<b>Quantity</b>
1	5X VILO™ Reaction Mix	4 µl
2	10X SuperScript™ Enzyme Mix	2 µl
3	RNA (up to 2.5 µg)	x µl
4	DEPC-treated water to	20 µL (add to make-up 20 µl)

2. Gently mix tube contents and incubate at 25°C for 10 minutes.
3. Incubate tube at 42°C for 60 minutes.
4. Terminate the reaction at 85°C at 5 minutes.
5. Use diluted or undiluted cDNA in Real time PCR (including SYBR™ Green)

Note the process step 2-4 can be automated using PCR machine for cDNA synthesis.

## Appendix T. Real Time PCR protocol adopted for SYBR Green Mastermix

The standard recommended protocol for SYBR<sup>®</sup> Green mastermix (Bio-Rad, Catalog # 172-5121)

The table below indicates typical components and their concentration.

Components	Vol. of Reaction	Final Concentration
Forward Primer	1 µl	0.5 pmol/ µl
Reverse Primer	1 µl	0.5 pmol/ µl
iTaq <sup>™</sup> Universal SYBR <sup>®</sup> Green Supermix (2X)	10 µl	1X
H <sub>2</sub> O	6 µl	--

1. Mix all components carefully by pipetting up and down (do not vortex), tap gently to mix several times to mix.
2. Short Centrifuge (3-5 sec) for spinning down.
3. Add 18 µl of PCR reaction mix (from Table) to each well
4. Carefully pipet 2 µl of each cDNA template (500 ng-1 µg) to each well of iCycler 96 well qPCR plate. You may need to mix by tapping and spin down cDNA before pipetting. This will result in final volume approximately 20 µl, which is optimum for the Bio-Rad thermocycler.
5. Seal the Multiwell Plate with 96 well plate sealing sticker.
6. Tap gently on the side of plate to mix but be careful not to splatter samples
7. Load the Multiwell plate into the Real time thermocycler and run appropriate program.

**Appendix U.** Calculation of the real time PCR results using  $2^{-\Delta\Delta C_T}$  Method adopted from (149)

Relative quantification of the mRNA gene expression for target gene is conducted of Real Time PCR results. For this purpose the housekeeping Gene (reference gene, such as GAPDH is taken as internal control).

Relative quantification method ( $\Delta\Delta C_T$  Method also known as Livak Method)

The  $C_T$ : “Cross threshold” is a basic principle of real time PCR and is an essential component in producing accurate and reproducible data.

Key Assumption: Amplification efficiency is 2 for both the target and reference gene which denotes a doubling of PCR product with each cycle (exponential growth).

Represented as **Ratio** =  $2^{-\Delta\Delta C_T}$

Where  $\Delta\Delta C_T = \Delta C_{T_{\text{treated}}} - \Delta C_{T_{\text{control}}}$

$\Delta C_{T_{\text{treated}}} = C_T$  difference of a reference and target gene for a treatment sample

$\Delta C_{T_{\text{treated}}} = C_{T_{\text{target}}} - C_{T_{\text{ref}}}$

$\Delta C_{T_{\text{control}}} = C_T$  difference of a reference and target gene for a control sample

$\Delta C_{T_{\text{control}}} = C_{T_{\text{target}}} - C_{T_{\text{ref}}}$

The procedure results in relative expression of target based on normalization with reference gene. Further details regarding theory and optimization can be obtained by reading the reference.

**Appendix V.** Approval certification for the satisfaction and quality control of the animal cell culture laboratory.



**คณะกรรมการควบคุมความปลอดภัยทางชีวภาพ มหาวิทยาลัยธรรมศาสตร์**

หนังสือรับรองเลขที่.....071/2560.....

รหัสโครงการ.....055/2560.....

ชื่อโครงการวิจัย.....การศึกษาความเป็นพิษและเป้าหมายการออกฤทธิ์ของสารอะพริกทีโดติน สารเนต้า-  
ยูเคสมอลและสารไฮนโซลต่อเซลล์มะเร็งท่อน้ำดี.....

ชื่อผู้วิจัยหลัก.....Mr. Vivek Bhakta Mathema.....

หน่วยงานที่รับผิดชอบ.....วิทยาลัยแพทยศาสตร์นานาชาติจุฬาภรณ์ มหาวิทยาลัยธรรมศาสตร์.....

ผลการพิจารณา

ประเภทของโครงการวิจัย.....ประเภทที่ 2.....

ระดับความปลอดภัยของห้องปฏิบัติการ.....ความปลอดภัยระดับที่ 1 (Biosafety Level 1) โดยต้องมี  
BSC และ Autoclave

คณะกรรมการควบคุมความปลอดภัยทางชีวภาพ มหาวิทยาลัยธรรมศาสตร์ ได้พิจารณาประเภทของ  
โครงการวิจัย และระดับความปลอดภัยของห้องปฏิบัติการ

ระยะเวลาที่อนุมัติ 1 ปี (เอกสารอนุมัติฉบับนี้มีผลตั้งแต่วันที่ 3 ตุลาคม 2560 ถึง วันที่ 2 ตุลาคม 2561)

กำหนดส่งรายงานความก้าวหน้า.....6 เดือน.....(3 เมษายน 2561).....

ลงชื่อ..........  
(รองศาสตราจารย์ ดร. วีระชัย ชนานันต์)  
ประธานกรรมการ

ลงชื่อ..........  
(ผู้ช่วยศาสตราจารย์ ดร. วีระชัย ทิตถาการ)  
กรรมการและเลขานุการ

อนุมัติ ณ วันที่ 3 ตุลาคม 2560



## BIOGRAPHY

**Name** Mr. Vivek Bhakta Mathema

**Date of Birth** November 9, 1985

**Educational Attainment** 2014: Graduate Degree, in Biotechnology

**Work Position** PhD Student/Researcher in CICM, Thammasat University, Thailand

**Scholarship** 2015 : Chulabhorn International College of Medicine(CICM), Thammasat University for PhD in Bioclinical Sciences

### Publications

- **Vivek Bhakta Mathema**, Chaijaroenkul W, Karbwang J, Na-Bangchang K. Growth inhibitory effect of  $\beta$ -eudesmol on cholangiocarcinoma cells and its potential suppressive effect on heme oxygenase-1 production, STAT1/3 activation, and NF- $\kappa$ B downregulation. Clinical Experimental Pharmacology Physiology. 2017; doi: 10.1111/1440-1681.12818
- **Vivek Bhakta Mathema**, Kesara Na-Bangchang. Current insights on cholangiocarcinoma research: a brief review. Asian Pacific Journal for Cancer Prevention. 2015 16:1307-1313
- **Vivek Bhakta Mathema**, Kesara Na-Bangchang. A brief review on biomarkers and proteomic approach for malaria research. Asian Pacific Journal of Tropical Medicine. 2015;8:253-262
- **Vivek Bhakta Mathema**, Bal Krishna Chand Thakuri, Mika Sillanpää, Reena Amatya Shrestha. Study of mercury (II) chloride tolerant bacterial isolates from

Baghmati river with estimation of plasmid size and growth variation for the high mercury (II) resistant *Enterobacter spp.* Journal of Biotech Research 2011;3:72-77

- **Vivek Bhakta Mathema**, Na-Bangchang K. Regulatory roles of brain-specific angiogenesis inhibitor 1(BAI1) protein in inflammation, tumorigenesis and phagocytosis: A brief review. Critical Reviews Oncology Hematology. 2017; doi: 10.1016/j.critrevonc.2017.01.006
- **Vivek Bhakta Mathema**, Zahid Manzoor, Jung-Eun Koo et al. Inhibition of cell death of bone marrow-derived macrophages infected with Ehrlichia muris. Ticks and Tick-borne Diseases 2013.doi:10.1016/j.ttbdis.2012.11.011
- **Vivek Bhakta Mathema**, Young-Sang Koh. Inhibitor of growth-4 mediates chromatin modification and has a suppressive effect on tumorigenesis and innate immunity. Tumor Biology 2011; 33:1-7
- **Vivek Bhakta Mathema**, Balkrishna Chand Thakuri, Mika Sillanpää. Bacterial mer operon-mediated detoxification of mercurial compounds: a short review. Archives of Microbiology 2011;193:837-844
- Zahid Manzoor, **Vivek Bhakta Mathema**, Doobyeong Chae, Eun-Sook Yoo, Hee-Kyoung Kang, Jin-Won Hyun, Nam Ho Lee, Dong-Sam Kim. *Sargasum macrocarpum* inhibits CpG-induced inflammatory response by attenuating NF-κB pathway. Food Science and Biotechnology 2014;23: 293-297

- Zahid Manzoor, **Vivek Bhakta Mathema**, Doobyeong Chae, Hee-Kyoung Kang, Eun-sook Yoo, You-Jin Jeon, Young-Sang Koh. Octaphlorethol A Inhibits CpG-Induced Inflammatory Response by Attenuating Mitogen-Activated Protein Kinase and NF- $\kappa$ B Pathways. *Bioscience, Biotechnology, and Biochemistry* 2013; doi:10.1271/bbb.130299
- Tran Hong Quang, Nguyen Thanh Ngan, Doobyeog Chae, **Vivek Bhakta Mathema**, Young-Sang Koh, Young Ho Kim. Inhibitory effects of oleananetype triterpenes and saponins from the stem bark of *Kalopanax pictus* on LPS-stimulated proinflammatory cytokine production in bone marrow-derived dendritic cells. *Archives of Pharmacal Research* 2013; doi:10.1007/s12272-013-0031-8
- Phan Van Kiem, Hoang Le Tuan Anh, Nguyen Xuan Nhiem, Chau Van Min, Pham Hai Yen, **Vivek Bhakta Mathema**, Young-Sang Koh, Young Ho Kim. Labdanetype diterpenoids from the rhizomes of *Hedychium coronarium* inhibit lipopolysaccharide-stimulated production of pro-inflammatory cytokines in bone marrow-derived dendritic cells. *Chemical & pharmaceutical bulletin* 2012. 60(2) 246-250

Expected publications:

- **Vivek Bhakta Mathema**, Wannana Chaijaroenkul, Kesara Na-bangchang. Growth inhibitory effect of atractylodin on cholangiocarcinoma cells and its potential suppressive effect on heme oxygenase-1 production, STAT1/3 activation and NF- $\kappa$ B downregulation. *Oncology letters*

### Oral presentation

- **Vivek Bhakta Mathema**, Kesara Na-Bangchang. Growth inhibitory activity of  $\beta$ -eudesmol on cholangiocarcinoma cells is associated with suppression of heme oxygenase-1 production and STAT3 phosphorylation. The 1st CICM International. Conference organizer CICM, Thammasat University, 28-29 August 2017

### Poster presentation

- **Vivek Bhakta Mathema** and Kesara Na-Bangchang. Atractylodin from *Atractylodin lancea* induces Apoptosis and inhibits growth of Human Cholangiocarcinoma Cells. *Conference on Illustrious Issues in Pharmacology 2017*. Conference organizer: Burapha University, May 18-20, 2017
- **Vivek Bhakta Mathema** and Kesara Na-Bangchang. Cytotoxic Activity and suppression of JAK/STAT and NF-KB pathway by Bioactive Compound from *Atractylodes lancea* (Thunb.) DC. A. *The second international conference on Herbal and Traditional Medicine (HTM2017)*. Conference: Jan 25-27 Asia Hotel, Bangkok, Thailand
- **Vivek Bhakta Mathema** and Kesara Na-Bangchang. Cytotoxic activity of bioactive compound from *Atractylodes lancea* (Thunb.) DC. against cholangiocarcinoma cell lines. Conference: The 13th Asian-Pacific Federation of Pharmacologist meeting "New Paradigms in Pharmacology for Global Health". The Berkeley Hotel Pratunam, Bangkok, Thailand

### Work experience

- Teaching Assistant at department of Biotechnology, Kathmandu University (2007-2009 AD)